# An Exploration of the Synthesis, Coordination Chemistry and Properties of Novel Thiourea Ligands and their Complexes

**Ali Abdulimam Abdulzahra Al-Riyahee**

**A thesis submitted to Cardiff University in accordance with the requirements for the degree of Doctor of Philosophy at School of Chemistry, Cardiff University, United Kingdom.**


**August 2016**

# DECLARATION

This work has not been submitted in substance for any other degree or award at this or any other university or place of learning, nor is being submitted concurrently in candidature for any degree or other award.

Signed …… (Ali A. A. Al-Riyahee) Date ……..……

## STATEMENT 1

This thesis is being submitted in partial fulfillment of the requirements for the degree of (PhD)

Signed …… (Ali A. A. Al-Riyahee) Date ……

## STATEMENT 2

This thesis is the result of my own independent work/investigation, except where otherwise stated. Other sources are acknowledged by explicit references. The views expressed are my own.

Signed …… (Ali A. A. Al-Riyahee) Date ……

## STATEMENT 3

I hereby give consent for my thesis, if accepted, to be available for photocopying and for inter-library loan, and for the title and summary to be made available to outside organizations.

Signed …… (Ali A. A. Al-Riyahee) Date ……

## STATEMENT 4: PREVIOUSLY APPROVED BAR ON ACCESS

I hereby give consent for my thesis, if accepted, to be available online in the university´s Open Access repository and for inter-library loans after expiry of a bar on access previously approved by the Academic Standards & Quality Committee.

Signed …… (Ali A. A. Al-Riyahee) Date ……

# ACKNOWLEDGMENTS

Although only my name appears on the cover of my PhD thesis, many people have participated in some way to its creation. I owe my thankfulness to all those people who support my PhD study journey and have made this thesis possible and an unforgettable experience for me.

Foremost, I would like to express my deepest sense of **G**ratitude (with a capital and bold g) to my supervisors Dr. Angelo Amoroso and Dr. Simon Pope, who offered their continuous advice, encouragement and support throughout the period of my PhD study, and especially in their confidence in me. I have been amazingly fortunate to have those supervisors who gave me the freedom to find out on my own, and at the same time the instruction to recover when my steps faltered.

A very special thanks goes out to Dr. Ben Ward for his precious notices, advice and support which he provided me during my PhD study.

I would like to acknowledge all the technical staff especially Dr. Rob Jenkins, Sham, Robin, Gaz and Dave for their help. I would also like to thank all members in inorganic groups for sharing chemicals and enjoyments moments in and outside the university.

I would like to say a big thank you to my parents for their love and support they provided me through my entire life. My sisters and brother deserve my wholehearted thanks as well.

I must express my big gratitude to Ashwaq (my wife), Shahad, Mohammed and Noor (my kids) for their continued support, encouragement and patience for me throughout my PhD study period. Lastly, I would like to thank the Iraqi government for giving me this opportunity to study PhD in Cardiff University.

## ABSTRACT

In order to highlight the presentation of this thesis and to provide more detailed investigations, the thesis was separated into five chapters according to the sequence of the work.

**Chapter One:** This chapter gives an overview of the coordination chemistry of different metal complexes focusing on Cr(III), Ni(II), Cu(II), Cu(I), and Zn(II) ions with common, uncommon, rare ligands and their geometric preferences. A brief introduction to magnetic susceptibility and their magnetic properties are also discussed. The cyclic voltammogram and the various types of redox processes are explained. Different electronic transitions in addition to *d-d* transition with the expected UV-vis. spectra bands are illustrated. HSAB theory is presented to show the stability of the metal complexes. Lastly, aims and the objectives of this thesis are shown in detail.

**Chapters Two and Four:** These chapters focus on the preparation and full characterization of novel molecules based upon thiourea derivatives and the subsequent synthesis of their complexes with Ni(II), Cu(II), Cu(I) and Zn(II) ions. Fully characterization was achieved successfully by Infrared Spectroscopy (IR), Electronic transition (UV-vis.), Mass Spectrometry (MS), Magnetic Susceptibility (and Magnetic Moment), elemental analysis (CHN), Nuclear Magnetic Resonance (NMR), Cyclic voltammetry (CV) and Single Crystal X-Ray Crystallography. Many of the complexes have been crystallographically characterised to elucidate the solid state geometry. The influence of increasing the reaction temperature on the hydrolysis of amide link within thiourea was investigated to probe the ease of cleavage of the benzoyl or pivaloyl group at varying temperature. All N-benzoyl and N-pivaloyl thiourea complexes showed intramolecular H-bonding (N-H….O) between the N-H of the thiourea and the oxygen of the acyl group. This result in the familiar of a six membered ring. The electrochemical studies (cyclic voltammoram) for the Cu(II), Cu(I) and Ni(II) complexes showed a quasi-reversible process in the reductive region for all the Cu(II) and Cu(I) complexes while two irreversible peaks in the reductive region are observed in the Ni(II) complexes.

**Chapter Three:** Describes the synthesis and characterization of thiosemicarbazone derivatives and their complexes with Ni(II), Cu(II) and Zn(II) ions. All thiosemicarbazone derivatives behave as tridentate ligands with two forms, keto (deprotonated) and enol (protonated). The hydrolysis of the thiosemicarbazone and cleavage of pivaloyl group were observed and attributed to increasing the reaction temperature. Cleavage may occur before complexation. The cyclic voltammogram showed one quasi-reversible process in the Cu(II) complexes in the reductive region whilst two irreversible peaks are observed in the Ni(II) complexes.

**Chapter Five:** The synthesis and characterisation of the novel Cr(III) complexes with 8-hydroxyquinoline derivatives is reported in this chapter. The X-ray crystal structures and UV-vis. spectra of all Cr(III) complexes confirmed the preference for an octahedral geometry. The electrochemical studies showed two reversible peaks for all Cr(III) complexes which was attributed to a Cr(III)/Cr(II) couple and a ligand based process. The optical properties were investigated and showed one emission peak which is assigned to fluorescence based on the 8-hydroxyquinoline group. An investigation of how the electron donating and electron withdrawing effects of substituents on the 8-hydroxyquinoline effect emission wavelength and intensity was carried out. In addition, the effect of coordinating water on the emission properties of these types of complexes was all investigated.

# *Contents*

## *Abbreviations*

## *Chapter one: An Introduction*



## *Chapter Two: Synthesis, characterization, X-ray crystal structures of Cu(I), Cu(II), Ni(II) and Zn(II) complexes with N,N'-substituted thiourea derivatives*

***Chapter Four: Spectral, magnetic and electrochemical studies of Cu(I), Cu(II) and Ni(II) complexes with N-((6-benzamido or pivalamido pyridin-2-yl)carbamothioyl benzamide or pivalamide derivatives ($L^5$-$L^{7A}$).***

# Abbreviations

| | |
|---|---|
| CFSE | Crystal field splitting energy |
| $\Delta_o$ | The crystal field splitting in an octahedral field |
| P | Pairing energy |
| LFSE | Ligand field stabilization energy |
| $PPh_3$ | Triphenyl phosphine |
| Py | Pyridine |
| UV-vis. | Ultra violet- visible |
| $\mu_{eff}$ | Magnetic moment |
| $^1H$ NMR | Proton nuclear magnetic resonance |
| TMS | Tetra methyl silane |
| $Cm^3$ | Cubic centimeter |
| G | Gram |
| Hz | Hertz |
| M | Mass |
| M | Molecular weight |
| T | Temperature in centigrade degree |
| ºC | Degrees centigrade |
| CV | Cyclic Voltammetry |
| TBAF | Tetrabutylammonium hexafluoro phosphate |
| I | Current |
| Mv | millivolts |
| V | Volts |
| Sec | seconds |
| Nm | nanometers |
| HOMO | Highest occupied molecular orbital |
| LUMO | Lowest unoccupied molecular orbital |
| M | Concentration in molarity/ Metal |
| Cm | centimeters |
| $\varepsilon$ | Extinction coefficient |
| LMCT | Ligand metal charge transfer |
| MLCT | Metal ligand charge transfer |
| CFT | crystal field theory |
| IR | Infrared |
| MS | Mass spectrometry |
| ESMS | Electroscopy ionization mass spectroscopy |
| $^{13}C$ NMR | Carbon 13 isotope nuclear magnetic resonance |
| $CDCl_3$ | Deuterated chloroform |
| DMSO-$d^6$ | Deuterated dimethylsulfoxide |
| Mmol | Millimoles |
| m.p | Melting point |
| *m/z* | Mass /Charge ratio |
| $cm^{-1}$ | Wavenumber reciprocal centimeters |
| $\lambda_{max}$ | Wavelength of the peak at the maximum absorption |
| MHz | Mega hertz |
| Ppm | Parts per million |

| | |
|---|---|
| D | Doublet |
| T | Triplet |
| S | Singlet |
| M | multiple |
| Ar | Aryl |
| *J* | Coupling constant (in Hz) |
| DMF | N,N-Dimethyl form amide |
| DCM | Dichloromethane |
| THF | Tetrahydrofuran |
| MeCN | acetonitrile |
| MeOH | Methanol |
| EtOH | Ethanol |
| *t*-butyl | Tertiary butyl |
| Fc | ferrocene |
| asu | Asymmetric unit |
| CCDC | Cambridge crystallography data centre |
| Å | Angstrom |
| r.t. | Room temperature |

# Chapter One
## An
## Introduction

# 1.1 Introduction

## 1.1.1 Coordination chemistry

**Coordination chemistry** is defined as the study of the bonding in compounds formed between metal ions and neutral or negatively charged ligands that donate electrons to the metal. The Nobel Prize winner, Alfred Werner (1866-1919), was the first scientist who majorly contributed to the discovery of this branch of chemistry by his coordination theory of metal-ammine complexes, such as $[Co(NH_3)_6Cl_3]$ in 1913.[1] Coordination compounds are of great importance in different fields due to their existence in different shapes and structures. There are tremendous examples of coordination compounds in biochemistry. For example, the iron, magnesium, cobalt and copper coordination compounds are exemplified by hemoglobin,[2] chlorophyll,[3] Vitamin B-12[4] and hemocyanin[5] respectively.

The knowledge of the oxidation state of the transition metals in their complexes as well as their geometric preference is very important for an understanding of the coordination chemistry of transition metal complexes. **Table 1.1** shows the distribution of different oxidation states for the d-block elements. It is very helpful for researchers to have a general idea of the oxidation states and coordination geometries before starting practical work. Recently, it was shown that the coordination bond of the metal-ligand allows the construction of supramolecular complexes.[6-10] In spite of the qualitative information of the coordination geometries and the oxidation states reported in inorganic textbooks,[11,12] quantitative data of coordination geometries of d-block elements is still rare.[13] In 1997, Venkataraman *et al*.[14] reported the occurrence of the different coordination numbers and geometries in d-block complexes. This thesis describes the complexation between Ni, Cu or Zn with thiourea and Cr with the 8-hydroxyquinoline derivatives. Thus, Venkataraman's results for groups 6, 10, 11 and 12 which contain Cr, Ni, Cu and Zn elements are relevant to this study. **Tables 1.2-1.5** show the coordination geometries of homoleptic complexes of the Cr, Ni, Cu and Zn elements and the different oxidation states (0, I, II, III and IV) in these coordination complexes.

**Table 1.1:** The distribution of different oxidation states (0, I, II, III, IV, V and VI) for the d-block elements. n: the number of the studied complexes,

| Group | Metal | n | % (number of its complexes) | | | | | | |
|---|---|---|---|---|---|---|---|---|---|
| | | | **0** | **I** | **II** | **III** | **IV** | **V** | **VI** |
| **6** | Cr | 129 | 27(35) | - | 17(22) | 55(71) | 1(1) | - | - |
| | Mo | 31 | 29(9) | - | 13(4) | 29(9) | 18(6) | 7(2) | 4(1) |
| | W | 23 | 51(11) | - | 3(1) | 10(2) | 14(3) | 6(2) | 16(4) |
| **10** | Ni | 301 | - | 1(3) | 98(295) | 1(3) | - | - | - |
| | Pd | 265 | - | - | 99(262) | - | 1(3) | - | - |
| | Pt | 570 | - | - | 90(513) | - | 10(57) | - | - |
| **11** | Cu | 530 | - | 33(175) | 67(355) | - | - | - | - |
| | Ag | 90 | - | 100(90) | - | - | - | - | - |
| | Au | 373 | - | 88(328) | 1(4) | 11(41) | - | - | - |
| **12** | Zn | 132 | - | - | 100(132) | - | - | - | - |
| | Cd | 44 | - | 2(1) | 98(43) | - | - | - | - |
| | Hg | 319 | - | - | 98(313) | 2(6) | - | - | - |

From this report, Cr has 129 published homoleptic coordination complexes, the highest percentage (55%, 71 complexes) of them are for Cr(III) and the least at 1% is for Cr(IV). While 301 structures were published for Ni, 98% (295) of them are for Ni(II). Cu has 530 published coordination complexes, 67% of them in Cu(II) oxidation state and 33% complexes are in Cu(I). For Zn, the oxidation state (II) was unique (100%,132). It is apparent from **Table 1.1** that the most common oxidation states for Cr, Ni, Cu and Zn elements are Cr(III), Ni(II), Cu(II) and Zn(II), respectively.

**Table 1.2:** Coordination geometries of Cr in different oxidation states (0, I, II, III and IV) in 129 coordination complexes.

| **Coordination geometry** | **% (number of its complexes)** | | | | |
|---|---|---|---|---|---|
| | **0** | **I** | **II** | **III** | **IV** |
| Trigonal planar | 1(1) | - | - | - | - |
| T- shaped | 1(1) | - | - | - | - |
| Pyramidal | - | - | - | - | - |
| Tetrahedral | - | - | - | - | 1(1) |
| Square planar | - | - | 11(14) | - | - |
| Trigonal bipyramidal | - | - | - | - | - |
| square pyramidal | - | - | 2(2) | - | - |
| Octahedral | 25(33) | - | 4(6) | 55(71) | - |

**Table 1.3:** Coordination geometries of Ni in different oxidation states (0, I, II, III and IV) in 301 coordination complexes.

| **Coordination geometry** | **% (number of its complexes)** | | | | |
|---|---|---|---|---|---|
| | **0** | **I** | **II** | **III** | **IV** |
| Trigonal planar | - | - | - | - | - |
| T- shaped | - | - | 8(24) | 0.6(2) | - |
| Pyramidal | - | - | | - | - |
| Tetrahedral | - | 1(3) | 4(12) | - | - |
| Trigonal pyramidal | - | - | 4(12) | - | - |
| Square planar | - | - | 32(94) | 0.3(1) | - |
| Trigonal bipyramidal | - | - | - | - | - |
| square pyramidal | - | - | - | - | - |
| Octahedral | - | - | 50(153) | - | - |

**Table 1.4:** Coordination geometries of Cu in different oxidation states (0, I, II, III and IV) in 530 coordination complexes.

| **Coordination geometry** | **% (number of its complexes)** | | | | |
|---|---|---|---|---|---|
| | **0** | **I** | **II** | **III** | **IV** |
| Trigonal planar | - | 17(88) | - | - | - |
| Pyramidal | - | 3(14) | 4(18) | - | - |
| Tetrahedral | - | 13(73) | - | - | - |
| Trigonal pyramidal | - | - | 3(14) | - | - |
| Square planar | - | - | 26(142) | - | - |
| Trigonal bipyramidal | - | - | 3(14) | - | - |
| square pyramidal | - | - | 11(60) | - | - |
| Octahedral | - | - | 20(107) | - | - |

**Table 1.5:** Coordination geometries of Zn in different oxidation states (0, I, II, III and IV) in 132 coordination complexes.

| **Coordination geometry** | **% (number of its complexes)** | | | | |
|---|---|---|---|---|---|
| | **0** | **I** | **II** | **III** | **IV** |
| Tetrahedral | - | - | 67(88) | - | - |
| Trigonal pyramidal | - | - | 3(4) | - | - |
| Square planar | - | - | - | - | - |
| Trigonal bipyramidal | - | - | 8(11) | - | - |
| Octahedral | - | - | 22(29) | - | - |

In reality, Cr(III) is the most common stable oxidation state of Cr and **Table 1.2** shows how the Cr(III) complex prefers an octahedral geometry. The reason of this preference is it lies in the high CFSE for $d^3$ ion (**-1.2** $\Delta_o$), see **Figure 1.1**. The Cr(III) complexes are kinetically inert complexes due to the high CFSE compared to reaction intermediates leading to the extremely slow rate of exchange of ligands.

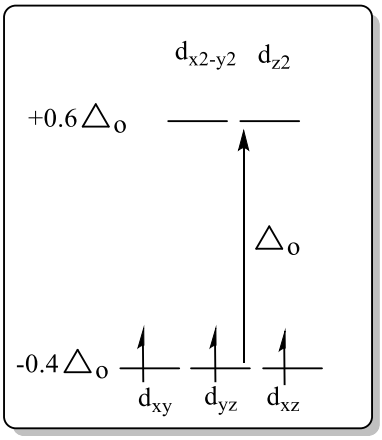


**Figure 1.1**: The preference of $d^3$ Cr(III) complexes to exhibit an octahedral geometry supported by the crystal field theory.

**Table 1.3** shows how the Ni(II) complexes prefer octahedral or square planar coordination geometries. This preference again depends on the value of CFSE for octahedral complexes (-1.2 $\Delta_o$), while the CFSE of square planar complexes is -2.44 $\Delta_o$ +P, P= pairing energy. Prima facie, it seems that square planar geometry are more stable than octahedral (CFSE $_{\text{square planar}}$ > CFSE $_{\text{octahedral}}$), but the preference depends on the relative difference of $\Delta_o$ versus P, with complexes with large $\Delta_o$ values favouring square planar geometries, see **Figure 1.2**.

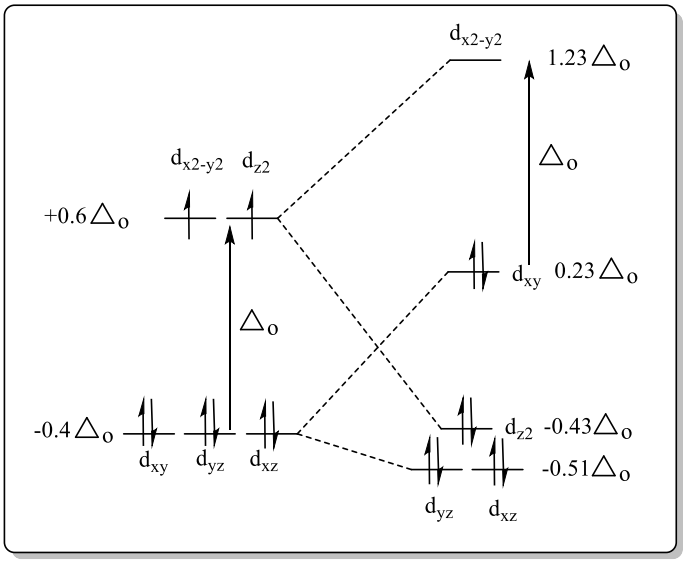


**Figure 1.2**: The preference of $d^8$ Ni(II) complexes to exhibit an octahedral geometry vs. a square planar geometry support by the crystal field theory.

The zero value of LFSE (ligand field stabilization energy) of Cu(I), $d^{10}$ electronic configuration complexes indicates there is no obvious preference of octahedral over tetrahedral geometry. **Table 1.4** shows there are two common geometries of Cu(I) complexes, trigonal planar and tetrahedral and this depends on the steric requirements of the ligands and thermochemical considerations. In **Table 1.4**, Cu(II) complexes show stronger preference to square planar than octahedral geometries around the Cu(II) centre. This may be due to the structure stability of the square planar over the octahedral complex (CFSE $d^9$ octahedral **-0.6** $\Delta_o$ while the CFSE $d^9$ square planar **-1.21** $\Delta_o$). The square planar geometry is the extreme example of the typical Jahn-Teller distortion observed in Cu(II) complexes.

The Jahn-Teller distortion is typically observed among $d^9$, Cu(II) octahedral complexes where it is described as a z-elongation. The z-elongation or the z-compression is observed where the two axial bonds are longer or shorter than those of the equatorial bonds respectively, see **Figure 1.3**. In elongated Jahn-Teller distortions, the d orbitals with a *z*-component ($d_Z^2$, $d_{XZ}$ and $d_{yz}$) are lowered in energy, while the orbitals without a z-component ($d_{xy}$ and $d_{X^2-y^2}$) are relatively destabilized. This is due to the relatively greater overlap between the $d_{xy}$ and $d_{x^2-y^2}$ orbitals with the ligand orbitals. The $d_{xy}$ orbital is still nonbonding, but is destabilized due to the interactions while the $d_{x^2-y^2}$ orbital is antibonding and it is expected to promote in energy due to elongation. In compression Jahn-Teller distortions, the situation is the converse, see **Figure 1.3**.[15,16]

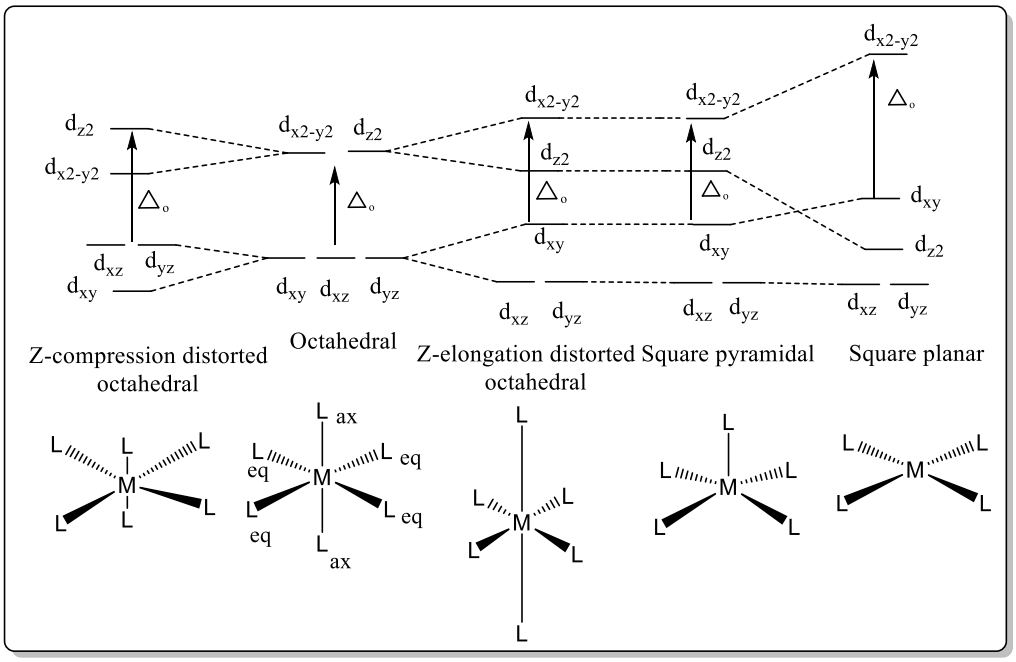


**Figure 1.3:** Crystal field energy diagram showing the transformation from octahedral to square planar geometry after distortion of octahedral and Jahn-Teller effect of octahedral geometry.

**Figure 1.3** shows the new ordering of the d-orbital energy diagram for octahedral complexes after distorting by the elongation, by removing one ligand to obtain a square pyramid, or removing the two ligands along the z-axis to form a square planar complex. Some octahedral complexes readily lose two ligands to form square planar complexes, such as complexes with a $3d^8$ configuration with strong field ligands (e.g. $[Ni(CN)_4]^{2-}$), or some $d^9$ complexes. This is due to the large $\Delta_o$.

The $d^{10}$ electronic configuration Zn(II) complexes, see **Figure 1.4**, has no electronic preference for an octahedral geometry over a tetrahedral geometry. This is due to the LFSE being zero for both geometries. **Table 1.5** shows that the Zn(II) ion commonly has tetrahedral geometry and this often depends on the steric requirements of the ligands and thermochemical considerations.

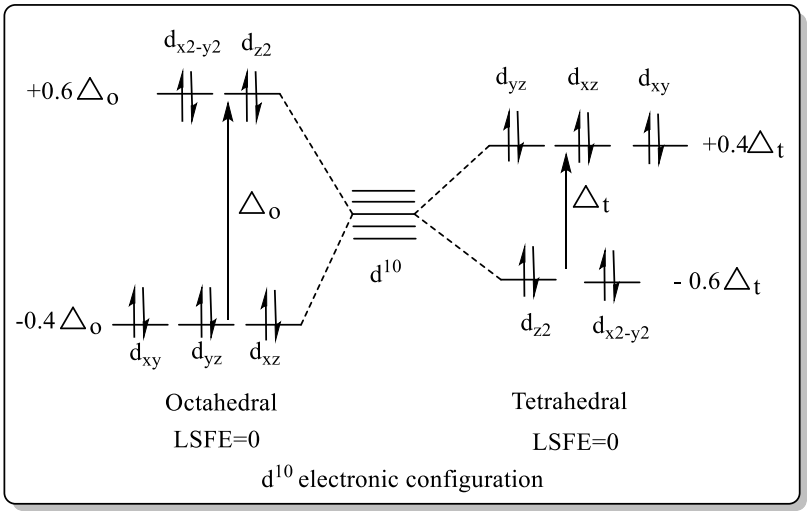


**Figure 1.4**: Shows no preference of $d^{10}$ electronic configuration, for example Zn(II) and Cu(I) complexes for octahedral geometry over tetrahedral geometry.

Important conclusions drawn from **Tables 1.2-1.5**, include: **i)** Cr(III) has the greatest propensity to adopt an octahedral geometry; **ii)** an octahedral coordination is strongly favoured by the Ni(II) ion, but square planar geometries form with strong field ligands; **iii)** the ion most likely to enter into a trigonal planar coordination mode is Cu(I), (it will be discussed and shown in **chapter two**) but the tetrahedral geometry is common. In contrast, Cu(II) prefers the octahedral and square planar geometries **iv)** tetrahedral coordination is common for Zn(II) ions (67% of structures) and octahedral geometry is less common (22% of structures) **v)** trigonal pyramidal coordination is observed rarely for Ni(II) (4%, 12 structures), Cu(II) (14 of 355 total structures) and Zn(II) (3%, 4 structures) **vi)** less commonly, square pyramidal and trigonal bipyramidal geometries are adopted by Cu(II) (11%) and Zn(II) (8%) respectively. **vii)** Cr(III) is the most likely towards an octahedral geometry than Ni(II), Cu(II) and Zn(II) ions while Ni(II) has the greatest preference to square planar geometry. **ix)** Zn(II) is much more likely to adopt a tetrahedral geometry compared to Ni(II) and Cu(I) ions.

One ligand framework of interest in our study is based around the thiourea group. Many different metal complexes of thiourea have been prepared and their coordination chemistry was studied due to their potential ability for use in various fields (as it will be shown extensively and in detail with many examples in **chapters two**, **three** and **four**). Different geometries were shown for the complexes of the

thiourea with different transition metal ions depending on the donating or withdrawing groups within the thiourea ligands. In the Cu(I) complexes of thiourea, the ligand can arrange in a three coordinate trigonal planar manner[17-22],(for example, bis(N-O-methylphenyl-N′-ethoxycarbonylthiourea)CuCl, see **Figure 1.5a**), four coordinated tetrahedral[23-28] (for example, $[CuCl(HL)(PPh_3)_2]$, HL=N-(dibenzylcarbamothioyl) benzamide), five coordinated square pyramidal[29,30] around the Cu(I) ion (for example, $[Cu_3L_2(Py)_6(H_{Im})](H_2O)_2$**,** $H_3L$=l-(2-carboxybenzoyl) thiosemicarbazide Py=pyridine, $H_{Im}$= imidazole). The Ni(II) complexes of the thiourea were prepared and showed four coordinate square planar[31-33], (for example, $[Ni(NH_2NHCSNH_2)_2](NO_3)_2$) and octahedral[34-36] geometries (for example, $[Ni(phen)_2(thiourea)Cl]Cl$, phen=1,10-phenanthroline). The coordination chemistry of the Zn(II) complexes of thiourea were also studied, they were shown four coordinate tetrahedral[37-39] (for example, $[Zn(L)Cl_2]$, L=3-phenyl-1,1-bis(pyridin-2-ylmethyl)thiourea) and octahedral geometries[40,41], (for example $[Zn(CH_5N_3S)_2(H_2O)_2]^{2+}$).

The thiosemicabazone complexes with Cu(II) ions show different geometries (see **Figure 1.5b**, four coordinated square planar [42-44] (for example, $[Cu(H_2L)Cl]$, $H_2L$=2-[(2-hydroxyphenyl)methylene]hydrazine-N-(2-propenyl)carbothioamide), tetrahedral (for example $[Cu(LH_2)](ClO_4)_2$,$LH_2$= thiosemicarbazone-pyridylhydrazine ligand) [45], five coordinated trigonal bipyramidal[46-48] (for example, $[Cu(LH)Cl_2].H_2O$, LH=(E)-1-(1-hydroxypropan-2-ylidene)thiosemicarbazide), square pyramidal[49,50] (for example, $[CuCl_2(H_2\text{-}OQtscH)]\cdot 2H_2O$, (H2-OQtsc-H)=2-oxo-1,2-dihydro quinoline-3-carbaldehyde thiosemicarbazone) and six coordinate octahedral.[51,52] Ni(II) complexes of thiosemicarbazone were also prepared. They showed various environments around the Ni(II) ion, four coordinate square planar[53-55] (for example, $[Ni(PLTSC\text{-}H)py]NO_3$ , PLTSC-H=pyridoxal thiosemicarbazone, py=pyridine) and octahedral[56-58] geometries (for example $[Ni(HAcb4DM)_2]^{+2}$, HAcb4DM = 5-acetylbarbituric-4N-dimethylthiosemicarbazone). The Zn(II) complexes of thiosemicabazone were studied and showed four coordinate tetrahedral,[59] five coordinate trigonal bipyramidal[60-66] (for example $[Zn(Triapine)Cl_2]$, Triapine=3-aminopyridine-2-carboxaldehyde thiosemicarbazone) as well as octahedral geometries[61,67,68] were observed. **Figures 1.5 a+b:** show the coordination

geometry of the metal complexes of thiourea and thiosemicarbazone derivatives respectively.

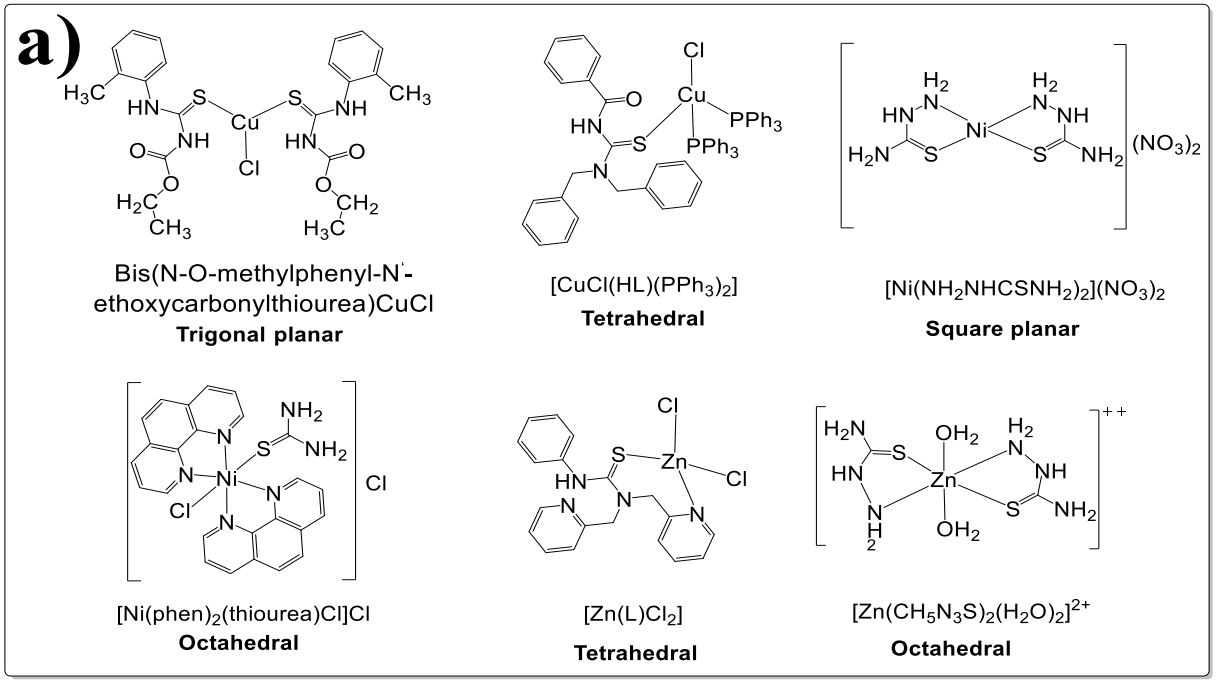


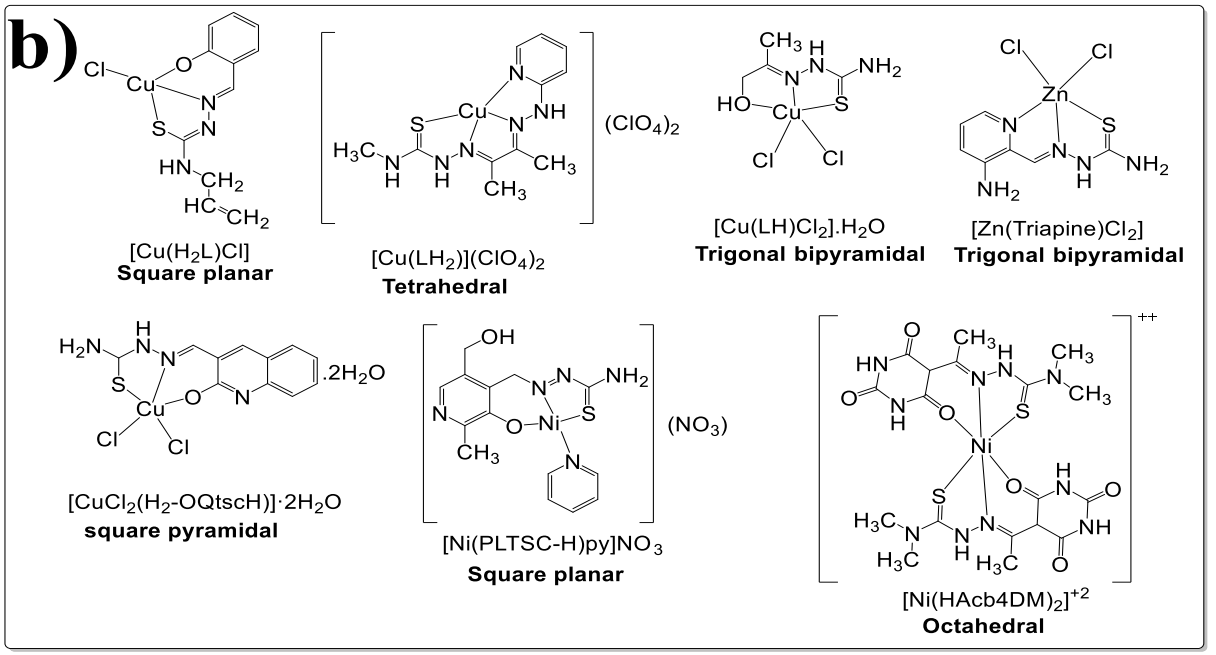


**Figures 1.5 a+b:** show the coordination geometry of the metal complexes of thiourea and thiosemicarbazone derivatives respectively.

We are interested in studying and developing the chemistry of mono and di substituted benzoyl and pivaloyl pyridyl thiourea and pyridyl thiosemicarbazone

derivatives and investigating the coordination chemistry of the newly prepared ligands as these ligands have different functional groups, for example C=O, C=S, N-pyridyl, NH-amine, which make these ligands capable of coordinating to Ni(II), Cu(I), Cu(II) and Zn(II) ions in a number of possible ways. In addition, our interest comes from their potential use in different fields, such as highly selective reagents for liquid-liquid extraction, pre-concentration and separation of the platinum-group metals. They also may act as building blocks in the synthesis of heterocyclic compounds, and have a broad spectrum of biological activities such as antifungal, antibacterial, anticancer or antiviral agents.

In chemistry, a Lewis acid-base reaction produces a coordination compound or metal complex and the central atom or ion is surrounded by anions or neutral molecules possessing lone pairs of electrons. Many metal-containing compounds, especially those of transition metals, are coordination complexes.[69] Different methods are used to characterise the coordination complexes: Mass spectrometry, Infrared spectroscopy, UV-Visible spectroscopy, Nuclear magnetic resonance spectroscopy, Elemental analysis and the most important method is X-ray crystallography.

In this first chapter, physical techniques such as UV-Visible, magnetic susceptibility and cyclic voltammetry will be discussed.

## 1.1.2 Magnetic susceptibility ($\chi$) and magnetic moments ($\mu_{eff}$)

The magnetic susceptibility value gives a major insight into the magnetic properties, structure, bonding and energy levels of a material. The magnetic susceptibility values determine whether a material is paramagnetic or diamagnetic. The coordination complexes containing metals are characterized via magnetic moments which are often used together with electronic spectra to gain information about the stereochemistry, oxidation state and the electronic configuration of the central metal ion.[70-73] The effective magnetic moment ($\mu_{eff}$) values can be calculated for all complexes depending on the total number of unpaired electrons. $\mu_{eff} \approx \mu_{s.o} = 2\sqrt{S(S+1)} = \sqrt{n(n+2)}\ \mu_B$, ($\mu_{eff}$**:** magnetic moment in (Bohr-magneton) unit., **S:** the total electron spin quantum number, **n:** the number of unpaired

electrons). Different practical devices are available for the measurement of magnetic susceptibility and magnetic moment of transition metal compounds such as Gouy and Faraday methods. The Gouy method is where a sample is hung between the poles of an electromagnet depends on the difference in the weight of sample in the presence and absence of a magnetic field. The change in weight is proportional to the magnetic susceptibility.[74-76] Gouy and Faraday balances, whilst very sensitive and accurate, were very time consuming.

Another device used to measure the magnetic susceptibility is called the Evans balance.[77] There are many advantages of this device over other traditional methods. Advantages include: cheapness, the digital readout supplies rapid, accurate readings, high sensitivity and the smaller amount of sample required (about 50 mg). The Evans method depends on the difference in the $^{1}$H NMR chemical shift in a solvent caused by the presence of a paramagnetic species. This method is used to calculate the susceptibility and hence magnetic moment, showing the number of unpaired electrons in the paramagnetic species.[78-83] The procedure of this method consists of a NMR tube containing the solution of paramagnetic compound in NMR solvent with TMS as reference. A sealed capillary tube contains the same pure deuterated NMR solvent with TMS insert in the NMR tube (**Figure 1.6**). The $^{1}$H NMR spectrum is then measured. Two peaks are observed in the spectrum, one of them used as reference assignable to the NMR solvent in the NMR tube and the other shifted peak due to NMR solvent in the capillary tube. The shifted peak is due to the paramagnetic properties of the compound solution in the magnetic field. The shift between the two peaks is measured and the magnetic susceptibility calculated.[84-91] The most common equation to calculate the total mass magnetic susceptibility: $\chi_{mass} = 3\Delta v/4\pi v_o m + \chi_o + \chi_o(d_o - d_s)/m$ ($\chi_{mass}$ : total mass magnetic susceptibility $cm^3.g^{-1}$ , $\Delta v$: observed frequency shift in Hz , $v_o$: frequency of the NMR spectrometer in Hz. , $m$: the mass in g of the complex in 1 $cm^3$ of the solution , $\chi_o$ : mass susceptibility of the solvent in $cm^3.g^{-1}$ , $d_o$ and $d_s$ : the densities of the solvent and solution respectively). The mass susceptibility may be converted to molar susceptibility: $\chi_{molar} = M.\chi_{mass}$ ($\chi_{molar}$ : molar magnetic susceptibility in $cm^3.mole^{-1}$., **M:** molecular weight of the complex in

g.mole$^{-1}$). Molar susceptibility may be converted to the effective magnetic moment: $\mu_{eff} = 2.828\ (\chi_{molar}.T)^{1/2}\ \mu_B$ ($\mu_{eff}$: magnetic moment and its unit (Bohr-magneton).,**T:** temperature in ºK).

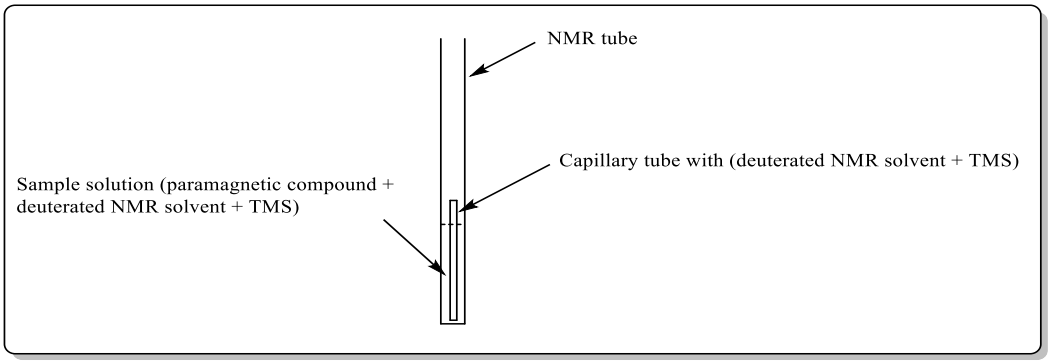


**Figure 1.6:** NMR tube and capillary tube for Evans method.

## 1.1.3 Cyclic voltammetry

Cyclic voltammetry (CV) is the most commonly used method in many areas of chemistry for gaining qualitative information about electrochemical reactions. The importance of cyclic voltammetry results from its capability to rapidly supply significant information on the thermodynamics of redox processes, the kinetics of heterogeneous electron-transfer reactions, transport properties of electrolysis reactions,[92] and on coupled chemical reactions. Cyclic voltammetry is often the first experiment performed in an electroanalytical study. It is used to study the presence of intermediates and the stability of reaction products of the redox reactions.[93] CV can also be used to determine the reversibility of a reaction.[94] Further, the effect of media upon the redox process and a rapid assessment of redox potentials of the electroactive species can be studied by using cyclic voltammetry. A standard CV experiment consists of three electrodes: working, reference and counter electrodes. The counter electrode is made from platinum and is called the auxiliary electrode, while the working electrode is made commonly from platinum or gold. To obtain sufficient conductivity, electrolyte is inserted in the sample solution. Many electrolytes are available but tetrabutylammonium hexafluorophosphate ($Bu_4N^+PF_6^+$) is frequently used.[95] The potential of the working electrode is controlled against the reference electrode (Ag/AgCl) and the current flows between

the working electrode and the counter electrode.[96] The basics of CV involve keeping the electrodes immobile and inserting them in an unstirred solution during the cyclic voltammetry experiment. The potential of the working electrode is ramped linearly versus time. Then, the potential returns to the initial step by ramping in the opposite direction. The resulting change in current is measured. **Figure 1.7** shows a forward and a backward scan of two cycles and the potential sweep of the cyclic voltammogram.

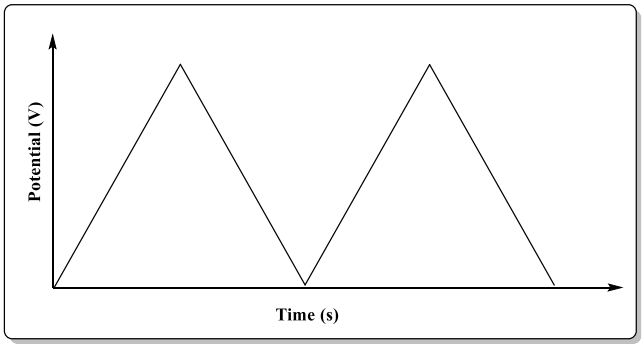


**Figure 1.7:** Cyclic voltammogram waveform.

**Figure 1.8** shows a typical cyclic voltammogramm and the current at the working electrode against the applied voltage. The $i_p^c$ and $i_p^a$ show the peak heights, $E^c_p$ and $E^a_p$ are the maximum potential values for cathodic and anodic current respectively for a reversible reaction.[97]

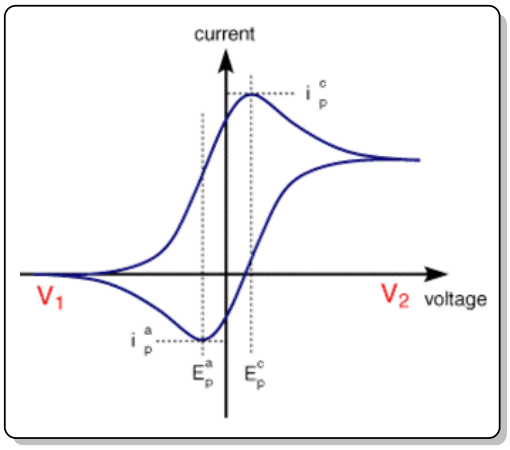


**Figure 1.8:** Typical cyclic voltammogram.

Reversibility is an important concept in cyclic voltammetry. The reaction is considered as reversible when an equilibrium is formed at the electrode surface

between the reduced and oxidised forms.[98] For a fully reversible electrochemical process the CV recorded has certain well defined characteristics, such as: **a)** The voltage separation between the two peaks, $\Delta E = E_p^a - E_p^c = 59/n$ mV, (n represents the number of electrons transferred per molecule). **b)** The positions of peak voltage do not show any change as a function of voltage scan rate even different scan rate is applied. **c)** The values of $I_p^a$ and $I_p^c$ should be identical and the ratio of the peak currents ($I_p^a$ / $I_p^c$) is equal to one. **d)** There is a proportional relation between the peak currents to the square root of the scan rate, (**Figure 1.9**). For a reversible process, the average of the peak potentials is defined as $E^o$ or $E_{1/2}$ which is equal to $(E_p^a + E_p^c)/2$. The reversible process follows the Nernst equation: (**$E=E^o-(RT/nF)$ ln Q, $Q=[R]/[O]$**, $E^o$= the formal or standard reduction potential, R= the gas constant, T= the temperature, F= the Faraday constant, [R]= the concentration of the reduced form, [O]= the concentration of the oxidised form).

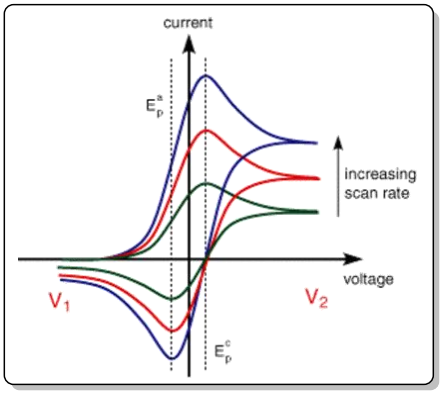


**Figure 1.9:** CV experiment in different scan rate.

The effect of the scan rate on the peak current for a reversible couple is given by the Randles-Sevcik equation. The proportional relation between the current and the square root of the scan rate is very clear in this equation.[99] **$i_p = (2.69x10^5) n^{3/2}ACD^{1/2}v^{1/2}$**, **$i_p$**= the current in ampere, **A**= the electrode area in $cm^2$ , **C**= the concentration in $mole.cm^{-3}$ , **D**= the diffusion coefficient in $cm^2.sec^{-1}$ **v**= the scan rate in $v.sec^{-1}$. In addition to the reversible redox process, there are quasi-reversible and irreversible processes in CV measurements. The quasi-reversible process is characterised when peaks can shift further apart on increasing the scan rate of the potential sweep. Overall, the voltammograms of a quasi-reversible

process exhibit a bigger separation in peak potentials and are more drawn out compared to a reversible system. Totally irreversible systems have peaks that do not overlap at all and the individual peaks are reduced in size and widely separated. The chemically irreversible systems are defined as the systems that do not have a return peak, as the oxidised species cannot reduce back to its original state.[100]

## 1.1.4 Electronic transitions (UV-vis.)

UV-visible absorption spectroscopy (UV = 200-400 nm, visible = 400-800 nm) is one of the most widely and routinely used techniques in clinical and chemical laboratories. The absorption transitions happen from the ground electronic state to the excited electronic state; the opposite process describes the concept of luminescence which occurs from the excited state to ground state. Therefore, UV-visible absorption spectroscopy is considered complementary to fluorescence spectroscopy.[101] The simple principle of UV-visible absorption is: electrons in molecules absorb the energy in UV or visible region to excite to the higher anti-bonding molecular orbitals.[102] The transition between the highest occupied molecular orbital (**HOMO**) and the lowest unoccupied molecular orbital (**LUMO**) is defined as the lowest energy transition. **Figure 1.10** shows the HOMO and LUMO molecular orbitals and the π - π* transition in 1,3,5-hexatriene. The ∆E is the HOMO – LUMO energy gap.[103] The lower energy gap between the HOMO and the LUMO leads to a lower frequency and a longer wavelength.

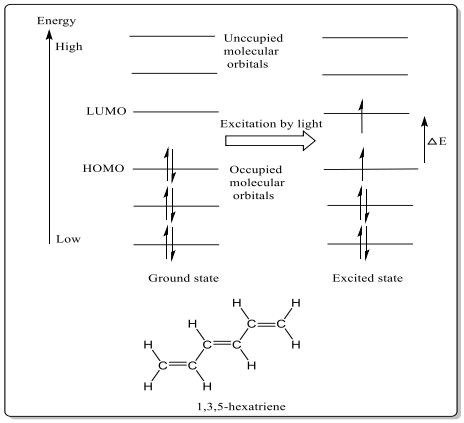


**Figure 1.10:** shows the molecular orbitals of the HOMO and LUMO and the π - π* transition in 1,3,5-hexatriene.

UV-visible absorption spectroscopy is considered to be a simpler, more versatile, rapid, accurate and cost-effective method than other spectrometry techniques. It is used in qualitative analysis for the identification of chemicals and in analytical chemistry for the quantitative determination of various analytes, such as transition metal ions, highly conjugated organic compounds, and biological macromolecules. The electronic transitions between energy levels are governed by selection rules. If one or more of these rules are not applied, the peak will be weak, such as in *d-d* transitions. These selection rules are:

1) The spin rule: The rule says that only one electron is involved in any transition and these transitions will be allowed when it occurs between the ground and excited states without a change in their spin ($\Delta S=0$). For example: Spin allowed octahedral $[Ti(H_2O)_6]^{+3}$ $Ti^{+3}$, $3d^1$ $\varepsilon$= 10 $M^{-1}$ $cm^{-1}$, Spin forbidden octahedral $[Mn(H_2O)_6]^{+2}$ $Mn^{+2}$, $3d^5$ $\varepsilon$= 0.1 $M^{-1}$ $cm^{-1}$

2) Laporte (symmetry) selection rule: The second rule states that allowed transition occur between atomic orbitals of different symmetry which means the transitions within the same symmetry is forbidden. That means the orbital angular momentum quantum number (l) should change. To have an allowed transition, $\Delta l=\pm 1$.[104] u→g, g→u, s→p, p→d are allowed transitions, u→u, g→g, d→d, f→f are forbidden transitions

Electronic transitions can be divided in to allowed and forbidden transitions. The allowed transitions are the transitions which have ε of $10^4$-$10^6$ $M^{-1}cm^{-1}$ such as $\pi \rightarrow \pi^*$ transitions, (for example the organic compound 1,3-butadiene shows an allowed transition at 217nm and has ε value= 21000 $M^{-1}cm^{-1}$). While the forbidden transitions have ε less than $10^4$ $M^{-1}cm^{-1}$. For example, the complex $[Mn(H_2O)_6]^{+2}$ has a spin and Laporte forbidden *d-d* transition and ε = 0.1 $M^{-1}cm^{-1}$, and the complex $[Co(H_2O)_6]^{2+}$ has ε = 1-10 $M^{-1}cm^{-1}$ as it is spin allowed and Laporte forbidden (*d-d*).[105] Three types of electronic transitions are observed in coordination complexes.

1. Ligand centred transitions ($\pi \rightarrow \pi^*$ and $n \rightarrow \pi^*$) which involve electrons in pi and *n* orbitals. These transitions are often observed at higher energy than other transitions and with varying intensity.
2. Charge-transfer transitions (LMCT or MLCT) involve the temporary transfer of an electron from the ligand to metal, or metal to ligand, respectively. In this type of transition, complexes should contain two components. The first must be electron donating and the second component must be able to accept electrons. The electron movement from donating species to accepting species occurs by absorption of radiation. In a LMCT transition, the ligand often corresponds to electron donating species such as Br-, $I^-$, $OH^-$, $RS^-$, $S_2^-$, $NCS^-$, $NCO^-$. e.g in $IrBr_6^{2-}$. While in MLCT transition, the ligand represents the accepting species, (for example CO, NO, $CN^-$, $N_2$, bipy, phen, RNC, $C_5H_5^-$, C=C), such as e.g. $W(CO)_4(phen)$ and $Ru(bipy)_3^{2+}$. The charge transfer bands are of higher intensity than *d-d* transition and the molar extinction coefficient are about $10^2$-$10^4$ $M^{-1}$ $cm^{-1}$. This is due to the charge transfer transitions being spin allowed and Laporte allowed.[106]
3. *d-d* transitions are the excitation of an electron from one d-orbital to another. A *d-d* transition may be an allowed or forbidden transition with respect to the spin rule. The *d-d* transition is forbidden in centrosymmetric complexes according to the Laporte rule. Knowledge of crystal field theory (CFT)[107] is important in understanding the nature of *d-d* transitions.

According to the ground terms, one electronic transition is observed for the metal complexes with D ground term and the transition energy relates directly with D. Then, $d^1$, $d^4$, $d^6$ and $d^9$ are covered with the following high spin configuration. The left-hand side is applicable to $d^4$, $d^9$ octahedral and $d^1$, $d^6$ tetrahedral complexes. The right-hand side is applicable to $d^1$, $d^6$ octahedral and $d^4$, $d^9$ tetrahedral complexes. See **Figure 1.11**.

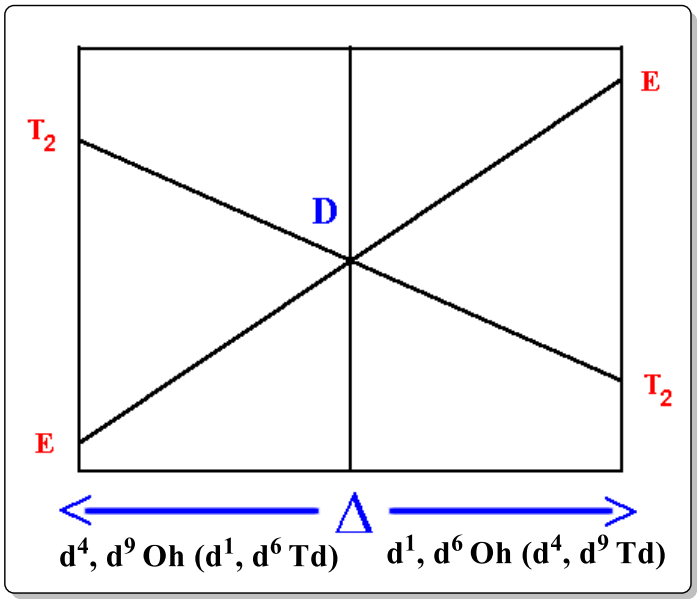


**Figure 1.11:** Orgel diagram of complexes with D term.

Three electronic transitions are observed when the complexes have F ground terms. See **Figure 1.12**, and $d^2$, $d^3$, high spin $d^7$ and $d^8$ are covered with the following configurations. The left-hand side is applicable to $d^3$, $d^8$ octahedral and $d^2$, $d^7$ tetrahedral complexes. The right-hand side is applicable to $d^2$ and high spin $d^7$ octahedral and $d^3$, $d^8$ tetrahedral complexes.

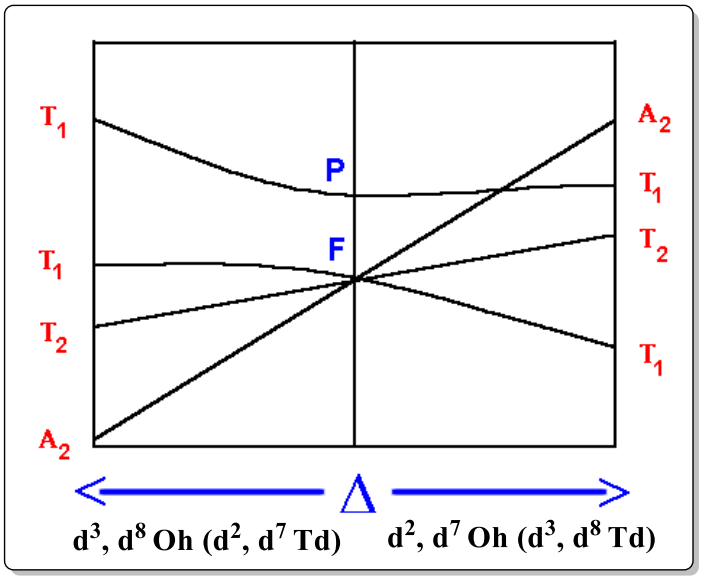


**Figure 1.12:** Orgel diagram of complexes with P and F term.

The two Orgel diagrams in **Figures 1.11**, **1.12**, are useful to show the expected spectra, and their relative energy levels with the spin allowed transitions of octahedral and tetrahedral transition metal complexes.

The knowledge of the expected UV-vis. spectra in characterization of the complexes is important for an understanding of the geometry of the complexes. Some of the UV-vis. transitions of the different geometries of the Cr(III), Ni(II), Cu(II), Cu(I) and Zn(II) complexes will be shown.

**i) Cr(III) $d^3$:** Previous studies have widely reported the UV-vis. spectra of the six coordinate octahedral geometry of Cr(III) complexes. These Cr(III) complexes show three spin allowed *d-d* transitions which are assigned to $^4A_{2g}\rightarrow{}^4T_{2g}$, $^4A_{2g}\rightarrow{}^4T_{1g}(F)$ and $^4A_{2g}\rightarrow{}^4T_{1g}(P)$ respectively.

**ii) Ni(II) $d^8$:** Octahedral Ni(II) complexes are expected to show three spin allowed transitions from $^3A_{2g}\rightarrow{}^3T_{2g}$, $^3A_{2g}\rightarrow{}^3T_{1g}$ and $^3A_{2g}\rightarrow{}^3T_{1g}(p)$ in the range 7000-13,000 $cm^{-1}$ (1429-769 nm), 11,000-20,000 $cm^{-1}$ (909-500 nm) and 19000-27000 $cm^{-1}$ (526-370 nm) respectively, with weak intensities less than 35 $M^{-1}cm^{-1}$. The four coordinate square diamagnetic planar complexes are formed specially for the electronic configuration $d^8$ Ni(II), particularly with strong field ligands. Typically of the square planar complexes, a single band at 16,667-25,000 $cm^{-1}$ (600-400 nm) with intensity about 50-500 $M^{-1}cm^{-1}$ are observed and assigned to a $d_{xy}$-$d_{x^2-y^2}$ transition. Charge transfer transition may also be observed at 23,000-30,000 $cm^{-1}$ (435-333 nm) with more intensity than *d-d* transitions. The four coordinate tetrahedral Ni(II) complexes exhibit one transition which may be split into two peaks by spin-orbit coupling in the range (16,667-12,500 $cm^{-1}$) 600-800 nm due to $^3T_1(P)\rightarrow{}^3T_1(F)$ with intensity $10^2$-$10^3$ $M^{-1}$ $cm^{-1}$.

**iii) Cu(II) $d^9$:** The electronic spectra of Cu(II) complexes have been studied extensively for various geometries. The $t_{2g}\rightarrow e_g$ transition in a regular six coordinate octahedral Cu(II) complexes ranges from 13,000-18,000 $cm^{-1}$ (769-556 nm) while in the distorted octahedral $D_{4h}$ several absorption bands may be expected in these regions relating to transitions from components of $t_{2g}$ to $e_g$ orbitals. The five coordinate Cu(II) complexes are described by two structures, the square pyramidal

and trigonal bipyramid. The square pyramidal Cu(II) complexes have a singlet band extending from 11,400-15,000 $cm^{-1}$(877-667 nm) and is assigned to a $d_{z2} \rightarrow d_{x2-y2}$ transition. Regular trigonal bipyramid Cu(II) complexes show multiple peaks (a strong low energy peak followed a weaker or shoulder peak to higher energy) extending from 10,500-14,000 $cm^{-1}$(952-714 nm). The four coordinate square planar Cu(II) complexes commonly exhibit a broad peak centered between 13,000-20,000 $cm^{-1}$ (769-500 nm) and is assigned to a $d_{xy} \rightarrow d_{x2-y2}$ transition. While a single transition at comparatively low energy when compared with square planar complexes is observed and assigned to $^2E \rightarrow {}^2T_2$ transition for a regular tetrahedral Cu(II) complexes( in the absence of spin orbit splitting).[105]

**iv) Cu(I) and Zn(II) $d^{10}$:** It is expected that the electronic spectra of $d^{10}$ Zn(II) and Cu(I) complexes to show ligand centred transitions. These complexes do not show any *d-d* transitions which occur within the metal centre. The transitions which centred about 400 nm are attributed to MLCT (metal ligand charge transfer). Many relevant examples will be seen in **chapters two**, **three** and **four**.

## 1.1.5 HSAB Theory

Hard and Soft (Lewis) Acids and Bases (HSAB) Theory or HSAB concept is a qualitative notion introduced by Pearson in 1960.[110] It is widely used to clarify the stability of metal complexes and the mechanism of their reactions. According to this theory, the Lewis acids and bases can be divided into hard or soft or borderline types. ***Hard Lewis acids*** apply to species which have small ionic radii, high positive charge state, strongly solvated, weakly polarizable, empty orbitals in the valence shell. ***Soft Lewis acids*** apply to species which have large ionic radii, low positive charge state, completely filled atomic orbitals and strongly polarizable. ***Hard Lewis bases*** apply to species which have small ionic radii, strongly solvated, highly electronegative, weakly polarizable. ***Soft Lewis bases*** apply to species which have large ionic radii, intermediate electronegativity and are strongly polarizable. Lewis acids and bases which have intermediate properties lie on ***the border line***. A summary of the theory is that soft acids prefer binding and react faster with soft bases to form stronger bonds giving covalent complexes, where hard acids prefer to bond and react faster with Hard Bases to form bonds giving

ionic complexes. In coordination chemistry soft-soft and hard-hard interactions exist between ligands and metal centers.[111-113] **Table 1.7** summarizes typical examples of hard and soft bases and acids.

HSAB theory explains the stability of product for the specific reaction. As an example, the Pb(II) ion prefers to form PbS over $Pb(OH)_2$. While Mg(II) will form $Mg(OH)_2$, Mg and hydroxide are considered as hard species. As discussed earlier, thiourea ligands are able to coordinate with different metal centres. The soft sulfur and hard nitrogen atoms allow them to bind to a wide range of metal centres. From Pearson's HSAB theory, soft acids will form stronger complexes with soft bases. On the contrary, hard acids will form stronger complexes with hard bases. Cu(I) is defined as a soft Lewis acid, and from the HSAB concept, it is expected to have a high affinity to the ligand derivatives of sulfur (a soft base). On the other hand, N-pyridine is classed as a border line Lewis base, therefore it would be suitable for thiourea containing pyridine ring to coordinate to border line Lewis acid metals such as those metal ions in our studies Ni(II), Cu(II) and Zn(II) to form stable transition metal complexes. From HSAB theory, Cr(III) ion is hard acid which prefers to form stable complexes which having some ionic character with hard bases, for example, ligands contain $OH^-$ or amines.

**Table 1.7:** Examples of hard, soft and borderline acids and bases.

| **Type of acid/base** | **example** |
|---|---|
| Hard acid | $H^+$, $Li^+$, $Na^+$, $K^+$, $Mg^{2+}$, $Ca^{2+}$, $Sr^{2+}$, $Mn^{+2}$<br>$Al^{3+}$, $Ga^{3+}$, $In^{3+}$, $Cr^{3+}$, $Co^{3+}$, $Fe^{3+}$, $Ir^{3+}$, $Si^{4+}$, $Ti^{4+}$, $VO^{2+}$<br>$BeMe_2$, $BF_3$, $BCl_3$, $AlMe_3$ |
| Soft acid | $Cu^+$, $Ag^+$, $Au^+$, $Hg^+$,$Tl^+$ , $Hg^{2+}$, $Pd^{2+}$, $Cd^{2+}$, $Pt^{2+}$<br>Metal atoms in zero oxidation states $M^0$ |
| Border line acid | $Fe^{2+}$ , $Co^{2+}$, $Ni^{2+}$, $Cu^{2+}$, $Zn^{2+}$, $Pb^{2+}$, $SO_2$, $NO^+$, $Ru^{+2}$ |
| Hard base | $H_2O$, $OH^-$, $F^-$, $Cl^-$, $CH_3CO_2$-, $PO_4^{3-}$, $SO_4^{2-}$, $CO_3^{2-}$, $ClO_4^-$, ROH, $RO^-$, $NH_3$, $RNH_2$, $N_2H_4$ |
| Soft base | RSH, $RS^-$, $R_2S$, $I^-$, $SCN^-$, $S_2O_3^-$, $R_3P$, RNC, CO, $C_6H_6$, $R^-$, $H^-$ |
| Border line base | Aniline, pyridine, $Br^-$, $NO_2^-$, $SO_3^{2-}$ |

## 1.2 Aims and the objectives of this thesis

**1-** To synthesis novel ligand molecules based upon thiourea or thiosemicarbazone derivatives and their metal complexes with Ni(II), Cu(II), Cu(I) and Zn(II) ions.

**2-** To prepare novel molecules based upon 8-hydroxyquinoline derivatives and their metal complexes with Cr(III) ion.

**3-** To study the spectral and magnetic properties of these metal complexes, together with any solid state structural investigations via X–ray crystal structures.

**4-** To investigate the coordination geometry of the metal centre and chelating behaviour of the thiourea, thiosemicarbazone and 8-hydroxyquinoline derivatives ligands in their complexes,

**5-** To examine the influence of different temperatures of the synthetic routes ending with different products.

**6-** To identify the nature and the number of the H-bonding interactions (intramolecular, intermolecular).

**7-** To focus on the intramolecular H-bonding which is typical to N-pivaloyl and N-benzoyl thiourea derivatives.

**8-** To study the redox process, recognize typical redox processes and their origin.

**9-** To explore the photoluminescence properties of the Cr(III) complexes and their origins.

**10-** To explore how different electron donating and withdrawing groups on ligands in Cr(III) complexes effect the photoluminescence energy and intensity.

**11-** To develop NS, NSS′ and SO donor thiourea and NN′S donor thiosemicarbazone ligand systems and characterise their metal complexes. Future work will investigate the potential medicinal and biological activity as antibacterial, antifungal, antimalarial and anticancer reagents for these ligand systems and their complexes.

## 1.3 References


**(1)** G. B. Kauffman, *Am. Chem. Soc.,* **1994**.

**(2)** J. W. Buchler, *Angew. Chem. In. Ed. Engl.*, **1978**, 17, 407-423.

**(3)** M. O. Senge, A. A. Ryan, K. A. Letchford, S. A. MacGowan and T. Mielke, *Symmetry.,* **2014**, 6, 781–843.

**(4)** L. Randaccio, S. Geremia, N. Demitri and J. Wuerges, *Molecules,* **2010**, 15(*5*), 3228–3259.

**(5)** K. E. Van Holde, K. I. Miller and H. Decker, *J. Biol. Chem.,* **2001**, 276 (*19*), 15563–15566.

**(6)** G. B. Gardner, D. Venkataraman, J. S. Moore and S. Lee, *Nature*, **1995**, 374, 792–795.

**(7)** P. J. Stang, D. H. Cao, S. Saito and A. M. Arif, *J. Am. Chem. Soc.,* **1995**, 117, 6273–6283.

**(8)** L. Carlucci, G. Ciani, D. M. Proserpio and A. Sironi, *J. Am. Chem. Soc.,* **1995**, 117, 4562–4569.

**(9)** B. F. Hoskins and R. Robson, *J. Am. Chem. Soc.,* **1990**, 112, 1546–1554.

**(10)** M. Fujita, Y. J. Kwon, S. Washizu and K. Ogura, *J. Am. Chem. Soc.,* **1994**, 116, 1151–1152.

**(11)** J. E. Huheey, *Inorganic Chemistry*, 3rd ed.; Harper & Row: New York, **1983**.

**(12)** F. A. Cotton and G. Wilkinson, *Advanced Inorganic Chemistry*, 5th ed.; Wiley: New York, **1988**.

**(13)** I. D. Brown, *Acta Crystallogr.,* **1988**, B44, 545–553.

**(14)** D. Venkataraman, Y. Du, S. R. Wilson, K. A. Hirsch, P. Zhang and J. S. Moore, *J. Chem. Educ.,***1997**, 74(*8*), 915-918.

**(15)** H. A. Jahn and E. Teller, *Proc. R. Soc. London A*, **1937**, 161, 220-235.

**(16)** C. Housecroft and A. G. Sharpe, *Inorganic Chemistry*. Prentice Hall, 3rd Ed., **2008**, 644.

**(17)** N. G. Ballesteros, D. P. Álvarez, M. S. C. Henriques, B. F. O. Nascimento, M. Laranjo, K. Santos, J. C. Lopes, A. M. Abrantes, M. F. Botelho, M. Pineiro, J. A. Paixão and M. C. R. Argüelles, *Inorg. Chim. Acta,* **2015**, 438,160-167.

**(18)** T. S. Lobana, R. Sharma, G. Hundal, A. Castineiras and R. J. Butcher, *Polyhedron*, **2012**, 47(*1*), 134–142.

**(19)** M. Gennari, M. Lanfranchi, L. Marchiò, M. A. Pellinghelli, M. Tegoni and R. Cammi, *Inorg. Chem.*, **2006**, 45(*8*), 3456–3466.

**(20)** Y. M. Zhang, L. Xian and T. B. Wei, *Acta Cryst.*, **2003**, C59, m473-m474.

**(21)** P. Aslanidis S. Kyritsis, M. L. Kantouri, B. Wicher and M. Gdaniec, *Polyhedron*, **2012**, 48(*1*), 140–145.

**(22)** L. Xian, T. B. Wei and Y. M. Zhang, *J. Coord. Chem.,* **2004**, 57(*6*), 453-457.

**(23)** S. Walia, S. Kaur, J. Kaur, A. K. Sandhu, T. S. Lobana, G. Hundal and J. P. Jasinski, *Z. Anorg. Allg. Chem*., **2015**, 641(*10*), 1728–1736.

**(24)** S. Shakhatreh, M. L.Kantouri, M. Gdaniec and P. D. Akrivos, *J. Coord. Chem.*, **2012**, 65(*2*), 251-261.

**(25)** N. Gunasekaran, S. W. Ng, E. R. T. Tiekink and R. Karvembu, *Polyhedron*, **2012**, 34(*1*), 41–45.
**(26)** L. P. Battaglia, A. B. Corradi, M. Nardelli and M. E. V. Tani, *J. Chem. Soc., Dalton Trans.*, **1976**, 2, 143-146.
**(27)** R. L. Girling and E. L. Amma, *Inorg. Chem.*, **1971**, 10, 335.
**(28)** M. Mufakkar, A. A. Isab**,** T. Rüffer, H. Lang, S. Ahmad, N. Arshad and A. Waheed, *Trans. Met. Chem.*, **2011**, 36(*5*), 505-512.
**(29)** X. Shen, D. Wu, X. Huang, Q. Liu, Z. Huang and B. Kang, *Polyhedron*, **1997**, 16(*9*), 1477–1482.
**(30)** M. Dennehy, O. V. Quinzani, R. Faccio, E. Freire and A. W. Mombrue, *Acta Cryst.*, **2012**, C68, m12-m16.
**(31)** N. J. Burke, A. D. Burrows, M. F. Mahon and L. S. Pritchard, *Cryst. Eng. Comm,* **2003**, 5, 355-357.
**(32)** R. G. Hazell, *Acta Chem. Scand*., **1972**, 26, 1365-1374.
**(33)** E. S. Raper, A. M. Britton and W. Clegg, *Trans. Met. Chem.*, **1989**, 14(*5*), 351-355.
**(34)** A. D. Burrows, R. W. Harrington, M. F. Mahon and S. J. Teat, *Crys. Grow. Des.*, **2004**, 4(*4*), 813–822.
**(35)** L. Suescun, A. W. Mombrú, R. A. Mariezcurrena, H. Pardo, S. Russi and R. Baggio, *Acta Cryst.*, **2000**, C56, 179-181.
**(36)** K. K. Du and S. X. Liu, *J. Molec. Struc.,* **2008**, 874(*1*),138–144.
**(37)** M. Vonlanthen, C. M. Connelly, A. Deiters, A. Linden and N. S. Finney, *J. Org. Chem.*, **2014**, 79(*13*), 6054–6060.
**(38)** P. Bombicz, J. Madarász, M. Krunks, L. Niinistö and G. Pokol, *J. Coord. Chem*., **2007**, 60(*4*), 457-464.
**(39)** A. I. Matesanz, C. Pastor and P. Souza, *Eur. J. Inorg. Chem*., **2007**, 2007(*34*), 5433–5438.
**(40)** A. D. Burrows, R. W. Harrington, M. F. Mahon and S. J. Teat, *Eur. J. Inorg. Chem.,* **2003**, 2003(*4*), 766–776.
**(41)** S. L. Li, J. Y. Wu, Y. P. Tian, H. K. Fun and S. Chantrapromma, *Acta Cryst.*, **2005**, E61, m2701-m2703.
**(42)** M. N. M. Milunovic, É. A. Enyedy, N. V. Nagy, T. Kiss, R. Trondl, M. A. Jakupec, B. K. Keppler, R. Krachler, G. Novitchi and V. B. Arion, *Inorg. Chem.*, **2012**, 51(*17*), 9309–9321.
**(43)** S. I. Orysyk, G. G. Repich, V. V. Bon, V. V. Dyakonenko, V. V. Orysyk, Yu. L. Zborovskii, O. V. Shishkin, V. I. Pekhnyo and M. V. Vovk, *Inorg. Chim. Acta*, **2014**, 423(Part A), 496–503.
**(44)** F. A. El-Saied, A. A. El-Asmy, W. Kaminsky and D. X. West, *Trans. Met. Chem.,* **2003**, 28(*8*), 954-960.
**(45)** A. R. Cowley, J. R. Dilworth, P. S. Donnelly and J. M. White, *Inorg. Chem.*, **2006**, *45*(*2*), 496–498.
**(46)** P. P. Netalkar, S. P. Netalkar and V. K. Revankar, *Polyhedron*, **2015**, 100, 215–222.
**(47)** M. B. Ferrari, F. Bisceglie, G. Pelosi, P. Tarasconi, R. Albertini, P. P. Dall'Aglio, S. Pinelli, A. Bergamo and G. Sava, *J. Inorg. Biochem.,* **2004**, 98(*2*), 301–312.
**(48)** P. G. Saiz, J. G.Tojal, M. Maestro, J. Mahía, L. Lezama and T. Rojo, *European J. Inorg. Chem.*, **2003**, 2003(*11*), 2123–2132.

**(49)** P. G. Saiz, R. G. García, M. A. Maestro, J. L. Pizarro, M. I. Arriortua, L. Lezama, T. Rojo, M. G. Álvarez, J. Borrás and J. G. Tojal, *J. Inorg. Biochem.,* **2008**,102(*10*),1910–1920.

**(50)** D. S. Raja, G. Paramaguru, N. S. P. Bhuvanesh, J. H. Reibenspies, R. Renganathan and K. Natarajan, *Dalton Trans*., **2011**, 40, 4548-4559.

**(51)** L. Yi, L. N. Zhu, B. Ding, P. Cheng, D. Z. Liao, Y. P. Zhai, S. P. Yan and Z. H. Jiang, *Trans. Met. Chem.,* **2004**, 29(*2*), 200-204.

**(52)** R. W. Clark, P. J. Squattrito, A. K Sen and S. N. Dubey, *Inorg. Chim. Acta,* **1999**, 293(*1*), 61–69.

**(53)** K. Alomar, A. Landreau, M. Allain, G. Bouet and G. Larcher, *J. Inorg. Biochem,* **2013**, 126, 76–83.

**(54)** J. V. Martínez, R. A. Toscano, M. S. García, M. Rubio, J. G. Lara and M. A. M. Vázquez, *Polyhedron*, **1989**, 8(*6*), 727–730.

**(55)** V. M. Leovac, L. S. Jovanović, V. Divjaković, A. Pevec, I. Leban and T. Armbruster, *Polyhedron*, **2007**, 26(*1*), 49–58.

**(56)** F. Bisceglie, A. Musiari, S. Pinelli, R. Alinovi, I. Menozzi, E. Polverini, P. Tarasconi, M. Tavone and G. Pelosi, *J. Inorg. Biochem*., **2015**, 152, 10–19.

**(57)** A. Castiñeiras, N. F. Hermida, I. G. Santos and L. G. Rodríguez, *Dalton Trans.*, **2012**, 41, 13486-13495.

**(58)** N. C. Kasuga, K. Sekino, C. Koumo, N. Shimada, M. Ishikawa and K. Nomiya, *J. Inorg. Biochem.,* **2001**, 84(*1*), 55–65.

**(59)** M. Matthew and G. J. Palenik, *Inorganica Chimica Acta,* **1971**, 5, 349–353.

**(60)** J. Shao, Z. Y. Ma, A. Li, Y. H. Liu, C. Z. Xie, Z. Y. Qiang and J. Y. Xu, *J. Inorg. Biochem.,* **2014**,136, 13–23.

**(61)** M. B. Ferrari, G. G. Fava, C. Pelizzi and P. Tarasconi, *J. Chem. Soc., Dalton Trans.*, **1992**, 14, 2153-2159.

**(62)** C. R. Kowol, R. Trondl, V. B. Arion, M. Jakupec, I. K. Lichtscheidl and B. K. Keppler, *Dalton trans*., **2010**, 39, 704.

**(63)** E. V. Zahínos, F. L. Giles, P. T. García and M. C. F. Calderón, *Eur. J. Med. Chem.,* **2011**, 46(*1*),150–159.

**(64)** D. K. Demertzi, P. N. Yadav, J. Wiecek, S. Skoulika, T. Varadinova and M. A. Demertzis, *J. Inorg. Biochem.,* **2006**,100(*9*),1558–1567.

**(65)** M. B. Ferrari, G. G. Fava , G. Pelosi and P. Tarasconi, *Polyhedron*, **2000**, 19(*16–17*),1895–1901.

**(66)** D. G. Calatayud, E. L. Torres and M. A. Mendiola, *Polyhedron*, **2013**, 54, 39–46.

**(67)** T. W. Kajdan, P. J. Squattrito and S. N. Dubey, *Inorg. Chim. Acta,* **2000**, 300–302, 1082–1089.

**(68)** R. W. Clark, P. J. Squattrito, A. K. Sen and S. N. Dubey, *Inorg. Chim. Acta*, **1999**, 293(*1*), 61–69.

**(69)** Greenwood, N. Norman and A. Earnshaw, *Chemistry of the Elements* (2nd ed.),**1997**.

**(70)** D. Jiles, *Introduction to Magnetism and Magnetic Materials*, Chapman & Hall, New York, **1991**.

**(71)** O. Kahn, *Molecular Magnetism*, VCH: Weinheim, Germany, **1993**.

**(72)** L. M. Smart, *Solid State Chemistry*, Chapman & Hall: New York, **1993**.
**(73)** J. I. Hoppe, "Effective magnetic moment". *J. Chem. Educ.*, **1972**, 49(*7*), 505.
**(74)** A. Sella, *Royal Society of Chemistry*, **2010**.
**(75)** A. Saunderson, "A Permanent Magnet Gouy Balance". *Physics Education,* **1968**, 3(*5*): 272–273.
**(76)** L. Brucacher and F. Stafford, "Magnetic Susceptibility". *J. Chem. Educ.*, **1962**, 39, 574.
**(77)** C. J. O'Connor and S. J. Lippard, *ed. Magnetic susceptibility measurements. Progress in Inorganic Chemistry, Wiley*, **1982**, 29, 203.
**(78)** D. F. Evans, *J. Chem. Soc.,* **1959**, 36, 2003-2005.
**(79)** D. F. Evans, G. V. Fazakerley and R. F. Phillips, *J. Chem. Soc.,* **1971**, A, 1931.
**(80)** D. F. Evans and D. A. Jakubovic, *J. Chem. Soc., Dalton Trans.,* **1988**, 2927.
**(81)** D. H. Grant, *J. Chem. Educ.,* **1995**, 72, 39.
**(82)** C. W. Garland, J. W. Nibler and D. P. Shoemaker, *Experiments in Physical Chemistry*, 8th Ed.; McGraw-Hill; New York, **2003**, 371-379.
**(83)** C. Piguet, *J. Chem. Educ.*, **1997**, 74, 815-816.
**(84)** J. L. Deutsch and S. M. Poling, *J. Chem. Educ.,* **1979**, 46,167-168.
**(85)** R. A. Bailey, *J. Chem. Educ.,* **1972**, 49, 297-299.
**(86)** J. M. White, *Physical Chemistry Laboratory Experiments*; Prentice-Hall: New Jersey, **1975**, 428.
**(87)** D. P. Shoemaker, C. W. Garland, J. I. Steinfeld and J. W. Nibler, *Experiments in Physical Chemistry*, 4th ed.; MeGraw-Hill: New York, **1981**, 405.
**(88)** Z. Szafran, R. M. Pike and M. M. Singh, *Microscale Inorganic Chemistry*; Wiley: New York, **1991**, 52.
**(89)** A. S. Chacravarti and B. Prasad, *Trans. Faraday Soc.*, **1939**, 35, 1466-1471.
**(90)** D. Ostfeld and I. A. Cohen, *J. Chem. Educ.,* **1972**, 49, 829.
**(91)** E. M. Schubert, *J. Chem. Educ.,* **1992**, 69, 62.
**(92)** S. H. Duvall and R. L. McCreery*, Anal. Chem.,* **1999**, 7(*20*), 4594–4602.
**(93)** R. S. Nicholson, *Anal. Chem.,* **1965**, 37(*11*)*,* 1351–1355.
**(94)** A. M. Bond and S. W. Feldberg, *J. Phys. Chem.,* **1998**, 102(*49*), 9966–9974*.*
**(95)** W. E. Geiger and F. Barriere, *Acc. of Chem. Res.*, **2010**, 43(*7*), 1030-1039.
**(96)** *X.* Cetó, C. Apetrei, M. D. Valle and M. L. Rodriguez, *Electrochimica Acta*, **2014**,120, 180-186.
**(97)** J. E. B. Randles, *Trans. Faraday Soc.*, **1952**, 48, 828-832.
**(98)** G. Mabbott, *J. Chem. Ed.*, **1983**, 60, 697-702.
**(99)** P. Kissinger and W. Heineman, *J. Chem. Ed.*, **1983**, 60, 702-707.
**(100)** K. B. Oldham and C. G. Zoski, *J. Electroanal. Chem.*, **1988**, 256(*1*),11.
**(101)** D. A. Skoog, F. J. Holler and S. R. Crouch, *Principles of Instrumental Analysis* (6th ed.). Belmont, CA: Thomson Brooks/Cole., **2007**, 169–173.
**(102)** R. J. Anderson, D. J. Bendell and P. W. Groundwater, *Organic Spectroscopic Analysis,* **2004**.

**(103)** J. M. Hornback, *Organic chemistry*, (2nd ed.), Thomson learning, **2006**, 961-962.
**(104)** A. B. P. Lever, INORGANIC ELECTRONIC SPECTROSCOPY, Elsevier Science and Technology, **1968**.
**(105)** A. B. P. Lever, INORGANIC ELECTRONIC SPECTROSCOPY( Studies in Physical and Theoretical Chemistry), Elsevier Science Ltd, **1984**.
**(106)** A. K. Brisdon, *Inorganic Spectroscopic Methods,* Oxford Chemistry Primers, **2003**.
**(107)** J. H. Van Vleck, *Phys. Rev.,* **1932**, 41, 208 –215.
**(108)** *International Tables for Crystallography Volume A: Space-group symmetry*, Kluwer Academic Publishers, **2002**.
**(109)** W. Clegg, *Crystal Structure Determination*, Oxford Chemistry Primers, **1998**.
**(110)** R. G.Pearson, *J. Chem. Educ.,* **1968**, 45(*9*), 581-587.
**(111)** R. G.Pearson, *J. Chem. Educ.,* **1968**, 45(*10*), 643-648.
**(112)** E. C. Koch, *Prop., Expl., Pyrotech*, **2005**, 30(*1*), 5-16.
**(113)** R. G. Pearson, *J. Am. Chem. Soc.,* **1963**, 85(*22*): 3533–3539.

# Chapter Two

## Synthesis, characterization, X-ray crystal structures of Cu(I), Cu(II), Ni(II) and Zn(II) complexes with N,N′-substituted thiourea derivatives

# 2.1 Introduction

In 1828, the German chemist Friedrich Wöhler first synthesized urea. Urea, **Figure 2.1** is important for a wide range of scientific and industrial processes. It was considered as the first organic compound that was synthesized in the laboratory. This development was an important step in the history of synthetic organic chemistry and the molecule has obviously played a vital physiological and biological role in the animal kingdom.[1-3]

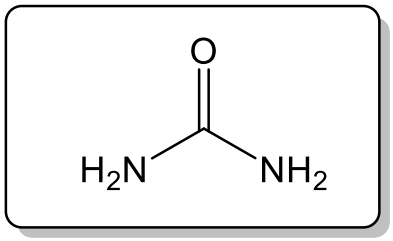


**Figure 2.1**: Structure of urea.

Thiourea, **Figure 2.2**, is structurally similar to urea. It is produced by the substitution of the oxygen atom in urea by a sulfur atom but the properties of urea and thiourea vary significantly because of the difference in electronegativity between sulfur and oxygen.[4]

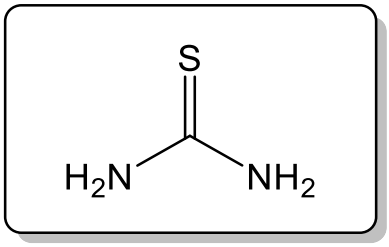


**Figure 2.2**: Structure of thiourea.

"Thiourea" refers to a broad class of compounds with the general structure $(R^1R^2N)(R^3R^4N)C=S$, (where R= H, alkyl or aryl groups). Previous studies have reported that the two possible conformational forms, *trans* and *cis* were observed in the N-alkyl substituted thiourea with the coplanar $N_2CS$ skeletal atoms, whilst three different conformations are possible for N,N'-dialkyl substituted thioureas: the *cis-cis*, *trans-trans* and *cis-trans* isomers **Figure 2.3**.[5,6] The structural conformation

of N-methylthiourea have been studied, both in the solid state and solution. It was confirmed through Raman and IR spectroscopy and X-ray structural analyses of N-methylthiourea that the compound assumes the *cis* configuration **Figure 2.3** in the solid state.[7] The study found that N,N'-dimethylthiourea and N,N'-diethylthiourea were *trans-trans* isomers. Subsequent studies on the coordination of these molecules were made using IR spectra to determine their binding sites.[8-11]

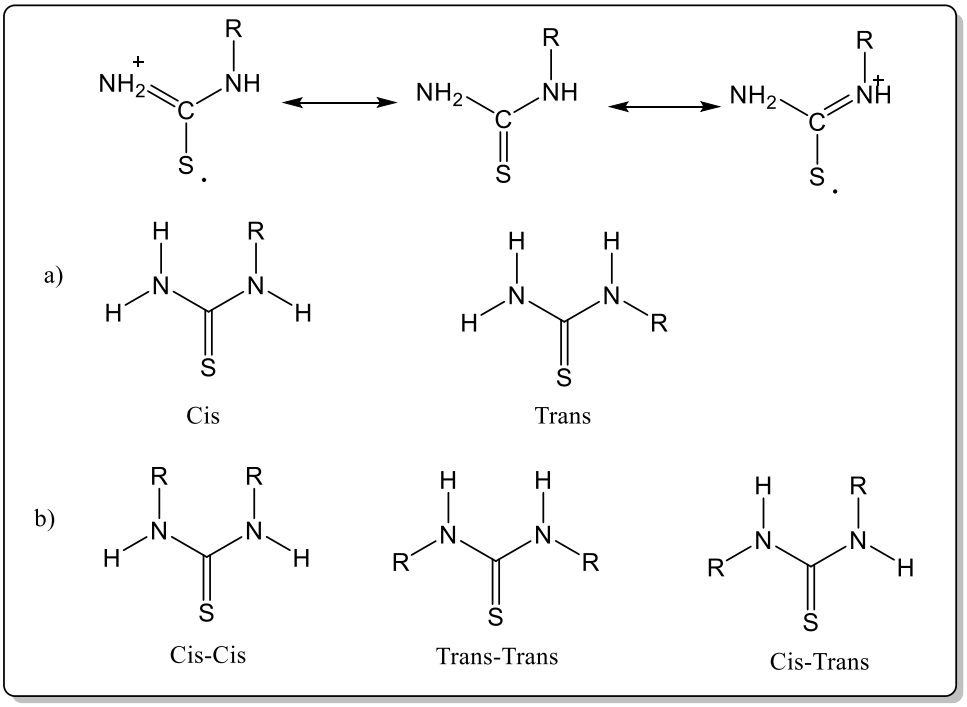


**Figure 2.3**: Structure of substituted thiourea showing: a) resonance states of mono substituted alkyl/aryl thiourea; (b) conformational isomers for both mono and disubstituted alkyl/aryl thiourea.

Synthetic methods for thiourea have been described and investigated by numerous studies and a range of common routes to synthesise substituted thioureas is given in **Scheme 2.1**: i) benzoyl isothiocyanate reacts with amines and then hydrolysis in basic solution to give thiourea derivative and benzoic acid;[12] ii) alkyl or aryl isothiocyanate reacts with ammonia or amines;[13] iii) primary amines react with $CS_2$ in aqueous solution/ mercury acetate;[14] iv) primary amines react with ammonium thiocyanate and then with strong acids such as HCl;[15] v) disubstituted cyanamide reacts with $H_2S/NH_3$;[16] vi) thiourea compounds react at high temperature 180ºC with primary alkyl amine.[17]

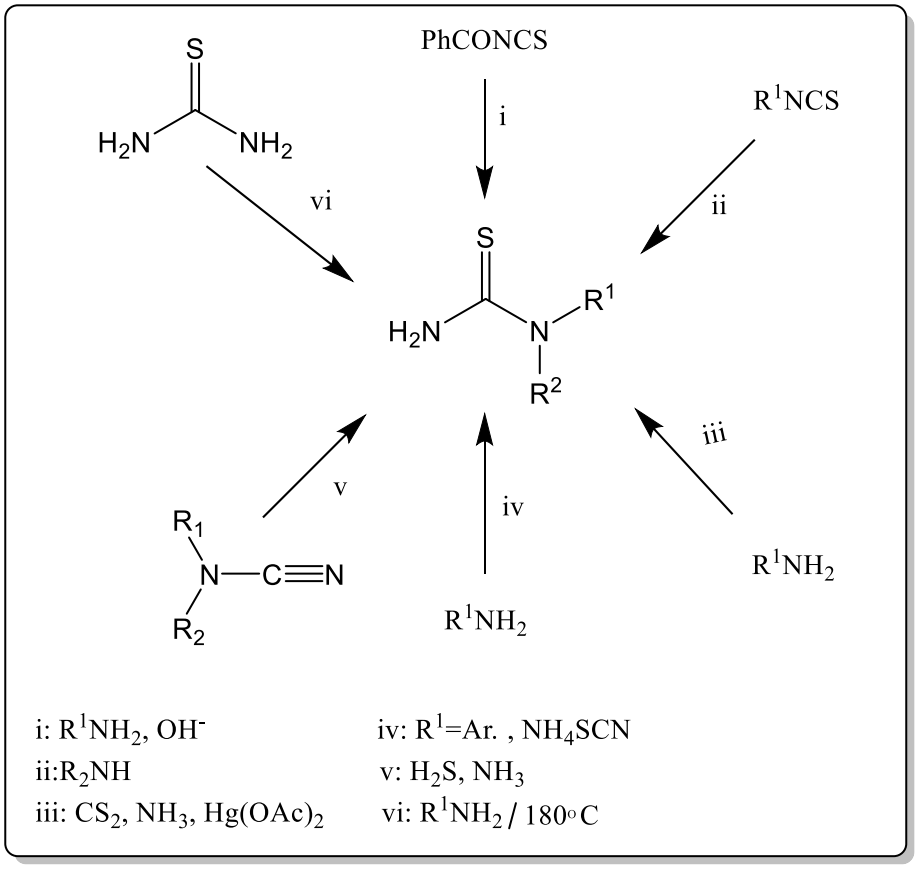


**Scheme 2.1**: Common routes to synthesis substituted thiourea.

Thiourea and its derivatives represent a well-known essential group of organic compounds due to their diverse application in different fields, such as highly selective reagents for the liquid-liquid extraction, pre-concentration and separation of the platinum-group metals.[18] Thiourea compounds also act as building blocks in the synthesis of heterocyclic compounds.[19] On the other hand, some thiourea derivatives show a broad spectrum of biological activities as antifungal,[20,21] antibacterial,[22] or antiviral agents.[23]

The application of thioureas in coordination chemistry is also well known. Co(II), Cu(II), Zn(II) and Fe(III) complexes of diisopropylthiourea, **Figure 2.4**, were synthesized and characterized by Ajibade and Zulu in 2011. The spectroscopic data of the complexes are consistent with a 4-coordinate geometry for the metal(II) complexes in the general form $[M^{II}Cl_2(diptu)_2]$, diptu=diisopropylthiourea, M= Co(II), Cu(II) and Zn(II), and six coordinate octahedral for the Fe(III) complex in the

general form $[Fe^{III}Cl_3(diptu)_3]$. In all cases the diisopropylthiourea ligand acts as a monodentate ligand through the sulfur atom.[24]

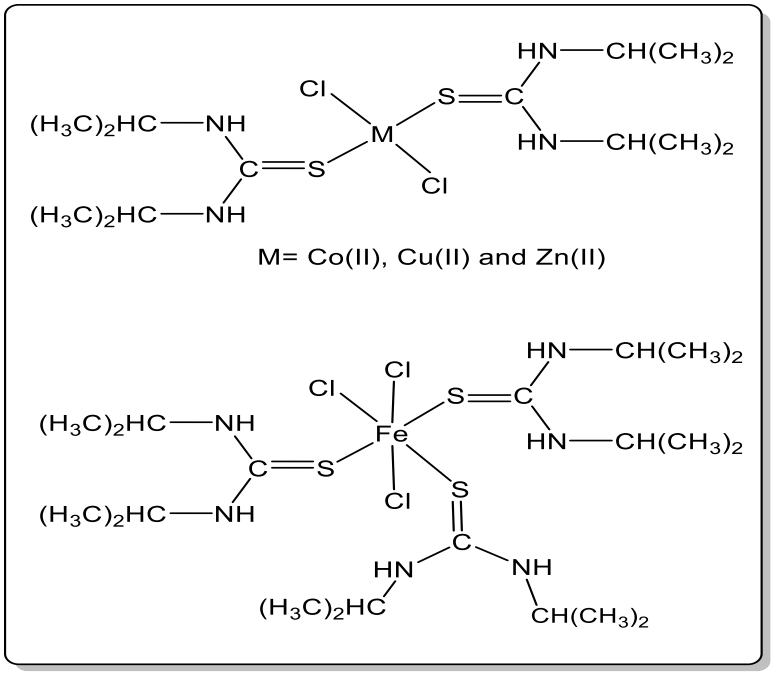


**Figure 2.4**: Structures for square planar Co(II), Cu(II) and Zn(II) and octahedral Fe(III) complex of disopropylthiourea.

For many years, thiourea derivatives with different alkyl and aryl substituents and their coordination to metals via the soft sulfur donor[25] atom have been studied. Metal complexes can be formed between thiourea derivatives and softer ions such as Hg(II), Au(I), Ag(I) and Cu(I).[26-33] Conformational evidence from crystallographically studied examples highlight the interaction between the metal ion and the thiourea through the sulfur atom, while some evidence from IR spectra suggested bonding through the nitrogen atom. Early reports studied the coordination chemistry of the aliphatic substituted thiourea and reported the complexes of Pt(II),[34] Zn(II),[35,36] Cd(II),[37,38] Ni(II),[39-42] Pb(II),[43] Pd(II),[44,45] and Co(II).[46-48]

In 1934, the first benzoylthiourea derivatives were prepared by Douglass *et al.* Their synthetic route was carried out by heating a mixture of equimolar ratio of $NH_4SCN$ and benzoyl chloride in acetone for a few minutes to prepare benzoyl isothiocyanate. A primary or secondary amine was then added to obtain a series of β-benzoyl-α-ethanolthiourea, β-benzoyl-α-ethanol-α-phenyl thiourea, β-benzoyl-α-

ethanol-α-(o-tolyl)-thiourea and β-benzoyl-α-ethanol-α-(p-tolyl)-thiourea, **Scheme 2.2**.[49]

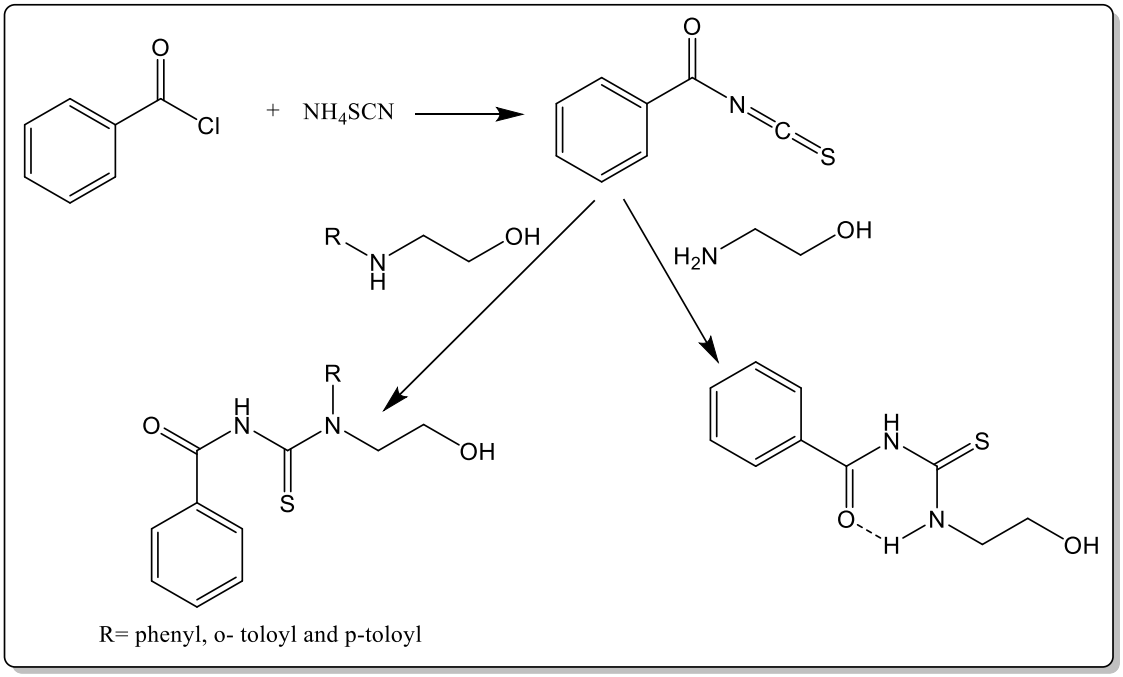


**Scheme 2.2**: Synthetic route of benzoylthiourea derivatives.

Recently, considerable literature has grown around the study of the compounds of benzoyl thiourea which is considered as one of the important thiourea derivatives and this is due to the wide range of potential uses in different fields. N-benzoyl-N'-alkylthiourea and N-benzoyl-N',N'-dialkylthiourea, **Figure 2.5** and their complexes with transition metal ions Pt(II), Au(III), Cd(II), Co(III), Cu(I), Pd(II), Ni(II), Zn(II) and Ru(III), have potential use in different fields: firstly, in the medical field as use as antimalarial,[50] antibacterial,[51-54] or antifungal agents;[55] secondly, in the analytical field, [56,57] thirdly, in the materials field [58-60] and fourthly, in coordination chemistry.[61-63] N-Benzoyl-N',N'-dialkyl thioureas are versatile ligands showing different kinds of coordination modes and they are able to coordinate as bidentate or monodentate ligands **(Figure 2.5**) through coordination via O, S atoms or S atom respectively.

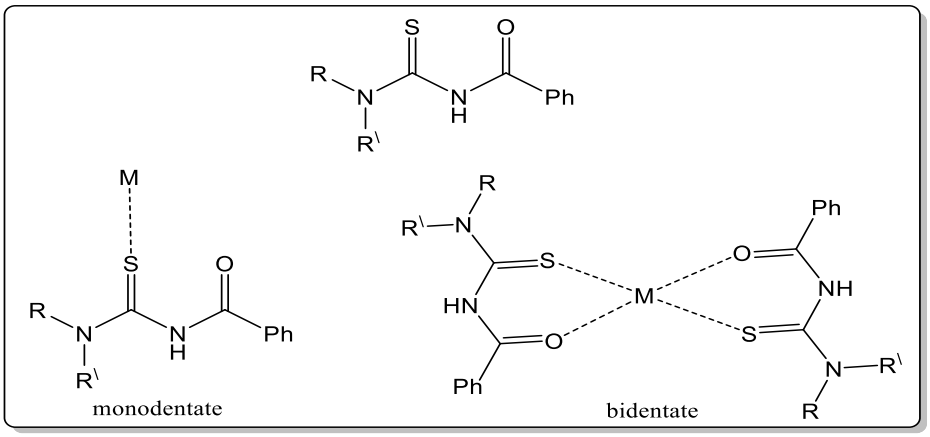


**Figure 2.5**: Structure of the general form of benzoyl thiourea derivatives and their mono and bi-dentate complexes.

Complexes with a monodentate coordination mode of the ligand through the sulfur donor atom have been reported with Ag(I),[64] Au(I)[65] and Pt(II),[66] (**Figure 2.6**). Many of the benzoyl thiourea ligands coordinate as mono-anionic bidentate O,S donors. Furthermore, a square planar geometry was observed in the complexes of Pt(II),[67,68] Hg(II),[69] Ni(II)[20] and Cu(II)[70] while octahedral coordination was reported for Pt(II),[71] Co(III),[72] Re(II) and Tc(III)[73] metal ion complexes, **Figure 2.6**.

The coordination chemistry of N,N-dialkyl-N'-4-fluoro or chloro benzoyl thiourea (where alkyl = methyl, ethyl, n-propyl, n-butyl and phenyl) with Ni(II) and Cu(II) ions was investigated in 2013 by Arslan *et al.* The ligands coordinated with Ni(II) and Cu(II) ions through oxygen and sulfur atoms to form complexes with a square planar geometry. In the crystal structures, intermolecular N–H···S, C–H···O and N–H···O hydrogen bonds in the ligands separately and C-H···S and C-H···O intermolecular hydrogen bonds in the complexes of Ni(II) and Cu(II) play a dominant role in the stabilities of crystal structures. In all examples, molecules form dimers through strong intermolecular hydrogen bonds.[74,75]

Zhang *et al.* investigated a Ni(II) complex with bis(1,1-diethyl-3(3-fluorobenzoyl) thiourea and the central Ni(II) ion is coordinated by sulfur and oxygen atoms to give a square planar conformation.[76] Co(III) complexes with N-(morpholinothiocarbonyl)benzamide and N-(piperidyl thiocarbonyl)benzamide were studied by Weiqun *et al.* The Co(III) ion was bound by bidentate ligands coordinating through S and O atoms.[55]

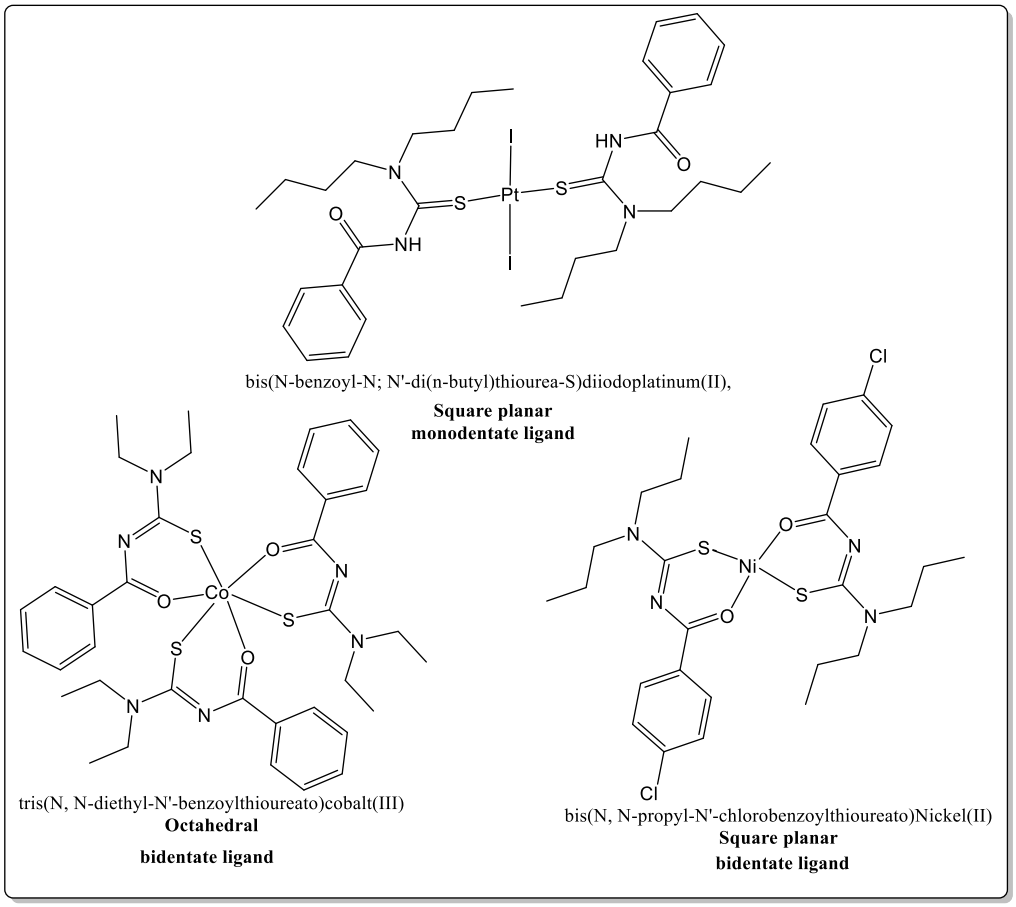


**Figure 2.6**: Examples of monodentate and bidentate coordination modes square planar and octahedral geometries.

In 2002, Kaminsky *et al.* published a paper in which they described the synthesis of *N*-(2-Pyridyl)-*N*́-benzoylthiourea by gently heating for 2 hours a mixture of equimolar amounts of benzoyl isothiocyanate and 2-aminopyridine in 95% ethanol. Prismatic crystals of *N*-(2-Pyridyl)-*N*́-benzoylthiourea was obtained by slow evaporation of the solution.[77] However, to the best of our knowledge, no report has been found so far focusing on the synthesis of any of the *N*-(2-Pyridyl)-*N*′-pivaloylthiourea derivatives and their coordination chemistry. Among the thioureas, N-benzoyl and N-carbonyl caught our attention because previously published results concerning the low toxicity of these thiourea derivatives, suggested their potential use in fields such as antibiotic drugs.

In this study, the synthesis of N,N′-substituted benzoyl thioureas derivatives (**L**$^{1a}$-**L**$^{3a}$) and N,N′-substituted pivaloyl thioureas derivatives (**L**$^{1b}$-**L**$^{3b}$) were carried out

according to the procedure of Kaminsky *et al.* with modification. The synthesis of N,N′-substituted thioureas (**$L^{1a}$-$L^{3b}$**) was achieved in two steps. First, the reaction was refluxed for 3 hours using an equimolar ratio of an organic acid chloride (benzoyl or pivaloyl chloride) with potassium thiocyanate in acetonitrile to give the corresponding isothiocyanates, pivaloyl or benzoyl isothiocyanate. The isothiocyante compound was refluxed for 15 hours with two amines, 5-methyl-2-amino pyridine or 2,6-diaminopyridine (equimolar and bimolar of 2,6-diaminopyridine) to yield the final thiourea ligands.

In this chapter, the investigation, synthesis, full characterization and crystallographic studies of mono and di benzoyl and pivaloyl thiourea ligands and their Cu(I), Cu(II), Ni(II) and Zn(II) complexes are reported in detail.

## 2.2 Experimental

### 2.2.1 Instrumentation

All reagents and solvents were of reagent grade quality and obtained from commercial suppliers, and used without further purification. Elemental analyses for carbon, hydrogen and nitrogen were performed on London Metropolitan University. Magnetic susceptibilities were determined at room temperature (20ºC) using the Evans method.[78] Electronic spectra were recorded using a (UV-1800) UV spectrophotometer (SHIMADZU). IR spectra were carried out with a shimadzu IR AFFINITY-1S. Electroscopy ionization mass spectroscopy (ESMS) were measured on a Waters LCT Premier XE (oa-TOF) mass spectrometer. The $^{1}H$ and $^{13}C$ NMR spectra were obtained on a Bruker AC 250 instrument using $CDCl_3$, DMSO-$d^6$, acetone-$d^6$ and acetonitrile-$d^3$ as solvents. Cyclic voltammetric measurements were performed in a one compartment three-electrodes cell using a platinum disk (2 mm diameter) working electrode and a platinum wire auxiliary electrode were used. The reference electrode was a non aqueous Ag/AgCl. All experiments were carried out under an atmosphere of dry nitrogen. The concentration of electroactive species was approximately $1.5 \times 10^{-3}$ M with tetrabutylammonium hexafluoro phosphate (0.1 M) as the supporting electrolyte.

## 2.2.2 Synthesis of ligands ($L^{1a}$-$L^{3b}$)

### 2.2.2.1.Synthesis of N-((5-methylpyridin-2-yl)carbamothioyl)benzamide $L^{1a}$ :

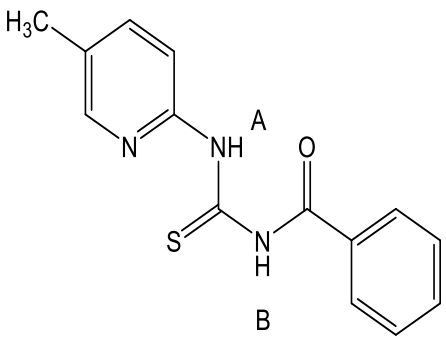


The ligand was synthesized by a modification to a previously described method.[77] To a suspension of potassium thiocyanate (3.89 g, 40 mmol) in acetonitrile (40 $cm^3$) was added dropwise a solution of benzoyl chloride (5.62 g, 40 mmol) in acetonitrile (10 $cm^3$). The reaction mixture was refluxed for 3 hours. After this time, the mixture was a yellow solution with a white precipitate. The mixture was filtered to remove the white precipitate (KCl). The yellow solution was added to a solution of 2-amino-5-methyl pyridine (4.32 g, 40 mmol) in acetonitrile (15 $cm^3$) and the reaction mixture was refluxed for a further 15 hours. The solution was left to cool and the white precipitate was collected by filtration. This product was washed with acetonitrile (30 $cm^3$) and purified by recrystallization from chloroform: ethanol (1:1) to obtain white crystals. Yield: (3.7 g, 85%); m.p= 158-159ºC, ESMS *(m/z)*(%): 272.10 [M+H] (100%); Mass: 272.0845, calc. Mass: 272.0858; FT-IR ($cm^{-1}$): ν(N-H) 3298, ν(C=O) 1672, ν(C=S) 1333; UV-vis. spectrum, $\lambda_{max}$ nm (εM, $M^{-1}cm^{-1}$): 245(11150), 269(15200), 316(9200); $^1$H NMR (250 MHz, DMSO-$d^6$), δ(ppm): 13.22 (1H, s, N-$H_A$), 11.68 (1H, s, N-$H_B$), 8.63 (1H, t, Ar $J_{HH}$ = 5 Hz ), 8.26 (1H, s, Py ), 7.97 (2H, d, Ar $J_{HH}$ = 7.5 Hz), 7.72 (1H, d, py $J_{HH}$ = 5 Hz), 7.65 (1H, d, Py $J_{HH}$ = 5 Hz), 7.54 (2H, t, Ar $J_{HH}$ =7.5 Hz), 2.29 (3H, s, $CH_3$); $^{13}$C NMR (62.5 MHz, DMSO-$d^6$), δ(ppm): 177.39 (C=S), 168.48 (C=O), 148.75, 148.31, 137.95, 133.01, 131.91, 130.69, 128.58, 128.31, 115.02, 17.42($CH_3$).

### 2.2.2.2 Synthesis of N-((6-aminopyridin-2-yl)carbamothioyl)benzamide $L^{2a}$ :

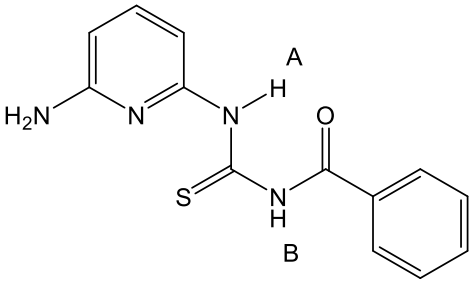


Using the same procedure as described for **$L^{1a}$** : potassium thiocyanate (3.89 g, 40 mmol), benzoyl chloride (5.62 g, 40 mmol) and 2,6-diamino pyridine (4.36 g, 40 mmol). Yield: (3.5 g 80%); m.p= 180-182ºC, yellow crystals; ESI-MS (*m/z*)(%): 272.07 [M+] (100%); Mass: 272.0617, calc. Mass: 272.0630; FT-IR ($cm^{-1}$): ν(N-H) 3485,3364, ν (C=O) 1672, ν(C=S) 1341; UV-vis. spectrum, $\lambda_{max}$ nm (εM, $M^{-1}cm^{-1}$): 248(14900), 278(8050), 301(6600), 337(5900); $^{1}$H NMR (250 MHz, DMSO-$d^6$), δ(ppm): 12.99 (1H, s, N-$H_A$), 11.53 (1H, s, N-$H_B$), 7.96 (3H, m, Ar ), 7.66 (1H, t, Py $J_{HH}$ =7.5 Hz), 7.53 (2H, d, Ar, $J_{HH}$ =7.5 Hz), 7.46 (1H, d, Py, $J_{HH}$ =10 Hz), 6.31 (1H, d, Py, $J_{HH}$ =7.5 Hz), 6.14 (2H, s, $NH_2$); $^{13}$C NMR (62.5 MHz, DMSO-$d^6$), δ(ppm): 177.09 (C=S), 168.68 (C=O), 159.03, 149.54, 138.75, 133.24, 132.18, 128.77, 128.54, 106.07, 102.82.

### 2.2.2.3 Synthesis of N,N'-((pyridine-2,6-diylbis(azanediyl))bis(carbonothioyl)) dibenzamide $L^{3a}$:

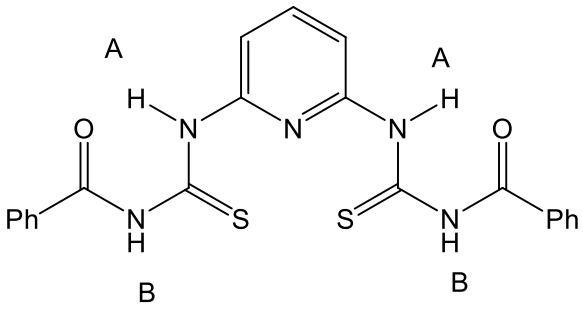


Using the same procedure as described for **$L^{1a}$**: potassium thiocyanate (3.89 g, 40 mmol), benzoyl chloride (5.62 g, 40 mmol) and 2,6-diamino pyridine (2.18 g, 20 mmol). Yield: (2 g, 91%); m.p= 197-198ºC, white crystals; ESI-MS (*m/z*)(%): 436.09 [M+H] (75%); Mass: 436.0915, calc. Mass: 436.0902; FT-IR ($cm^{-1}$): ν(N-H) 3321, ν(C=O) 1667, ν(C=S) 1325; UV-vis. spectrum, $\lambda_{max}$ nm (εM, $M^{-1}cm^{-1}$): 278(19400), 331(12200); $^{1}$H NMR (250 MHz, DMSO-$d^6$), δ(ppm): 13.15 (2H, s, 2N-$H_A$), 11.85 (2H, s, N-$H_B$), 8.53 (2H, d , $H_2$, Py, $J_{HH}$ =5 Hz), 8.01 (1H, t, py, $J_{HH}$ =10 Hz), 7.98 (4H, d, Ar, $J_{HH}$ =7.5 Hz), 7.65 (2H, t, Ar, $J_{HH}$ =7.5 Hz), 7.53 (4H, t, Ar, $J_{HH}$ =7.5 Hz); $^{13}$C NMR (62.5 MHz, DMSO-$d^6$),

δ(ppm): 178.47 (C=S), 168.92 (C=O), 150.18, 140.38, 133.59, 132.40, 129.13, 128.78, 113.41.

### 2.2.2.4 Synthesis of N-((5-methylpyridin-2-yl)carbamothioyl)pivalamide $L^{1b}$ :

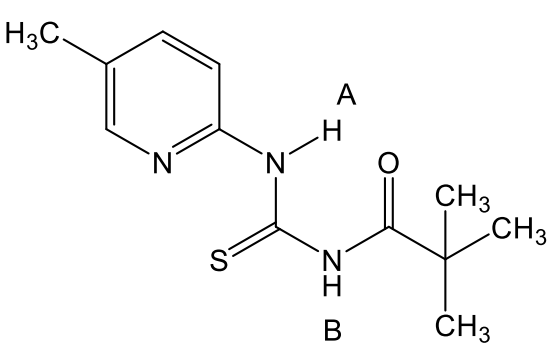


To a suspension of potassium thiocyanate (0.81 g, 8.3 mmol) in acetonitrile (15 $cm^3$) was added dropwise the solution of trimethyl acetyl chloride (1 g, 8.3 mmol) in acetonitrile (10 $cm^3$). The reaction mixture was refluxed for 3 hours. After this time, the mixture was a yellow solution with a white precipitate. The mixture was filtered to remove the white precipitate (KCl). The yellow solution was added to a solution of 2-amino-5-methyl pyridine (0.9 g, 8.3 mmol) in acetonitrile (5 $cm^3$) and the reaction mixture was refluxed for 21 hours. The solution of product was concentrated to half of its original volume and the white precipitate of product was collected by filtration. The product was washed with acetonitrile (5 $cm^3$) and purified by recrystallization from ethanol. Yield: (0.78 g, 87%); m.p= 86-88ºC, white crystals; ESI-MS(*m/z*)(%): 252.08 [M+H] (100%); Mass: 252.1169, calc. Mass: 252.1171, FT-IR ($cm^{-1}$): ν(N-H) 3341, ν(C=O) 1676, ν(C=S) 1331; UV-vis. spectrum, $\lambda_{max}$ nm (εM, $M^{-1}$ $cm^{-1}$): 254(11700), 306(10850); $^1$H NMR (250 MHz, DMSO-$d^6$), δ(ppm): 13.16 (1H, s, N-$H_A$), 10.75 (1H, s, N-$H_B$), 8.57 (1H, d, Py $J_{HH}$ =10 Hz), 8.25 (1H, s, Py), 7.72 (1H, d, Py $J_{HH}$ =2.5 Hz), 2.29 (3H, s, 1$CH_3$), 1.25 (9H, s, 3$CH_3$); $^{13}$C NMR (100 MHz, DMSO-$d^6$), δ(ppm): 180.65 (C=S), 177.84 (C=O), 148.86, 148.44, 138.10, 131.00, 115.32, 40.11, 26.13 ($CH_3$), 17.39 ($CH_3$).

### 2.2.2.5 Synthesis of N-((6-aminopyridin-2-yl)carbamothioyl)pivalamide $L^{2b}$:

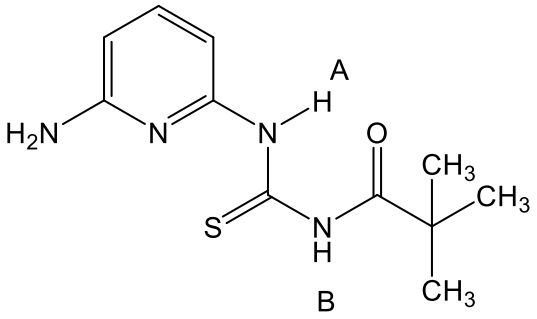

Using the same procedure as described for $L^{1b}$: potassium thiocyanate (0.81 g, 8.3 mmol), tri methyl acetyl chloride (1 g, 8.3 mmol) and 2,6-diaminopyridine (0.9 g, 8.3 mmol). Yield: (0.71 g, 79%); m.p= 164-165ºC, white crystals; ESI-MS *(m/z)*(%)*:* 252.08 [M] (91%); Mass: 252.1044, calc. Mass: 252.1045, FT-IR ($cm^{-1}$): ν(N-H) 3401, 3302, ν(C=O) 1685, ν(C=S) 1356; UV-vis. spectrum, $\lambda_{max}$ nm (εM, $M^{-1}$ $cm^{-1}$): 232(31900), 267(17750), 292(12850), 328(14850); $^{1}$H NMR (250 MHz, DMSO-$d^6$), δ(ppm): 12.93 (1H, s, N-$H_A$), 10.58 (1H, s, N-$H_B$), 7.91(1H, d, py, $J_{HH}$ =7.5 Hz), 7.44(1H, t, py, $J_{HH}$ =7.5 Hz), 6.30 (1H, d, py, $J_{HH}$ =7.5 Hz), 6.12 (2H, s, $NH_2$), 1.25 (9H, s, $3CH_3$ ); $^{13}$C NMR (100 MHz, DMSO-$d^6$), δ(ppm): 180.34 (C=S), 176.86 (C=O), 158.83, 149.38, 138.62, 105.97, 102.51, 40.02, 26.17 ($CH_3$ ).

### 2.2.2.6 Synthesis of N,N'-((pyridine-2,6-diylbis(azanediyl))bis(carbonothioyl)) bis (2,2-dimethylpropanamide) $L^{3b}$:

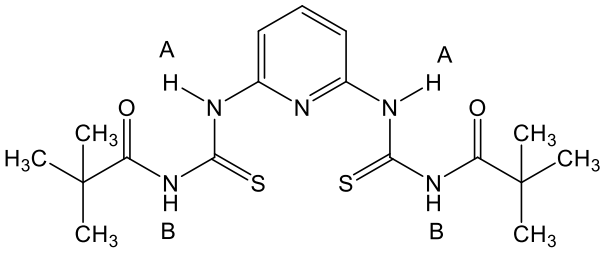

Using the same procedure as described for $L^{1b}$: potassium thiocyanate (1.94 g, 20 mmol), trimethyl acetyl chloride (2.4 g, 20 mmol) and 2,6-diamino pyridine (1.09 g, 10 mmol). Yield: (2 g, 86 %); m.p= 176-177ºC, white crystals; ESI-MS *(m/z)*(%): 396.14 [M+H] (60%); Mass: 396.1522, calc. Mass: 396.1528; FT-IR ($cm^{-1}$): ν(N-H) 3445, 3414, ν(C=O) 1692, 1673, ν(C=S) 1366; UV-vis. spectrum, $\lambda_{max}$ nm (εM, $M^{-1}$ $cm^{-1}$): 267(42000), 322(47200); $^{1}$H NMR (250 MHz, DMSO-$d^6$), δ(ppm): 13.19 (2H, s, 2N-$H_A$), 10.90 (2H, s, 2N-$H_B$), 8.53 (2H, d, Py, $J_{HH}$ =7.5 Hz), 7.97 (1H, t, Py, $J_{HH}$ =10 Hz), 1.26 (18H, s, $6CH_3$); $^{13}$C NMR (100 MHz, DMSO-$d^6$), δ(ppm): 180.64 (C=S), 178.30 (C=O), 149.78, 139.99, 113.27, 40.19, 26.12 ($CH_3$).

## 2.2.3 Synthesis of complexes 2.1-2.27

***CAUTION***: Perchlorate compounds of metal ions are potentially explosive especially in presence of organic ligands. Only a small amount of material should be prepared and handled with care.

### 2.2.3.1 Synthesis of $[Cu(L^{1a})_2]ClO_4$ (2.1)

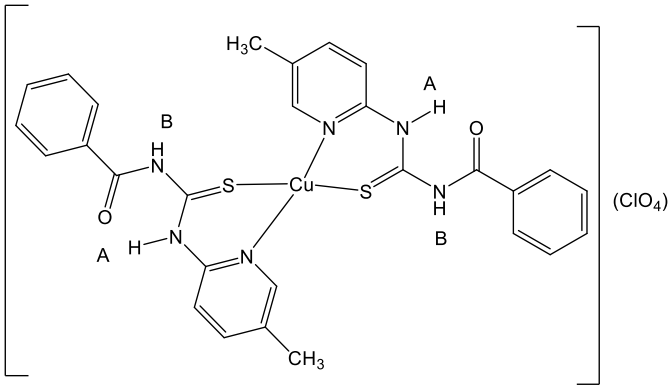


A solution of $Cu(ClO_4)_2.6H_2O$ (0.2 g, 0.5 mmol) in $H_2O$ (3 $cm^3$) was added to a solution of **$L^{1a}$** (0.292 g, 0.10 mmol) in DMF (4 $cm^3$). The mixture was stirred at room temperature for 3 hours. The colorless solution turned orange and formed a precipitate. The orange precipitate was filtered, washed with $CHCl_3$ (20 $cm^3$) to remove unreacted ligand and dried under vaccum. Red crystals of **2.1** were grown at room temperature by the diffusion of diethyl ether vapor into an acetonitrile solution. Yield: (0.25 g, 88 %); red crystals; ESI-MS *(m/z)*(%): 605.09 [M+] (100%); Mass: 605.0854, calc. Mass: 605.0855; FT-IR ( $cm^{-1}$): ν(N-H) 3267, ν(C=O) 1672, ν(C=S) 1281; ν(Cl-O) 1091, 625; UV-vis. spectrum, $\lambda_{max}$ nm (εM, $M^{-1}$ $cm^{-1}$): 248(24250), 268(30600), 315(17550); $^1$H NMR (250 MHz, acetone-$d^6$), δ(ppm): 14.10 (2H, s, 2N-$H_A$), 11.14 (2H, s, 2N-$H_B$), 8.28 (2H, s, py), 8.06 (4H, d, Ar, $J_{HH}$ =7.5 Hz), 7.91(2H, d, py, $J_{HH}$ =7.5 Hz), 7.72 (2H, t, Ar, $J_{HH}$ =7.5 Hz), 7.59 (4H, t, Ar, $J_{HH}$ =7.5 Hz), 7.35(2H, t, Py., $J_{HH}$ =10 Hz), 2.25 (6H, s, 2$CH_3$). $^{13}$C NMR (62.5 MHz, acetone-$d^6$), δ(ppm): 170.47(C=S), 149.49(C=O), 148.99, 142.04, 135.03, 133.81, 132.68, 129.93, 129.65, 119.06, 111.87, 17.86. Anal. Calcd. for **$C_{28}H_{26}ClCuN_6O_6S_2$** (%): C, 47.66; H, 3.71; N,11.91. Found (%): C, 47.58; H, 3.68; N, 11.97.

### 2.2.3.2 Synthesis of $[Ni(L^{1a})(L^{1C})](ClO_4)_2$ (2.2)

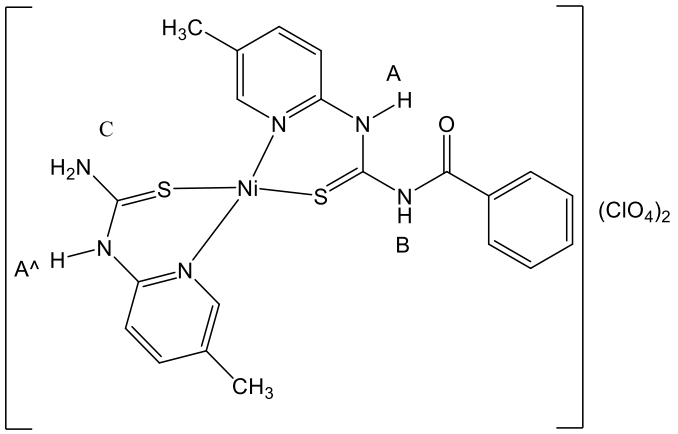

$[Ni(L^{1a})(L^{1C})](ClO_4)$ was obtained by adding a solution of $Ni(ClO_4)_2.6H_2O$ (0.236 g, 0.65 mmol) in methanol (5 $cm^3$) to a solution of **$L^{1a}$** (0.35 g, 1.3 mmol) in $CHCl_3$ (10 $cm^3$). The mixture was refluxed 5 hours. The colorless solution turned green and then a brown precipitate formed and was filtered off, washed with $CHCl_3$ (20 $cm^3$) to remove the unreacted ligand and dried under vaccum. Yield: (0.28 g, 80%); brown powder; ESI-MS *(m/z)*(%): 495.04 [M+] (100%); Mass: 495.0575, calc. Mass: 495.0572; FT-IR ($cm^{-1}$): ν(N-H) 3314, ν(C=O) 1672, ν(C=S) 1283; ν(Cl-O) 1090, 627; UV-vis. spectrum, $\lambda_{max}$ nm, (εM, $M^{-1}$ $cm^{-1}$): 242(15100), 272(21500), 303(14100), 411(390), 584(56); $^1$H NMR (250 MHz, DMSO-$d^6$), δ(ppm): 13.24 (1H, s, 1N-$H_A$), 11.70 (1H, s, 1N-$H_{A^\wedge}$), 10.46 (2H, s, $NH_2$), 8.81 (1H, s, 1N-$H_B$), 8.64 (1H, d, Py $J_{HH}$ =5 Hz), 8.27 (1H, s, Py), 8.05 (1H, s, HPy), 7.96 (2H, d, Ar, $J_{HH}$ =7.5 Hz), 7.73 (1H, d, Py, $J_{HH}$ =5 Hz), 7.66 (1H, d, Py, $J_{HH}$ =7.5 Hz), 7.58 (3H, t, Ar, $J_{HH}$ =7.5 Hz), 7.05 (1H, d, Py $J_{HH}$ =7.5 Hz), 2.29 (3H, s, 1$CH_3$), 2.20 (3H, s, 1$CH_3$). $^{13}$C NMR (62.5 MHz, DMSO-$d^6$), δ(ppm): 177.38(C=S), 168.51(C=O), 151.44, 145.31, 139.48, 133.17, 132.41, 128.68, 128.44, 127.01, 112.32, 17.37 ($CH_3$). Anal. Calcd. for **$C_{21}H_{22}Cl_2N_6NiO_9S_2$**(%): C,36.23; H, 3.19; N,12.07. Found (%): C, 36.31; H, 3.12; N, 12.06.

### 2.2.3.3 Synthesis of $[Ni(L^{1a})_2](ClO_4)_2$ (2.3)

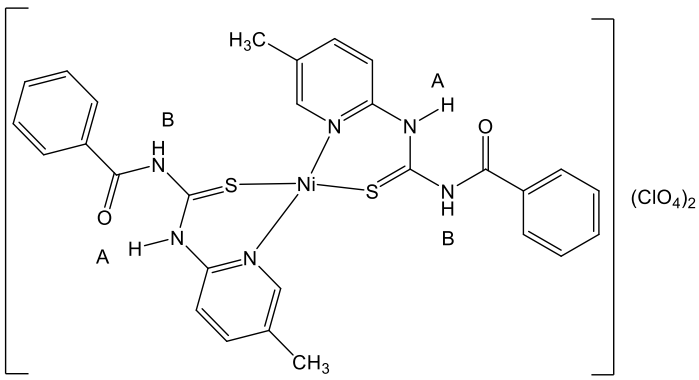

$[Ni(L^{1a})_2](ClO_4)_2$ was obtained by stirring for 5 hours a mixture of $Ni(ClO_4)_2.6H_2O$ (0.337 g, 0.92 mmol) in methanol (5 $cm^3$) and a solution of **$L^{1a}$** (0.5 g, 1.9 mmol) in $CHCl_3$ (10 $cm^3$) at 50ºC. The colorless solution turned green and then a brown precipitate

formed and was filtered off, washed with $CHCl_3$ (20 $cm^3$) to remove the unreacted ligand and dried under vaccum. Yield: (0.38 g, 76%); brown powder; ESI-MS *(m/z)*(%): 599.01 [M+] (100%); Mass: 599.0837, calc. Mass: 599.0834; FT-IR ($cm^{-1}$): ν(N-H) 3404, ν(C=O) 1668, ν(C=S) 1283; ν(Cl-O) 1087, 624; UV-vis. spectrum, $\lambda_{max}$ nm, (εM, $M^{-1}$ $cm^{-1}$): 245(16600), 269(24400), 314(12500), 394(377), 598(11); $^1$H NMR (250 MHz, DMSO-$d^6$), δ(ppm): 13.24 (2H, s, 2N-$H_A$), 11.71 (2H, s, 2N-$H_B$), 8.66 (2H, t , Ar, $J_{HH}$ = 7.5 Hz), 8.27 (2H, s, Py,), 7.96 (4H, d, Ar, $J_{HH}$ = 7.5 Hz), 7.73 (2H, d, Py, $J_{HH}$ =7.5 Hz), 7.65 (2H, d, Py, $J_{HH}$ =7.5 Hz), 7.55 (4H, t, Ar., $J_{HH}$ =5 Hz), 2.29 (6H, s, $2CH_3$). $^{13}$C NMR (62.5 MHz, DMSO-$d^6$), δ(ppm): 176.08(C=S), 167.22(C=O), 157.59, 147.11, 136.76, 131.99, 127.53, 127.44, 116.26, 110.61, 16.21 ($CH_3$). Anal. Calcd. for **$C_{28}H_{26}Cl_2N_6NiO_{10}S_2$** (%): C, 42.02; H, 3.27; N, 10.50. Found (%): C, 41.95; H, 3.34; N, 10.39.

### 2.2.3.4 Synthesis of $[Zn(L^{1C})_2](ClO_4)_2$ (2.4)

A methanolic solution (5 $cm^3$) of $Zn(ClO_4)_2.6H_2O$ (0.28 g, 0.75 mmol) was added drop wise to a solution of **$L^{1a}$** (0.408 g, 1.5 mmol) in $CHCl_3$ (10 $cm^3$). The mixture was refluxed for 8 hours. The white precipitate formed was filtered, washed with $CHCl_3$ (20 $cm^3$) to remove the unreacted ligand and dried under vaccum. Colorless crystals of **2.4** were grown at room temperature by the diffusion of diethyl ether vapor into an acetonitrile solution. Yield: (0.34 g, 85%); white powder; ESI-MS *(m/z)*(%): 397.05 [M+] (100%); Mass: 397.0230, calc. Mass: 397.0248; FT-IR ($cm^{-1}$): ν(N-H) 3381, ν(C=S) 1279; ν(Cl-O) 1080, 626; UV-vis. spectrum, $\lambda_{max}$ nm, (εM, $M^{-1}$ $cm^{-1}$): 240(14900), 273(28450), 299(25600); $^1$H NMR (250 MHz, DMSO-$d^6$), δ(ppm): 10.52 (2H, s, 2N-$H_A$), 10.47 (2H, s, 2N-H, $NH_{2B}$), 8.83 (2H, s, 2N-H, $NH_{2B^\wedge}$), 8.06 (2H, s, py), 7.60 (2H, d, py, $J_{HH}$ =10 Hz), 7.06 (2H, d, py, $J_{HH}$ =7.5 Hz), 2.21 (6H, s, $2CH_3$). $^{13}$C NMR (62.5 MHz, DMSO-$d^6$), δ(ppm): 180.44 (C=S), 151.78, 145.47, 139.84, 126.59, 112.84, 17.37($CH_3$). Anal. Calcd. for **$C_{14}H_{18}Cl_2N_6O_8S_2Zn$** (%): C, 28.09; H, 3.03; N, 14.04. Found (%): C, 28.16; H, 3.01; N, 14.12.

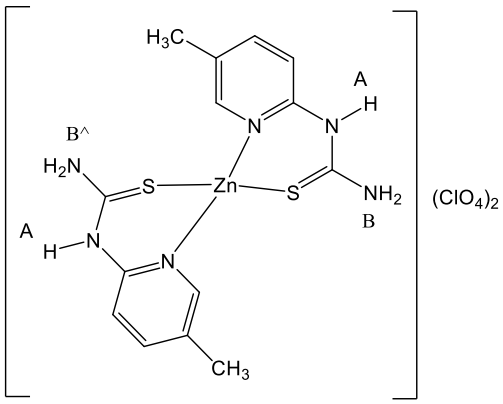

### 2.2.3.5 Synthesis of $[Zn(L^{1a})(L^{1C})](ClO_4)_2$ (2.5)

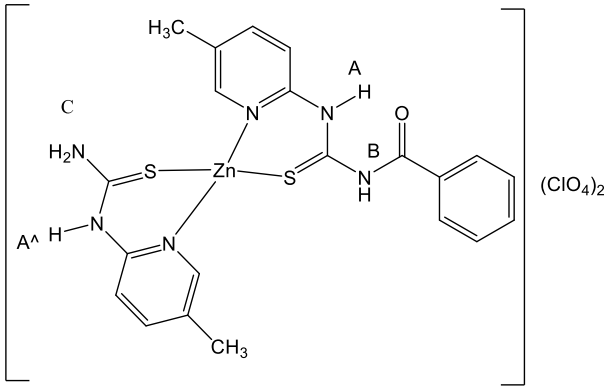


A methanolic solution (5 $cm^3$) of $Zn(ClO_4)_2.6H_2O$ (0.34 g, 0.92 mmol) was added drop wise to a solution of **$L^{1a}$** (0.5 g, 1.9 mmol) in $CHCl_3$ (10 $cm^3$). The mixture was stirred at room temperature for 8 hours. The white precipitate formed was filtered, washed with $CHCl_3$ (20 $cm^3$) to remove the unreacted ligand and dried under vaccum. Yield: (0.36 g, 72%); white powder; ESI-MS *(m/z)*(%): 501.00 [M-H] (100%); Mass: 501.0331, Calc. Mass: 501.0339; FT-IR ($cm^{-1}$): ν(N-H) 3377, ν(C=O) 1670, ν(C=S) 1278; ν(Cl-O) 1084, 627; UV-vis. spectrum, $\lambda_{max}$ nm, (εM, $M^{-1}$ $cm^{-1}$): 235(24300), 273(33950), 299(29800), $^1$H NMR (250 MHz, DMSO-$d^6$), δ(ppm): 10.52 (1H, s, 1N-$H_A$), 10.46 (1H, s, 1N-$H_{A^\wedge}$ ), 8.82 (1H, s, 1N-$H_B$), 8.05 (2H, s, py), 7.95 (2H, d, py, $J_{HH}$ =7.5 Hz), 7.65 (1H, t, Ar, $J_{HH}$ = 7.5 Hz), 7.60 (1H, d, Ar, $J_{HH}$ =2.5 Hz), 7.57 (1H, d, Ar, $J_{HH}$ =2.5 Hz), 7.52 (2H, t, Ar, $J_{HH}$ =7.5 Hz), 7.05 (2H, d, Py, $J_{HH}$ =7.5 Hz), 4.01 (2H, s, 1$NH_{2C}$ ), 2.20 (6H, s, 2$CH_3$). $^{13}$C NMR (62.5 MHz, DMSO-$d^6$), δ(ppm): 180.35 (C=S), 166.30 (C=O), 151.65, 145.53, 139.77, 133.47, 129.71, 129.25, 128.92, 127.14, 112.43, 17.33. Anal. Calcd. for **$C_{21}H_{22}Cl_2N_6O_9S_2Zn$** (%): C, 35.89; H, 3.16; N, 11.96. Found (%): C, 35.72 ; H, 2.88 ; N, 11.82.

### 2.2.3.6 Synthesis of $[Cu(L^{2a})_2]ClO_4$ (2.6)

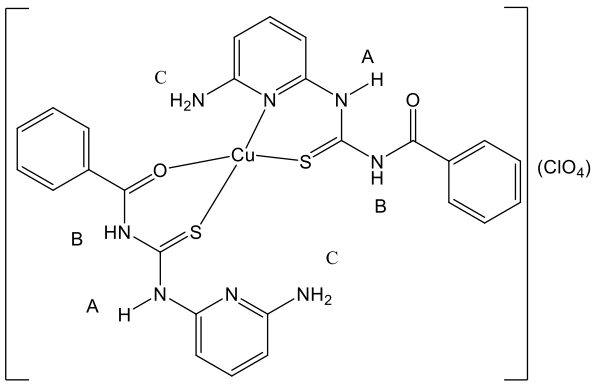


Using the same procedure as described for **1.1** followed using: $Cu(ClO_4)_2.6H_2O$ (0.4 g, 1.1 mmol), **$L^{2a}$** (0.589 g, 2.2 mmol). Dark orange crystals of **2.6** were grown at room temperature by the diffusion of diethyl ether vapour into an acetonitrile: methanol (2:1) solution of it. Yield: (0.51 g, 88%); red crystals; ESI-

MS *(m/z)*(%): 607.08 [M+] (100%); Mass: 607.0754, Calc. Mass: 607.0760, FT-IR ($cm^{-1}$): ν(N-H) 3323, ν(C=O) 1661, ν(C=S) 1258; ν(Cl-O) 1080, 624; UV-vis. spectrum, $\lambda_{max}$ nm, (εM, $M^{-1}$ $cm^{-1}$): 247(33650), 279(18200), 302(14700), 344(12850); $^1$H NMR (250 MHz, acetonitrile-$d^3$), δ(ppm): 13.23 (2H, s, 2N-$H_A$), 9.68 (2H, s, 2N-$H_B$), 7.91 (4H, d, Ar, $J_{HH}$ =7.5 Hz), 7.69 (2H, t, Py, $J_{HH}$ =7.5 Hz), 7.55 (6H, t, Ar, $J_{HH}$ =7.5 Hz), 7.34 (2H, d, Py., $J_{HH}$ =10 Hz), 6.49 (2H, d, Py., $J_{HH}$ =7.5 Hz), 5.29 (4H, s, 2$NH_{2C}$),$^{13}$C NMR (62.5 MHz, acetonitrile-$d^3$), δ(ppm): 174.72(C=S), 168.88(C=O), 158.06, 149.87, 140.22, 133.52, 132.61, 128.68, 128.59, 103.07, 100.66. Anal. Calcd. for **$C_{26}H_{24}ClCuN_8O_6S_2$**(%): C,44.13; H, 3.42; N,15.84. Found (%): C, 44.04; H, 3.47; N, 15.72.

### 2.2.3.7 Synthesis of $[Ni(L^{2C})_2](ClO_4)_2$ (2.7)

$[Ni(L^{2C})_2](ClO_4)_2$ was obtained by using the same procedure as described for **2.2**: $Ni(ClO_4)_2.6H_2O$ (0.2 g, 0.5 mmol) and **$L^{2a}$** (0.3 g, 1 mmol). Red crystals of **2.7** were grown at room temperature by the diffusion of diethyl ether vapour into an ethyl acetate solution. Yield: (0.21 g, 71%); brown crystals; ESI-MS *(m/z)*(%): 393.02 [M+] (90%); Mass: 393.0206, Calc. Mass: 393.0215, FT-IR ($cm^{-1}$): ν(N-H) 3343, ν(C=S) 1271; ν(Cl-O) 1071, 627; UV-vis. spectrum, $\lambda_{max}$ nm, (εM, $M^{-1}$ $cm^{-1}$): 215(16900), 251(20050), 272(18950), 319(22950), 401(205), 603(17); $^1$H NMR (250 MHz, DMSO-$d^6$), δ(ppm): 10.61 (2H, s, 2N-$H_A$), 10.05 (2H, s, 2N-H ($NH_{2B}$)), 8.66 (2H, s, 2N-H ($NH_{2B^\wedge}$)), 7.28 (2H, t, Py, $J_{HH}$ = 7.5 Hz), 6.20 [(6H, m, 4N-H(2$NH_{2C}$) + 2H, Py)], 6.00 (2H, d, Py, $J_{HH}$ =7.5 Hz),$^{13}$C NMR (62.5 MHz, DMSO-$d^6$), δ(ppm): 179.99 (C=S), 157.50, 139.08, 129.08, 128.78, 100.98, 98.88. Anal. Calcd. for **$C_{12}H_{16}Cl_2N_8NiO_8S_2$** (%): C,24.26; H, 2.72; N,18.86. Found (%): C, 24.20; H, 2.83; N, 18.79.

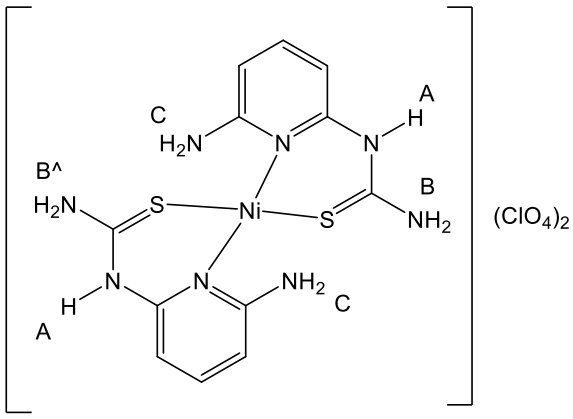

### 2.2.3.8 Synthesis of $[Ni(L^{2a})_2](ClO_4)_2$ (2.8)

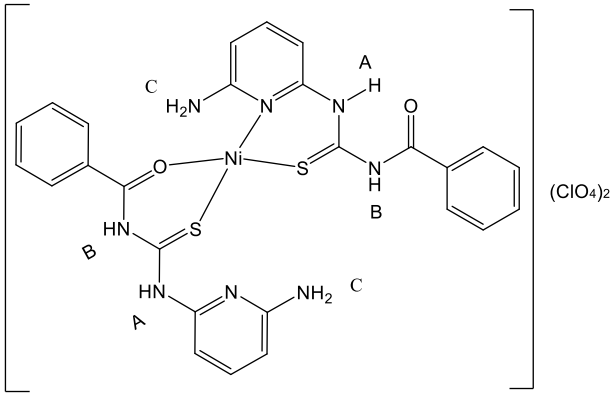

$[Ni(L^{2a})_2](ClO_4)_2$ was obtained by using the same procedure as described for **2.3**: $Ni(ClO_4)_2.6H_2O$ (0.336 g, 0.92 mmol) of $\mathbf{L^{2a}}$ (0.5 g, 1.9 mmol). Yield: (0.34 g, 69%); brown powder; ESI-MS *(m/z)*(%): 601.08 [M+] (100%); Mass: 601.0742, Calc. Mass: 601.0739; FT-IR ($cm^{-1}$): ν(N-H) 3331, ν(C=O) 1660, ν(C=S) 1275, ν(Cl-O) 1071, 626; UV-vis. spectrum, $\lambda_{max}$ nm, (εM, $M^{-1}$ $cm^{-1}$): 235(16550), 250(19300),273 (13550), 324(11500), 421(423), 612(5); $^1$H NMR (250 MHz, DMSO-$d^6$), δ(ppm): 13.00 (2H, s, 2N-$H_A$), 11.55 (2H, s, 2N-$H_B$), 7.95 (4H, d, Ar, $J_{HH}$ =5 Hz), 7.64 (4H, d, Py, $J_{HH}$ =5 Hz), 7.52 (4H, t, Ar, $J_{HH}$ =7.5 Hz), 7.28 (2H, t, Py., $J_{HH}$ =7 Hz), 6.21 (4H, s, 4N-H(2$NH_{2C}$)), 6.18 (2H, t, Ar., $J_{HH}$ =10 Hz), $^{13}$C NMR (62.5 MHz, DMSO-$d^6$), δ(ppm): 176.09 (C=S), 165.60 (C=O), 158.36, 156.75, 138.90, 132.87, 132.77, 128.33, 128.04, 109.43, 105.80. Anal. Calcd. for $\mathbf{C_{26}H_{24}Cl_2N_8NiO_{10}S_2}$ (%): C,38.93; H, 3.02; N,13.97. Found (%): C, 38.87; H, 3.13; N, 13.92.

### 2.2.3.9 Synthesis of $[Zn(L^{2C})_2](ClO_4)_2$ (2.9)

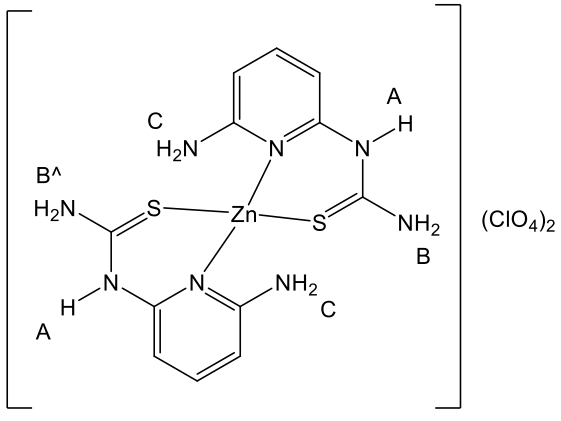

Using the same procedure as described for **2.4** was followed by using: $Zn(ClO_4)_2.6H_2O$ (0.24 g, 0.64 mmol) and $\mathbf{L^{2a}}$ (0.35 g, 1.3 mmol). Yield: (0.28 g, 81%); white powder; ESI-MS *(m/z)*(%): 399.00 [M+] (100%); Mass: 399.0000, Calc. Mass: 399.0000; FT-IR ($cm^{-1}$): ν(N-H) 3375, ν(C=S) 1267; ν(Cl-O) 1067, 626; UV-vis. spectrum, $\lambda_{max}$ nm, (εM, $M^{-1}$ $cm^{-1}$): 214(28200), 251(34100), 272(31750), 320(38250); $^1$H NMR (400 MHz, DMSO-$d^6$), δ(ppm): 10.63 (2H, s, 2N-$H_A$), 10.06 (2H, s, 2N-H($NH_{2B}$)), 8.68 (2H, s, 2N-H($NH_{2B^\wedge}$)), 7.29 (2H, t, Py, $J_{HH}$ =2.5 Hz), 6.22 [(6H, m, 4N-H(2$NH_{2C}$)+ 2H Py], 6.02 (2H, d, Py, $J_{HH}$ =5 Hz), $^{13}$C NMR (100 MHz, DMSO-$d^6$),

δ(ppm): 180.05 (C=S), 157.74, 152.40, 139.39, 101.00, 98.79. Anal. Calcd. for **$C_{12}H_{16}Cl_2N_8O_8S_2Zn$** (%): C,23.99; H, 2.68; N,18.65. Found (%): C, 24.13; H, 2.73; N, 18.48.

### 2.2.3.10 Synthesis of $[Zn(L^{2a})(L^{2C})](ClO_4)_2$ (2.10)

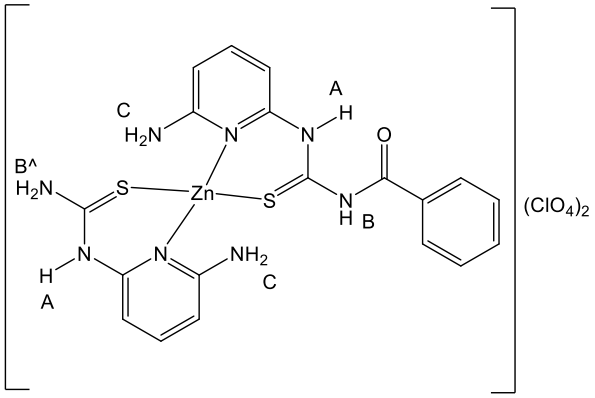


Using the same procedure as described for **2.5** was followed by using: $Zn(ClO_4)_2.6H_2O$ (0.17 g, 0.46 mmol) was added drop wise to a solution of **$L^{2a}$** (0.25 g, 0.92 mmol). Yield: (0.18 g, 73%); white powder; ESI-MS *(m/z)*(%): 504.05 [M+] (100%); Mass: 504.0663, Calc. Mass: 504.0674; FT-IR ($cm^{-1}$): ν(N-H) 3366, ν(C=O) 1668, ν(C=S) 1277; ν(Cl-O) 1070, 626; UV-vis. spectrum, $\lambda_{max}$ nm, (εM, $M^{-1}$ $cm^{-1}$): 222(21100), 275(14000), 326(8150), 367(10300). $^1$H NMR (250 MHz, DMSO-$d^6$), δ(ppm): 10.62 (2H, s, 2N-$H_A$), 10.06 (1H, s, 1N-$H_B$), 8.67 (2H, s, 2N-H($NH_{2B^\wedge}$)), 7.95 (2H, d, Ar, $J_{HH}$ =7.5 Hz), 7.66 (1H, t, Ar, $J_{HH}$ =7.5 Hz), 7.52 (2H, t, Ar, $J_{HH}$ =7.5 Hz), 7.29 (2H, t, Py, $J_{HH}$ =7.5 Hz), 6.19 (2H, d, Py, $J_{HH}$ =7.5 Hz), 6.02 (2H, d, Py, $J_{HH}$ =7.5 Hz), 3.85 (4H, s, 4N-H($2NH_{2C}$)), $^{13}$C NMR (62.5 MHz, DMSO-$d^6$), δ(ppm): 180.35 (C=S), 166.26 (C=O), 157.86, 152.35, 139.55, 133.48, 129.65, 129.25, 128.93, 101.20, 98.79. Anal. Calcd. for **$C_{19}H_{20}Cl_2N_8O_9S_2Zn$** (%): C,32.38; H, 2.86; N,15.90. Found (%): C, 32.40; H, 3.14; N, 15.84.

### 2.2.3.11 Synthesis of $[Cu(L^{3a})]ClO_4$ (2.11)

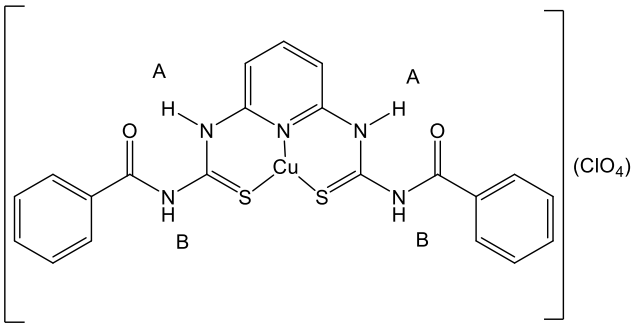


Using the same procedure as described for **2.1** was followed by using: $Cu(ClO_4)_2.6H_2O$ (0.21 g, 0.57 mmol) and **$L^{3a}$** (0.25 g, 0.57 mmol). Yield: (0.16 g, 65%); brown powder; ESI-MS *(m/z)*(%): 498.02 [M+] (100%); Mass: 498.0110, Calc. Mass:

498.0120; FT-IR ($cm^{-1}$): ν(N-H) 3387, ν(C=O) 1665, ν(C=S) 1260; ν(Cl-O) 1096, 621; UV-vis. spectrum, $\lambda_{max}$ nm, (εM, $M^{-1}$ $cm^{-1}$): 263(23200), 316(18400), 359(19400); $^{1}$H NMR (250 MHz, DMSO-$d^6$), δ(ppm): 12.14 (2H, s, 2N-$H_A$), 11.74 (2H, s, 2N-$H_B$), 8.25 (2H, d, Ar, $J_{HH}$ =7.5 Hz), 8.11 (2H, d, Py, $J_{HH}$ =7.5 Hz), 7.93 (1H, d, Py, $J_{HH}$ =7.5 Hz), 7.69 (1H, t, Py, $J_{HH}$ =7.5 Hz), 7.59 [( 7H, m, 1H, Py + 6H, Ar)], $^{13}$C NMR (62.5 MHz, DMSO-$d^6$), δ(ppm): 176.50 (C=S), 169.51 (C=O), 150.24, 140.39, 133.53, 132.77, 132.27,131.50, 128.66, 128.59, 113.19, 107.09. Anal. Calcd. for **$C_{21}H_{17}ClCuN_5O_6S_2$** (%): C,42.14; H, 2.86; N,11.70. Found (%): C, 42.30; H, 3.00; N, 11.69.

### 2.2.3.12 Synthesis of $[Cu(L^{3a})_2]ClO_4$ (2.12)

Using the same procedure as described for **2.1** was followed by using: $Cu(ClO_4)_2.6H_2O$ (0.106 g, 0.29 mmol) and **$L^{3a}$** (0.25 g, 0.57 mmol). Yield: (0.17 g, 69%); orange powder; ESI-MS *(m/z)*(%): 933.09 [M+] (100%); Mass: 933.1029, Calc. Mass: 933.1045; FT-IR ($cm^{-1}$): ν(N-H) 3340, ν(C=O) 1667, ν(C=S) 1252; ν(Cl-O) 1096, 621; UV-vis. spectrum, $\lambda_{max}$ nm, (εM, $M^{-1}$ $cm^{-1}$): 268(40950), 336(24600); $^{1}$H NMR (250 MHz, DMSO-$d^6$), δ(ppm): 12.15 (4H, s, 4N-$H_A$), 11.73 (4H, s, 4N-$H_B$), 8.23 (8H, d, Ar $J_{HH}$ =2.5 Hz), 8.14 (2H, t, Py $J_{HH}$ =5 Hz), 8.02 (4H, d, Py, $J_{HH}$ =5 Hz), 7.64 (4H, t, Ar $J_{HH}$ =5 Hz), 7.56 (8H, Ar $J_{HH}$ =5 Hz). $^{13}$C NMR (62.5 MHz, DMSO-$d^6$), δ(ppm): 176.42 (C=S), 168.78 (C=O), 162.32, 141.10, 133.58, 132.20, 129.05, 128.67, 114.61. Anal. Calcd. for **$C_{42}H_{34}ClCuN_{10}O_8S_4$** (%): C, 48.79; H, 3.31; N, 13.55. Found (%): C, 48.46; H, 2.92; N, 13.47.

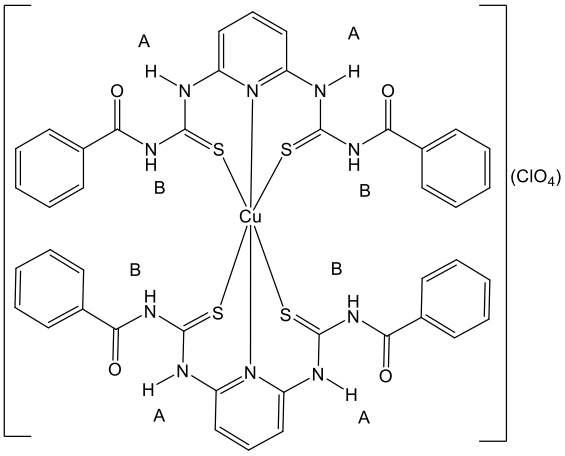

### 2.2.3.13 Synthesis of $[Ni(L^{3a})_2](ClO_4)_2$ (2.13)

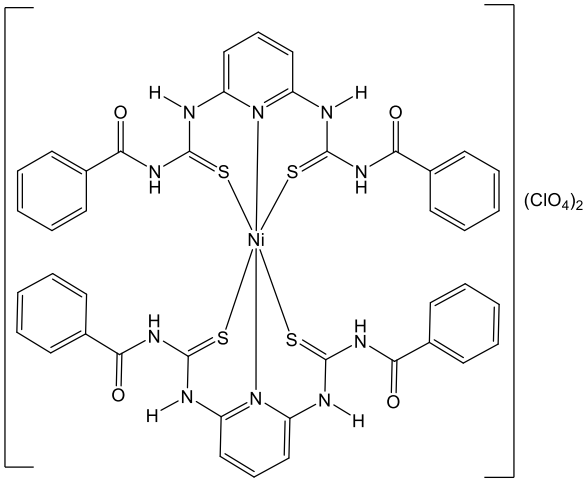

$[Ni(L^{3a})_2](ClO_4)_2$ was obtained by using the same procedure as described for **2.3**: $Ni(ClO_4)_2.6H_2O$ (0.11 g, 0.29 mmol) and $\mathbf{L^{3a}}$ (0.25 g, 0.57 mmol). Yield: (0.17 g, 71%); green powder; ESI-MS *(m/z)*(%): 928.10 [M+] (100%); Mass: 928.2207, Calc. Mass: 928.2233; FT-IR ($cm^{-1}$): ν(N-H) 3469, ν(C=O) 1663, ν(C=S) 1277; ν(Cl-O) 1064, 627; UV-vis. spectrum, $\lambda_{max}$ nm, (εM, $M^{-1}$ $cm^{-1}$): 281(24300), 331(14200), 413(212), 583(21), 936(12); Anal. Calcd. for $\mathbf{C_{42}H_{34}Cl_2N_{10}NiO_{12}S_4}$ (%): C, 44.70; H, 3.04; N, 12.41. Found (%): C, 44.67; H, 2.68; N, 12.39.

### 2.2.3.14 Synthesis of $[Zn(L^{3C*})_2](ClO_4)_2$ (2.14)

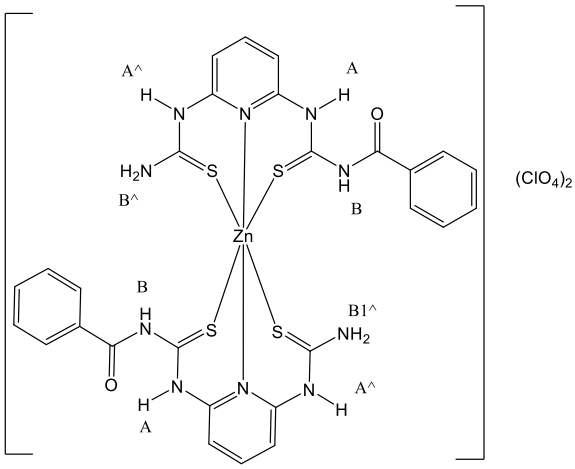

Using the same procedure as described for **2.5** was followed by using: $Zn(ClO_4)_2.6H_2O$ (0.214 g, 0.57 mmol) and $\mathbf{L^{3a}}$ (0.5 g, 1.1 mmol). Yield: (0.32 g, 65%); white powder; ESI-MS *(m/z)*(%): 934.09 [M+] (100%); Mass: 934.1150, Calc. Mass: 934.1169; FT-IR ($cm^{-1}$): ν(N-H) 3318, ν(C=O) 1664, ν ν(C=S) 1273; ν(Cl-O) 1095, 627; UV-vis. spectrum, $\lambda_{max}$ nm, (εM, $M^{-1}$ $cm^{-1}$): 281(29900), 326(20800); $^1$H NMR (250 MHz, DMSO-$d^6$), δ(ppm): 12.86 (2H, s, 2N-$H_A$), 11.67 (2H, s, 2N-$H_{A^\wedge}$), 10.61 (2H, s, 2N-$H_B$), 10.05 (2H, s, 2N-H($NH_{2B^\wedge}$)), 9.00 (2H, s, 2N-H($NH_{2B1^\wedge}$)), 7.94-7.99 (4H, m, 2H py + ,2H -Ar ), 7.84 (4H, d, Ar $J_{HH}$ =7.5 Hz), 7.66 (4H, t, Ar, $J_{HH}$ =7.5 Hz), 7.44 (2H, d, Py $J_{HH}$ =7.5 Hz), 7.02 (2H, d, py $J_{HH}$ =10 Hz).$^{13}$C NMR (62.5 MHz, DMSO-$d^6$), δ(ppm): 180.23 (C=S), 178.09 (C=S), 168.13 (C=O), 152.04, 148.35, 140.66, 133.51, 132.27, 128.94, 128.65, 109.97, 109.76. Anal. Calcd. for **$C_{28}H_{26}Cl_2N_{10}O_{10}S_4Zn$ (%)**: C, 36.28; H, 2.83; N, 15.11. Found (%): C, 35.90; H, 2.66; N, 14.95.

### 2.2.3.15 Synthesis of $[Cu(L^{1b})_2](ClO_4)$ (2.15)

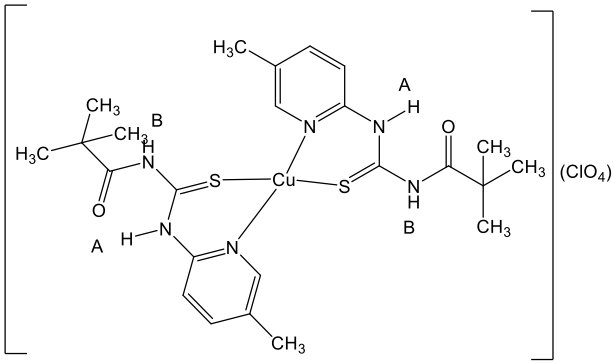

Using the same procedure as described for **2.1** was followed by using: $Cu(ClO_4)_2.6H_2O$ (0.22 g, 0.59 mmol) $\mathbf{L^{1b}}$ (0.298 g, 1.2 mmol). Orange crystals of **2.15** were grown at room temperature by the diffusion of diethyl ether vapor into a $CHCl_3$ solution. Yield: (0.2 g, 70%); yellow crystals; ESI-MS *(m/z)*(%): 565.15 [M+] (100%); Mass: 565.1482, Calc. Mass: 565.1481; FT-IR ($cm^{-1}$): ν(N-H) 3358, ν(C=O) 1676, ν(C=S) 1283; ν(Cl-O) 1096, 621; UV-vis. spectrum, $\lambda_{max}$ nm, (εM, $M^{-1}$ $cm^{-1}$): 254(23900), 307(22000); $^1$H NMR (400 MHz, acetonitrile-$d^3$), δ(ppm): 13.60 (2H, s, 2N-$H_A$), 9.09 (2H, s, 2N-$H_B$), 8.15 (2H, s, py), 7.75 (2H, d, Py $J_{HH}$= 5 Hz), 7.45 (2H, d, Py $J_{HH}$= 5 Hz), 2.29 (6H, s, 2$CH_3$), 1.29 (18H, s, 6$CH_3$). $^{13}$C NMR (100 MHz, acetonitrile-$d^3$), δ(ppm): 182.39 (C=S), 176.90 (C=O), 149.41, 148.51, 141.72, 133.93, 118.97, 41.21, 26.36 ($CH_3$), 18.19 ($CH_3$). Anal. Calcd. for $\mathbf{C_{24}H_{34}ClCuN_6O_6S_2}$ (%): C, 43.30; H, 5.15; N, 12.62. Found (%): C, 43.34; H, 5.06; N, 12.57.

### 2.2.3.16 Synthesis of $[Cu(L^{1b})Cl]$ (2.16)

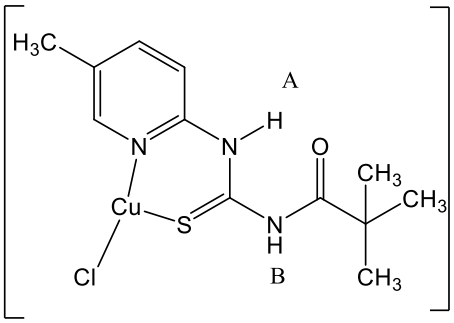

A solution of $\mathbf{L^{1b}}$ (0.30 g, 1.2 mmol) in $CHCl_3$ (4 $cm^3$) was added to a solution of $CuCl_2.2H_2O$ (0.10 g, 0.6 mmol) in methanol (4 $cm^3$)**.** The mixture was stirred for 4 hours at room temperature. The colorless solution turned orange with precipitate. The orange precipitate formed was filtered, washed with $CHCl_3$ (20 $cm^3$) to remove unreacted ligand, and dried under vaccum. Red crystals of **2.16** were grown at room temperature by the diffusion of diethyl ether vapor into a chloroform solution. Yield: (0.26 g, 88%); ESI-MS (m/z)(%): 371.13 [M+Na] (80%); FT-IR ($cm^{-1}$): ν(N-H) 3450, ν(C=O) 1673, ν(C=S) 1275; UV-vis. spectrum, $\lambda_{max}$ nm, (εM,

$M^{-1}$ $cm^{-1}$): 293(9500), 318(7600); $^{1}$H NMR (400 MHz, $CDCl_3$), δ(ppm): 13.73 (1H, s, N-$H_A$), 9.67 (1H, s, 1N-$H_B$), 8.50 (1H, s, py ), 7.67 (1H, d, Py $J_{HH}$= 5Hz), 7.17 (1H, d, Py $J_{HH}$= 5 Hz), 2.38 (3H, s, 1$CH_3$), 1.43 (9H, s, 3$CH_3$). $^{13}$C NMR (125 MHz, $CDCl_3$), δ(ppm): 181.94 (C=S), 174.69 (C=O), 149.19, 146.70, 140.06, 132.60, 117.88, 40.96, 26.65, 17.95. Anal. Calcd. for **$C_{12}H_{17}ClCuN_3OS$** (%): C,41.14; H, 4.89; N,11.99. Found (%): C, 40.94; H, 4.65; N, 12.04.

### 2.2.3.17 Synthesis of $[Ni(L^{1b})_2](ClO_4)_2$ (2.17)

$[Ni(L^{1b})_2](ClO_4)_2$ was obtained by using the same procedure as described for **2.3**: $Ni(ClO_4)_2.6H_2O$ (0.255 g, 0.7 mmol) and **$L^{1b}$** (0.35 g, 1.4 mmol). Yield: (0.27 g, 78%); brown powder; ESI-MS *(m/z)*(%): 559.15 [M+] (100%); Mass: 559.1451, Calc. Mass: 559.1460; FT-IR ($cm^{-1}$): ν(N-H) 3321, ν(C=O) 1675, ν(C=S) 1287, ν(Cl-O) 1092, 626; UV-vis. spectrum, $\lambda_{max}$ nm, (εM, $M^{-1}$ $cm^{-1}$): 257(9100), 304(9250), 390(329), 597(11); $^{1}$H NMR (250 MHz, DMSO-$d^6$), δ(ppm): 13.15 (2H, s, 2N-$H_A$), 10.74 (2H, s, 2N-$H_B$), 8.56 (2H, d, py $J_{HH}$= 5 Hz ), 8.23 (2H, s, Py), 7.69 (2H, d, Py $J_{HH}$= 10 Hz), 2.27 (6H, s, 2$CH_3$), 1.24 (18H, s, 6$CH_3$). $^{13}$C NMR (62.5 MHz, DMSO-$d^6$), δ(ppm): 177.23 (C=S), 174.83 (C=O), 161.21, 147.56, 137.53, 125.84, 114.22, 40.00, 25.52 ($CH_3$), 17.02 ($CH_3$). Anal. Calcd. for **$C_{24}H_{34}Cl_2N_6NiO_{10}S_2$** (%): C,37.92; H, 4.51; N,11.05. Found (%): C, 37.80; H, 4.58; N, 10.97.

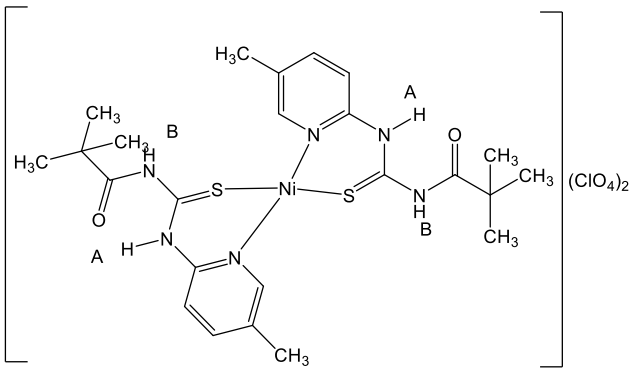

### 2.2.3.18 Synthesis of $[Zn(L^{1C})_2](ClO_4)_2$ (2.18)

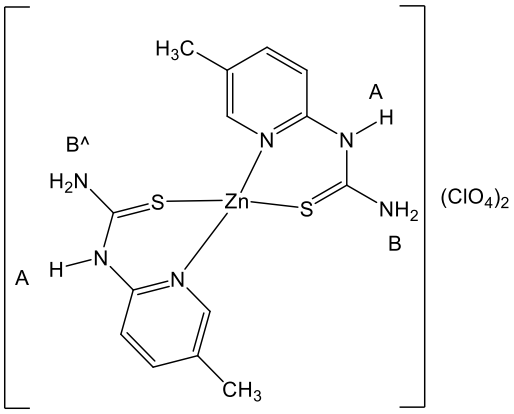

Using the same procedure as described for **2.4** was followed by using: $Zn(ClO_4)_2.6H_2O$ (0.22 g, 0.6 mmol) and $\mathbf{L^{1b}}$ (0.3 g, 1.2 mmol). Yield: (0.2 g, 69%); white powder; ESI-MS *(m/z)*(%): 397.02 [M+] (100%); Mass: 397.0235, Calc. Mass: 397.0248; FT-IR ($cm^{-1}$): ν(N-H) 3485, ν(C=S) 1280; ν(Cl-O) 1053, 627; UV-vis. spectrum, $\lambda_{max}$ nm, (εM, $M^{-1}$ $cm^{-1}$): 273(8500), 299(8100); $^1$H NMR (250 MHz, DMSO-$d^6$), δ(ppm): 10.52 (2H, s, 2N-$H_A$), 10.47 (2H, s, 2N-H($NH_{2B}$)), 8.82 (2H, s,2N-H($NH_{2B^\wedge}$)) 8.06 (2H, s, py ), 7.60 (2H, d, Py $J_{HH}$= 10 Hz), 7.06 (2H, d, Py $J_{HH}$= 7.5 Hz), 2.21 (6H, s, $2CH_3$). $^{13}$C NMR (62.5 MHz, DMSO-$d^6$), δ(ppm): 180.38 (C=S), 151.81, 145.48, 139.84, 126.95, 112.47, 17.34 ($CH_3$). Anal. Calcd. for **$C_{14}H_{18}Cl_2N_6O_8S_2Zn$** (%): C, 28.09; H, 3.03; N, 14.04. Found (%): C, 28.16 ; H, 3.01 ; N, 14.12.

### 2.2.3.19 Synthesis of $[Cu(L^{2b})_2](ClO_4)$ (2.19)

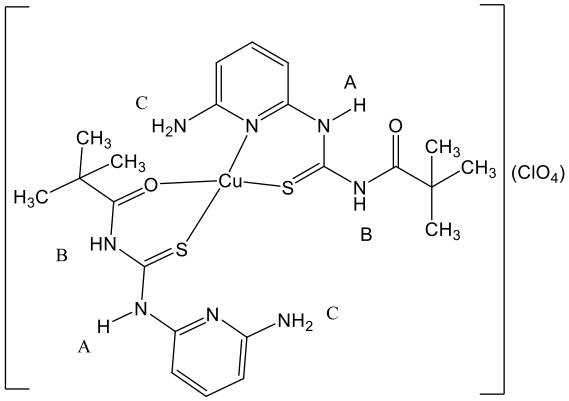

The same procedure as described for **2.1** was followed by using: A solution of $Cu(ClO_4)_2.6H_2O$ (0.26 g, 0.69 mmol) and $\mathbf{L^{2b}}$ (0.35 g, 1.4 mmol). Yield: (0.29 g, 83%); brown precipitate; ESI-MS *(m/z)*(%): 567.20 [M+] (100%); Mass: 567.1367, Calc. Mass: 567.1386; FT-IR ($cm^{-1}$): ν(N-H) 3343, ν(C=O) 1671, ν(C=S) 1267; ν(Cl-O) 1079, 625; UV-vis. spectrum $\lambda_{max}$ nm, (εM, $M^{-1}$ $cm^{-1}$): 230(12000), 268(6400), 296(4300), 332(5650); $^1$H NMR (250 MHz, acetonitrile-$d^3$), δ(ppm): 13.25 (2H, s, 2N-$H_A$), 8.94 (2H, s, 2N-$H_B$), 7.54 (2H, t, py $J_{HH}$= 7.5 Hz ), 7.01 (2H, d, Py $J_{HH}$= 7.5 Hz), 6.50 (2H, d, Py $J_{HH}$= 10 Hz), 5.37 (4H, s, 4N-H($2NH_{2C}$)), 1.26 (18H, s, $6CH_3$). $^{13}$C NMR (62.5 MHz, acetonitrile-$d^3$), δ(ppm): 182.51 (C=S), 176.62 (C=O), 159.48, 149.07, 141.61, 41.38, 27.18 ($CH_3$). Anal. Calcd. for

**$C_{22}H_{32}ClCuN_8O_6S_2$** (%): C, 39.58; H, 4.83; N, 16.78. Found (%): C, 39.37; H, 4.70 ; N, 16.46.

### 2.2.3.20 Synthesis of $[Cu(L^{2b*})_2Cl_2]$ (2.20)

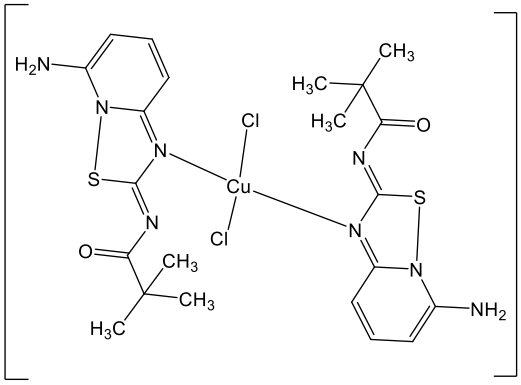

A solution of $CuCl_2.6H_2O$ (0.1 g, 0.59 mmol) in methanol (4 $cm^3$) was added to a solution of **$L^{2b}$** (0.3 g, 1.2 mmol) in $CHCl_3$ (8 $cm^3$). The mixture was stirred for 3 hours at room temperature. The colorless solution turned orange with precipitate. The orange precipitate formed was filtered, washed with $CHCl_3$ (20 $cm^3$) to remove unreacted ligand, and dried under vaccum**.** Dark orange crystals of **2.20** were grown at room temperature by the diffusion of diethyl ether vapor into an mixture DCM:ethanol(1:1) solution of it. Yield: (0.18 g, 61%); Dark green crystals ;ESI-MS (m/z)(%): 667.04 [M+meOH] (100%); FT-IR ($cm^{-1}$): ν(N-H) 3320, ν(C=O) 1683, ν(C=S) 1273; UV-vis. spectrum $\lambda_{max}$ nm, (εM, $M^{-1}$ $cm^{-1}$): 264(26900), 282(22800), 326(22100), 470(139). Anal. Calcd. for **$C_{22}H_{28}Cl_2CuN_8O_2S_2$** (%): C,41.61; H, 4.44; N,17.64. Found (%): C, 41.28; H, 4.43; N, 17.25.

### 2.2.3.21 Synthesis of $[Ni(L^{2C})_2](ClO_4)_2$ (2.21)

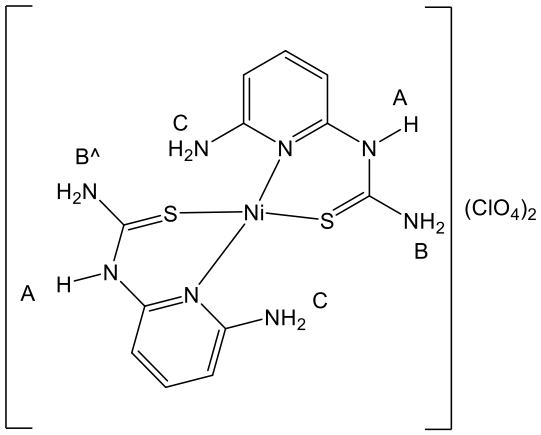

$[Ni(L^{2C})_2](ClO_4)_2$ was obtained by using the same procedure as described for **2.2**: $Ni(ClO_4)_2.6H_2O$ (0.25 g, 0.69 mmol) and **$L^{2b}$** (0.35 g, 1.4 mmol). Yield: (0.24 g, 69%); brown powder; ESI-MS *(m/z)*(%): 393.06 [M+] (90%); Mass: 393.0206 Calc. Mass: 393.0215, FT-IR ($cm^{-1}$): ν(N-H) 3321, ν(C=S) 1270; ν(Cl-O) 1073, 627; UV-vis. spectrum, $\lambda_{max}$ nm, (εM, $M^{-1}$ $cm^{-1}$): 215(16900), 251(20050), 272(18950), 319(22950), 401(205), 603(17); $^1$H NMR

(250 MHz, DMSO-$d^6$), δ(ppm): 10.61 (2H, s, 2N-$H_A$), 10.05 (2H, s, 2N-H($NH_{2B}$)), 8.66 (2H, s, 2N-H($NH_{2B^\wedge}$)), 7.28 (2H, t, Py, $J_{HH}$ = 7.5 Hz), 6.20 [(6H, m, 4N-H($2NH_{2C}$)+ 2H (Py)], 6.00 (2H, d, Py, $J_{HH}$ =7.5 Hz), $^{13}$C NMR (62.5 MHz, DMSO-$d^6$), δ(ppm): 179.99 (C=S), 157.50, 139.08, 129.08, 128.78, 100.98, 98.88. Anal. Calcd. for **$C_{12}H_{16}Cl_2N_8NiO_8S_2$** (%): C,24.26; H, 2.72; N,18.86. Found (%): C, 24.20; H, 2.83; N, 18.79.

### 2.2.3.22 Synthesis of $[Ni(L^{2b})_2](ClO_4)_2$ (2.22)

$[Ni(L^{2b})_2](ClO_4)_2$ was obtained by using the same procedure as described for **2.3**: $Ni(ClO_4)_2.6H_2O$ (0.36 g, 1 mmol) and **$L^{2b}$** (0.5 g, 2 mmol) Yield: (0.38 g, 76%); brown powder; ESI-MS *(m/z)*(%): 561.09 [M+] (100%); Mass: 561.1361, Calc. Mass: 561.1365; FT-IR ($cm^{-1}$): ν(N-H) 3377, ν(C=O) 1664, ν(C=S) 1277; ν(Cl-O) 1071, 627; UV-vis. spectrum, $\lambda_{max}$ nm, (εM, $M^{-1}$ $cm^{-1}$): 232(41600), 268(24100), 294(15500), 328(21550), 410(340), 606(7); $^1$H NMR (250 MHz, DMSO-$d^6$), δ(ppm): 12.91 (2H, s, 2N-$H_A$), 10.56 (2H, s, 2N-$H_B$), 7.88 (2H, d, py $J_{HH}$ = 7.5 Hz ), 7.42 (2H, t , py $J_{HH}$ = 7.5 Hz ), 6.28 (2H, d , py $J_{HH}$ = 7.5 Hz ), 6.10 (4H, s, 4N-H($2NH_{2C}$)), 1.22 (18H, s, $6CH_3$). $^{13}$C NMR (62.5 MHz, DMSO-$d^6$), δ(ppm): 179.81 (C=S), 176.03 (C=O), 158.53, 148.85, 138.08, 105.48, 102.15, 30.37, 25.81 ($CH_3$). Anal. Calcd. for **$C_{22}H_{32}Cl_2N_8NiO_{10}S_2$** (%): C,34.67; H, 4.23; N,14.70. Found (%): C, 34.58; H, 4.29; N, 14.72.

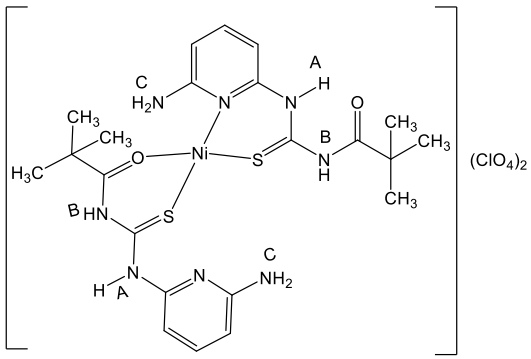


### 2.2.3.23 Synthesis of $[Zn(L^{2C})_2](ClO_4)_2$ (2.23)

Using the same procedure as described for **2.4** was followed by using: $Zn(ClO_4)_2.6H_2O$ (0.25 g, 0.67 mmol) and **$L^{2b}$** (0.34 g, 1.3 mmol). Yield: (0.27 g, 81%); white powder; ESI-MS (m/z)(%): 399.05 [M+] (100%); Mass: 399.0000, Calc. Mass: 399.0000; FT-IR

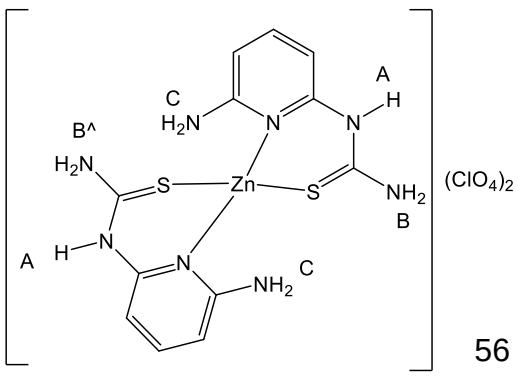

($cm^{-1}$): ν(N-H) 3370, ν(C=S) 1275; ν(Cl-O) 1071, 626**;** UV-vis. spectrum, $\lambda_{max}$ nm, (εM, $M^{-1}$ $cm^{-1}$): 214(28200), 251(34100), 272(31750), 320(38250); $^{1}$H NMR (250 MHz, DMSO-$d^6$), δ(ppm): 10.63 (2H, s, 2N-$H_A$), 10.06 (2H, s, 2N-H($NH_{2B}$)), 8.68 (2H, s, 2N-H($NH_{2B^{\wedge}}$)), 7.29 (2H, t, Py, $J_{HH}$ =2.5 Hz), 6.22 [(6H, m, 4N-H($2NH_{2C}$)+ 2H (Py)], 6.02 (2H, d, Py, $J_{HH}$ =5 Hz),$^{13}$C NMR (62.5 MHz, DMSO-$d^6$),δ(ppm): 180.05 (C=S), 157.74, 152.40, 139.39, 101.00, 98.79. Anal. Calcd. for **$C_{12}H_{16}Cl_2N_8O_8S_2Zn$** (%): C,23.99; H, 2.68; N,18.65. Found (%): C, 24.13; H, 2.73; N, 18.48.

### 2.2.3.24 Synthesis of $[Cu(L^{3b})]ClO_4$ (2.24)

Using the same procedure as described for **2.1** was followed by using: $Cu(ClO_4)_2.6H_2O$ (0.328 g, 0.89 mmol) and $\mathbf{L^{3b}}$ (0.35 g, 0.89 mmol). Yellow crystals of **2.24** were grown at room temperature by the diffusion of diethyl ether vapor into a mixture of ethanol:DCM(3:1) solution. Yield: (0.28 g, 80%); brown powder; ESI-MS *(m/z)*(%): 458.06 [M+] (100%); Mass: 458.0869, Calc. Mass: 458.0871; FT-IR ($cm^{-1}$): ν(N-H) 3400, ν(C=O) 1688, ν(C=S) 1277; ν(Cl-O) 1090, 625; UV-vis. spectrum, $\lambda_{max}$ nm, (εM, $M^{-1}$ $cm^{-1}$): 298(6650), 350(6500); $^{1}$H NMR (250 MHz, DMSO-$d^6$), δ(ppm): 11.99 (2H, s, 2N-$H_A$), 11.00 (2H, s, 2N-$H_B$), 8.17 (1H, t, py $J_{HH}$ =7.5 Hz), 7.94 (1H, d, py $J_{HH}$ =7.5 Hz), 7.64 (1H, d, py, $J_{HH}$ =7.5 Hz), 1.29 (18H, s, $6CH_3$). $^{13}$C NMR (62.5 MHz, DMSO-$d^6$), δ(ppm): 187.38 (C=S), 181.39 (C=O), 149.85, 140.40, 139.85, 112.84, 107.67, 26.23 ($CH_3$), 25.84, 25.32 ($CH_3$), 24.96**.** Anal. Calcul. For **$C_{17}H_{25}ClCuN_5O_6S_2$ (%)**: C, 36.56; H, 4.51; N, 12.54. Found (%): C, 36.31; H, 4.41; N, 12.68.

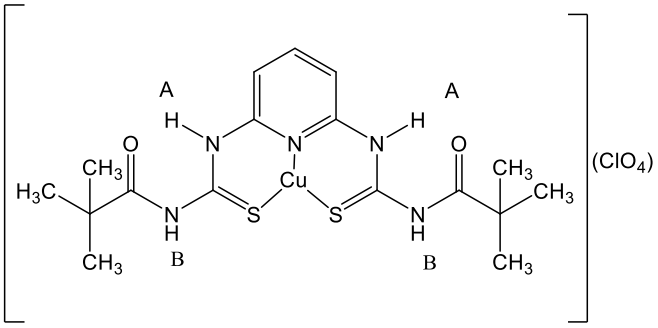

### 2.2.3.25 Synthesis of $[Cu(L^{3b})_2]ClO_4$ (2.25)

Using the same procedure as described for **2.1** was followed by using: $Cu(ClO_4)_2.6H_2O$ (0.164 g, 0.44 mmol) and $\mathbf{L^{3b}}$ (0.35 g, 0.89 mmol). Yield: (0.23 g, 68%); brown powder; ESI-MS *(m/z)*(%): 853.22 [M+] (100%); Mass: 853.2191, Calc. Mass: 853.2195; FT-IR ($cm^{-1}$): ν(N-H) 3397, ν(C=O) 1690, ν(C=S) 1277; ν(Cl-O) 1077, 624; UV-vis. Spectrum, $\lambda_{max}$ nm, (εM, $M^{-1}$ $cm^{-1}$): 278(20700), 290(20750), 326(14800); $^1$H NMR (250 MHz, acetonitrile-$d^3$), δ(ppm): 13.64 (4H, s, 4N-$H_A$), 9.18 (4H, s, 4N-$H_B$), 7.99 (2H, t , py $J_{HH}$ =7.5 Hz), 7.73 (4H, d, py $J_{HH}$ =10 Hz), 1.29 (36H, s, 12$CH_3$). $^{13}$C NMR (62.5 MHz, acetonitrile-$d^3$), δ(ppm): 182.79 (C=S), 178.32 (C=O), 149.38, 143.13, 117.19, 41.85, 26.96 ($CH_3$). Anal. Calcul. For **$C_{34}H_{50}ClCuN_{10}O_8S_4$ (%)**: C, 42.80; H, 5.28; N, 14.68. Found (%): C, 42.46; H, 4.93; N, 14.63.

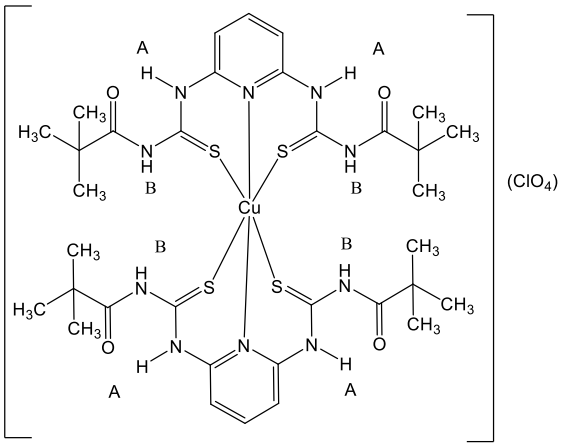


### 2.2.3.26 Synthesis of $[Ni(L^{3b})_2](ClO_4)_2$ (2.26)

$[Ni(L^{3b})_2](ClO_4)_2$ was obtained by using the same procedure as described for **2.3**: $Ni(ClO_4)_2.6H_2O$ (0.14 g, 0.38 mmol) and $\mathbf{L^{3b}}$ (0.3 g, 0.76 mmol). Yield: (0.2 g, 67%); green powder; ESI-MS *(m/z)*(%): 847.25 [M+] (100%); Mass: 847.2164, Calc. Mass: 847.2175; FT-IR ($cm^{-1}$): ν(N-H) 3312, ν(C=O) 1687, ν(C=S) 1262; ν(Cl-O) 1090, 626; UV-vis. spectrum, $\lambda_{max}$ nm, (εM, $M^{-1}$ $cm^{-1}$): 267(38800), 323(39050), 421(242), 591(5), 952(3). Anal. Calcul. For **$C_{34}H_{50}Cl_2N_{10}NiO_{12}S_4$ (%)**: C, 38.94; H, 4.81; N, 13.36. Found (%): C, 39.10; H, 4.72; N, 13.46.

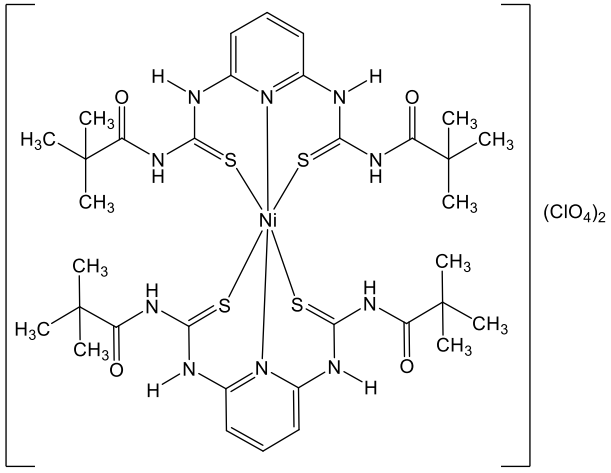

### 2.2.3.27 Synthesis of $[Zn(L^{3C})_2](ClO_4)_2$ (2.27)

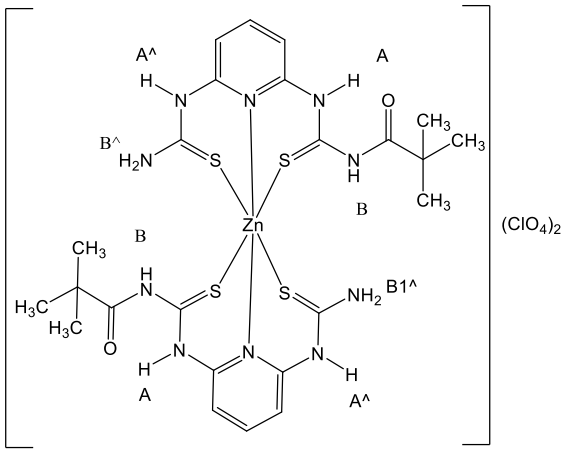


Using the same procedure as described for **2.5** was followed by using: $Zn(ClO_4)_2.6H_2O$ (0.165 g, 0.44 mmol) and $\mathbf{L^{3b}}$ (0.35 g, 0.89 mmol). Yield: (0.26 g, 74%); white powder; ESI-MS *(m/z)*(%): 685.09 [M+] (100%); Mass: 685.0972, Calc. Mass: 685.0962; FT-IR ($cm^{-1}$): ν(N-H) 3317, ν(C=O) 1689, ν(C=S) 1258; ν(Cl-O) 1075, 626; UV-vis. spectrum, $\lambda_{max}$ nm, (εM, $M^{-1}$ $cm^{-1}$): 282(27500), 326(21200); $^1$H NMR (250 MHz, DMSO-$d^6$), δ(ppm): 12.93 (2H, s, 2N-$H_A$), 10.77 (2H, s, 2N-H($NH_{2B^\wedge}$)), 10.60 (2H, s, 2N-H($NH_{2B^\wedge 1}$)), 10.00 (2H, s, 2N-$H_{A^\wedge}$), 8.99 (2H, s, 2N-$H_B$ ), 7.91 (2H, d, py $J_{HH}$ =7.5 Hz), 7.82 (2H, t, py $J_{HH}$ =7.5 Hz), 7.01 (2H, d, py, $J_{HH}$ =7.5 Hz), 1.25 (18H, s, 6 $CH_3$). $^{13}$C NMR (62.5 MHz, DMSO-$d^6$), δ(ppm): 180.23, 180.39 (C=S), 178.28 (C=O), 151.88, 148.22, 140.66, 110.09, 40.27, 26.30 ($CH_3$). Anal. Calcul. For $\mathbf{C_{24}H_{34}Cl_2N_{10}O_{10}S_4Zn}$ (%): C, 32.49; H, 3.86; N, 15.79. Found (%): C, 32.28; H, 3.54; N, 15.54.

## 2.3 Results and discussion

### 2.3.1 Synthesis of ligands $L^{1a}$-$L^{3a}$ and $L^{1b}$-$L^{3b}$

Two series of substituted thioureas were prepared by a modification of the method described by Kaminsky *et al*, [77] to evaluate the coordination properties of a set of thiourea derivatives with varied substitution patterns. The synthesis of the ligands $\mathbf{L^{1a}}$-$\mathbf{L^{3a}}$ and $\mathbf{L^{1b}}$-$\mathbf{L^{3b}}$ required the preparation of benzoyl isothiocyanate and pivaloyl isothiocyanate respectively as a first step, by refluxing for 3 hours a mixture of benzoyl chloride or pivaloyl chloride with potassium thiocyanate in acetonitrile. The final compounds $\mathbf{L^{1a}}$-$\mathbf{L^{3a}}$ and $\mathbf{L^{1b}}$-$\mathbf{L^{3b}}$ were obtained by refluxing the two primary amines, (either 2-amino-5-methyl pyridine or 2,6-diamino pyridine) with benzoyl isothiocyanate or pivaloyl isothiocyanate in acetonitrile for approximately 15 hours (**Scheme 2.3**). The crude compounds of $\mathbf{L^{1a}}$, $\mathbf{L^{2a}}$ and $\mathbf{L^{3a}}$ were purified by washing

in acetonitrile and were then recrystallized from a $CHCl_3$:ethanol solution to obtain white crystals of $\mathbf{L^{1a}}$ and $\mathbf{L^{3a}}$ and yellow crystals of $\mathbf{L^{2a}}$. While crude compounds of $\mathbf{L^{1b}}$, $\mathbf{L^{2b}}$ and $\mathbf{L^{3b}}$ were recrystallized from ethanol to obtain white crystals of pure ligand, $\mathbf{L^{1a}}$-$\mathbf{L^{3b}}$ were obtained in good yields (79-91%). $\mathbf{L^{1a}}$-$\mathbf{L^{3b}}$ are soluble in DMF and DMSO. $\mathbf{L^{1a}}$ and $\mathbf{L^{2a}}$ are partially soluble in acetone, acetonitrile, alcohol, ethyl acetate, $CHCl_3$ and DCM while $\mathbf{L^{1b}}$ and $\mathbf{L^{2b}}$ are completely soluble in these solvents. $\mathbf{L^{1a}}$, $\mathbf{L^{2a}}$, $\mathbf{L^{1b}}$ and $\mathbf{L^{2b}}$ are insoluble in n-hexane. $\mathbf{L^{3a}}$ is soluble in DMF, THF and DMSO and insoluble in all organic solvents while $\mathbf{L^{3b}}$ is soluble in all solvents above, except n-hexane.

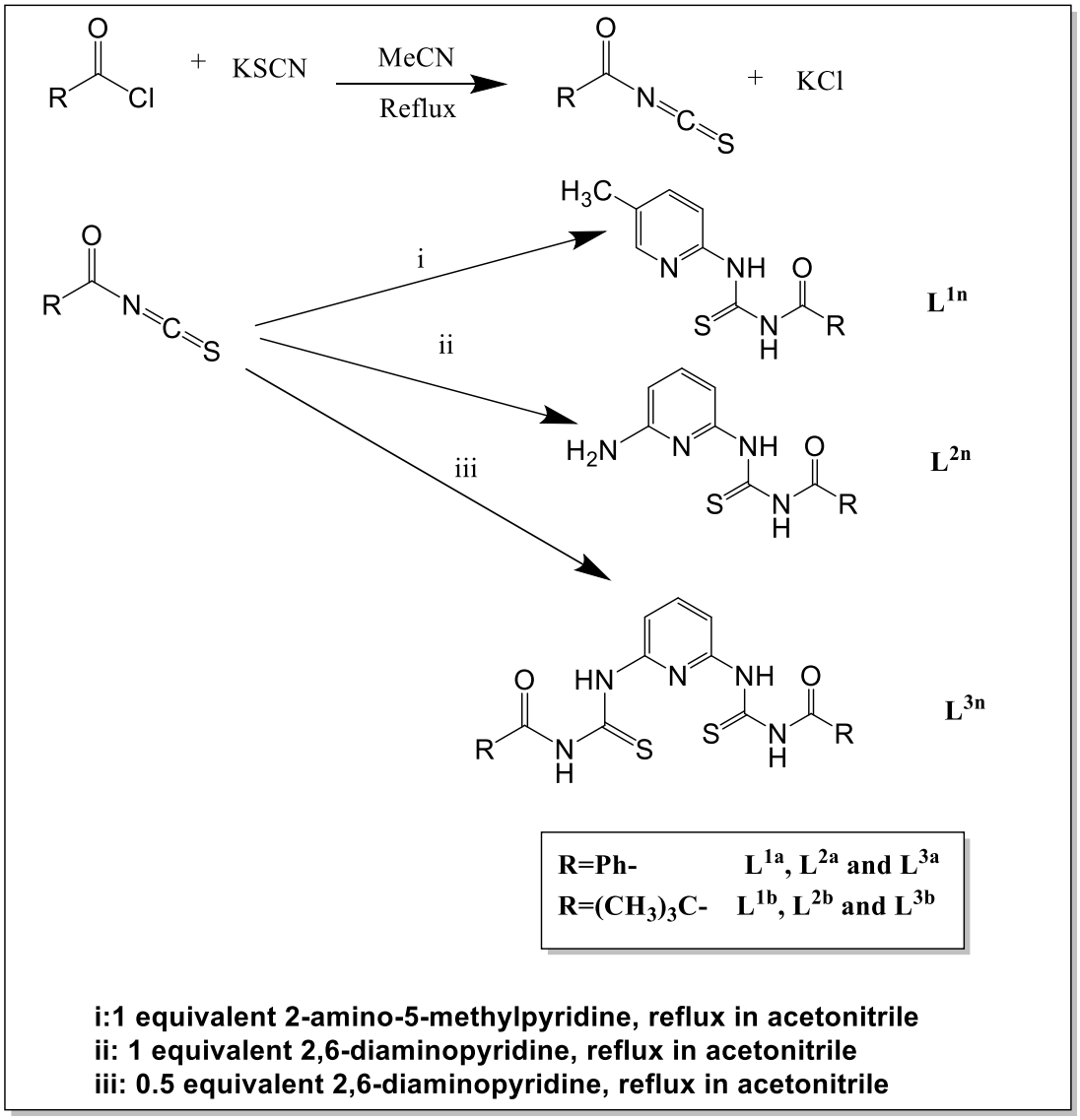


**Scheme 2.3:** Synthesis of the ligands $\mathbf{L^{1a}}$-$\mathbf{L^{3b}}$. (reaction conditions and reagents)

## 2.3.2 Synthesis of complexes (2.1- 2.27)

The reaction between **$L^{1a}$-$L^{3a}$** or **$L^{1b}$-$L^{3b}$** with $Cu(ClO_4)_2.6H_2O$ in a 2:1 stoichiometry was carried out in a DMF/water at room temperature. Analytical, spectral and X-ray crystallographic data indicated the formation of the Cu(I) complex, $[Cu^{I}(L)_2](ClO_4)$ (**Scheme 2.4**). Recently, it has been shown that the preparation of complexes of Cu(I) with some thiourea derivatives can be simply accomplished by mixing the solution of ligand and the corresponding Cu(II) salts. It has been reported that in such case the thiourea is also adding as reducing agent, [79-83] however in our experiments this appears unlikely due to the stoichiometry of the reaction.

Although, many researches of Cu(I) complexes have been accomplished by the reaction between thiourea and the Cu(II) salts, the precise mechanism of the conversion of Cu(II) to Cu(I) by using thiourea derivatives has not been reported. The stable and unchanged structure for the thiourea ligand in its Cu(I) complexes here in this chapter lead us to suggest that if the ligand is oxidized it then returns again to its normal oxidation state. In addition, it is possible that the solvents in the reaction may be have any role in the reduction process of Cu(II) to Cu(I). The Cu(I) complexes were isolated as red, orange or yellow solids, were stable at room temperature and completely soluble in DMF and DMSO. The complexes of **$L^{1a}$-$L^{3a}$** are partially soluble in acetone, acetonitrile, alcohol, ethyl acetate, but insoluble in $CHCl_3$, DCM and n-hexane. The complexes of **$L^{1b}$-$L^{3b}$** are completely soluble in acetone, acetonitrile, alcohol, ethyl acetate, $CHCl_3$, DCM and insoluble in n-hexane. Nickel (II) perchlorate complexes were prepared by the reaction of **$L^{1a}$- $L^{3a}$** and **$L^{1b}$- $L^{3b}$** with $Ni(ClO_4)_2.6H_2O$ in a 2:1 ratio in a mixture of $CHCl_3$/ methanol at 50ºC.

Initial work to prepare Ni(II) complexes heated the reaction mixture at 75ºC, but full characterization of these complexes indicated cleavage of at least one or two of the benzoyl or pivaloyl groups. These results led us to carry out the preparation of the complexes by heating the solution to lower temperatures (50ºC) to obtain complexes without cleavage. The analytical, spectral and crystallographic data showed the formation of **2.3** $[Ni^{II}(L^{1a})_2](ClO_4)_2$ in the reactions at 50ºC

(**Scheme 2.4**). The Ni(II) complexes are stable at room temperature and were collected as brown or green solids and were soluble in acetone, DMF and DMSO.

Four coordinate mononuclear Zn(II) complexes, $[Zn^{II}(L)(L^{C})](ClO_4)_2$ and $[Zn^{II}(L^{C})_2](ClO_4)_2$ were formed as colorless powders by the reaction of $\mathbf{L^{1a}}$-$\mathbf{L^{3b}}$ with $Zn(ClO_4)_2.6H_2O$ (2:1 molar ratio) in a mixture of $CHCl_3$/methanol at room temperature and 75ºC respectively. ($L^{C}$ indicated cleavage of benzoyl or pivaloyl groups from $\mathbf{L^{1a}}$-$\mathbf{L^{3b}}$ after complexation with Zn(II) ion). The zinc complexes formed with the cleavage of one of the acyl moieties in **2.5** and **2.10** at room temperature, or cleavage two in **2.4**, **2.9**, **2.14**, **2.18**, **2.23** and **2.27** when carried out by refluxing the reaction mixture, (**Scheme 2.4**). To explain the reason responsible for the hydrolysis of the amide in the Zn(II) complexes, one should consider the nature of Zn(II) ion; a Lewis acid acting as a catalyst for the acidic hydrolysis of the amide. So in **2.5** and **2.10** one acyl group is cleaved when the reaction was at room temperature, while the high temperature 75ºC helped to lose the second acyl group as well as the Zn(II) ion as acid Lewis to form **2.4**, **2.9**, **2.14**, **2.18**, **2.23** and **2.27**. Zn(II) complexes are soluble in acetone, acetonitrile, DMF and DMSO. The purification of the complexes of Cu(II), Ni(II) and Zn(II) salts was carried out by washing the obtained precipitates with the same solvents used in their synthesis and then recrystallizing from acetonitrile:MeOH, ethyl acetate, $CHCl_3$ or DCM:EtOH solutions. The yields of these complexes were moderate (61-88%).

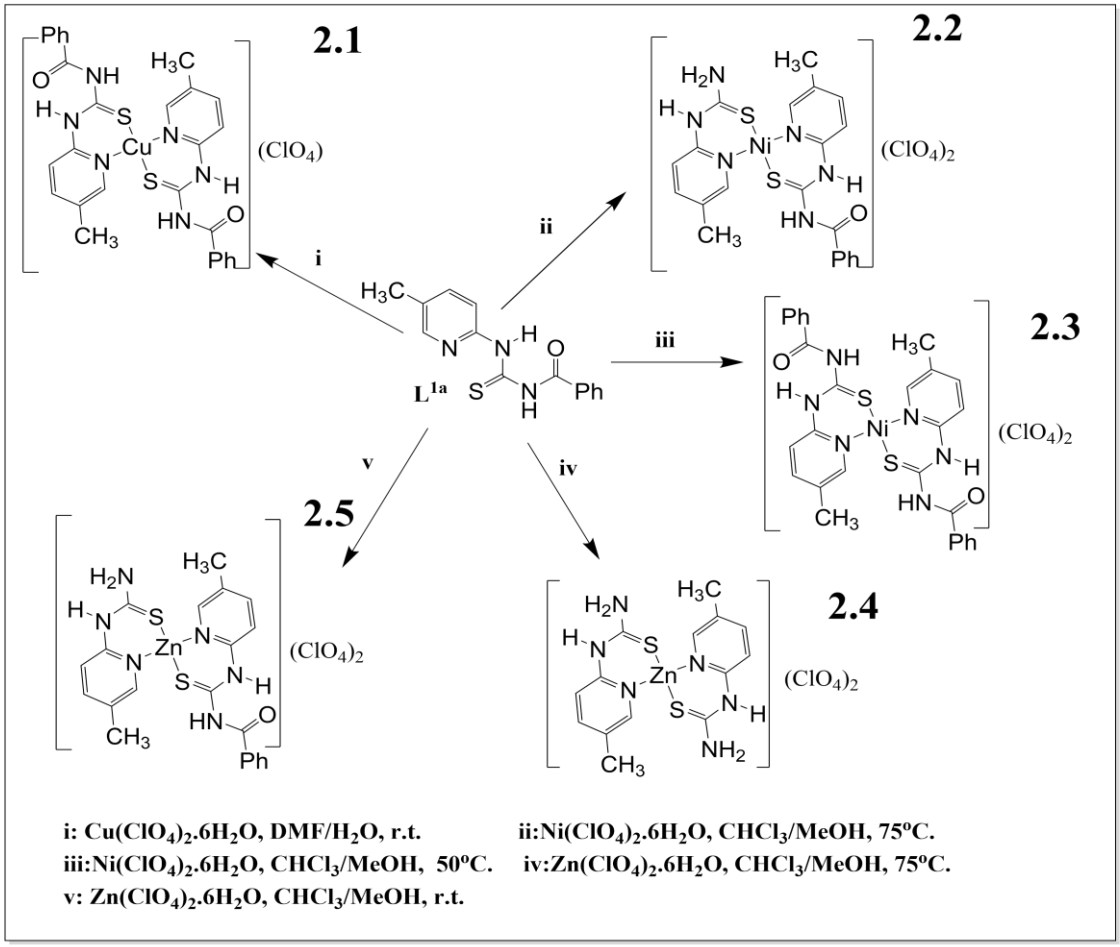


**Scheme 2.4:** Synthesis of the Cu(I), Ni(II) and Zn(II) complexes of **L$^{1a}$** ligand (**2.1**-**2.5**).

Experimental observations on the reactivity of the ligands can be summarized: i) ligands **L$^{1a}$-L$^{3a}$** and **L$^{1b}$-L$^{3b}$** are stable (without cleavage of carbonyl group) in refluxing mixtures of $CHCl_3$:methanol:$H_2O$ (3:3:0.5ml) at 75°C; ii) all prepared Cu(I) complexes are stable (without cleavage of carbonyl group) in refluxing mixture of $CHCl_3$:methanol:$H_2O$ (3:3:0.5ml) at 75°C; iii) all prepared Ni(II) complexes are stable (without cleavage of carbonyl group) in the mixture of $CHCl_3$:methanol:$H_2O$ (3:3:0.5ml) at 50°C, but they suffer from cleavage of carbonyl group at 75°C; iv) Zn(II) complexes demonstrate partial cleavage of one of the carbonyl groups at room temperature.

An interesting result is the Cu(II) complex **2.20.** The characterization of **2.20** reveals a Cu(II) complex where the thiourea has undergone a Hugershoff reaction,[84-86] resulting in a cyclised product. $CuCl_2$ oxidises the ligand **L$^{2b}$** which

then coordinates to the generated ligand **$L^{2b*}$**, forming a dark-green crystals compound. Two hydrogen atoms are removed during the oxidation and cyclizations occur. Each copper ion has a coordination number of four, surrounded by two monodentate ligands **$L^{2b*}$** coordinating through nitrogen atom of the ring and two chloride ions. **Scheme 2.5** shows the proposed method to synthesis **$L^{2b*}$** synthesis. We propose that under reaction conditions, the Cu(I) formed in the Hugershoff reaction undergoes aerial oxidation to Cu(II) which is the complexed by the formed **$L^{2b*}$**.

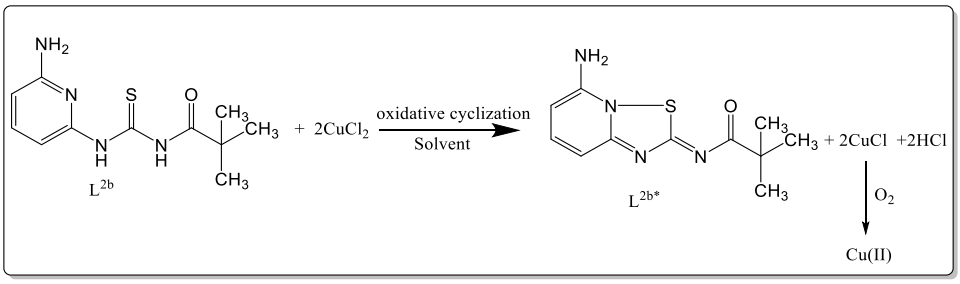


**Scheme 2.5:** the proposed method to synthesis **$L^{2b*}$**.

## 2.3.3 Spectroscopic studies of $L^{1a}$-$L^{3b}$ and their complexes (2.1 – 2.27)

### 2.3.3.1 $^{1}H$ and $^{13}C$ NMR spectra

The $^{1}H$ and $^{13}C$ NMR characterization for the investigated ligands (**$L^{1a}$-$L^{3b}$**) and their complexes with Cu(II), Ni(II) and Zn(II) ions (**2.1**-**2.27**) are listed in the experimental section. They have been recorded in DMSO-$d^6$, $CDCl_3$, acetone-$d^6$ and acetonitrile-$d^3$ solutions.

The $^{1}H$ and $^{13}C$ NMR data for ligands (**$L^{1a}$-$L^{3b}$**) and their complexes were characterized and discussed as two separated groups **$L^{1a}$-$L^{3a}$** and **$L^{1b}$-$L^{3b}$** with their complexes. The $^{1}H$ NMR spectra of the Cu(I), Ni(II) and Zn(II) complexes with **$L^{1a}$-$L^{3a}$** and **$L^{1b}$-$L^{3b}$** are both highly comparable to their ligands, the slight differences arising in the respective chemical shifts. All these complexes protons are more deshielded in comparison to their free ligands. This is due to the decrease in

electron density around the protons as compared to the protons in their corresponding free ligands because of the coordination of sulfur and nitrogen donors to the metal centre. The proton chemical shifts for hydrogen bonded and free N-H (CSNH and CONH respectively) are found around 12.99-13.22 and 11.53–11.85 ppm in **$L^{1a}$**-**$L^{3a}$** and around 12.93-13.19 and 10.58-10.90 ppm in **$L^{1b}$**-**$L^{3b}$**, respectively. The aromatic protons appear in the $^{1}$H NMR spectra for all ligands between 6.30-8.63 ppm. $^{1}$H NMR data for the Cu(I), Ni(II) and Zn(II) complexes showed the existence of aromatic protons in the range 6.49-8.50, 6.00-8.66 and 6.02-8.83 ppm respectively. The N-H peaks for CSNH and CONH were found in the range 14.10-11.99 and 11.74-8.94 ppm respectively for Cu(I) complexes, 13.24-10.61 and 11.71-10.46 for Ni(II) complexes and 12.93-10.46 and 10.61-8.82 ppm for Zn(II) complexes respectively. These changes due to the deshielding of the protons in the complexes by decreasing the electron density on sulfur, nitrogen and oxygen donor atoms through coordination with the metal centre. The 5-methyl pyridine derivative complexes **2.1-2.5** and **2.15-2.18** showed a singlet peak at 2.20-2.29 and 2.21-2.38 ppm respectively, assigned to the methyl group. The other singlet peak which appeared in the range 1.22-1.43 ppm in the pivaloyl group derivative complexes **2.15, 2.16, 2.17, 2.19, 2.22, 2.24, 2.25** and **2.27** were assigned to the methyl groups in the *t*-butyl groups. $^{1}$H NMR spectra for complexes **2.2, 2.4, 2.5, 2.7, 2.9, 2.10, 2.14 2.18, 2.21, 2.23** and **2.27** showed unexpected new peaks in the range 10.00-10.47 and 8.66-9.00 ppm. These new peaks are assigned to the N-H in one or two $NH_2$ groups formed by the cleavage of the benzoyl/pivaloyl groups. $^{1}$H NMR spectra for these complexes also showed the disappearance of the proton signals of the phenyl group in complexes **2.2**, **2.4**, **2.5**, **2.7**, **2.9**, **2.10** and **2.14** and of the *t*-butyl group in complexes **2.18**, **2.21**, **2.23** and **2.27** respectively.

The $^{13}$C NMR spectra of the complexes (**2.1-2.27**) showed the expected number of resonances at typical shifts. The signals observed in the range 102.51-159.03 and 98.79-162.32 ppm were assigned to the aromatic carbons for ligands **$L^{1a}$**-**$L^{3b}$**. The resonances due to the C=O and C=S carbon nuclei in the ligands **$L^{1a}$**-**$L^{3a}$** appeared in the regions of 168.48-168.92 and 177.09-178.47 ppm respectively; the related resonances in the ligands **$L^{1b}$**-**$L^{3b}$** appeared in the regions 176.86-

178.30 and 180.34-180.65 ppm, respectively. While the resonances due to the C=S in the Cu(I), Ni(II) and Zn(II) complexes have been observed with a change in comparison with the free corresponding ligands indicating the coordination of the ligands to the metal centre through C=S. The $^{13}$C NMR peaks of C=O and C=S of the Cu(I) complexes appeared in the regions of 168.78-181.39 and 176.42-187.38 ppm respectively for **2.11, 2.12** and **2.24**. In the Cu(I) complexes **2.1, 2.6, 2.15, 2.16, 2.19** and **2.25**, the $^{13}$C NMR peaks of C=O and C=S appeared in the regions 149.49-178.32 ppm and 170.47-182.79 ppm respectively. Sadly, it is not possible to directly compare these NMR of **2.1, 2.6, 2.15, 2.16, 2.19** and **2.25** with their corresponding free ligands due to the use of different NMR solvents due to the different solutions of the products. Ni(II) complexes showed $^{13}$C NMR peaks of C=O and C=S in the regions of 165.60-168.51 and 176.08-177.38 ppm respectively for **2.2, 2.3** and **2.8** and 174.83-176.03 and 177.23-179.81 ppm respectively for **2.17** and **2.22**. The Zn(II) complexes also gave resonances due to the C=O and C=S carbon nuclei in the regions of 166.26-168.13 and 178.09-180.35 ppm respectively for **2.5, 2.10, 2.14** and 178.28 and (180.23, 180.39) ppm respectively for **2.27**. $^{13}$C NMR of the Ni(II) and Zn(II) complexes showed a noticeable change in C=S peak in comparison with the free corresponding ligands indicating the coordination of the ligands to the metal centre through C=S. $^{13}$C NMR for complexes **2.4, 2.7, 2.9, 2.18, 2.21** and **2.23** showed the disappearance of the C=O signals consistent with the hydrolysis and cleavage of the benzoyl/pivaloyl thiourea groups.

### 2.3.3.2 Infrared spectra

The main vibrational bands of the ligands (**L$^{1a}$-L$^{3b}$**) and their complexes (**2.1-2.27**) are given in the experimental section and listed in **Table 2.1**. The IR spectra of free ligands (**L$^{1a}$-L$^{3b}$**) show characteristic absorption bands at 3298-3485 (N-H), 1672-1692 (C=O), 1468-1512 (C=N) and 1325-1366 (C=S) cm$^{-1}$. The IR spectra of thiourea complexes (**2.1**-**2.27**) show these absorption bands at 3267-3485 (N-H), 1660-1690 (C=O), 1439-1504 (C=N) and 1252-1287 (C=S) cm$^{-1}$. Related literature reports the amide carbonyl stretch at ~1630-1690 cm$^{-1}$.[87] The IR spectra of complexes **2.6**, **2.8**, **2.19** and **2.22** showed a considerable modulation of the C=O

stretching frequency and is red shifted (lower wavenumber) as compared with their corresponding free ligands, consistent with coordination to the metal through the oxygen carbonyl group. This is due to the electrons donating behaviour of the oxygen atom in C=O group to the metal centre which cause the reducing of the double bond property in C=O bond and weaken it. Then this reduce force constant of the bond and observes it in lower wavenumber.

For the complexes **2.4**, **2.7**, **2.9**, **2.18**, **2.21** and **2.23**, the most striking change is the C=O stretching frequency in the free ligands disappears completely from the IR spectra, indicating cleavage of the benzoyl and pivaloyl groups from the complexes. The complexes **2.1**, **2.2**, **2.3**, **2.5**, **2.10**, **2.11**, **2.12**, **2.13**, **2.14**, **2.15**, **2.16**, **2.17**, **2.20**, **2.24**, **2.25**, **2.26** and **2.27** show little change in C=O stretching frequency indicating the oxygen carbonyl group does not coordinate to the metal centre. A strong peak at 1325-1366 $cm^{-1}$, assigned as (C=S) in ligands $\mathbf{L^{1a}}$-$\mathbf{L^{3b}}$ also shifts to lower energy at 1252-1287 $cm^{-1}$ in all prepared complexes (**2.1-2.27**). This indicates coordination of the sulfur atom of the C=S group to the metal centre which weakens the C=S bond by the electrons donating from the sulfur atom to the electropositive metal and then reduces the bond order. The C=N stretching vibration was observed at lower frequency (1439-1504 $cm^{-1}$) compared to the corresponding free ligands (1468-1512 $cm^{-1}$) suggesting the coordination of the pyridyl nitrogen atom to the metal centre. In all perchlorate complexes the presence of two characteristic unsplit IR active bands at (1053-1096) and (621-627) $cm^{-1}$ indicates that the $T_d$ symmetry of $ClO_4^-$ was maintained in all complexes and suggests the presence of $ClO_4^-$ outside the coordination sphere.[88,89] All of these features are consistent with the X-ray crystal structures and the $^1H$, $^{13}C$ NMR spectra for all complexes.

**Table 2.1:** IR characterization ($\nu_{max}$, $cm^{-1}$) for ligands (**$L^{1a}$- $L^{3b}$**) and their complexes (**2.1-2.27**).

| Compound. | ν (N-H) | ν (C=O) | ν (C=S) | ν (Cl-O) |
|---|---|---|---|---|
| **$L^{1a}$** | 3298 | 1672 | 1333 | - |
| **2.1** | 3267 | 1672 | 1281 | 1091,625 |
| **2.2** | 3314 | 1672 | 1283 | 1090,627 |
| **2.3** | 3404 | 1668 | 1283 | 1087,624 |
| **2.4** | 3381 | - | 1279 | 1080, 626 |
| **2.5** | 3377 | 1670 | 1278 | 1084, 627 |
| **$L^{2a}$** | 3485,3364 | 1672 | 1341 | - |
| **2.6** | 3323 | 1661 | 1258 | 1081,624 |
| **2.7** | 3343 | - | 1271 | 1071,627 |
| **2.8** | 3331 | 1660 | 1275 | 1071, 626 |
| **2.9** | 3375 | - | 1267 | 1067 ,626 |
| **2.10** | 3366 | 1668 | 1277 | 1070 ,626 |
| **$L^{3a}$** | 3321 | 1667 | 1325 | - |
| **2.11** | 3387 | 1665 | 1260 | 1096, 621 |
| **2.12** | 3340 | 1667 | 1252 | 1096 ,621 |
| **2.13** | 3469 | 1663 | 1277 | 1064, 627 |
| **2.14** | 3318 | 1664 | 1273 | 1095, 627 |
| **$L^{1b}$** | 3341 | 1676 | 1331 | - |
| **2.15** | 3358 | 1676 | 1283 | 1096,621 |
| **2.16** | 3450 | 1673 | 1275 | - |
| **2.17** | 3321 | 1675 | 1287 | 1092,626 |
| **2.18** | 3485 | - | 1280 | 1053,627 |
| **$L^{2b}$** | 3401,3302 | 1685 | 1356 | - |
| **2.19** | 3343 | 1671 | 1267 | 1079,625 |
| **2.20** | 3320 | 1683 | 1273 | - |
| **2.21** | 3321 | - | 1270 | 1073,627 |
| **2.22** | 3377 | 1664 | 1277 | 1071,627 |
| **2.23** | 3370 | - | 1275 | 1071 ,626 |
| **$L^{3b}$** | 3445,3414 | 1692,1673 | 1366 | - |
| **2.24** | 3400 | 1688 | 1277 | 1090, 625 |
| **2.25** | 3397 | 1690 | 1277 | 1077,624 |
| **2.26** | 3312 | 1687 | 1262 | 1090, 626 |
| **2.27** | 3317 | 1689 | 1258 | 1075 ,626 |

### 2.3.3.3 Electronic absorption spectra

The UV-visible spectra of the ligands **$L^{1a}$-$L^{3b}$** and their complexes with Cu(I), Ni(II) and Zn(II) ions were recorded using DMF solutions and their full data are presented in the experimental section. Electronic spectra of the ligands **$L^{1a}$-$L^{3b}$** showed typical intraligand transitions, π→π* and n→π* transitions at 214-293 nm and 299-367 nm respectively. The complexes **2.1**-**2.27** also reveal these transitions at higher energy to those of their corresponding free ligands. A noticeable shift is observed for the bands in Cu(I) complexes. For example, these π→π* and n→π* transitions were observed in the ligand **$L^{3a}$** at 278 and 331 nm respectively, and were shifted to 263 and 316 nm in complex **2.11** and this may be due to the hindrance effect govern **$L^{3a}$** after coordination with metal centre and causes stronger C=S and C=N bonds. This is in good agreement with the previously reported complex [$Cu^{I}Cl(eitotH_2)_2$] ($eitotH_2$= 5-carbethoxy-2-thiouracil) which also reveals transitions at 264 and 311 nm.[90]

The electronic spectra of the Cu(II) complex **2.20** confirm a four coordinate environment around Cu(II) ion by showing a *d-d* band observed at 470 (139 $M^{-1}cm^{-1}$) nm. The diamagnetic $d^{10}$ Zn(II) complexes exhibited intraligand transitions of π→π* and n→π* without any *d-d* transitions as expected. Absorbance of the zinc complex of the ligand **$L^{2b}$** shifted from 232 to 214 nm for π→π* and from 328 to 320 nm for n→π*.

The spectra of the Ni(II) complexes confirmed a square planar four-coordinate environment around the nickel central ion for complexes **2.2, 2.3, 2.7, 2.8, 2.17, 2.21** and **2.22** and six-coordinate environment in complexes **2.13** and **2.26**. The electronic spectra for four coordinated complexes revealed one LMCT bands observed at around 400 nm. One *d-d* transition was observed in square planar four-coordinate Ni(II) complexes, and assigned to $d_{xy}$→ $d_{x^2-y^2}$ (**see Table 2.2**). This *d-d* transition is located around 600 nm (see **Figure 2.7**, **Table 2.2**). This is in good agreement with the complex, [Ni(DEP)] (DEP: (3E)-3-[(2-{(E)-[1-(2,4-Dihydroxy phenyl)ethylidene]amino}ethyl)imino]-1-phenylbutan-1-one) which also revealed two transitions at 433 and 568 nm which were assigned to a LMCT and $d_{xy}$→ $d_{x^2-y^2}$ transition respectively.[91,92]

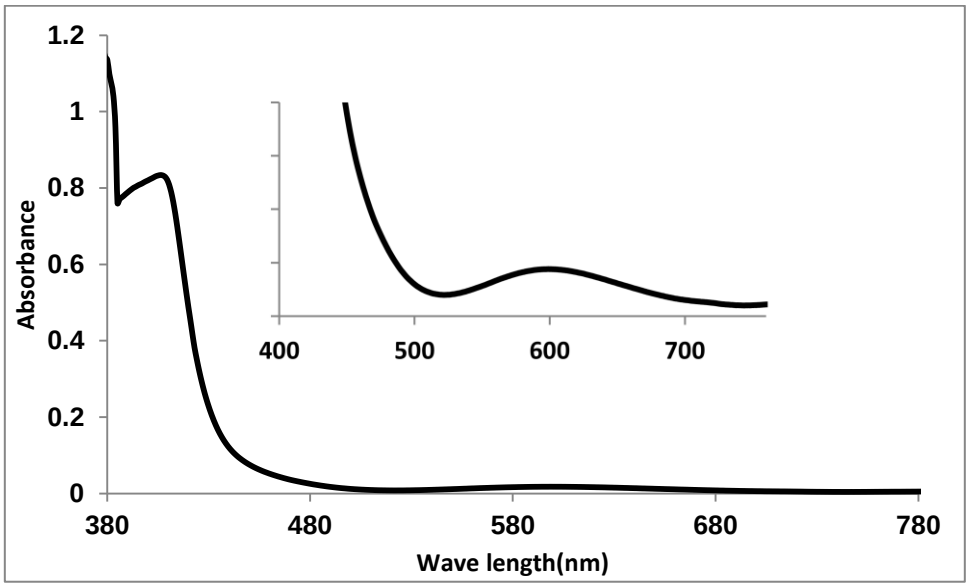


**Figure 2.7:** The electronic spectra of square planar Ni(II) complex **2.22.**

The UV-vis. spectra of octahedral six- coordinate Ni(II) complexes **2.13** and **2.26** showed two *d-d* transitions which are attributed to $^3A_{2g}\rightarrow{}^3T_{2g}$ ($\nu_1$) and $^3A_{2g}\rightarrow{}^3T_{1g}(F)$ ($\nu_2$) respectively. The third transition $^3A_{2g}\rightarrow{}^3T_{1g}(P)$ ($\nu_3$) has been shielded by ligand-metal charge transfer MLCT band at $\lambda_{max.}$ nm(ε,$M^{-1}cm^{-1}$) 413(212) and 421(242) in **2.13** and **2.26** respectively (see **Figure 2.8**, **Table 2.2**). The three spin allowed transitions generally fall within the ranges 7000-13000 $cm^{-1}$, 11000-20000 $cm^{-1}$ and 19000-27000 $cm^{-1}$, respectively, for regular octahedral systems.[92] The assignments yields spectrochemical parameters(10Dq, B and *β*) 1068.4 $cm^{-1}$, 854.7 $cm^{-1}$ and 0.82 for **2.13** and 1050.4 $cm^{-1}$, 875.3 $cm^{-1}$ and 0.84 for **2.26**. It is clear that these transitions for complexes **2.13** and **2.26** lie within these ranges and are in good agreement with those reported for an octahedral geometry around the Ni(II) ion. The octahedral complex $[Ni^{II}(C_{14}H_{13}N_3OS)_2(CH_3CN)_2](ClO_4)_2$ reported by Saad *et al*. exhibits the same environment around the nickel and shows three transitions at 10,549, 16,978 and 27,777 $cm^{-1}$, the bands have been assigned as to $^3A_{2g}\rightarrow{}^3T_{2g}$ ($\nu_1$), $^3A_{2g}\rightarrow{}^3T_{1g}(F)$ ($\nu_2$) and $^3A_{2g}\rightarrow{}^3T_{1g}(P)$ ($\nu_3$) respectively.[93]

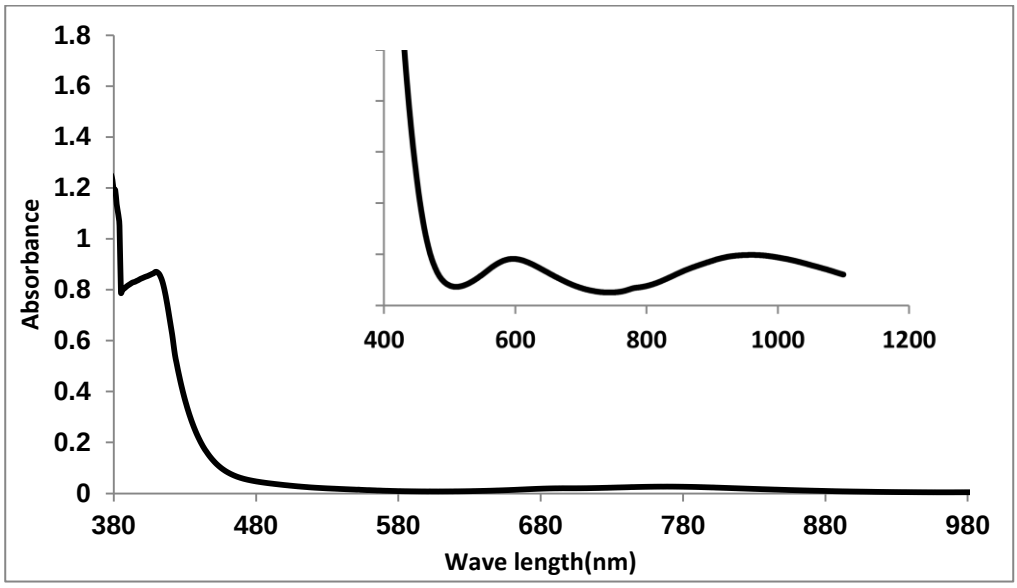


**Figure 2.8:** The electronic spectra of octahedral Ni(II) complex **2.13.**

**Table 2.2:** Electronic spectral assignment for Ni(II) complexes of **$L^{1a}$-$L^{3b}$.**

| | MLCT $\lambda_{max}$ nm, ($\varepsilon$, $M^{-1}cm^{-1}$) | d-d transition $\lambda_{max}$ nm, ($\varepsilon$, $M^{-1}$ $cm^{-1}$) | | | Δ $(cm)^{-1}$ | B $(cm)^{-1}$ | β |
|---|---|---|---|---|---|---|---|
| | | $d_{xy}\rightarrow d_{X}^{2}-y^{2}$ | $^{3}A_{2g}\rightarrow {}^{3}T_{1g}$ (F) ($v_2$) | $^{3}A_{2g}\rightarrow {}^{3}T_{2g}$ ($v_1$) | | | |
| **2.2** | 411(390) | 584(56) | - | - | - | - | - |
| **2.3** | 394(377) | 598(11) | - | - | - | - | - |
| **2.7** | 401(205) | 603(17) | - | - | - | - | - |
| **2.8** | 421(423) | 612(5) | - | - | - | - | - |
| **2.13** | 413(212) | - | 583(21) | 936(12) | 1068.4 | 854.7 | 0.82 |
| **2.17** | 390(329) | 597(11) | - | - | - | - | - |
| **2.21** | 401(205) | 603(17) | - | - | - | - | - |
| **2.22** | 410(340) | 606(7) | - | - | - | - | - |
| **2.26** | 421(242) | - | 591(5) | 952(3) | 1050.4 | 875.3 | 0.84 |

## 2.3.4 Magnetic susceptibility measurements

Magnetic susceptibility measurements were carried out at room temperature using the Evans method.[78] The observed magnetic moments of Ni(II) complexes **2.2**, **2.3**, **2.7**, **2.8**, **2.17**, **2.21** and **2.22** are zero confirming the diamagnetic properties and the square-planar structure of these complexes. The magnetic moments for the Ni(II) complexes **2.13** and **2.26** are 2.94 and 2.98 B.M. and correspond to two unpaired electrons consistent with an octahedral geometry around the Ni(II) complexes. The magnetic moment of the Cu(II) complex **2.20** was 1.80 B.M., consistent with a $d^9$ configuration. **Table 2.3** shows the magnetic data which includes mass magnetic susceptibility $\chi_{mass}$, molar magnetic susceptibility, $\chi_M$, and magnetic moments, $\mu_{eff.}$ Finally, measurements confirmed the Zn(II) and Cu(I) complexes were diamagnetic, as expected.

**Table 2.3:** Magnetic data of Cu(II) and octahedral Ni(II) complexes of **$L^{1a}$**-**$L^{3b}$**.

| Complex | $\chi_{mass}$ x$10^{-6}$ | $\chi_{molar}$ x$10^{-6}$ | $\mu_{obs}$B.M. experimental |
|---|---|---|---|
| 2.13 | 3.221 | 3636.16 | 2.939 |
| 2.20 | 2.150 | 1365.24 | 1.8014 |
| 2.26 | 3.561 | 3734.73 | 2.978 |

## 2.3.5 Electrochemical studies of Cu (I), Cu(II) and Ni(II) complexes

The electrochemical data for Cu(I), Cu(II) and Ni(II) complexes were measured in acetonitrile using $[Bu_4N][PF_6]$ (0.1 M) as supporting electrolyte. The data is summarized for Cu(I) and Cu(II) complexes in **Table 2.4** and for Ni(II) complexes in **Table 2.5**. The cyclic voltammogram of Cu(I) complexes **2.1**, **2.6**, **2.11**, **2.12**, **2.15**, **2.16**, **2.19**, **2.24** and **2.25** are very similar. **Figures 2.9-2.11** show representative cyclic voltammograms of the reductive region for **2.1, 2.11** and **2.12** respectively. Typically, a quasi-reversible process is observed between -0.23 to -0.30 V (vs $Fc/Fc^+$), with very large peak to peak separations being observed (200-350 mV); see **Table 2.4**. This potential is typical of a Cu(I)/Cu(II) couple and the peak to

peak separations, being much greater than those observed with the ferrocene internal standard, suggest a quasi-reversible nature. This is possibly due to a structural/geometric rearrangement occurring on the transitions between the Cu(I) and Cu(II) oxidation state. Furthermore, the ratio of $i_{pc}$ to $i_{pa}$ is less than 1, which also supports the quasi-reversible nature of this process.

It was noted that the application of a high negative potential for prolonged periods caused a sharp anodic peak between -0.5 to -0.7V suggestive of species being deposited upon the electrode. The cyclic voltammogram of Cu(II) complex, **2.20** showed quasi-reversible process at -0.4 V attributed to the Cu(II)/Cu(I) redox process. Interestingly, **2.20**, was unique among these copper complexes as the voltammogram (**Figure 2.12**) as it displays a single reversible process at + 0.250V vs $Fc/Fc^+$ ($\Delta E$= 72 mv). This complex contains the new cyclized group, formed via the Hugershoff reaction. The synthesis of such organic fragments has not been widely reported.[94] Furthermore, to the best of our knowledge, the electrochemical properties of these molecules has also not been reported. Therefore, it is suggested that the process observed at +0.250V may be associated with this moiety.

**Table 2.4:** Electrochemical parameters for the **absorbance spike**, **quasi-reversible** and **reversible** processes exhibited by copper(I) complexes, **2.1**, **2.6**, **2.11**, **2.12**, **2.15**, **2.16**, **2.19**, **2.24** and **2.25**, and copper(II) complex **2.20** in acetonitrile solution, supporting electrolyte $[Bu_4N][PF_6]$ (0.1 M), t =$25^0$ c measured at 100 mv/sec.

| **Complex** | ***$E_P$*/V vs FC/$FC^+$** | ***Quasi reversible* vs FC/$FC^+$** | | | | | ***reversible* vs FC/$FC^+$** | | | | |
|---|---|---|---|---|---|---|---|---|---|---|---|
| | ***Absorbance Spike*** | **$E_{Pa}$ V** | **$\Delta E_P$ mv** | **$I_{pa}$ µA** | **$I_{pc}$ µA** | **$I_{pc}/I_{Pa}$** | **$E_{Pa}$ V** | **$\Delta E_P$ mv** | **$I_{pa}$ µA** | **$I_{pc}$ µA** | **$I_{pc}/I_{Pa}$** |
| **2.1** | -0.646 | -0.274 | 266 | 5.01 | 2.80 | 0.559 | - | - | - | - | - |
| **2.6** | -0.632 | -0.297 | 339 | 1.38 | 1.07 | 0.775 | - | - | - | - | - |
| **2.11** | - | -0.234 | 206 | 3.68 | 1.75 | 0.476 | - | - | - | - | - |
| **2.12** | - | -0.228 | 232 | 2.38 | 1.32 | 0.555 | - | - | - | - | - |
| **2.15** | - | -0.249 | 302 | 1.50 | 0.82 | 0.547 | - | - | - | - | - |
| **2.16** | -0.552 | -0.284 | 254 | 2.18 | 0.66 | 0.303 | - | - | - | - | - |
| **2.19** | - | -0.274 | 322 | 1.35 | 0.84 | 0.622 | - | - | - | - | - |
| **2.20** | -0.538 | -0.394 | 304 | 3.16 | 1.24 | 0.392 | +0.250 | 72 | 3.44 | 3.32 | 0.965 |
| **2.24** | -0.696 | -0.246 | 262 | 13.80 | 9.40 | 0.681 | - | - | - | - | - |
| **2.25** | -0.660 | -0.237 | 302 | 13.31 | 8.21 | 0.617 | - | - | - | - | - |

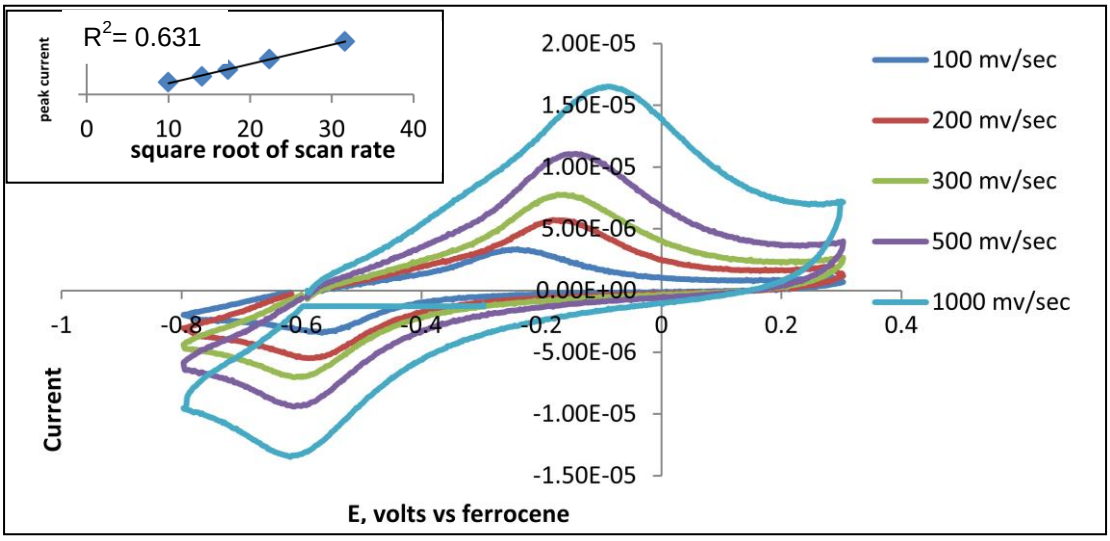


**Figure 2.9**: Cyclic voltammogram of complex **2.1** shows quasi-reversible process

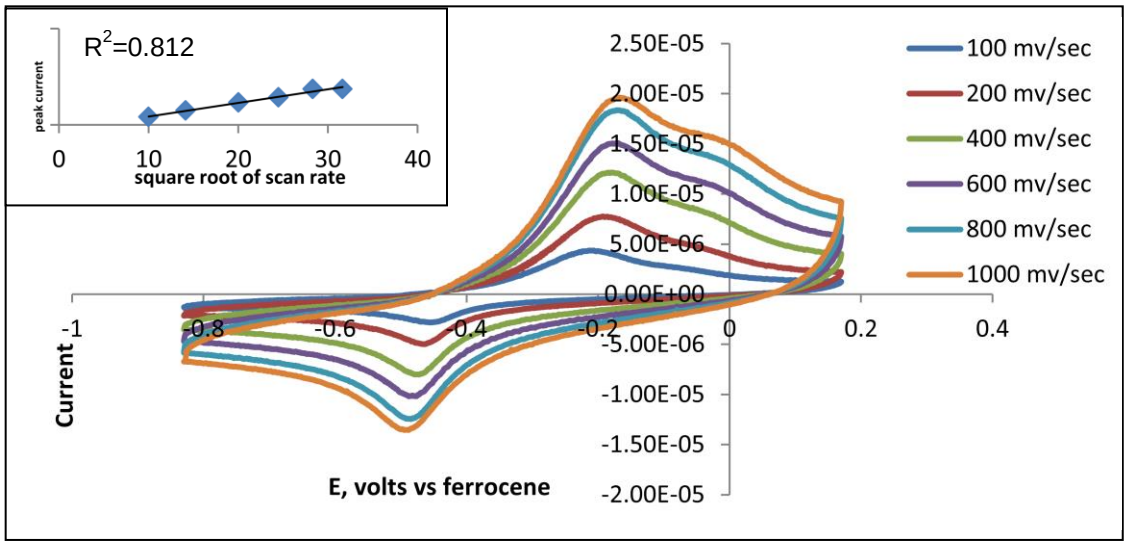


**Figure 2.10**: Cyclic voltammogram of complex **2.11** shows quasi-reversible process

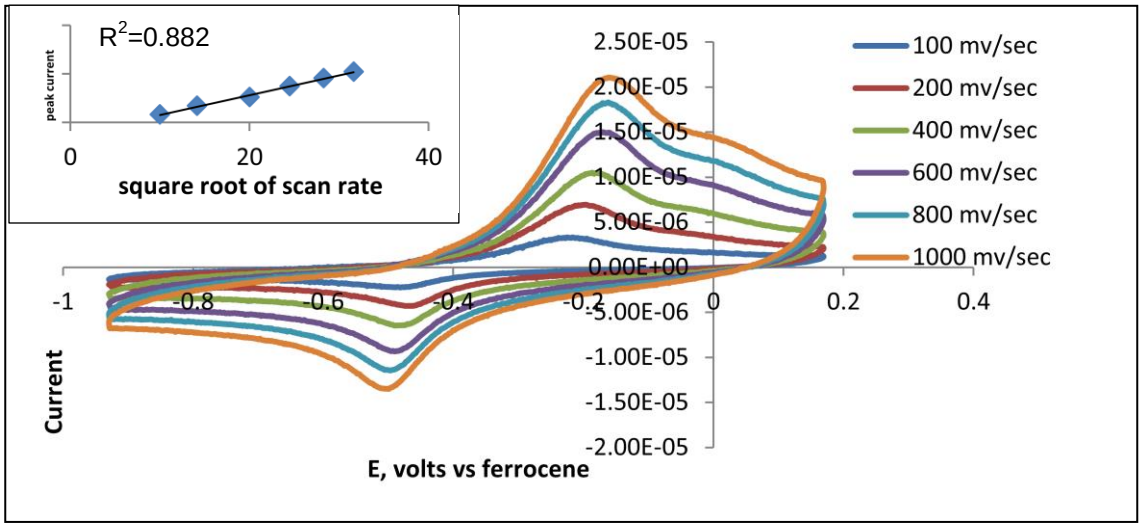


**Figure 2.11**: Cyclic voltammogram of complex **2.12** shows quasi-reversible process

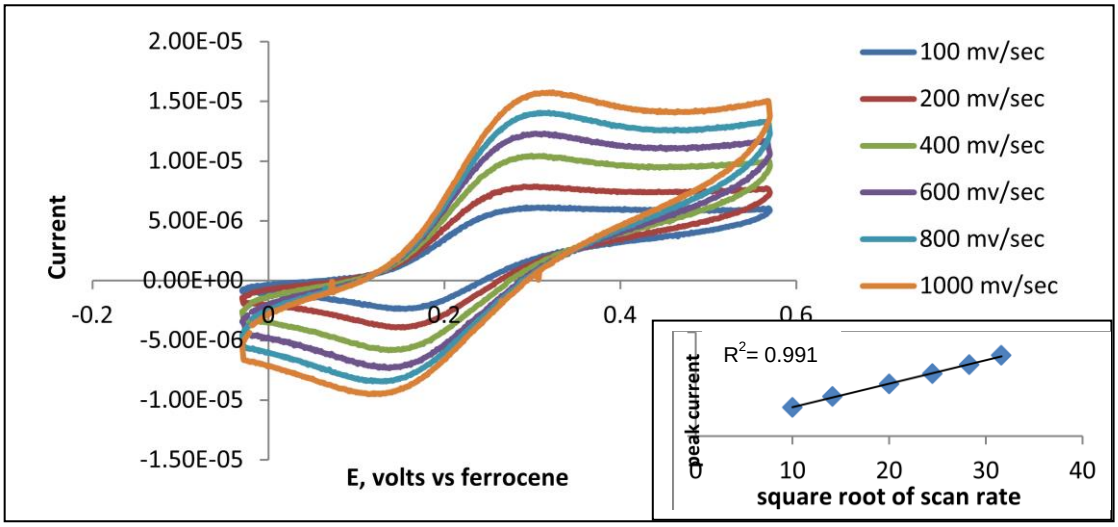


**Figure 2.12**: Cyclic voltammogram of complex **2.20** shows reversible process

The cyclic voltammogram of the Ni(II) complexes **2.2**, **2.3**, **2.7**, **2.8**, **2.13**, **2.17**, **2.21**, **2.22** and **2.26** revealed two irreversible reductions (-1.11 to -1.34V vs $Fc/Fc^+$) and (-1.63 to -1.99V vs $Fc/Fc^+$) respectively (**Table 2.5**). The cyclic voltammogram of **2.3** is shown in **Figure 2.13** as a representative example. Similar behaviour has been reported by Saad *et al.* for the Ni(II) complex of bis(6-benzoylthiourea-2-pyridylmethyl)(2-pyridylmethyl) amine which showed two similar irreversible reductions at -1.37 V and -1.78 V (vs Fc/Fc+) in acetonitrile solution.[95] Without further investigate, it is impossible to unequivocally assign these processes however Saad[95] has suggested that the first irreversible reduction may be ligand based. Moreover, the second irreversible reduction process may be attributed to Ni(II) to Ni(I) process.

**Table 2.5:** Electrochemical parameters for the irreversible reduction processes exhibited by Ni(II) complexes, **2.2**, **2.3**, **2.7**, **2.8**, **2.13**, **2.17**, **2.21**, **2.22** and **2.26** in acetonitrile solution, supporting electrolyte $[Bu_4N][PF_6]$ (0.1 M), t =$25^0$ c measured at 100 mV/sec.

| **complex** | $E_P$**/V vs** $Fc/Fc^+$ **irreversible reductions** | |
|---|---|---|
| **2.2** | -1.195 | -1.930 |
| **2.3** | -1.159 | -1.958 |
| **2.7** | -1.123 | -1.699 |
| **2.8** | -1.332 | -1.714 |
| **2.13** | -1.267 | -1.778 |
| **2.17** | -1.109 | -1.613 |
| **2.21** | -1.123 | -1.699 |
| **2.22** | -1.336 | -1.992 |
| **2.26** | -1.253 | -1.872 |

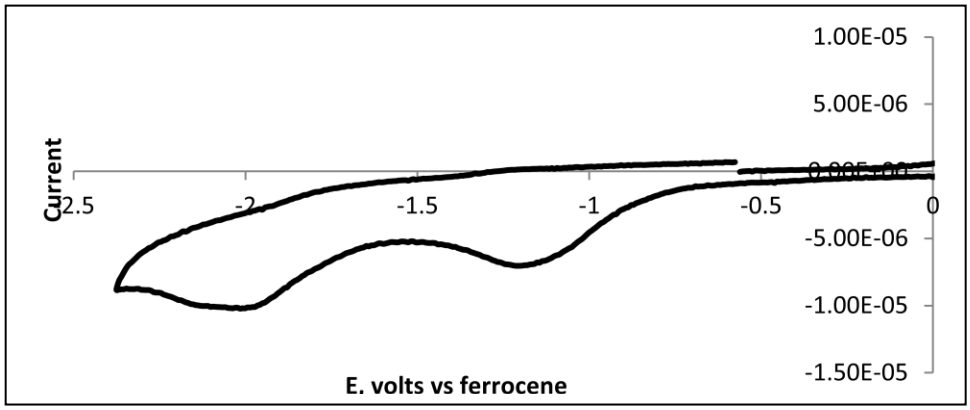


**Figure 2.13**: Cyclic voltammogram of complex **2.3** show irreversible reductive process at 100 mv.sec$^{-1}$.

## 2.3.6 Crystallographic studies

Crystal parameters, details of the data collection and structural refinements of **2.1, 2.4, 2.6** and **2.7** are presented in **Table 2.13** while **2.15, 2.16, 2.20** and **2.24** are presented in **Table 2.14**. Structure solution was refined by full-matrix least-squares on $F^2$.[96] Selected bond lengths and angles are given for all structures in **Tables 2.6-2.12**.

### 2.3.6.1 Crystal structures of $[Cu(L^{1a})_2]ClO_4 \cdot CH_3CN$ 2.1 and $[Cu(L^{1b})_2]ClO_4.H_2O$ 2.15

The Cu(I) complexes **2.1** and **2.15** crystallise in the monoclinic space $P2_1/n$ and Orthorhombic space $P2_12_12_1$ and contain single complexes within the asymmetric unit (asu), **Figure 2.14** and **Figure 2.15**. Red, monoclinic crystals of **2.1** and orange orthorhombic crystals of **2.15** were obtained by vapour diffusion of diethyl ether into an acetonitrile solution of **2.1** or a chloroform solution of **2.15**. Selected bond distances and bond angles are given in **Table 2.6**. **Figure 2.14** shows Cu(I) complex **2.1**, with the metal centre tetrahedrally coordinated by two bidentate ligands. Each ligand coordinates by a pyridine ring and the sulfur of the thiourea. Bond angles about the metal centre range from 98.04(6)-128.23(3) degrees, signifying a significant distortion, although the average angles are 109.5 degrees. This is due to the steric rigidity of the ligand making the N-Cu-S bond angle fixed in

its nature. This effect is observed in S21–Cu1–S1 angle at (128.23(3)º). The N and S donor atom sites from the bidentate ligands coordinates the Cu(I) centre forming two six membered $C_2N_2SCu$ rings. The sulfur bonds Cu1-S1 2.2235(7) and Cu1-S21 2.2191(7) in **2.1** is significantly longer than the nitrogen bonds with Cu(I) ion due to the greater atomic size of sulfur. A data search of the CCDC reveals there are 183 crystal structures of Cu(I) four coordinate with $N_2S_2$ donors. In 123 crystal structures, Cu(I) adopts a teteraheral geometry and square planar is adopted in 17. In a search for Cu(I) complexes of pyridyl thiourea derivatives, four crystal structures were found and all of them had a tetrahedral geometry and Cu(I) ion was coordinated by the nitrogen pyridyl group and the sulfur of C=S group.

Typical for this class of ligand, intramolecular hydrogen bond interactions are also observed (**Figure 2.14**). These two interactions N2–H2···O1 and N22–H22···O21 occur between the oxygen carbonyl atom and amide hydrogen atom. Furthermore, there are two intermolecular hydrogen bonds, N23–H23···N51 and N3–H3···O41$^{i}$ that are observed between thiourea and an acetonitrile molecule and perchlorate ion respectively. Complex **2.15** (**Figure 2.15**) has a *t*-butyl group in place of a phenyl group, but **2.1** and **2.15** have an almost identical coordination sphere. Comparable intramolecular hydrogen bonds N2–H2···O1 and N22–H22···O21 were observed in **2.1**. These hydrogen bonds are typical of benzoyl thioureas ligands. In 2004, N-(p-Methoxybenzoyl)-N'-(o-methoxyphenyl) thiourea was reported by Ali *et al.*,[97] and it showed similar intramolecular hydrogen bonding. In addition, there was an intermolecular hydrogen bond N3–H3A···O41$^{ii}$ between thiourea and a perchlorate ion.

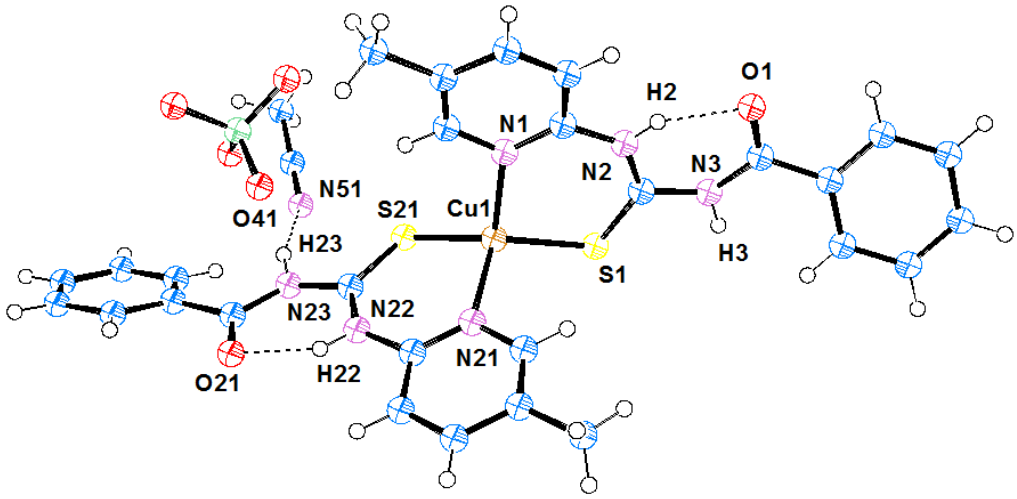


**Figure 2.14:** The asymmetric unit of **2.1**. Displacement ellipsoids are shown at 50% probability. H- atoms are drawn as spheres of arbitrary radius.

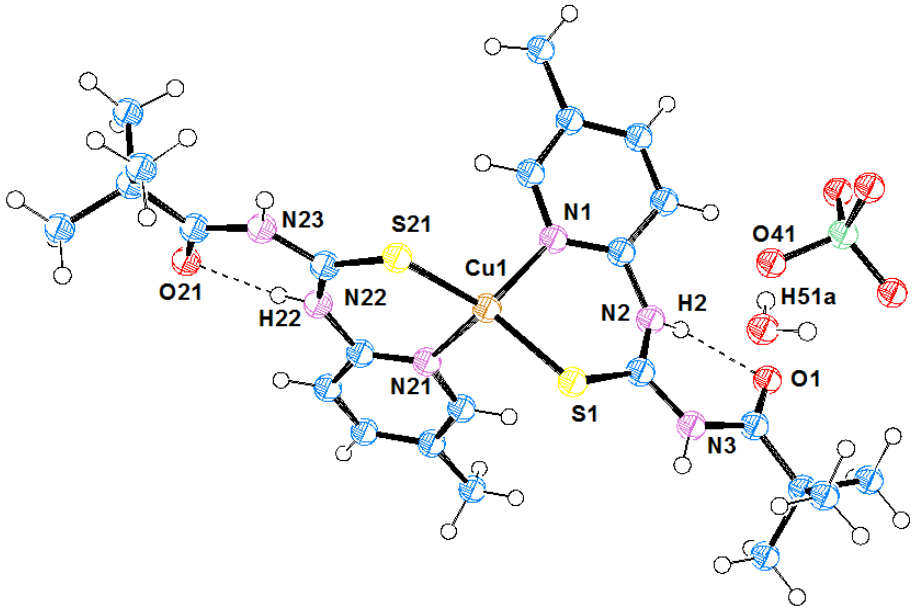


**Figure 2.15:** The asymmetric unit of **2.15**. Displacement ellipsoids are shown at 50% probability.

**Table 2.6:** Selected bond lengths (Å) and bond angles (º) for **2.1** and **2.15**.

| **Bond length (Å)** | **2.1** | **2.15** |
|---|---|---|
| Cu1–N1 | 2.074(2) | 2.055(7) |
| Cu1–N21 | 2.079(2) | 2.050(6) |
| Cu1–S21 | 2.2191(7) | 2.214(2) |
| Cu1–S1 | 2.2235(7) | 2.232(2) |
| C1/C6–S1 | 1.672(3) | 1.675(7) |
| C21/C26–S21 | 1.675(3) | 1.666(8) |
| **Bond Angles (º)** | | |
| N1–Cu1–N21 | 111.87(9) | 110.9(3) |
| N1–Cu1–S21 | 111.55(6) | 116.05(18) |
| N21–Cu1–S21 | 98.12(6) | 98.89(17) |
| N1–Cu1–S1 | 98.04(6) | 97.40(18) |
| N21–Cu1–S1 | 109.21(6) | 109.80(18) |
| S21–Cu1–S1 | 128.23(3) | 123.97(9) |

## 2.3.6.2 Crystal structure of $[Zn(L^{1C})_2](ClO_4)_2$ (2.4)

Monoclinic colourless crystals of **2.4** were obtained by vapour diffusion of diethyl ether into an acetonitrile solution of **2.4**. The Selected bond distances and bond angles are given in **Table 2.7, Figure 2.16**. The zinc complex crystallises in the monoclinic space group $P2_1$. A closer look at the coordination sphere of Zn(II) shows a tetrahedral geometry (**Figure 2.16**, **Table 2.7**). The bond angles about the metal centre range from 99.35(14)-115.56(18) degrees. The geometry about the Zn(II) centre is similar to that about Cu(I) centres in **2.1** and **2.15**. This again reflects the rigid nature of the ligand. On searching the CCDC, there is just one structure of tetrahedral Zn(II) with pyridyl thiourea ligands coordinated by two N-pyridyl and 2C=S donors.[98] However for $ZnN_aS_b$ structures, there are 526 crystal structures and the Zn(II) ion adopts a tetrahedral geometry in 265 through coordination with two nitrogen and two sulfur atoms. 125 and 136 crystal structures was found to Zn(II) ions in five and six-coordinated respectively.

The metal centre is bound by two bidentate ligands, each ligand coordinating via a pyridine donor and the sulfur atom of the thiourea. The nitrogen and sulfur donor sites from the bidentate ligands coordinates the Zn(II) centre to form two six membered $C_2N_2SZn$ rings. In the structure, intermolecular hydrogen bond interactions N1–H1A···O22, N2–H2···O23 and N1–H1B···O31$^{i}$ are observed (2.04, 2.01 and 2,04 Å) and occur due to the interaction between thiourea N-H and a perchlorate oxygen atom (**Figure 2.16**). The tetrahedral complex bis[(N-2-pyridinyl)morpholine-4-carbimidothiolat-K$^2$-N,S] zinc(II), reported in 2012 by Orysyk *et al.*, exhibits coordinative bond lengths Zn(1)–N(2) 2.025(2), Zn(1)–N(5) 2.032(2), Zn(1)–S(1) 2.2761(8) and Zn(1)–S(2) 2.2899(8) and bond angles N(2)–Zn(1)–N(5) 123.71(10), N(2)–Zn(1)–S(1) 97.18(7), N(5)–Zn(1)–S(1) 110.39(8), N(2)–Zn(1)–S(2) 108.62(7), N(5)–Zn(1)–S(2) 95.35(8) and S(1)–Zn(1)–S(2) 123.96(3),[99] similar to **2.4**.

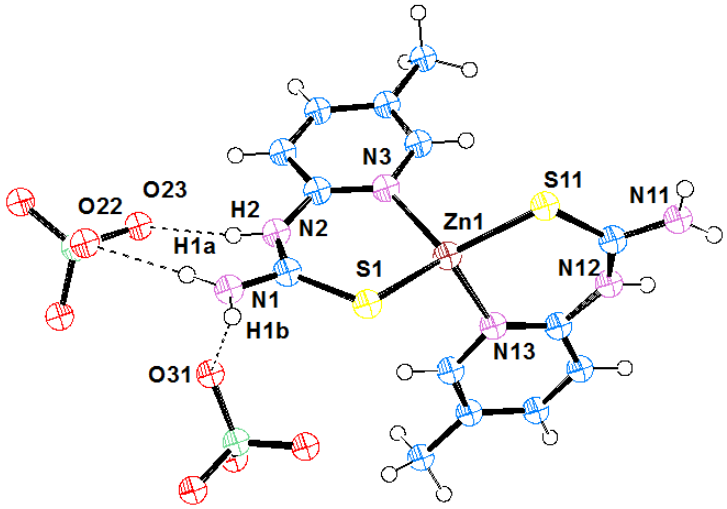


**Figure 2.16**: The asymmetric unit of **2.4**. Displacement ellipsoids are shown at 50% probability.

**Table 2.7:** Selected bond lengths (Å) and angles (º) for **2.4**.

| | | | |
|---|---|---|---|
| **Bond length (Å)** | | | |
| Zn1–N3 | 2.022(5) | Zn1–S11 | 2.2536(15) |
| Zn1–N13 | 2.025(5) | Zn1–S1 | 2.2595(16) |
| **Bond Angles (º)** | | | |
| N3–Zn1–N13 | 115.56(18) | N3–Zn1–S1 | 99.72(14) |
| N3–Zn1–S11 | 114.11(14) | N13–Zn1–S1 | 113.61(14) |
| N13–Zn1–S11 | 99.35(14) | S11–Zn1–S1 | 115.36(5) |

## 2.3.6.3 Crystal structure of $[Cu(L^{2a})_2](ClO_4)$ (2.6)

The molecular structure of the complex $[Cu(L^{2a})_2]ClO_4$ (**2.6**) was established by X-ray crystallography and is illustrated in **Figure 2.17**. The Cu(I) complex **2.6** crystallises in the monoclinic space $P2_1/c$ and contains a single complex within the (asu). The Cu(I) centre is chelated by two $\mathbf{L^{2a}}$. Each ligand coordinates by the sulfur atoms of the thiourea, but one ligand coordinates by a carbonyl oxygen group and the other by the pyridine ring. The Cu(I) complex is clearly tetrahedral with bond angles around the metal centre ranging from 83.50(4)-126.94(2) degrees (**Table 2.8**), and this distortion due to hindrance around metal centre. According to CCDC, there are just three crystal structures published for the $Cu^{I}S_2NO$ site and they were tetrahedral. The bond angles around the Cu(I) centre arrange between 82.156-128.671 degrees.[100,101] The more acute of these angles is associated with the bond angles between the two donors of the bidentate ligand. A large distortion is observed for S1–Cu1–S21 (126.94(2)). Similar to **2.1** and **2.15**, Cu-S bond is longer than Cu-N. As in benzoyl thiourea compounds, intramolecular hydrogen bonds are observed. These intramolecular interactions, N2–H2···O1 and N4–H4B···O21, occur between the carbonyl oxygen atom and the hydrogen atom of N-H in (NHCS) and $NH_2$ respectively in thiourea. Another intramolecular hydrogen bond N21-H21…N23 is observed between the nitrogen pyridyl group with the hydrogen atom of N-H. Such interactions may provide an explanation for the S/O donor behaviour of one of the ligands, where the $NH_2$ group of one ligand

hydrogen bonds to the oxygen (O21) also co-ordinated to the metal centre. The intramolecular hydrogen bond N2–H2···O1 is typical to benzoyl thiourea and it is similar to the **2.1** and **2.15**. It is clear that the bond length of the hydrogen bond N2–H2···O1 is shorter than N4–H4B···O21. This is due the short distance between H2-atom and the O1-atom which result of the free movement of the free carbonyl group as compared with the hindered movement of the carbonyl group which bonded with Cu(I) ion. Furthermore, intermolecular hydrogen bonds are observed between perchlorate oxygen atoms with the hydrogen atom in the thiourea N-H group, (see **Figure 2.17**).

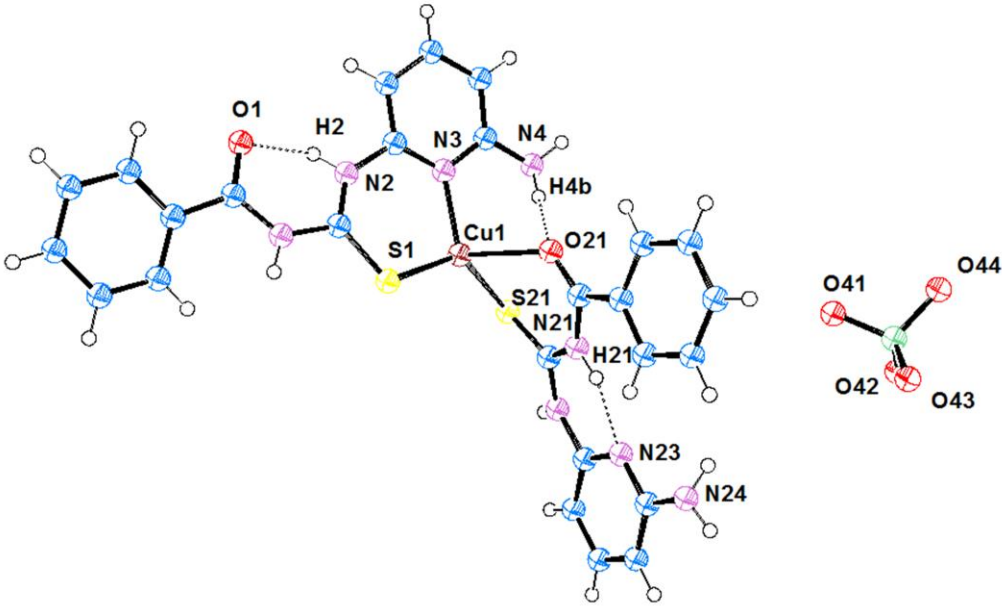


**Figure 2.17:** The asymmetric unit of **2.6**. Displacement ellipsoids are shown at 50% probability.

**Table 2.8:** Selected bond lengths (Å) and angles (º) for **2.6**.

| | | | |
|---|---|---|---|
| **Bond length (Å)** | | | |
| Cu1–N3 | 2.0149(17) | Cu1–S21 | 2.2514(6) |
| Cu1–S1 | 2.2129(6) | Cu1–O21 | 2.3697(16) |
| **Bond Angles (º)** | | | |
| N3–Cu1–S1 | 102.75(5) | N3–Cu1–O21 | 101.82(6) |
| N3–Cu1–S21 | 125.51(5) | S1–Cu1–O21 | 109.04(5) |
| S1–Cu1–S21 | 126.94(2) | S21–Cu1–O21 | 83.50(4) |

## 2.3.6.4 Crystal structure of $[Ni(L^{2C})_2](ClO_4)_2.H_2O.CH_3CH_2OH$ (2.7)

Monoclinic red crystals of **2.7** were obtained by vapour diffusion of diethyl ether into an ethyl acetate solution. Selected bond distances and bond angles are given in **Table 2.9**. An ORTEP diagram of **2.7**, with atomic numbering scheme for the coordinating sites, is shown in **Figure 2.18**. It contains two bidentate ligands which have lost the benzoyl groups. Each ligand coordinates by the nitrogen of the pyridine ring and the sulfur atom of the thiourea. The Ni(II) complex is clearly square planar (**Figure 2.18**, **Table 2.9**) with bond angles about the metal centre ranging from 88.08(3)-92.55(9), 169.95(6) and 170.57(6) degrees. It is not uncommon for Ni(II) to be surrounded by 2N and 2S. There are 626 published structures of this particular donor set according to the CCDC. 606 of them are square planar and the rest tetrahedral. The square planar complex $[Ni(L^2)_2]$.2DMSO ($L^2$ = 2-furancarbaldehyde thiosemicarbazone) reported by Argüelles[102] *et al.* exhibits a similar geometry and shows two bond lengths Ni–N(3) 1.9121(11), and two bond lengths Ni–S(1) 2.1797(4) which is similar to bond lengths in **2.7**. In the structure, intermolecular hydrogen bond interactions N4–H4B···O31, N14–H14A···O24 are observed in 2.26, 2.42 Å and occur due the interaction between thiourea N-H and perchlorate oxygen atom, **Figure 2.18**. These intermolecular hydrogen bonds are similar to those in **2.1, 2.4, 2.6** and **2.15**.

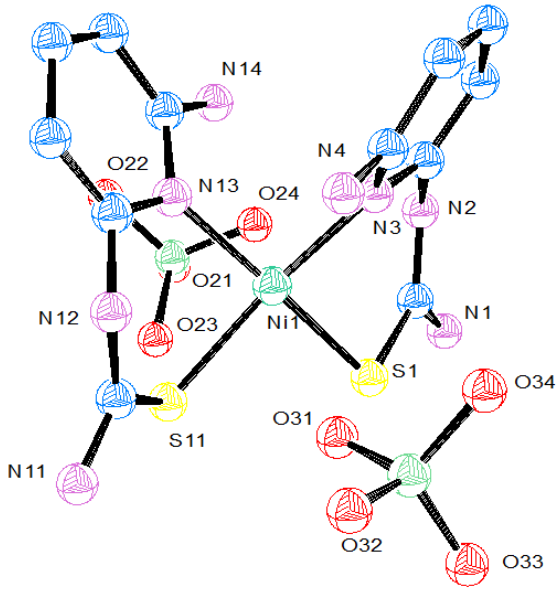


**Figure 2.18:** The asymmetric unit of **2.7**. Displacement ellipsoids are shown at 50% probability. Solvents and hydrogen atoms of crystallisation omitted for clarity.

**Table 2.9**: Selected bond lengths (Å) and angles (º) for **2.7**.

| | | | |
|---|---|---|---|
| **Bond length (Å)** | | | |
| Ni1–N13 | 1.927(2) | Ni1–S1 | 2.1651(7) |
| Ni1–N3 | 1.928(2) | Ni1–S11 | 2.1740(7) |
| **Bond Angles (º)** | | | |
| N13–Ni1–N3 | 92.55(9) | N13–Ni1–S11 | 90.28(6) |
| N13–Ni1–S1 | 170.57(6) | N3–Ni1–S11 | 169.95(6) |
| N3–Ni1–S1 | 90.65(6) | S1–Ni1–S11 | 88.08(3) |

## 2.3.6.5 Crystal structure of [Cu($L^{1b}$)Cl] (2.16)

Monoclinic red crystals of **2.16** were obtained by vapour diffusion of diethyl ether into an $CHCl_3$ solution of the complex. **Table 2.10** and **Figure 2.19** show the complex is tetrahedral and polymeric. Each copper atom is coordinated by two bidentate ligands. One ligand binds in a bidentate manner through a sulfur atom and a pyridine donor. The same sulfur donor also coordinates to a second metal

centre, and this arrangement, **Figure 2.19**, is reciprocated by another complex, leading to the formation of a polymeric chain. The final coordination sphere is completed by a chloride atom. Bond angles about the metal centre range from 92.13(5)-116.961(15) degrees, and as expected, the bond angle between the two donors of the bidentate ligand is the more acute due to the steric constraints of the ligand. Surprisingly, however, the bond angle (N1–Cu1–S1: 92.13(5)º) is slightly more acute than the analogus bite angles observed in **2.1** and **2.15**. An intramolecular hydrogen bond N2-H2....O1, **Figure 2.19**, is again observed in the acyl thiourea moiety (1.83 Å) and is similar to that in **2.1**, **2.6** and **2.15**. The polymeric tetrahedral complex **[Cu(L)Br]$_n$** L= N-(2-pyridyl)-N'-phenylthiourea reported by Saxena *et al.* exhibits the same polymeric nature and is similar to complex **2.16** when considering bond lengths Cu-S1 2.2611(6), Cu-S2 2.3147(6), Cu-Br 2.4395(3).[103]

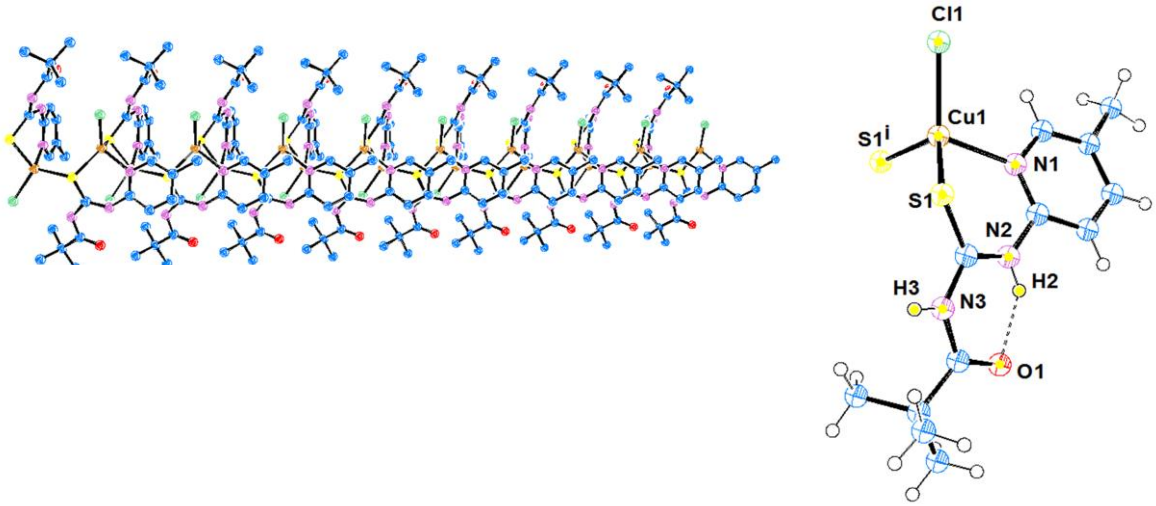


**Figure 2.19:** The polymeric nature of **2.16**, with tertiary butyl groups omitted for clarity.

**Table 2.10:** Selected bond lengths (Å) and angles (º) for **2.16**.

| | | | |
|---|---|---|---|
| **Bond length (Å)** | | | |
| Cl1–Cu1 | 2.2505(6) | Cu1–S1 | 2.3081(6) |
| Cu1–N1 | 2.0871(19) | C9–C11 | 1.540(3) |
| Cu1–S1$^{i}$ | 2.2881(6) | S1–Cu1$^{ii}$ | 2.2880(6) |
| **Bond Angles (º)** | | | |
| N1–Cu1–Cl1 | 112.58(5) | N1–Cu1–S1 | 92.13(5) |
| N1–Cu1–S1$^{i}$ | 103.38(5) | Cl1–Cu1–S1 | 114.26(2) |
| Cl1–Cu1–S1$^{i}$ | 114.57(2) | S1$^{i}$–Cu1–S1 | 116.961(15) |

## 2.3.6.6 Crystal structure of $[Cu(L^{2b*})_2Cl_2]$ (2.20)

The Cu(II) complex crystallises in the monoclinic space group $P2_1/c$ and contains one complex within the asu. Selected bond lengths and bond angles are given in **Table 2.11**. Each Cu(II) ion has a coordination number of four and is surrounded by two chloride ions and two ligands (**Figure 2.20**). The Cu(II) complex is clearly perfect square planar with bond angles about the metal center ranging from 89.28(6)-90.72(6) and two bond angles at 180.00 degrees. Formation of a square planar structure through binding of monodentate ligands to the Cu(II) ion has rarely been possible. The square planar complex $[Cu(L)_2Cl_2]$ (L= N-(7-methyl-2H-[1,2,4]thiadiazolo[2,3-a]pyridine-2-ylidene)benzamide) reported by Adhami *et al.* exhibits the same environment of $N_2Cl_2$ around the Cu(II) ion and formed a new compound by forming a new bond between sulfur atom and a pyridyl nitrogen, (see **Figure 2.21**). This complex reveals similar bond lengths as compared complex **2.20**,[94] which are: Cu–Cl1 2.2637(14), Cu–Cl2 2.2637(14), Cu–N2 1.988(2), Cu–N2' 1.988(2) and angles N2–Cu–N2' 180.0, N2–Cu–Cl1 91.10(6), N2'–Cu–Cl1 88.90(6), N2–Cu–Cl2 88.90(6), N2'–Cu–Cl2 91.10(6), Cl1–Cu–Cl2 180.0. Furthermore, the bond lengths and angles of **L** in $[Cu(L)_2Cl_2]$ are very close to the bond lengths and angles of the new oxidative cyclic compound $\mathbf{L^{2b*}}$ in **2.20**. The bond lengths in **L** range from 1.328(3)-1.364(3) Å for the C-N bonds. The C-S and N-S bonds in **L** are also very closely to their in **2.20.** The bond angles of the

oxidative cyclic compound **L** were at 111.69(19)-121.4(2)º to C-N-C angles. The other bond angles in **L**, C-S-N, C-N-S and C-C-N are observed closely to their in **2.20**. The large distortion from the perfect square planar bond angle is observed for $N2^{i}$–Cu1–$Cl1^{i}$ (89.28(6)º). An intramolecular hydrogen bond interaction (N4–H4A···S1) is observed (2.62 Å) due to the bonding between hydrogen in N-H and sulfur atoms in the new oxidative cyclic compound $\mathbf{L}^{\mathbf{2b*}}$. Furthermore, two intermolecular hydrogen bonds are observed. These interactions, N4–H4A···$Cl1^{ii}$ and N4–H4B···$Cl1^{iii}$, occur between chloride atoms and the thiourea N-H hydrogen atom. The hydrogen bond lengths are 2.79 and 2.43 Å.

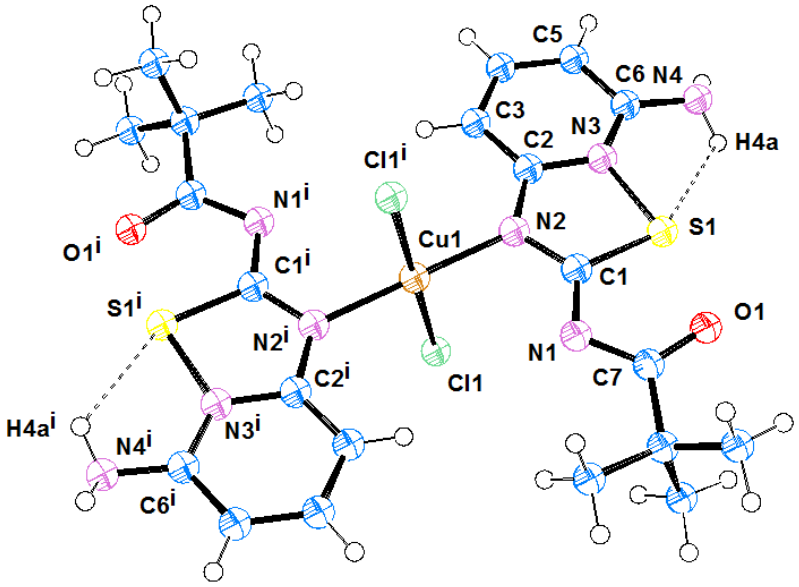


**Figure 2.20:** The asymmetric unit of **2.20**. Displacement ellipsoids are shown at 50% probability

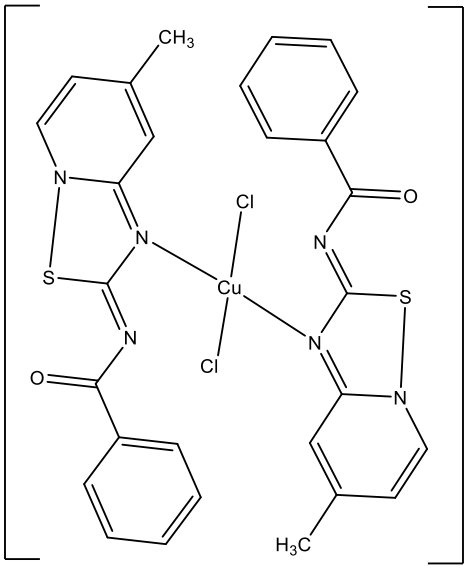


**Figure 2.21:** Chemical structure of the complex $[Cu(L)_2Cl_2]$.

**Table 2.11:** Selected bond lengths (Å) and angles ($^0$) for **2.20**.

| | | | |
|---|---|---|---|
| **Bond length (Å)** | | | |
| Cu1–Cl1 | 2.3046(6) | C1–N1 | 1.329(3) |
| Cu1–N2$^i$ | 1.962(2) | C1–N2 | 1.325(3) |
| Cu1–N2 | 1.962(2) | C2–N2 | 1.371(3) |
| Cu1–Cl1$^i$ | 2.3046(6) | C2–N3 | 1.364(3) |
| C1–S1 | 1.755(3) | C6–N3 | 1.362(3) |
| N3–S1 | 1.841(2) | C7–N1 | 1.342(3) |
| **Bond Angles (º)** | | | |
| N2$^i$–Cu1–N2 | 180.00(3) | C2–N3–S1 | 112.52(17) |
| N2$^i$–Cu1–Cl1$^i$ | 89.28(6) | C6–N3–S1 | 125.12(18) |
| N2–Cu1–Cl1$^i$ | 90.72(6) | C1–N1–C7 | 110.7(2) |
| N2$^i$–Cu1–Cl1 | 90.72(6) | C1–N2–C2 | 113.3(2) |
| N2–Cu1–Cl1 | 89.28(6) | C6–N3–C2 | 122.1(2) |
| Cl1$^i$–Cu1–Cl1 | 180.0 | C1–S1–N3 | 84.64(11) |
| C1–N2–Cu1 | 118.84(18) | N3–C6–C5 | 118.0(2) |
| C2–N2–Cu1 | 126.94(17) | | |

## 2.3.6.7 Crystal structure of $[Cu(L^{3b})](ClO_4).0.5H_2O$ (2.24)

The crystallographic data and the final refinement details are listed in **Table 2.14** and selected bond lengths and angles are given in **Table 2.12**. Monoclinic yellow crystals of **2.24** were obtained by vapour diffusion of diethyl ether into an ethanol:dichloromethane (3:1) solution of **2.24**. The Cu(I) complex, **2.24** crystallises in the monoclinic space group $P2_1$,(**Figure 2.22**). The Cu(I) cation lies at the centre of a slightly distorted trigonal planar geometry to form an $NS_2$ core. The Cu(I) ion is coordinated by one tridentate ligand through a nitrogen (pyridine ring) and two sulfur atoms. The bond angles around the metal centre are 107.40(18), 107.69(18) and 144.87(7) degrees. The complex **2.24** has two acute L-M-L angles (107.69(18)º) and one angle (S-Cu-S) is significantly larger (144.87(7)º). According to structures on the CCDC, there are no trigonal planar Cu(I) complexes of pyridyl thiourea derivatives. But with the general form $Cu^INS_2$, there are 64 crystal structures of Cu(I) complexes with the metal ion surrounded by 1N and 2S atoms adopting a trigonal planar geometry.[104,105] The related trigonal planar complex $[Cu(CETH)_2Cl]$ (CETH = cuminaldehyde-4-ethyl-3-thiosemicarbazone) reported by Krishna *et al.* exhibits similar bond lengths Cu(1)–S(1) 2.2110 (11), Cu(1)–S(2) 2.2211 (12),[106] (see **Figure 2.23**). Again and similar to **2.1**, **2.6**, **2.15** and **2.16**, typical for acyl thiourea derivatives, hydrogen bond interactions are again observed. Two interactions N2–H2A···O1 and N4–H4A···O2 (1.77 and 1.82 Å) occur within the thiourea between the oxygen carbonyl atom and hydrogen atom. Furthermore, intermolecular hydrogen bonds are observed between the hydrogen N-H in the thiourea and the oxygen atom in the perchlorate ion.

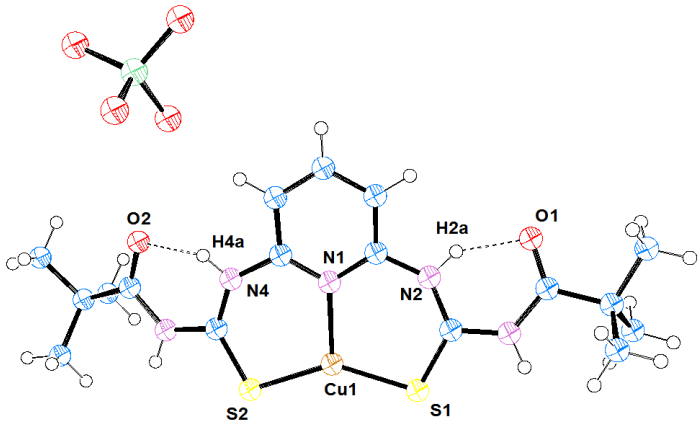


**Figure 2.22:** The asymmetric unit of **2.24**. Displacement ellipsoids are shown at 50% probability.

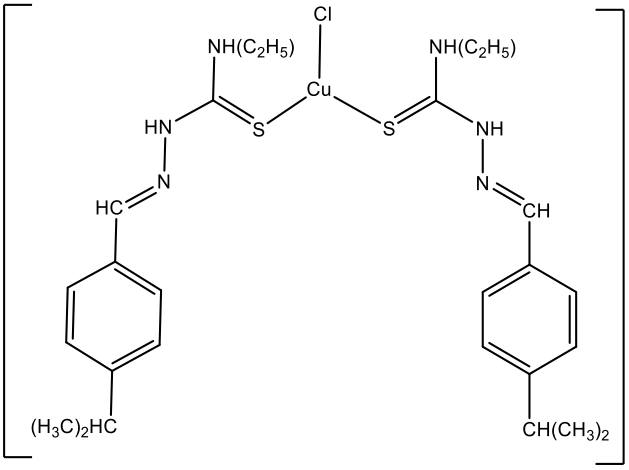


**Figure 2.23:** Chemical structure of the complex $[Cu(CETH)_2Cl]$.

**Table 2.12:** Selected bond lengths (Å) and angles (º) for **2.24**.

| | |
|---|---|
| **Bond length (Å)** | |
| Cu1–N1 | 1.993(5) |
| Cu1–S1 | 2.140(2) |
| Cu1–S2 | 2.140(2) |
| **Bond Angles (º)** | |
| N1–Cu1–S1 | 107.40(18) |
| N1–Cu1–S2 | 107.69(18) |
| S1–Cu1–S2 | 144.87(7) |

**Table 2.13:** Crystallographic data for $[Cu^{I}(L^{1a})_2]ClO_4.CH_3CN$ (**2.1**), $[Zn(L^{1C})_2](ClO_4)_2$ (**2.4**), $[Cu^{I}(L^{2a})_2]ClO_4$ (**2.6**) and $[Ni(L^{2C})_2](ClO_4)_2.H_2O.CH_3CH_2OH$ (**2.7**).

| **Compound** | **2.1** | **2.4** | **2.6** | **2.7** |
|---|---|---|---|---|
| **Chemical Formula** | $CuC_{30}H_{29}ClN_7O_6S_2$ | $ZnC_{14}H_{18}Cl_2N_6O_8S_2$ | $CuC_{26}H_{24}ClN_8O_6S_2$ | $NiC_{14}H_{22}Cl_2N_8O_{10}S_2$ |
| **Mr. g.mol$^{-1}$** | 746.71 | 598.73 | 707.64 | 656.12 |
| **Crystal system** | Monoclinic | Monoclinic | Monoclinic | Monoclinic |
| **Space group** | $P2_1/n$ | $P2_1$ | $P2_1/c$ | $C2/c$ |
| **T(K)** | 100(2) | 100(2) | 100(2) | 100(2) |
| **a, Å** | 15.4602(11) | 5.1243(2) | 10.4870(7) | 14.5374(10) |
| **b, Å** | 9.7669(7) | 11.4452(3) | 17.9141(13) | 17.6166(11) |
| **c, Å** | 21.9107(15) | 18.1830(5) | 15.3930(11) | 10.1978(7) |
| **α, degree** | 90 | 90 | 90 | 90 |
| **β, degree** | 109.196(2) | 91.109(3) | 106.4260(10) | 107.5720(10) |
| **γ, degree** | 90 | 90 | 90 | 90 |
| **Z** | 4 | 2 | 4 | 4 |
| **Dc. Mg/m$^3$** | 1.587 | 1.865 | 1.695 | 1.750 |
| **μ($M_O$ K α), mm$^{-1}$** | 0.975 | 1.656 | 1.094 | 1.228 |
| **Reflections collected** | 20493 | 7361 | 36950 | 37562 |
| **Unique reflections** | 7132 | 7361 | 6352 | 5704 |
| **$R_{int}$** | 0.0530 | ? | 0.0449 | 0.0439 |
| **R1[I>2σ<(I)]** | 0.0440 | 0.0323 | 0.0362 | 0.0423 |
| **wR2(all data)** | 0.1136 | 0.1102 | 0.0987 | 0.1258 |

**Table 2.14:** Crystallographic data for $[Cu^{I}(L^{1b})_2]ClO_4.H_2O$ (**2.15**) and $[Cu^{I}(L^{1b})Cl]$ (**2.16**), $[Cu^{II}(L^{2b*})_2Cl_2]$ (**2.20**), and $[Cu^{I}(L^{3b})]ClO_4.0.5\ H_2O$ (**2.24**).

| **Compound** | **2.15** | **2.16** | **2.20** | **2.24** |
|---|---|---|---|---|
| **Chemical Formula** | $CuC_{24}H_{36}ClN_6O_7S_2$ | $CuC_{12}H_{17}ClN_3OS$ | $CuC_{22}H_{28}Cl_2N_8O_2S_2$ | $CuC_{17}H_{26}ClN_5O_{6.50}S_2$ |
| **Mr. g.mol$^{-1}$** | 683.70 | 350.33 | 635.08 | 567.54 |
| **Crystal system** | Orthorhombic | Monoclinic | Monoclinic | Monoclinic |
| **Space group** | $P2_12_12_1$ | $P2_1/c$ | $P2_1/c$ | $P2_1$ |
| **T(K)** | 100(2) | 100(2) | 100(2) | 100(2) |
| **a, Å** | 9.0770(3) | 12.5881(9) | 10.7026(8) | 12.3999(3) |
| **b, Å** | 17.2213(8) | 6.0555(4) | 16.3850(11) | 14.2258(4) |
| **c, Å** | 19.5201(6) | 19.3671(14) | 7.9196(5) | 13.3826(3) |
| **α, degree** | 90 | 90 | 90 | 90 |
| **β, degree** | 90 | 101.012(2) | 97.287(2) | 90.462(2) |
| **γ, degree** | 90 | 90 | 90 | 90 |
| **Z** | 4 | 4 | 2 | 4 |
| **Dc. Mg/m$^3$** | 1.488 | 1.606 | 1.531 | 1.597 |
| **μ($M_O$ K α), mm$^{-1}$** | 0.992 | 1.830 | 1.175 | 1.261 |
| **Reflections collected** | 35113 | 14551 | 20899 | 30299 |
| **Unique reflections** | 6990 | 3349 | 3166 | 10291 |
| **$R_{int}$** | 0.1008 | 0.0518 | 0.0958 | 0.0477 |
| **R1[I>2σ<(I)]** | 0.0659 | 0.0310 | 0.0631 | 0.0571 |
| **wR2(all data)** | 0.1418 | 0.0943 | 0.1740 | 0.1577 |

## 2.4 Conclusion

A series of N,N'-disubstituted thiourea derivatives (**$L^{1a}$-$L^{3b}$**) and their complexes with Cu(I), Cu(II), Ni(II) and Zn(II) ions, **2.1-2.27**, were synthesized and fully characterized by elemental analysis, low and high resolution mass spectra, IR, UV-vis., $^{1}H$, $^{13}C$ NMR spectroscopy and X-ray crystallography. The redox behaviour of Cu(I), Cu(II) and Ni(II) species has been probed by cyclic voltammetry. Data shows that Cu(I) and Cu(II) complexes show one quasi-reversible process in the reductive region. Ni(II) complexes reveal two irreversible reductions. The spectroscopic characterization and crystallographic studies reveal the versatility of these ligands to form stable complexes with the transition metal ions listed above. The magnetic, spectroscopic data and X-ray crystal structures reveal that the complexes **2.1**, **2.4**, **2.6**, **2.15** are mononuclear whilst **2.16** is polymeric in the solid state. The four coordinate Cu(I) atom in **2.1**, **2.6, 2.15** and **2.16** and Zn(II) atom in **2.4** are arranged in a distorted tetrahedral geometry. The Cu(I) centre in **2.24** is three coordinate and adopts a trigonal planar geometry. From the magnetic and spectroscopic data especially the X-ray crystal structures for **2.7** and **2.20**, it is clear that four coordinate Ni(II) and Cu(II) centres have a square planar geometry. The ligands (**$L^{1a}$** and **$L^{1b}$**) have been found to bind as a neutral bidentate ligand through a sulfur atom of C=S and a nitrogen atom of the pyridyl group. The ligands **$L^{2a}$** and **$L^{2b}$** bind through the sulfur atom in C=S and the oxygen atom in C=O group, while **$L^{3a}$** and **$L^{3b}$** bind as a neutral tridentate donors via two sulfur atoms and one nitrogen atom of the pyridyl group. One of the more significant findings to emerge from this investigation is that the stability of the ligands **$L^{1a}$**-**$L^{3a}$** and **$L^{1b}$**-**$L^{3b}$** and their complexes with Cu(I), Cu(II) and Ni(II) ions at high temperatures. Interestingly, the characterization of **2.20** reveals that it is oxidized by using a weak oxidizing agent (copper chloride) to form a new kind of metal complex by an oxidative cyclisation rearrangement (Hugershoff synthesis).

## 2.5 References


**(1)** A. M. Alkherraz, Z. I. Lusta and A. E. Zubi, *International Journal of Chemical, Molecular, Nuclear, Materials and Metallurgical Engineering*, **2014**, 8 (*2*), 108–110.

**(2)** S. Edrah, *J. Appl. Scien. R*, **2010**, 4(*8*), 1014-1018.

**(3)** W. Rabb, *J. Appl. Cosmetol*, **1997**, 15(*4*), 115-123.

**(4)** C. Alkan, Y. Tek and D. Kahraman, *Turk J Chem,* **2011**, 35, 769 –777.

**(5)** M. J. Moloto, M. A. Malik, P. O'Brien, M. Motevalli and G. A. Kolawole, *Polyhedron*, **2003**, 22(*4*), 595–603.

**(6)** T.H. Sidall and W.E. Stewart, *J. Org. Chem.*, **1967**, 32, 3261.

**(7)** G. Vassilev, V. Koleva, M. Ilieva and B. Galabov, *J. Mol. Struct.*, **1982**, 82, 35–41.

**(8)** V. Joy and T. K. Srinivasan, *Spectrochim. Acta Part A,* **1999**, 55(*14*), 2899–2909.

**(9)** Y. Mido, I. Kitagawa, M. Hashimoto and H. Matsuura, *Spectrochim. Acta Part A*, **1999**, 55, 2623–2633.

**(10)** C. Marcos, J. M. Alía, V. Adovasio, M. Prieto and S. García-Granda, *Acta Crystallogr. Sect. C*, **1998**, 54(*9*), 1225–1229.

**(11)** X. Shen, X. Shi, B. Kang, Y. Liu, Y. Tong, H. Jiangc and K. Chen, *Polyhedron*, **1998**, 17(*23*), 4049-4058.

**(12)** C. R. Rasmussen, L. E. Weaner, B. E. Reynolds, A. R. Hood, L. R. Hecker and S. O. Nortey, *J. Synthesis,* **1988**, 456.

**(13)** W. Fathalla and P. Pazdera, *Arkivoc,* **2002**, 2002, 7–11.

**(14)** J. Bernstein, H.L. Yale, K. Losee, M. Holsing, J. Martins and W.A. Lott, *J. Am. Chem. Soc.*, **1951**, 73, 906-912.

**(15)** B. Loev, P. E. Bender, H. Bowman, A. Helt, R. McLean and T. Jen, *J. Med. Chem.*, **1972**, 15(*10*), 1024–1027.

**(16)** H. W. Cressman, *J. Org. Synth. Coll.*, **1955**, Vol. III, 609.

**(17)** J. G. Erickson, *J. Org. Chem.*, **1956**, 21, 483.

**(18)** S. Bourne and K. R. K. P, *J. CHEM. SOC. DALTON TRANS,* **1993**, 1, 2071.

**(19)** M. Kodomari, M. Suzuki, K. Tanigawa and T. Aoyama, *Tetrahedron Lett.*, **2005**, 46, 5841–5843.

**(20)** R. D. Campo, J. J. Criado, E. Garcia, M. R. Hermosa, A. Jimenez-Sanchez, J. L. Manzano, E. Monte, E. Rodriguez-Fernandez and F. Sanz, *J. Inorg. Biochem.*, **2002**, 89, 74-82.

**(21)** T. Phuong, T. Khac-Minh, N. T. Van Ha and H. T. Ngoc Phuong, *Bioorg. Med. Chem. Lett.*, **2004**, 14, 653–656.

**(22)** I. Küçükgüzel, S. G. Küçükgüzel, S. Rollas and M. Kiraz, *Bioorganic Med. Chem. Lett.*, **2001**, 11, 1703–1707.

**(23)** T. K. Venkatachalam, E. A. Sudbeck and F. M. Uckun, *Tetrahedron Lett.*, **2001**, 42, 6629–6632.

**(24)** P. A. Ajibade and N. H. Zulu, *Int. J. Mol. Sci.*, **2011**, 12(*10*), 7186–7189.

**(25)** R. G. Pearson, Chemical Hardness: Applications from Molecules to Solids; *Wiley-VCH, Weinheim*, **1997**.

**(26)** T. J. Lane, A. Yamaguchi, J. V. Quagliano, J. A. Ryan and S. Mizushima, *J. Am. Chem. Soc.*, **1959**, 81, 3824-3826.
**(27)** M. Schafer and C.Curran, *Inorg. Chem.*, **1966**, 5, 265-268.
**(28)** R. K. Gosavi, U. Agarwala and C. N. R. Rao, *J. Am. Chem. Soc.*, **1967**, 89, 235-239.
**(29)** R. K. Gosavi and C. N. R. Rao, *J. Inorg. Nucl. Chem.*, **1967**, 29, 1937-1945.
**(30)** L. P. Battaglia, A. B. Corradi and G. Marcotrigiano, *J.C.S. Dalton*, **1979**, 1089-1092.
**(31)** M. S. Weininger, G. W. Hunt and E. L. Amma, *J.C.S. CHEM. COMM.*, **1972**, 1140-1141.
**(32)** G. A Bowmaker, J. V Hanna, C. Pakawatchai, B. W. Skelton, Y. Thanyasirikul and A. H. White, *Inorg. Chem.*, **2009**, 48(*1*) 350–368.
**(33)** G. A. Bowmaker, C. Pakawatchai, B. W. Skelton, Y. Thanyasirikul and A. H. White, *Z. Anorg. Allg. Chem.* **2008**, 634(*14*), 2583-2588.
**(34)** F. D. Rochon, J. Bariyanga and P. C. Kong, *Can. J. Chem.*, **1985**, 63(*9*), 2425–2429.
**(35)** N. R. Kunchur and M. R. Truter, *J. Chem. Soc.*, **1958**, 2551.
**(36)** R. Mahmood, S. Sadaf, A. A. Isab, M. Akkurt, S. Sharif, I. U. Khan, J. Tariq and S. Ahmad, *Russ. J. Coord. Chem.*, **2012**, 38(*7*), 456–460.
**(37)** L. Cavalca, M. Nardelli and G. Fava, *Acta Crystallogr.*, **1960**,13, 125.
**(38)** M. Nardelli, G. F. Gasparri and P. Boldrini, *Acta Crystallogr.*, **1965**,18, 618.
**(39)** D. R. Eaton and K. Zaw, *Can. J. Chem.*, **1975**, 53, 633–643.
**(40)** H. Luth and M.R. Truter, *J. Chem. Soc. A.*, **1968**, 1879-1886.
**(41)** M. S. Weininge, J. E. O'Connor and E. L. Amma, *Inorg Chem.*, **1969**, 8(*3*), 424-431.
**(42)** D. M. Adams and R. R. Smardzew, *J. Chem. Soc. A.*, **1971**, 10-12.
**(43)** M. Nardelli and G. Fava, *Acta Crystallogr.*, **1959**,12, 727.
**(44)** S. Ooi, T. Kawase, K. Nakatsu and H. Kuroya, *Chem. Soc. Jpn.*, **1960**, 33(*6*), 861-862.
**(45)** D. A. Berta, W. A. Spofford, P. Boldrini and E. L. Amma, *Inorg Chem.*, **1970**, 9(*1*), 136-142.
**(46)** J. E. O'Connor and E. L. Amma, *Chem. Commun*., **1968**, 892-893.
**(47)** D. D. Hall and W. D. Horrocks, *Inorg Chem.*, **1969**, 8, 1809-1810.
**(48)** J. E. O'Connor and E. L. Amma, *Inorg Chem.*, **1969**, 8(*11*), 2367-2374.
**(49)** I. B. Douglass and F. B. Dains, *J. Am. Chem. Soc.,* **1934**, 56, 719-721.
**(50)** T. J. Egan, K. R. Koch, P. L. Swan, C. Clarkson, D. A. Van Schalkwyk, and P. J. Smith, *J. Med. Chem.*, **2004**, 47, 2926–2934.
**(51)** U. Paderborn, *Turkish J. Chem.*, **2010**, 34, 335–345.
**(52)** M. K. Rauf, Imtiaz-ud-Din, A. Badshah, M. Gielen, M. Ebihara, D. De Vos and S. Ahmed, *J. Inorg. Biochem.*, **2009**, 103(*8*), 1135–1144.
**(53)** N. Selvakumaran, S. W. Ng, E. R. T. Tiekink and R. Karvembu, *Inorganica Chim. Acta*, **2011**, 376(*1*), 278–284.
**(54)** N. T. Branch, *European Journal of Chemistry*, **2010**, 1(*3*), 200-205.
**(55)** Z. Weiqun, Y. Wen, X. Liqun and C. Xianchen, *J. Inorg. Biochem.*, **2005**, 99, 1314–1319.

**(56)** V. Cîrcu, M. Ilie, M. Iliş, F. Dumitraşcu, I. Neagoe and S. Păsculescu, *Polyhedron*, **2009**, 28, 3739–3746.
**(57)** R. C. Luckay, F. Mebrahtu, C. Esterhuysen and K. R. Koch, *Inorg. Chem. Commun.*, **2010**, 13, 468–470.
**(58)** J. C. Bruce, N. Revaprasadu and K. R. Koch, *New J. Chem.*, **2007**, 31, 1647-1653.
**(59)** N. Gunasekaran, P. Jerome, S. W. Ng, E. R. T. Tiekink and R. Karvembu, *J. Mol. Catal. A Chem.*, **2012**, 353, 156–162.
**(60)** N. Gunasekaran, P. Ramesh, M. N. G. Ponnuswamy and R. Karvembu, *Dalt. Trans.*, **2011**, 40, 12519-12526.
**(61)** M. S. Rathod and S. Z. Jadhao, *J. Chem. Pharm. Res.*, **2012**, 4(*3*), 1562-1565.
**(62)** N. Gunasekaran and R. Karvembu, *Inorg. Chem. Commun.*, **2010**, 13, 952–955.
**(63)** D. P. Singh, S. Pratap and M. Shukla, *Inorganica Chim. Acta*, **2014**, 423, 386–396.
**(64)** U. Braun, R. Richter, J. Sieler, A. I. Yanovsky and Y. T. Struchkov, *Z. Anorg. Allg. Chem.*, **1985**, 529, 201.
**(65)** W. Bensch and M. Schuster, *Z. Anorg. Allg. Chem.*, **1992**, 611, 99.
**(66)** K. R. Koch and S. Bourne, *J. Mol. Struct.*, **1998**, 441, 11-16.
**(67)** T. J. Egan, K. R. Koch, P. L. Swan, C. Clarkson, D. A. Van Schalkwyk and P. J. Smith, *J. Med. Chem.*, **2004**, 47(*11*), 2926-2934.
**(68)** A. Irving, K. R. Koch and M. Matoetoe, *Inorg. Chim. Acta*, **1993**, 206, 193-199.
**(69)** W. Q. Zhou, Y. Wen, L. H. Qiu, Y. Zhang and Z. F. Yu, *J. Mol. Struct.*, **2005**, 749, 89-95.
**(70)** H. Arslan, N. Külcü and U. Flörke, *Transition Met. Chem.*, **2003**, 28, 816-819.
**(71)** A. N. Westra, S. A. Bourne, C. Esterhuysen and K. R. Koch, *Dalton Trans.*, **2005**, 2162-2172.
**(72)** W. Bensch and M. Schuster, *Zeitschrift Fur Kristallographie*, **1995**, 210, 68.
**(73)** N. H. Huy and U. Abram, *Inorg. Chem.*, **2007**, 46(*13*), 5310-5319.
**(74)** G. Binzet, G. Kavak, N. Külcü, S.Özbey, U. Flörke and H. Arslan, *Transit. Met. Chem.*, **2003**, 2013(*2*), 816–819.
**(75)** H. Arslan, U. Flörke, N. Külcü and E. Kayhan, *Turk J. Chem.*, **2006**, 30, 429 –440.
**(76)** Y. Zhang, H. Pang, C. Cao and T. Wei, *Indian J. Chem.*, **2007**, 46, 1787–1791.
**(77)** W. Kaminsky, K. I. Goldberg and D. X. West, *J. Mol. Struct.*, **2002**, 605, 9–15.

**(78)** D. F. Evans, *J. Chem. Soc.*, **1959**, 2003–2005.
**(79)** M. Zhao, X. Dong, G. Li and X. Yang, *Asian Journal of Chemistry,* **2014**, 26(*1*) 277-279.
**(80)** B.-Q. Su, L. Xian, H.-B. Song and L. Sheng, *Acta Crystallogr. Sect. C Cryst. Struct. Commun.*, **2004**, 60 (*12*), m661–m662.

**(81)** Y. M. Zhang, L. Xian and T. B. Wei, *Acta Crystallogr. Sect. C Cryst. Struct. Commun.*, **2003**, 59 (*11*), m473–m474.
**(82)** S. Xu, W. Ting-Bin, L. Qiu-Tian, H. Xiao-Ying, K. Bei-Sheng, W. Xiao-Lin, H. Zhi-Shu and G. Lian-Quan, *Polyhedron*, **1997**, 16 (*15*), 2605–2611.
**(83)** X.-Y. Zhao, C.-B. Zhu, H.-P. Li, Y. Yang and H. W. Roesky, *Zeitschrift für Anorg. und Allg. Chemie,* **2014**, 640 (*8-9*), 1614–1621.
**(84)** G. Li, D.-J. Che, Z.-F. Li, Y. Zhu and D.-P. Zou, *New J. Chem.*, **2002**, 26 (*11*), 1629–1633.
**(85)** D. X. Westa, L. F. Szczepura, J. M. Giesen, W. Kaminsky, J. Kelley and K. I. Goldberg, *J. Mol. Struct.*, **2003**, 646, 95–102.
**(86)** J. Garin, E. Melendez, F. L. Merchan, P. Merino, J. Orduna and T. Tejero, *Synth. Commun*., **1990**, 20(*15*), 2327-2334.
**(87)** J. Coates;**"Interpretation of Infrared Spectra, A Practical Approach",** *Encyclopedia of Analytical Chemistry,* R.A. Meyers (Ed.) ©John Wiley & Sons Ltd, Chichester, **2000**, 10815–10837.
**(88)** C. Lodeiro, J. L. Capelo, E. Bértolo and R. Bastida, *Z. Anorg. Allg. Chem.,* **2004**, 630 (*7*), 1110–1115.
**(89)** Hathaway, *Proc. Chem. Soc.,* **1958,** 344.
**(90)** I. Papazoglou, P. J. Cox, A. G. Hatzidimitriou, C. Kokotidou, T. Choli-Papadopoulou and P. Aslanidis, *Eur. J. Med. Chem.*, **2014**, 78, 383–391.
**(91)** I. Ejidike and P. Ajibade, *Molecules*, **2015**, 20 (*6*), 9788–9802.
**(92)** A.B.P. Lever, INORGANIC ELECTRONIC SPECTROSCOPY, second eddition, (Amsterdam: Elsevier) **1986**, 534.
**(93)** F. A. Saad, *Spectrochim. Acta - Part A Mol. Biomol. Spectrosc.*, **2014**, 128, 386–392.
**(94)** F. Adhami, M. Safavi, M. Ehsani, S. K. Ardestani, F. Emmerling and F. Simyari, *Dalton Trans.*, **2014**, 43, 7945-7957.
**(95)** F. Saad, N. J. Buurma, A. J. Amoroso, J. C. Knight and B. Kariuki, *Dalton Trans*., **2012**, 41, 4608–4617.
**(96)** G. M. Sheldrick, SHELXL-97, University of Göttingen, Germany, **1997**.
**(97)** H. Ali, S. N. A. Halim, N. A. Khamis, M. S. Yusof and B. M. Yamin, *Acta Cryst.*, **2004**, E60 (*9*), o1497–o1498.
**(98)** Y. Fan, H. Lu, H. Hou, Z. Zhou, Q. Zhao, L. Zhang and F. Cheng, *J. Coord. Chem.,* **2000**, 50(*1*), 65-72.
**(99)** S. I. Orysyk, V. V. Bon, V. I. Pekhnyo, Y. L. Zborovskii, V. V. Orysyk and M. V. Vovk, *Polyhedron*, **2012**, 38(*1*), 15–25.
**(100)** A. C. Jahnke, A. Herter, S.Dechert, M. John and F. Meyer, *Inorg. Chim, Acta*, **2011**, 374(*1*), 601-605.
**(101)** M. Rittmeier, S. Demeshko, S. Dechert and F. Meyer, *Z. Angor. Allg. Chem.,* **2013**, 639,1445.
**(102)** M. C. RodÍguez-Argüelles, P. Tourón-Touceda, R. Cao; A. M. GarcÍa-Deibe, P. Pelagatti, C. Pelizzi and F. Zani, *J. Inorg. Biochem.*, **2009**, 103 (*1*), 35-42.
**(103)** A. Saxena, E. C. Dugan, J. Liaw, M. D. Dembo and R. D. Pike, *Polyhedron*, **2009**, 28(*18*), 4017–4031.

**(104)** R. Pattacini, L. Barbieri, A. Stercoli, D. Cauzzi, C. Graiff, M. Lanfranchi , A. Tiripicchio and L. Elviri, *J. Am. Chem. Soc.*, **2006**, 128 (*3*), 866–876.

**(105)** L. Han, X. Bu, Q. Zhang and P. Feng, *Inorg. Chem.*, **2006**, 45 (*15*), 5736–5738.

**(106)** P. M. Krishna and K. H. Reddy, *Inorg. Chim. Acta,* **2009**, 362 (*11*), 4185–4190.

# Chapter Three

## Cu(II), Ni(II) and Zn(II) complexes of thiosemicarbazone derivatives, (E)-N-(2-(1-(pyridin-2-yl)ethylidene)hydrazine-1-carbonothioyl)benzamide and pivalamide (ACbe-H and ACTM-H): Synthesis, characterization, structural studies and electrochemical investigations.

# 3.1 Introduction

A semicarbazone, **Scheme 3.1**, is the product resulting from the condensation reaction between a ketone or aldehyde and a semicarbazide.

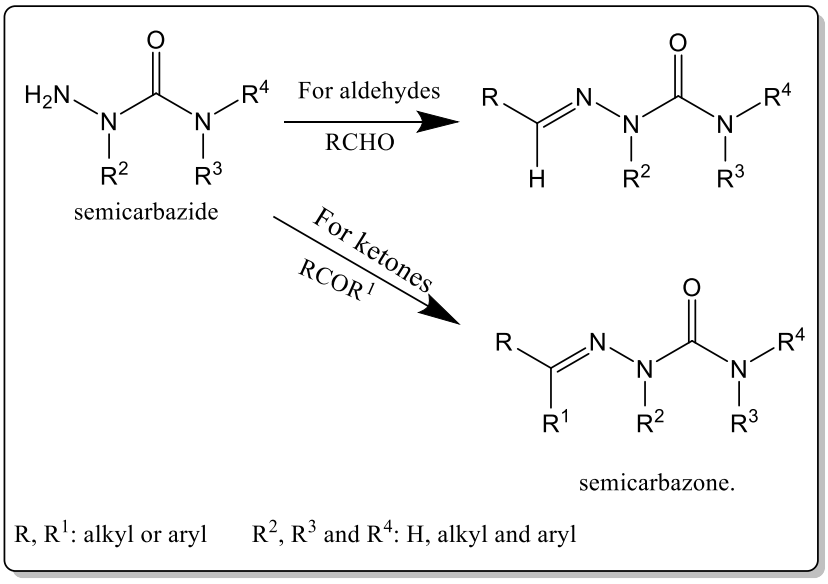


**Scheme 3.1:** Synthetic routes to a semicarbazone.

A thiosemicarbazone, **Figure 3.1**, is structurally similar to semicarbazone, except that the *oxygen* atom is replaced by a *sulfur* atom.

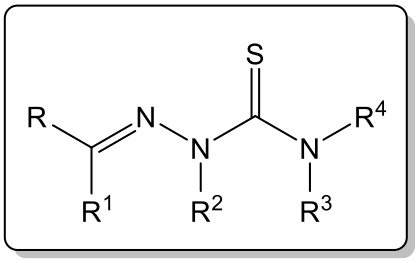

**Figure 3.1:** General chemical structure of a thiosemicarbazone.

The first study, discussions and analyses of thiosemicarbazones, emerged during the 1950s by Hamre *et al.* when they discovered the antiviral activity of thiosemicarbazones. They studied the activity of benzaldehyde thiosemicarbazone against neurovaccinial infection in mice.[1,2] These results encouraged and prompted researchers to study and create new classes of thiosemicarbazones. The main method for the synthesis of thiosemicarbazone ligands is the

condensation of a thiosemicarbazide and a ketone or an aldehyde. For example, in 1960, Gingras *et al.* synthesized a number of thiosemicarbazones, **Figure 3.2**, by the reaction of the mixture of thiosemicarbazide ($H_2NCSNHNH_2$) and the suitable aldehyde or ketone.[3,4] Similarly, the 2-hydroxyacetophenone $^4$N-dimethyl thiosemicarbazone was prepared via the reaction 2-hydroxyacetophenone and the $^4$N-methylthiosemicarbazide.[5]

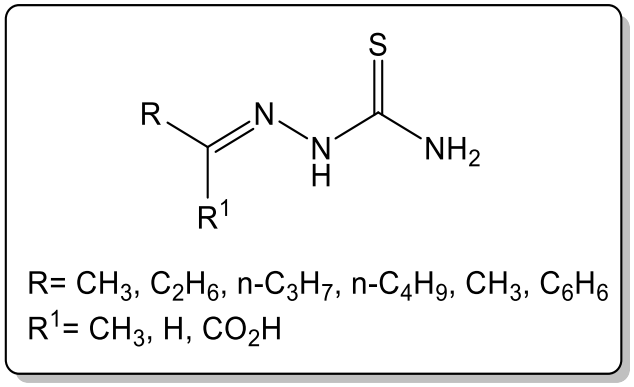


**Figure 3.2:** Thiosemicarbazone derivatives.

In recent years, thiosemicarbazones and their transition metal (Ni(II),Cu(II), Pd(II), Pt(II)) complexes have received considerable interest due to their potential use in biological fields. As an example in medicinal chemistry, these complexes have shown pharmacological activity, such as antibacterial,[6-9] antifungal,[10,11] antiviral,[12] and antitumor.[13-15] In 2001, the coordination chemistry of methyl pyruvate thiosemicarbazone with Zn(II) ion [Zn(Me–Hmpt)$Cl_2$], **Figure 3.3**, was reported by Ferrari *et al*. The Zn(II) metal centre was arranged in a penta-coordinate way with a geometry intermediate between square pyramidal and trigonal bipyramidal. One position in the base and one apex are occupied by two chloride ions while the three other positions are occupied by the three donor (N,O and S) atoms of the tridentate ligand.[16]

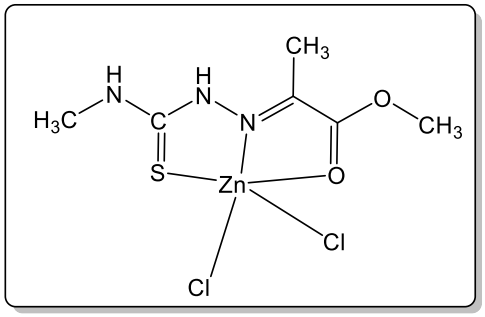


**Figure 3.3:** Chemical structure of [Zn(Me–Hmpt)$Cl_2$]

Heterocyclic thiosemicarbazones, as well as their metal complexes, are considered as a very important class of compounds. In the last few decades, researchers have shown an increased interest to investigate and study this class of thiosemicarbazone. They possess considerable biological properties and have medicinal applications such as antimalarial Cu(II),[17,18] antitumor Fe(II), Fe(III),[19] Cu(II),[20,21] antiviral,[22] antibacterial[23] Pt,[24] antitrypanosomal Pd(II),[25] antifungal Pd(II),[26] antiamoebic Cu(II).[27,28] Heterocyclic thiosemicarbazones also have applications in analytical fields. Some of these complexes are darkly coloured with metal ions. These complexes have been proposed as colourimetric analytical reagents that can be used in selective and sensitive determinations of metal ions. That means that this kind of thiosemicarbazone acts as a chelating agent for metal ions by bonding as bidentate or tridentate ligands via the sulfur and the hydrazino nitrogen atom. Sometimes they coordinate as unidentate ligands by bonding only through the sulfur atom.[29,30] An equilibrium mixture of keto (thione) (I) and enol (thiol) (II) forms, **Figure 3.4**, is observed in a thiosemicarbazone solution. This equilibrium is called thione-thiol tautomerism.

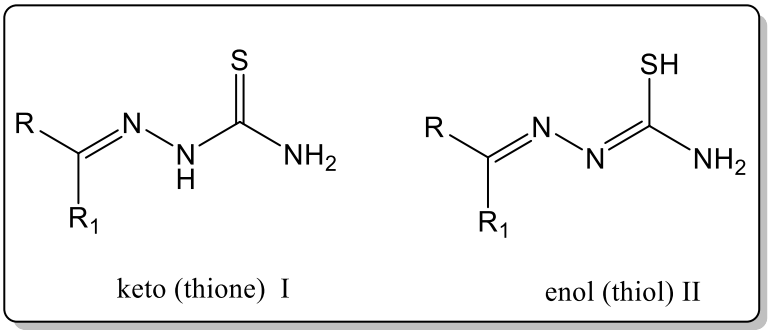


**Figure 3.4:** Thione and thiol tautomerism of thiosemicarbazones

The coordination of thiosemicarbazone ligands to metal ions may occur in two (thione-thiol) forms, in neutral thione form (common case) and in the thiol or anion form (occurs by deprotonation N-H group through enolization to the thiol form). The coordination chemistry of transition metals has been studied for thiosemicarbazone complexes. For example, Hernández *et al.* have prepared bis[4-phenyl-1-(acetone)thiosemicarbazonato]palladium (II), $[Pd(TSC)_2]$, **Figure 3.5**. The thiosemicarbazone coordinates as a bidentate deprotonated ligand via the azomethine nitrogen and thione/thiolato sulfur to form a neutral Pd(II) complex and the metal ion is situated in a square planar environment.[31] In most cases, thiosemicarbazones act as bidentate ligands such as above but when thiosemicarbazones have an additional coordination functionality in close proximity to the donating centres, the ligands may coordinate in a tri, tetra or pentadentate manner. For example, $[Fe(Ampip)_2]ClO_4$, Ampip = 2-pyridineformamide 3-piperidyl thiosemicarbazone, **Figure 3.5**, was prepared by Ketcham *et al.* The Fe(III) has an octahedral geometry and the ligand coordinates as a tridentate deprotonated ligand through a pyridyl nitrogen, azomethine nitrogen and a thione/thiolato sulfur to form a mono-anionic Fe(III) complex.[32] Argüelles *et al.* prepared the complex $[Zn(H_2dapipt)(OH_2)](ClO_4)_2$, $H_2$dapipt = 2,6-diacetylpyridine bis(hydrazinopyruvoyl thiosemicarbazone), **Figure 3.5**. The ligand $H_2$dapipt coordinates in a pentadentate manner and the Zn(II) is coordinated with two oxygen atoms from two water molecules and neutral ligand through $N_3O_2$, three nitrogen and two oxygen donating atoms to showing a planar pentagon with seven-coordinate stereochemistry.[33] Sometimes thiosemicarbazones act as monodentate ligands such as in $[Cd(L^2)_2I_2]$, $L^2$= 2-[1-(pyrrol-2-yl)ethylidene]hydrazinecarbothioamide, **Figure 3.5**, which was published by Castiñeiras *et al*. The thiosemicarbazone ligand $L^2$ is neutral and monodentate. The Cd(II) ion is coordinated to the two iodides and the S atom in the two molecules of $L^2$ to form a distorted tetrahedral geometry.[34] Further, some researchers studied and published the coordination chemistry of the metal ions Cu(II),[35-37] Cu(I),[38] VO(V),[39,40] Pd(II),[41] Pb(II),[42] Sn(II),[43] Pt(II),[44] Cd(II),[45,46] with other thiosemicarbazone derivatives.

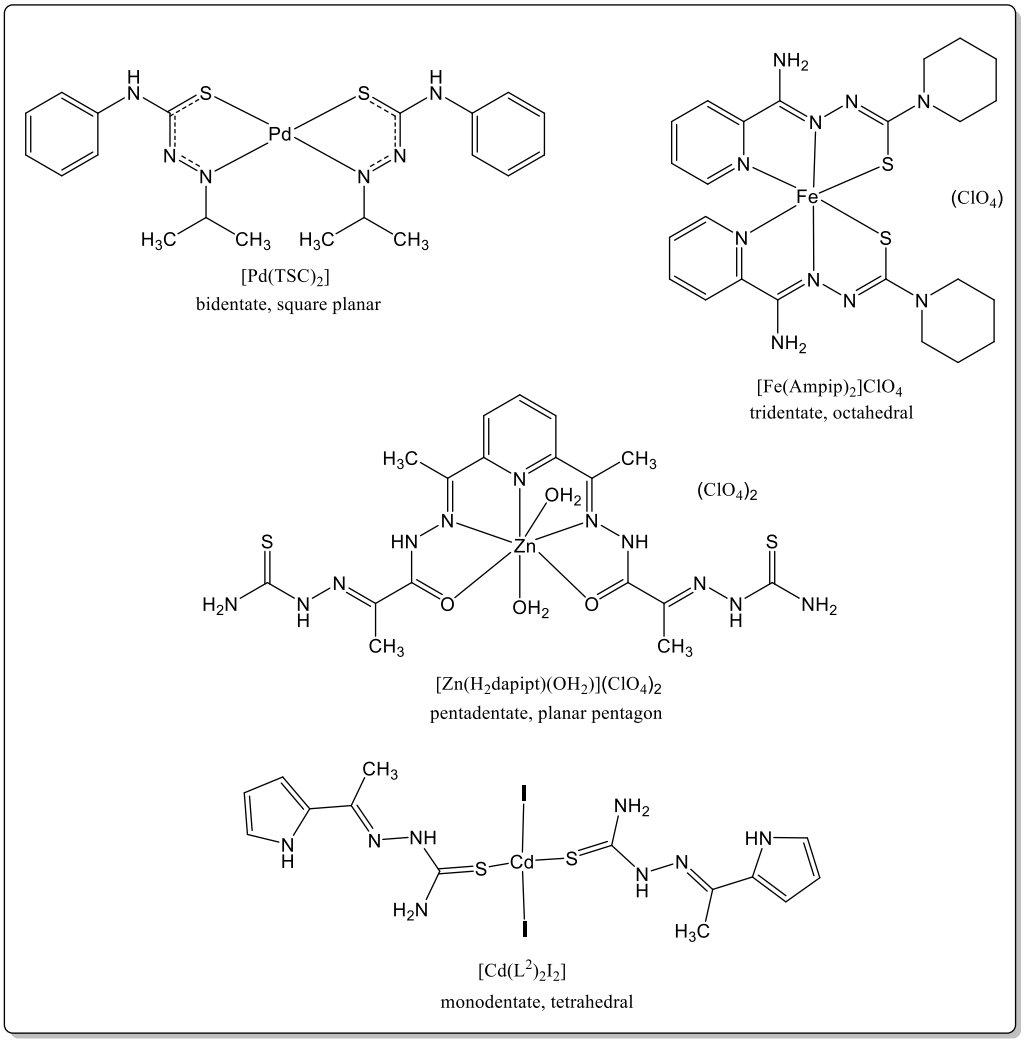


**Figure 3.5:** Examples of various coordination modes of thiosemicarbazones.

However, to the best of our knowledge, no report focused on the synthesis of any benzoyl or pivaloyl thiourea derivatives of 2-acetyl pyridine thiosemicarbazone. The coordinative behaviour of these ligands would be of interest, as the deprotonation of the N-H to form a thiol like donor may be influenced by the acyl group.

In this work, the new N,N′-substituted thiosemicarbazone derivatives (**ACbe-H** and **ACTM-H**) were synthesized by modification of the method described by Kaminsky *et al.*[47,48] In this chapter, the synthesis, full characterization and crystal structures of the new 2-acetyl pyridine thiosemicarbazone derivatives **ACbe-H** and **ACTM-H** and their Cu(II), Ni(II) and Zn(II) complexes are reported in detail. The Evans method was used to investigate the magnetic properties of these complexes. Electrochemical properties were measured for Cu(II), Ni(II) complexes.

Full characterization data led to the identification of the geometric conformations for the prepared complexes.

# 3.2 Experimental

## 3.2.1 Instrumentation

Mass spectrometry, NMR, Infrared, UV-vis., elemental analyses, magnetic susceptibilities[49] and electrochemical measurements were carried out as explained in Chapter two.

## 3.2.2 Synthesis of ligands (ACbe-H and ACTM-H)

### 3.2.2.1 Synthesis of (E)-N-(2-(1-(pyridin-2-yl)ethylidene)hydrazine-1-carbono thioyl)benzamide ACbe-H

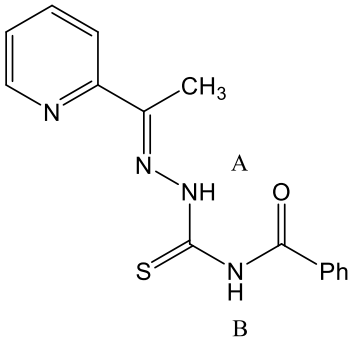


ACbe-H was synthesized via the method described before with some modification.[47] The starting material (E)-2-(1-hydrazonoethyl) pyridine was prepared as described before.[48] Its solution (1.35 g, 10 mmol) in acetonitrile (20 $cm^3$) and benzoyl isothiocyanate (1.63 g, 10 mmol) in acetonitrile (15 $cm^3$) were refluxed for 3 hours. Yellow precipitate was formed, washed with acetonitrile (10 $cm^3$) and recrystallized from acetonitrile to get yellow crystals. The crystals were dried under vacuum. Yield (1.2 g, 90%); m.p= 174-176ºC, EI-MS (m/z) (%): 298.09 [M] (80%); Mass: 298.0884, Calc Mass: 298.0888; FT-IR ($cm^{-1}$): ν(N-H) 3391, ν(C=O) 1663, ν(C=S) 1332; UV-vis. spectrum, $\lambda_{max}$ nm, (εM, $M^{-1}$ $cm^{-1}$): 287(14500), 345(10800). $^1$H NMR (400 MHz, DMSO-$d^6$), δ(ppm): 13.88 (1H, s, N-$H_A$), 11.88 (1H, s, N-$H_B$), 8.66 (1H, d, Py $J_{HH}$= 2.5 Hz), 8.18 (1H, d, Py $J_{HH}$= 5 Hz), 8.01 (2H, d, Ar $J_{HH}$= 5 Hz), 7.93 (1H, t, py $J_{HH}$= 7.5 Hz), 7.68 (1H, t, py $J_{HH}$= 7.5 Hz), 7.55 (2H, t, Ar $J_{HH}$= 5 Hz), 7.49 (1H, t, Ar $J_{HH}$= 5 Hz), 2.48 (3H, s, 1$CH_3$); $^{13}$C NMR (125 MHz, DMSO-$d^6$), δ(ppm): 177.81 (C=S), 168.69 (C=O), 156.51, 154.16, 148.80, 136.77, 133.22, 131.81, 128.76, 128.46, 124.65, 120.94, 12.44 ($CH_3$).

### 3.2.2.2 Synthesis of (E)-N-(2-(1-(pyridin-2-yl)ethylidene)hydrazine-1-carbono thioyl) pivalamide ACTM-H

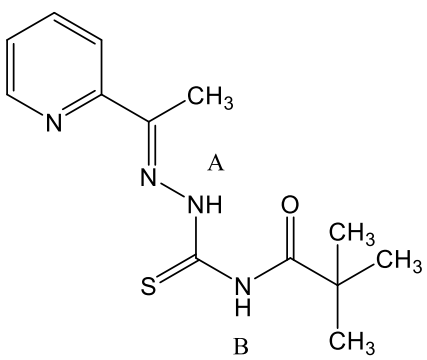


To a suspension of potassium thiocyanate (0.97 g, 10 mmol) in acetonitrile (10 $cm^3$) was added dropwise, the solution of trimethyl acetyl chloride (1.2 g, 10 mmol) in acetonitrile (15 $cm^3$). The reaction mixture was refluxed for 3 hours. The mixture was a yellow solution with white precipitate. The mixture was filtered to remove the white precipitate (KCl). The yellow filtrate solution was added to a solution of (E)-2-(1-hydrazonoethyl)pyridine (1.35 g, 10 mmol) in acetonitrile (5 $cm^3$) and the reaction mixture was stirred at room temperature for 24 hours. The light yellow precipitate was formed, collected by filtration and washed with acetonitrile:ethanol (1:1 10 $cm^3$) and purified by recrystallization from ethanol to obtain light yellow crystals. Yield (1 g, 81%); m.p= 141-142ºC, ES-MS (m/z)(%): 278.12 [M] (70%); Mass: 278.1206, Calc. Mass: 278.1201, FT-IR ($cm^{-1}$): ν(N-H) 3298, ν(C=O) 1672, ν(C=S) 1371; UV-vis. spectrum, $\lambda_{max}$ nm, (εM, $M^{-1}$ $cm^{-1}$): 270(21800), 337(23350). $^1$H NMR (400 MHz, DMSO-$d^6$), δ(ppm): 13.79 (1H, s, N-$H_A$), 10.91(1H, s, N-$H_B$), 8.64 (1H, d, Py $J_{HH}$= *2.*5Hz), 8.14 (1H, d, Py $J_{HH}$= *2.*5 Hz), 7.92 (1H, t, Py $J_{HH}$= 7.5 Hz), 7.48 (1H, t, Py $J_{HH}$= 5 Hz), 2.42 (3H, s, 1$CH_3$), 1.27 (9H, s, 3$CH_3$);$^{13}$C NMR (100 MHz, DMSO-$d^6$), δ(ppm): 180.84 (C=S), 178.13 (C=O), 156.23, 154.09, 148.77, 136.78, 124.68, 120.93, 39.88, 26.15 ($CH_3$), 12.47 ($CH_3$).

## 3.2.3 Synthesis of complexes 3.1-3.12

***CAUTION***: Perchlorate compounds of metal ions are potentially explosive especially in presence of organic ligands. Only a small amount of material should be prepared and handled with care.

### 3.2.3.1 Synthesis of $[Cu^{II}(ACbe)(MeCN)(H_2O)]ClO_4$ (3.1)

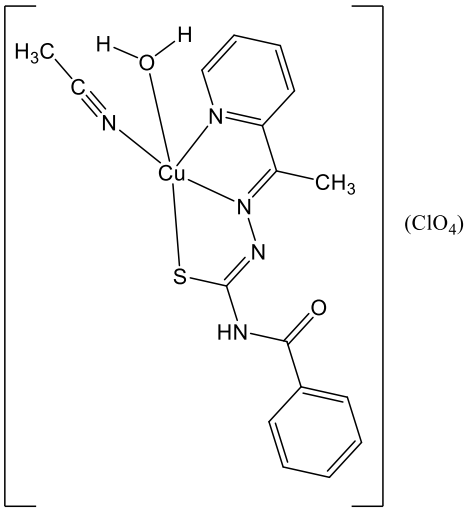

A solution of $Cu(ClO_4)_2.6H_2O$ (0.37 g, 1 mmol) in $H_2O$ (5 $cm^3$) was added to a solution of **ACbe-H** (0.3 g, 1 mmol) in DMF (5 $cm^3$). The mixture was allowed to stirring at room temperature for 3 hours. The colourless solution turned to dark green with precipitate. The green precipitate formed was filtered, washed with DMF (2 $cm^3$) to remove unreacted ACbe-H and dried under vacuum. Green crystals of **3.1** were grown at room temperature by the diffusion of diethyl ether vapour into an acetonitrile solution. Yield: (0.20 g, 65%); Pale green crystals; ESI-MS (m/z)(%): 417.98 [M-H] (100%); FT-IR ($cm^{-1}$): ν(N-H) 3429, ν(C=O) 1660, ν(Cl-O) 1092, 621; UV-vis. spectrum, $\lambda_{max}$ nm, (εM, $M^{-1}$ $cm^{-1}$): 267(50000), 303(44150), 421(2600), 455(2550), 620(47); Anal. Calcd. for **$C_{17}H_{18}ClCuN_5O_6S$:** C,39.31; H, 3.49; N,13.48. Found: C, 39.15; H, 3.49; N, 13.47.

### 3.2.3.2 Synthesis of $[Cu^{II}(ACbe\text{-}H)_2](ClO_4)_2$ (3.2)

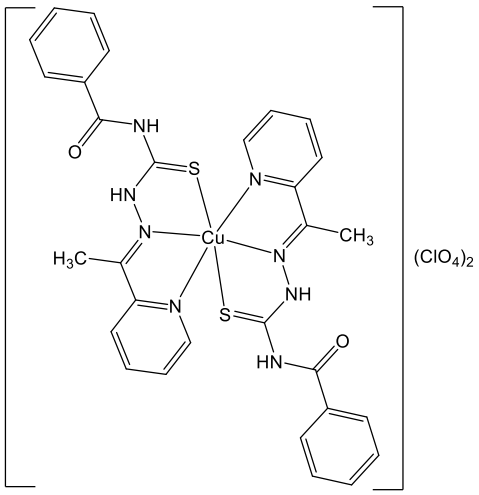

A solution of $Cu(ClO_4)_2.6H_2O$ (0.186 g, 0.5 mmol) in $H_2O$ (5 $cm^3$) was added to a solution of **ACbe-H** (0.3 g, 1 mmol) in DMF (5 $cm^3$). The mixture was allowed to stirring at room temperature for 3 hours. The colourless solution turned to green with precipitate. The green precipitate formed was filtered, washed with DMF (2 $cm^3$) to remove unreacted ACbe-H and dried under vacuum. Yield:

(0.21 g, 71%); green powder; ESI-MS (m/z)(%): 658.15 [M-H] (100%); Mass: 658.1480, calc. Mass: 658.1471; FT-IR ($cm^{-1}$): ν(N-H) 3410, ν(C=O) 1662, ν(C=S) 1258, ν(Cl-O) 1096, 621; UV-vis. spectrum, $\lambda_{max}$ nm, (εM, $M^{-1}$ $cm^{-1}$): 274(21300), 299(23200), 441(7600), 457(2300), 634(25); Anal. Calcd. for **$C_{30}H_{28}Cl_2CuN_8O_{10}S_2$:** C,41.94; H, 3.29; N,13.04. Found: C, 42.02; H, 3.20; N, 13.27.

### 3.2.3.3 Synthesis of $[Ni(ACbe\text{-}H)_2](ClO_4)_2$ (3.3)

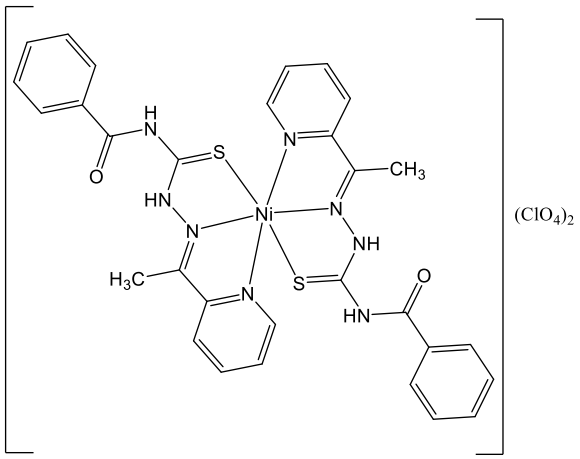


$[Ni(ACbe\text{-}H)_2](ClO_4)_2$ was obtained by stirring for 7 hours at 50ºC the mixture solution of $Ni(ClO_4)_2.6H_2O$ (0.183 g, 0.5 mmol) in methanol (5 $cm^3$) and a solution of **ACbe-H** (0.3 g, 0.10 mmol) in $CHCl_3$ (10 $cm^3$). The colourless solution turned to brown. The brown precipitate formed was filtered, washed with $CHCl_3$ (20 $cm^3$) to remove the unreacted ligand and dried under vacuum. Yield: (0.26 g, 87%); greenish brown powder; ESI-MS (m/z)(%): 653.13 [M+] (100%); Mass: 653.1057, Calc. Mass: 653.1052; FT-IR ($cm^{-1}$): ν(N-H) 3350, ν(C=O) 1660, ν(C=S) 1252, ν(Cl-O) 1093, 622; UV-vis. spectrum, $\lambda_{max}$ nm, (εM, $M^{-1}$ $cm^{-1}$): 267(15150), 296(19500), 448(7300), 476(1300), 816(23). Anal. Calcd. for **$C_{30}H_{28}Cl_2N_8NiO_{10}S_2$**: C,42.18; H, 3.30; N,13.12. Found: C, 42.25; H, 3.24; N, 13.13.

### 3.2.3.4 Synthesis of $[Zn(ACbe\text{-}H)_2](ClO_4)_2$ (3.4)

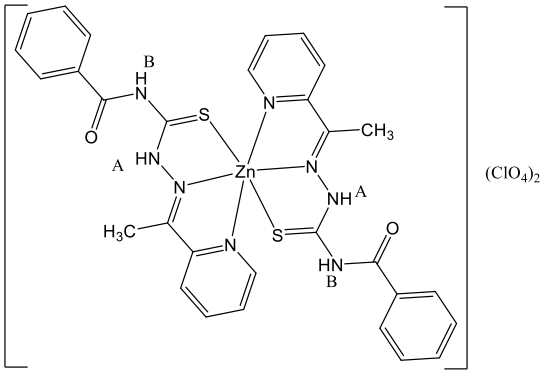


A methanolic solution (5 $cm^3$) of $Zn(ClO_4)_2.6H_2O$ (0.186 g, 0.5 mmol) was added drop wise to a solution of **ACbe-H** (0.3 g, 0.10 mmol) in $CHCl_3$ (5 $cm^3$). The mixture was stirred for 6 hours at 50ºC. The white-creamy precipitate formed was filtered, washed with $CHCl_3$ (20 $cm^3$), methanol (10 $cm^3$) to remove the unreacted ligand, Zn salt and dried under vacuum. Yield: (0.23 g, 77%); white-

creamy powder; ESI-MS (m/z)(%): 659.12 [M+] (100%); Mass: 659.0995, Calc. Mass: 659.0990; FT-IR ($cm^{-1}$): ν(N-H) 3366, ν(C=O) 1663, ν(C=S) 1250, ν(Cl-O) 1096, 619; UV-vis. spectrum, $\lambda_{max}$ nm, (εM, $M^{-1}$ $cm^{-1}$): 290(89400), 360(38000), 409(32800); $^{1}H$ NMR (400 MHz, DMSO-$d^6$), δ(ppm): 13.40 (2H, s, 2N-$H_A$), 11.53 (2H, s, 2N-$H_B$), 8.39 (2H, m, Py), 8.08 (2H, d, Py $J_{HH}$= 5 Hz), 8.02 (2H, m, py ), 7.83 (4H, d, Ar $J_{HH}$= 5 Hz), 7.54 (4H, m, 2H, Ar + 2H, py ), 7.43 (4H, t, Ar $J_{HH}$= 5 Hz), 2.39 (6H, s, $2CH_3$); $^{13}C$ NMR (100 MHz, DMSO-$d^6$), δ(ppm): 177.57 (C=S), 167.71 (C=O)**,** 155.79, 150.51, 148.10, 140.94, 133.31, 132.94, 128.86, 128.71, 124.67, 122.00, 14.09 ($CH_3$). Anal. Calcd. for **$C_{30}H_{28}Cl_2N_8O_{10}S_2Zn$:** C,41.85; H, 3.28; N,13.01. Found: C, 41.76; H, 3.27; N, 13.14.

### 3.2.3.5 Synthesis of [Ni(ACbe)Cl] (3.5)

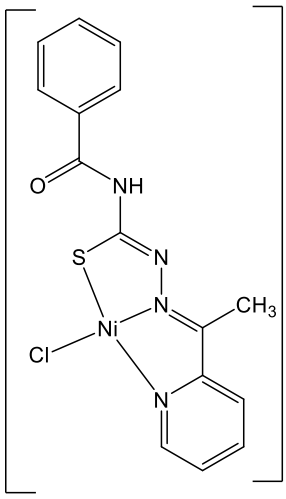


[Ni(ACbe)Cl] was obtained by stirring for 6 hours at 50ºC a solution of $NiCl_2.6H_2O$ (0.24 g, 0.10 mmol) in methanol (5 $cm^3$) and a solution of **ACbe-H** (0.3 g, 0.10 mmol) in $CHCl_3$ (10 $cm^3$). The colourless solution turned to brown. The brown precipitate formed was filtered, washed with $CHCl_3$ (20 $cm^3$) and methanol (10 $cm^3$) to remove the unreacted ligand and Ni salt and dried under vacuum. Red crystals of **3.5** were grown at room temperature by the diffusion of diethyl ether vapour into a DMF solution. Yield: (0.21 g, 70%); Red crystals; ESI-MS (m/z)(%): 389.01 [M+] (100%); 388.9760 Calc. Mass: 388.9774; FT-IR ($cm^{-1}$): ν(N-H) 3310, ν(C=O) 1664; UV-vis. spectrum, $\lambda_{max}$ nm, (εM, $M^{-1}$ $cm^{-1}$): 281(10400), 300(12200), 382(5500), 490(1300), 609(59). Anal. Calcd. for **$C_{15}H_{13}ClN_4NiOS$**: C,46.02; H, 3.35; N,14.31. Found: C, 46.24; H, 3.07; N, 14.29.

### 3.2.3.6 Synthesis of $[Zn(ACbe\text{-}H)Cl_2]$ (3.6)

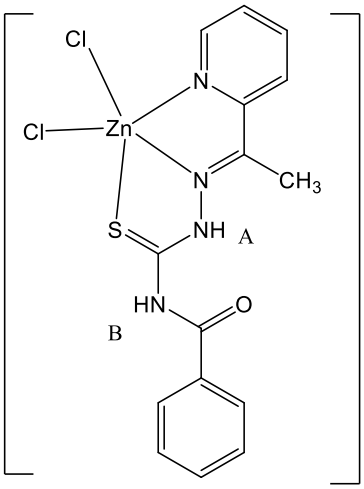


An ethanolic solution (5 $cm^3$) of $ZnCl_2$ (0.14 g, 0.10 mmol) was added drop wise to a solution of **ACbe-H** (0.3 g, 0.10 mmol) in $CHCl_3$ (5 $cm^3$). The mixture was stirred for 6 hours at 50ºC. The white-creamy precipitate formed was filtered, washed with $CHCl_3$ (10 $cm^3$), and then ethanol (5 $cm^3$) to remove the unreacted ligand and Zn salt, and then dried under vacuum. Yellow crystals of **3.6** were grown at room temperature by the diffusion of diethyl ether vapour into a DMF solution. Yield: (0.2 g, 67%); light yellow crystals; ESI-MS (m/z)(%): 463.95 [M+ MeOH] (100%); FT-IR ($cm^{-1}$): ν(N-H) 3279, ν(C=O) 1663, ν(C=S) 1270; UV-vis. spectrum, $\lambda_{max}$ nm, (εM, $M^{-1}$ $cm^{-1}$): 289(11400), 355(5100), 409(3250); $^1H$ NMR (400 MHz, DMSO-$d^6$), δ(ppm): 13.87 (1H, s, N-$H_A$), 11.74 (1H, s, N-$H_B$), 8.64 (1H, m, Py), 8.14 (1H, d, Py $J_{HH}$= 5 Hz), 8.03 (1H, m, py), 7.93 (2H, d, Ar $J_{HH}$= 5 Hz), 7.62 (2H, m, 1H-Ar + 1H-py), 7.51 (2H, t, Ar $J_{HH}$= 5 Hz), 2.47 (3H, s, 1$CH_3$); $^{13}C$ NMR (100 MHz, DMSO-$d^6$), δ(ppm): 177.40 (C=S), 168.29 (C=O), 155.57, 148.22, 137.63, 133.34, 132.43,128.87, 128.66, 125.86, 123.07, 13.45 ($CH_3$). Anal. Calcd. for **$C_{15}H_{14}Cl_2N_4OSZn$**: C,41.45; H, 3.25; N,12.89. Found: C, 41.29; H, 3.27; N, 12.93.

### 3.2.3.7 Synthesis of $[Cu^{II}(ACTM^{*}).DMF]\,BF_4$ (3.7)

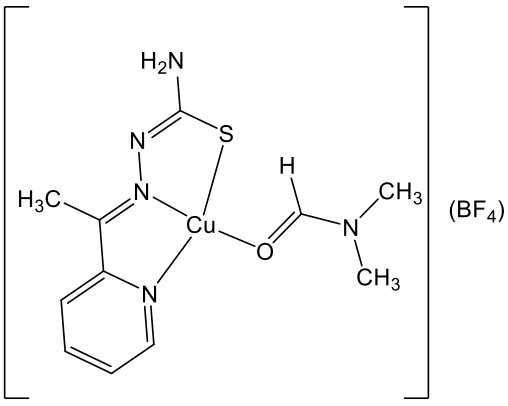


A solution of $Cu(BF_4)_2.6H_2O$ (0.26 g, 0.11 mmol) in $H_2O$ (5 $cm^3$) was added to a solution of **ACTM-H** (0.3 g, 0.11 mmol) in DMF (5 $cm^3$). The mixture was allowed to stirring for 4 hours at 50ºC. The colorless solution turned to dark green with precipitate. The green precipitate formed was filtered, washed with DMF (2 $cm^3$) to remove unreacted ACTM-H and dried under vacuum. Green crystals of **3.7** were grown at room temperature by the diffusion of diethyl ether vapour into a DMF solution. Yield: (0.22 g, 74%); dark

green crystals; ESI-MS (m/z)(%): 353.31 [M+$Na^+$,$H^+$] (100%); FT-IR ($cm^{-1}$): ν(N-H) 3333, ν(C=O)$_1$ 1710 (DMF), ν(C=O)$_2$ absent; UV-vis. spectrum, $\lambda_{max}$ nm, (εM, $M^{-1}$ $cm^{-1}$): 297(12800), 414(6150), 611(19). Anal. Calcd. for **$C_{11}H_{16}BCuF_4N_5OS$**: C,31.71; H, 3.87; N,16.81. Found: C, 31.82; H, 3.78; N, 16.72.

### 3.2.3.8 Synthesis of [$Cu^{II}$(ACTM).DMF] $BF_4$ (3.8)

A solution of $Cu(BF_4)_2.6H_2O$ (0.26 g, 0.11 mmol) in $H_2O$ (5 $cm^3$) was added to a solution of **ACTM-H** (0.3 g, 0.11 mmol) in DMF (5 $cm^3$). The mixture was allowed to stirring for 4 hours at room temperature. The colorless solution turned to dark green with precipitate. The green precipitate formed was filtered, washed with DMF (3 $cm^3$) to remove unreacted reactants and dried under vacuum. Green crystals of **3.8** were grown at room temperature by the diffusion of diethyl ether vapour into an DMF solution. Yield: (0.19 g, 64%); green crystals; ESI-MS (m/z)(%): 413.11 (100%); Mass: 413.0947, Calc. Mass: 413.0947; FT-IR ($cm^{-1}$): ν(N-H) 3335, ν(C=O)$_1$ 1707(DMF), ν(C=O)$_2$ 1670; UV-vis. spectrum, $\lambda_{max}$ nm, (εM, $M^{-1}$ $cm^{-1}$): 287(13500), 393(4650), 588(23). Anal. Calcd. for **$C_{16}H_{24}BCuF_4N_5O_2S$**: C,38.37; H, 4.83; N,13.98. Found: C, 38.26; H, 4.89; N, 13.86.

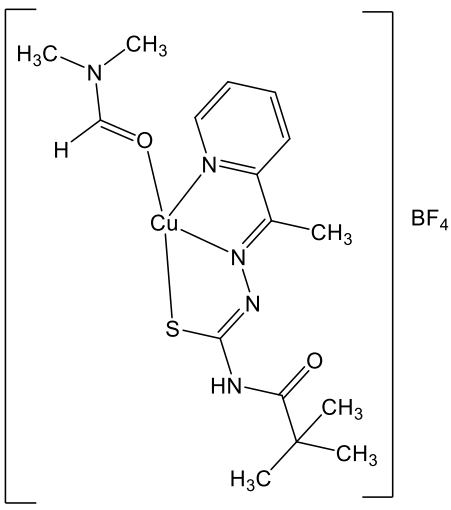


### 3.2.3.9 Synthesis of [$Cu^{II}$(ACTM-H)$_2$] $(BF_4)_2$ (3.9)

A solution of $Cu(BF_4)_2.6H_2O$ (0.13 g, 0.5 mmol) in $H_2O$ (5 $cm^3$) was added to a solution of **ACTM-H** (0.3 g, 1 mmol) in DMF (5 $cm^3$). The mixture was allowed to stir for 3 hours at room temperature. The colourless solution turned to dark green with a precipitate. The green precipitate formed was filtered, washed with DMF (3 $cm^3$) to remove unreacted reactants and dried under vacuum. Green crystals of **3.9** were grown at room temperature by the diffusion of diethyl ether vapour into DMF

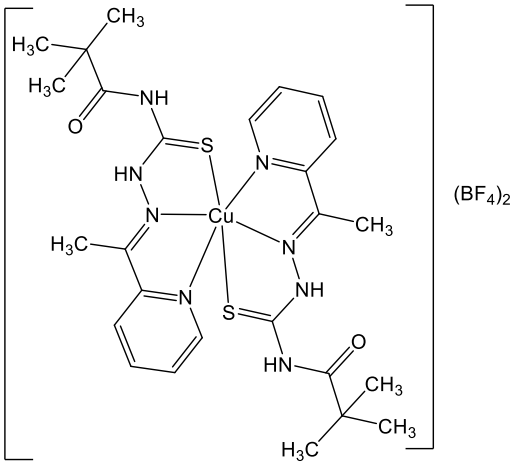

solution. Yield: (0.2 g, 68%); green crystals; ESI-MS (m/z)(%): 618.11 [M-H] (100%); Mass: 617.1889, Calc. Mass: 617.1897; FT-IR ($cm^{-1}$): ν(N-H) 3329, ν(C=O) 1669, ν(C=S) 1330; UV-vis. spectrum, $\lambda_{max}$ nm, (εM, $M^{-1}$ $cm^{-1}$): 278(67450), 412(4200), 594(11); Anal. Calcd. for **$C_{26}H_{36}B_2CuF_8N_8O_2S_2$:** C,39.34; H, 4.57; N,14.11. Found: C, 39.41; H, 4.67; N, 14.14.

### 3.2.3.10 Synthesis of [Ni(ACTM)Cl] (3.10)

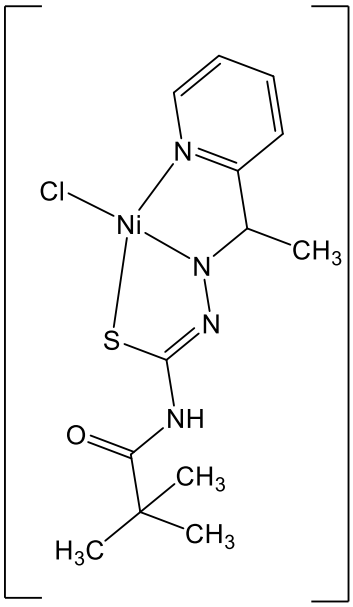


[Ni(ACTM)Cl] was obtained by stirring for 6 hours at room temperature a solution of $NiCl_2.6H_2O$ (0.26 g, 0.11 mmol) in methanol (5 $cm^3$) and a solution of **ACTM-H** (0.3 g, 0.11 mmol) in $CHCl_3$ (10 $cm^3$). The colourless solution turned to brown. The brown precipitate formed was filtered, washed with diethyl ether (20 $cm^3$) to remove the unreacted ligand and dried under vacuum. Orange crystals of **3.10** were grown at room temperature by the diffusion of diethyl ether vapour into an acetonitrile solution. Yield: (2.4 g, 80%); orange crystals; ESI-MS (m/z)(%): 393.00 [M+Na] (80%); FT-IR ($cm^{-1}$): ν(N-H) 3314, ν(C=O) 1671; UV-vis. spectrum, $\lambda_{max}$ nm, (εM, $M^{-1}$ $cm^{-1}$): 266(19800), 303(19500), 381(12300), 482(2000), 607(55). Anal. Calcd. for **$C_{13}H_{17}ClN_4NiOS$:** C,42.03; H, 4.61; N,15.08. Found: C, 41.95; H, 4.57; N, 14.78.

### 3.2.3.11 Synthesis of [Zn(ACTM*-H)$Cl_2$] (3.11)

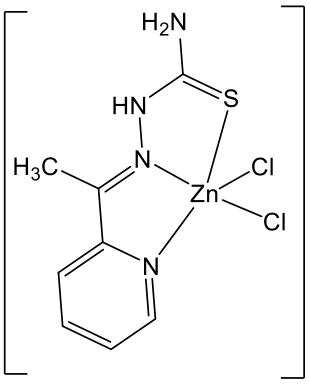


An ethanolic solution (10 $cm^3$) of $ZnCl_2$ (0.147 g, 0.11 mmol) was added drop wise to a solution of **ACTM-H** (0.3 g, 0.11 mmol) in $CHCl_3$ (5 $cm^3$). The mixture was heating for 6 hours at 50ºC. The white-creamy precipitate formed was filtered, washed with $CHCl_3$ (5 $cm^3$), ethanol (5 $cm^3$) to remove the unreacted ligand, Zn salt and dried under vacuum. Yellow crystals of **3.11** were grown at room temperature by the diffusion of diethyl ether vapour into a DMF solution. Yield: (0.22 g, 75%); Yellow crystals; ESI-MS (m/z)(%): 328.90 [M+H] (100%); FT-IR ($cm^{-1}$): ν (N-H) 3170, ν(C=S) 1321; UV-vis. spectrum, $\lambda_{max}$

nm, (εM, $M^{-1}$ $cm^{-1}$): 269(17500), 332(14800), 405(5600); $^{1}$H NMR (400 MHz, DMSO-$d^6$), δ(ppm): 10.91 (1H, s, N-H), 8.66 (1H, d, Py $J_{HH}$= 5Hz), 8.16 (1H, d, Py $J_{HH}$= 5 Hz), 8.05 (1H, t, Py $J_{HH}$= 5 Hz), 7.60 (1H, t, Py $J_{HH}$= 5 Hz), 4.34 (2H, s, $NH_2$), 2.46 (3H, s, $1CH_3$); $^{13}$C NMR (100 MHz, DMSO-$d^6$), δ(ppm): 178.52 (C=S), 155.82, 148.95, 148.64, 137.68, 126.64, 123.76, 13.17 ($CH_3$) ppm. Anal.Calcd. for **$C_8H_{10}Cl_2N_4SZn$:** C,29.07; H, 3.05; N,16.95. Found: C, 29.04; H, 2.95; N, 16.81.

### 3.2.3.12 Synthesis of [Zn(ACTM-H)$Cl_2$] (3.12)

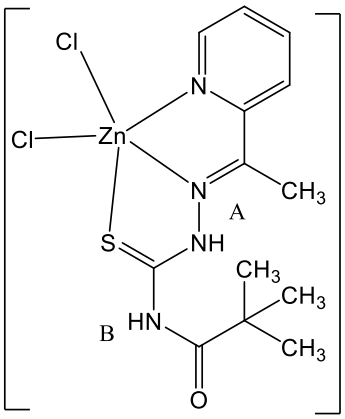


An ethanolic solution (10 $cm^3$) of $ZnCl_2$ (0.147 g, 0.11 mmol) was added drop wise to a solution of **ACTM-H** (0.3 g, 0.11 mmol) in $CHCl_3$ (5 $cm^3$). The mixture was stirred for 6 hours at room temperature. The white-creamy precipitate formed was filtered, washed with $CHCl_3$ (5 $cm^3$) and ethanol (5 $cm^3$) to remove the unreacted ligand and Zn salt and dried under vacuum. Yellow crystals of **3.12** were grown at room temperature by the diffusion of diethyl ether vapour into a DMF solution. Yield: (0.18 g, 63%); white-creamy powder; ESI-MS (m/z)(%): 411.93 [M+H] (70%); Mass: 412.1566, Calc. Mass: 412.1575; FT-IR ($cm^{-1}$): ν (N-H) 3167, ν (C=O) 1670, ν (C=S) 1340; UV-vis. spectrum, $\lambda_{max}$ nm, (εM, $M^{-1}$ $cm^{-1}$): 266(12400), 321(9300), 381(5600); $^{1}$H NMR (400 MHz, DMSO-$d^6$), δ(ppm): 14.06 (1H, s, N-$H_A$), 11.28 (1H, s, N-$H_B$), 8.66 (1H, d, Py $J_{HH}$= 2.5Hz), 8.15 (1H, d, Py $J_{HH}$= 5 Hz), 8.04(1H, t, Py $J_{HH}$= 7.5 Hz), 7.59 (1H, t, Py $J_{HH}$= 7.5 Hz), 2.46 (3H, s, $1CH_3$), 1.25 (9H, s, $3CH_3$); $^{13}$C NMR (100 MHz, DMSO-$d^6$), δ(ppm): 177.99 (C=S), 171.32 (C=O), 159.21, 155.84, 148.60, 138.09, 127.97, 120.56, 39.58, 26.05 ($CH_3$), 13.51 ($CH_3$). Anal. Calcd. for **$C_{13}H_{18}Cl_2N_4OSZn$**: C,37.66; H, 4.38; N,13.51. Found: C, 38.05; H, 4.69; N, 13.41.

# 3.3 Results and discussion

## 3.3.1 Synthesis of ligands (ACbe-H and ACTM-H)

The new N,N′-substituted thiosemicarbazone derivatives (**ACbe-H** and **ACTM-H**) were synthesized by a modification of the described method of Kaminsky *et al.*[47] Our synthesis commenced with a 3 hours reflux of the reaction mixture of an acid chloride (pivaloyl or benzoyl chloride) with potassium thiocyanate in acetonitrile to produce pivaloyl or benzoyl isothiocyanate. The final ligands, (E)-N-(2-(1-(pyridin-2-yl)ethylidene)hydrazine-1-carbonothioyl) benzamide and pivalamide (**ACbe-H** and **ACTM-H,** respectively), were prepared by conversion of an acylisothiocyanate to acylthiosemicarbazone by refluxing (3 hours) the mixture of equimolar benzoyl isothiocyanate and (E)-2-(1-hydrazonoethyl) pyridine in acetonitrile to get **ACbe-H,** while **ACTM-H** was synthesized by stirring the mixture of equimolar pivaloyl isothiocyanate with (E)-2-(1-hydrazonoethyl) pyridine in acetonitrile at room temperature. The starting material (E)-2-(1-hydrazonoethyl) pyridine was prepared as reported previously[48] by stirring at room temperature, for 24 hours, the mixture of 2-acetyl pyridine(1-(pyridin-2-yl)ethan-1-one) and hydrazine hydrate. The crude **ACbe-H** was washed and recrystallized using acetonitrile to obtain yellow crystals. Crude **ACTM-H** was washed using a mixture of acetonitrile and ethanol and recrystallized from ethanol to yield yellow crystals. The **ACbe-H** and **ACTM-H** ligands were prepared in good yields (81-90%). The synthetic route to **ACbe-H** and **ACTM-H** is shown in **Scheme 3.2**. **ACbe-H** and **ACTM-H** are soluble in acetone, acetonitrile, alcohols, ethyl acetate, $CHCl_3$, DMF and DMSO, while they are insoluble in n-hexane.

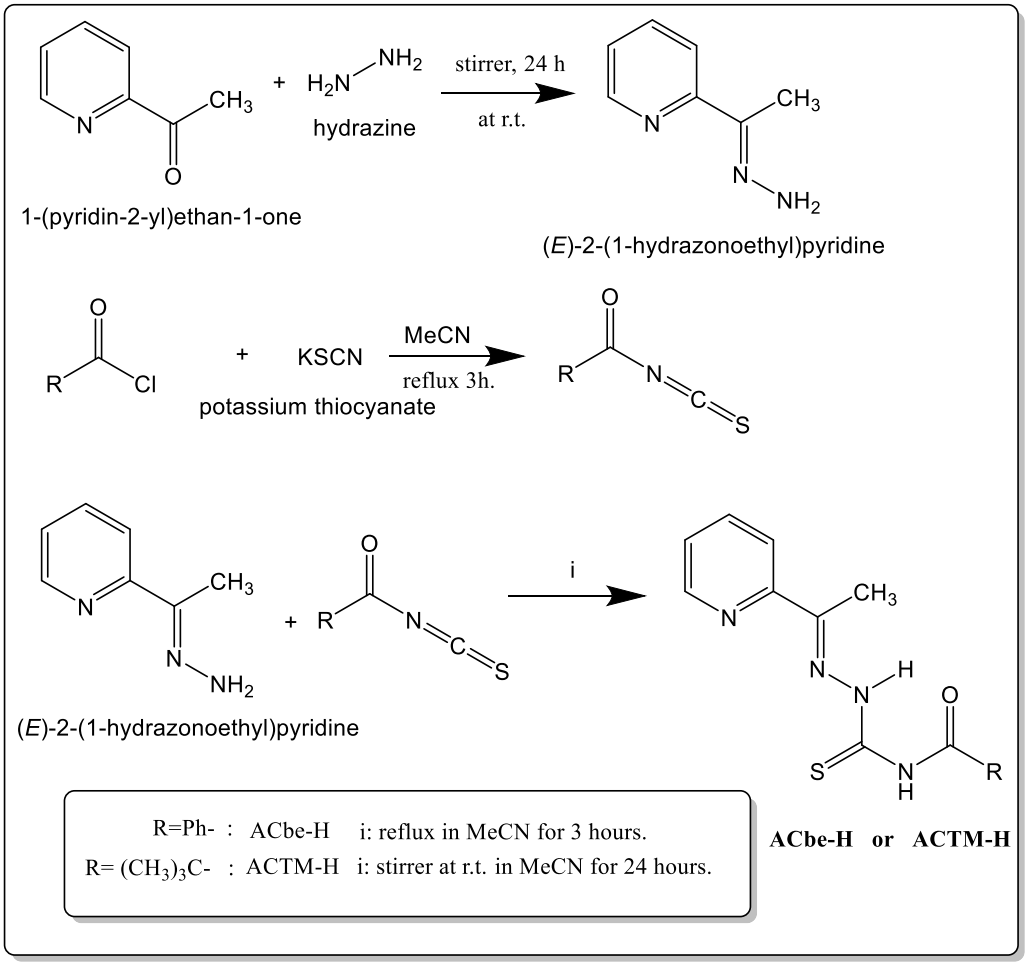


**Scheme 3.2:** Synthesis of ligands **Acbe-H** and **ACTM-H**. (Reaction conditions and reagents)

## 3.3.2 Synthesis of complexes (3.1-3.12)

The reaction between **ACbe-H** and $Cu(ClO_4)_2.6H_2O$ in 1:1 and 2:1 stoichiometries was carried out by stirring the mixture in a DMF/water solution at room temperature. Analytical, spectral and crystallographic data indicated the formation of $[Cu^{II}(\mathbf{ACbe})](ClO_4)$ **3.1** and $[Cu^{II}(\mathbf{ACbe\text{-}H})_2](ClO_4)_2$ **3.2**, (**ACbe** refers to **ACbe-H** ligand with deprotonation of one proton (N-H)), **Scheme 3.3**. Reactions between **ACTM-H** with $Cu(BF_4)_2.6H_2O$ in 1:1 and 2:1 stoichiometries were carried out by stirring mixtures in a DMF/water solution at room temperature. Analytical data indicated the formation of $[Cu^{II}(\mathbf{ACTM})](BF_4)$ **3.8** and $[Cu^{II}(\mathbf{ACTM\text{-}H})_2](BF_4)_2$ **3.9**, (**ACTM** refers to **ACTM-H** ligand with deprotonation of one proton (N-H)). The

Cu(II) complexes were isolated as green crystals and these are stable at room temperature and completely soluble in DMF and DMSO. The Cu(II) complexes with **ACbe-H** were partially soluble in acetone, acetonitrile and alcohols, but insoluble in $CHCl_3$, DCM, n-hexane. The Cu(II) complexes with **ACTM-H** were completely soluble in acetone, acetonitrile, alcohol, ethyl acetate, $CHCl_3$, DCM and insoluble in n-hexane. Importantly, the analytical, spectral and crystallographic data showed cleavage of the pivaloyl group from complex **3.7** [$Cu^{II}$(**ACTM**$^{*}$)DMF]($BF_4$), **(ACTM**$^{*}$ refers to **ACTM-H** ligand with cleavage of pivaloyl group and loss of one proton) when the reaction was carried out at 50$^{o}$C in a DMF/$H_2O$ solution, **Scheme 3.3**.

New Ni(II) complexes were prepared by stirring the reaction mixture of **ACbe-H** or **ACTM-H** with $NiCl_2.6H_2O$ in (1:1 or 2:1 ratios) in a $CHCl_3$/methanol solution to obtain **3.5** [Ni(**ACbe**)Cl] and **3.10** [Ni(**ACTM**)Cl] respectively. **3.5** was prepared at 50$^{o}$C and **3.10** at room temperature due to the **ACTM-H** ligand suffering cleavage of the pivaloyl group at 50$^{o}$C, while **ACbe-H** is stable at high temperature (this property was noted in the synthetic step). **3.5** and **3.10** were collected as brown crystals and were completely soluble in acetone, DMF and DMSO. The complex [(**ACbe-H**)$_2$Ni]($ClO_4$)$_2$, **3.3**, was obtained by stirring **ACbe-H** and $Ni(ClO_4)_2.6H_2O$ in 1:1 or 2:1 ratios at 50$^{o}$C in the mixture of $CHCl_3$/methanol solution. The complex [(**ACbe-H**)$_2$Zn]($ClO_4$)$_2$, **3.4**, was obtained by stirring **ACbe-H** and $Zn(ClO_4)_2.6H_2O$ in 1:1 or 2:1 ratios at 50$^{o}$C in the mixture of $CHCl_3$/methanol solution. Yellow crystals of the five coordinate monometallic Zn(II) complexes [$Zn^{II}$(**ACbe-H**)$Cl_2$] **3.6** and [$Zn^{II}$(**ACTM**$^{*}$**-H**)$Cl_2$] **3.11** were obtained by stirring the reaction mixture at 50$^{o}$C in a $CHCl_3$/ethanol solution of (1:1 or 1:2 ratio) of the $ZnCl_2.6H_2O$ and **ACbe-H** or **ACTM-H**. Analytical data showed there was cleavage of the pivaloyl group in [Zn(**ACTM**$^{*}$**-H**)$Cl_2$] **3.11**. The pivaloyl group may be retained to form [Zn(**ACTM-H**)$Cl_2$] **3.12** by doing the reaction at room temperature instead of 50$^{o}$C.

In summary, the **ACbe-H** ligand appears to be more stable than **ACTM-H** at higher reaction temperatures. The presence of the phenyl group in **ACbe-H** has promoted the stability due to the unique properties of aromatic *molecular orbitals* in

comparison to equivalent bonding in aliphatic groups such as methyl groups in **ACTM-H**. This also increases the rigidity of **ACbe-H** as compared to **ACTM-H**.

Green and orange crystals of **3.1** and **3.10** respectively were obtained from the diffusion of diethyl ether vapour in an acetonitrile solution. While using the same recrystallization method in DMF solution gave red crystals of **3.5**, yellow crystals of **3.6** and **3.11** and green crystals of **3.7** and **3.8**. The yields of the complexes of **ACbe-H** and **ACTM-H** and Cu(II), Ni(II) and Zn(II) ions were moderate (63-87%).

There are more interesting observations which we can summarize: **(1) ACbe-H** ligand is stable in the refluxing mixture of $CHCl_3$:methanol:$H_2O$ (3:3:0.5) at different temperatures (25, 37, 50 and 75$^oC$) (there is no cleavage of benzoyl group); **(2) ACTM-H** ligand is stable at room temperature and 37$^oC$ but suffers cleavage of the pivaloyl group at 50$^oC$ in the mixture of $CHCl_3$:methanol:$H_2O$ (3:3:0.5); **(3)** Cu(II) complexes of **ACbe-H**, **3.1** and **3.2**, are stable in a refluxing mixture of $CHCl_3$:methanol:$H_2O$ (3:3:0.5) at different temperatures (25, 37, 50 and 75$^oC$) (there is no cleavage of benzoyl group); **(4)** Cu(II) complexes of **ACTM-H**, **3.8** and **3.9**, are stable at room temperature and 37$^oC$ but they suffer cleavage of the pivaloyl group when heated to 50$^oC$ in the mixture of $CHCl_3$:methanol:$H_2O$ (3:3:0.5); **(5)** the Ni(II) complex of **ACbe-H**, **3.3**, is stable in a mixture of $CHCl_3$:methanol:$H_2O$ (3:3:0.5) at 50$^oC$ but suffers from cleavage of benzoyl group at 75$^oC$, while **3.5** is stable in the same mixture solution at high temperature; **(6)** the Ni(II) complex of **ACTM-H** (**3.10**) is stable at room temperature but suffers from cleavage of the pivaloyl group with heating at 50$^oC$ in the mixture of $CHCl_3$:methanol:$H_2O$ (3:3:0.5); **(7)** the Zn(II) complex of **ACbe-H** (**3.4**) is stable in $CHCl_3$:methanol:$H_2O$ (3:3:0.5) at 50$^oC$ but suffers from cleavage of benzoyl group at 75$^oC$, **3.6** does not show any cleavage in the solution mixture even at 75$^oC$ (similar to the stability of nickel chloride complexes). The Zn(II) complex of **ACTM-H** (**3.11**) is stable at room temperature but suffers from cleavage of pivaloyl group at 50$^oC$; **(8)** In **3.7** and **3.11** complexes, we suggest pivaloyl group cleavage in **ACTM-H** at 50$^oC$ before complexation with metal salt.

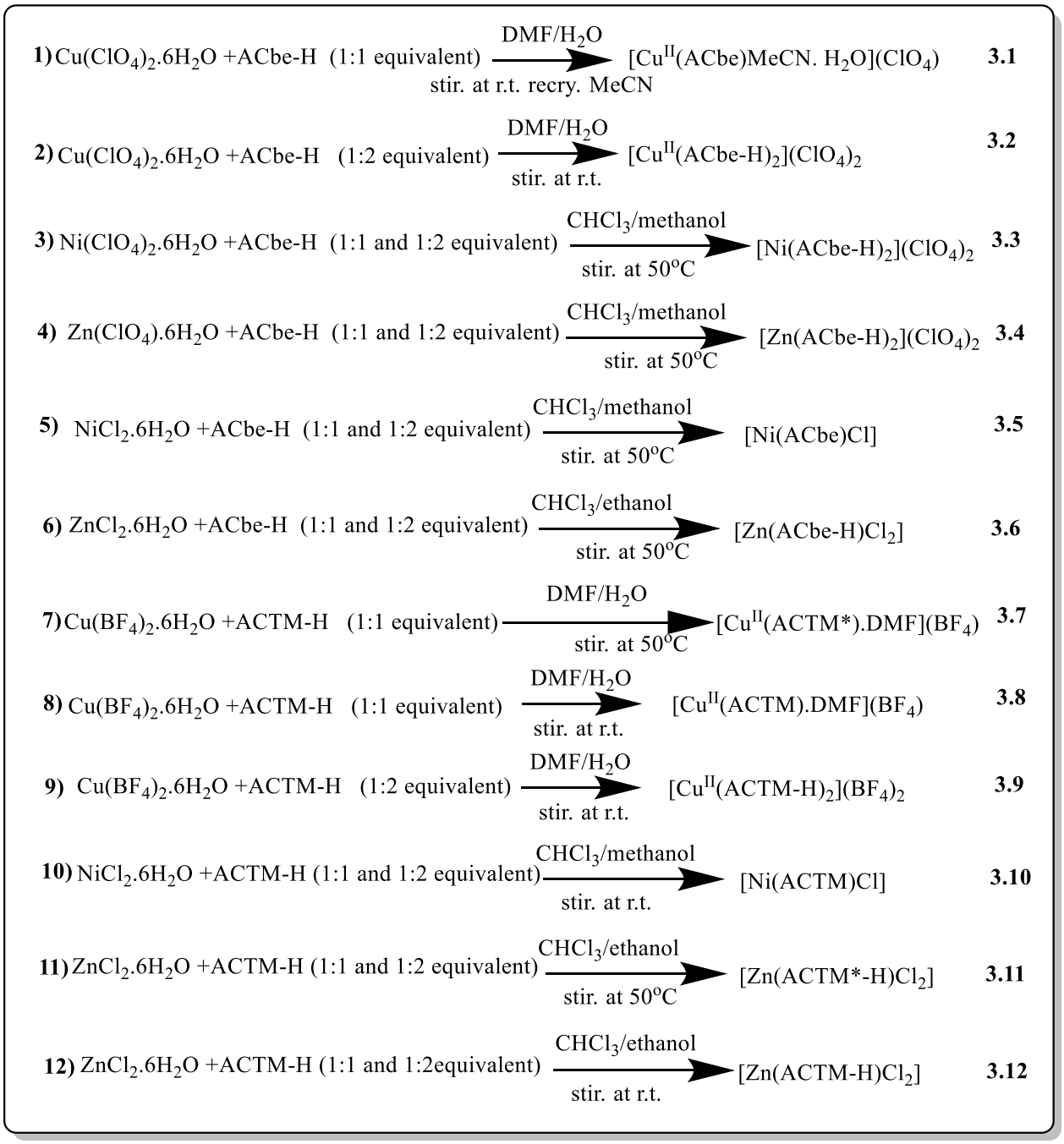


**Scheme 3.3:** Synthesis of the Cu(II), Ni(II) and Zn(II) complexes of **ACbe-H** and **ACTM-H (3.1-3.12).**

## 3.3.3 Spectroscopic studies of ligands (ACbe-H and ACTM-H) and their complexes (3.1 – 3.12)

### 3.3.3.1 $^{1}$H and $^{13}$C-NMR spectra

The $^{1}$H-NMR and $^{13}$C-NMR data of the newly prepared ligands **ACbe-H** and **ACTM-H** and their complexes with Zn(II), (**3.4**, **3.6**) and (**3.11**, **3.12**) respectively in DMSO-d$^{6}$ solution are listed in the experimental section. The $^{1}$H-NMR data for the ligands showed that the N*H* hydrogen resonates considerably downfield from other resonances in the spectra. Their $^{1}$H-NMR spectra show two singlet signals at 13.88 and 11.88 ppm for **ACbe-H** and at 13.79 and 10.91 ppm for **ACTM-H** assigned to the hydrogen bonded N-$H_A$ and free N-$H_B$ respectively. Singlet signals at 2.48 and 2.42 ppm are assigned to the methyl groups in **ACbe-H** and **ACTM-H** ligands respectively. Moreover, the $^{1}$H-NMR spectrum of the **ACTM-H** ligand showed a singlet signal at 1.27 ppm due to three methyl groups in the pivaloyl group. In addition, **ACbe-H** shows multiple peaks around 7.49-8.66 ppm, which are attributed to the aromatic protons in the aryl and pyridyl rings. In **ACTM-H**, the aromatic protons in the pyridyl ring appear as multiple peaks around 7.48-8.64 ppm. The $^{13}$C-NMR spectra of the **ACbe-H** and **ACTM-H** ligands show expected resonances, around 120.94-156.51 ppm and 120.93-156.23 ppm respectively which are assigned to the aromatic carbons, while peaks at 12.44 and 12.47 ppm respectively are assigned to the carbon of the methyl group. In addition, significant signals appear at 168.69 and 178.13 ppm respectively and are attributed to the carbon atom in the C=O group in **ACbe-H** and **ACTM-H** respectively. The signal for carbon in the C=S group is observed at 177.81 and 180.84 ppm respectively.

The $^{1}$H-NMR spectra of Zn(II) complexes **3.4, 3.6**, **3.11** and **3.12** show aromatic protons due to aryl and pyridyl rings in the range 7.43-8.66 ppm. The two resonances in the range 13.40-14.06 and 11.28-11.74 ppm are assigned to the presence of hydrogen bonded N-$H_A$ and free N-$H_B$ respectively and these two resonances shifted downfield after complexation due to the intramolecular hydrogen bonds N-H···O which is common in carbonyl thiourea complexes. Since it is involved in an intramolecular hydrogen-bond the carbonyl oxygen withdraws

electron density causing the proton to be highly deshielded and shifted downfield. As comparing between **3.4** and **3.6**, it is clear that all proton signals in **3.6** are downfield a little more than **3.4** and this is might be due to the presence of two chloride atoms in **3.6** coordinated directly with Zn(II) ion. The higher electronegativity of the two chloride atoms may cause deshielding of the protons in **ACbe-H**.

The $^{1}$H-NMR spectra of **3.11** shows the disappearance of the singlet signal in **ACTM-H** assigned to the three methyl groups, indicating cleavage of the pivaloyl group. The $^{13}$C-NMR spectra of the complexes showed all the expected resonances signals due to the unique carbon atoms. All complexes exhibited resonances due to aliphatic carbons in the expected regions. The signals observed in the range 120.56-159.21 ppm for all complexes have been assigned to the aromatic carbons of thiosemicarbazone ligands **ACbe-H** and **ACTM-H**. The resonances due to the C=S and C=O carbon nuclei in the Zn(II) complexes (**3.4, 3.6, 3.11** and **3.12)** were significantly shifted compared to their corresponding free ligands **ACbe-H** and **ACTM-H**, and appeared in the regions of 177.40-178.52 and 167.71-171.32 ppm respectively in the complexes **3.4, 3.6, 3.11** and **3.12** indicating that the C=S is taking part in the coordination to the Zn(II) ion and the possibility of the presence of hydrogen bonds with the carbonyl group in the ligands. The striking result to emerge from the data is that the C=O peak disappeared from **3.11** giving good evidence to confirm cleavage of the pivaloyl group.

### 3.3.3.2 Infrared spectra

The main vibrational bands of ligands (**ACbe-H** and **ACTM-H**) and their complexes (**3.1**-**3.12**) are given in the experimental section and listed in **Table 3.1**. The IR spectrum of free ligand **ACbe-H** shows characteristic absorption bands at $\nu_{max}$ ($cm^{-1}$): 3391(N-H), 1663(C=O) and 1332(C=S). The IR spectra of the prepared thiosemicarbazone complexes (**3.1**-**3.6**) show these absorption bands at $\nu_{max}$ ($cm^{-1}$) 3279-3429(N-H), 1660-1664(C=O) and 1250-1270(C=S). While the IR spectra of free ligand **ACTM-H** show characteristic absorption bands at $\nu_{max}$ ($cm^{-1}$) 3298(N-H), 1672(C=O) and 1371(C=S). The IR spectra of the prepared thiosemicarbazone complexes (**3.7**-**3.12**) show these absorption bands at $\nu_{max}$ ($cm^{-1}$) 3167-3335(N-H), 1669-1671(C=O) and 1310-1340(C=S). According to literature, the amide carbonyl stretch typically appears at ~1630-1690 $cm^{-1}$.[50] The carbonyl stretch of the ligands **ACbe-H** and **ACTM-H** are observed at 1663 and 1672 $cm^{-1}$ respectively. A small decrease in C=O stretching frequency of **ACbe-H** may be due to the presence of the phenyl aromatic ring, decreases the double bond character of C=O, through resonance.

The FT-IR spectra of the complexes (**3.1-3.12**) except **3.7** and **3.11** show a little change of the C=O stretching frequency indicating the oxygen carbonyl group does not coordinate to the metal centre. For the complexes **3.7** and **3.11**, the most striking changes are the disappearance of the C=O stretching frequency, indicating cleavage of the pivaloyl group from these complexes. A strong peak at 1332 and 1371 $cm^{-1}$, assigned to the $\nu$(C=S) in **ACbe-H** and **ACTM-H** respectively shifted to lower frequency at 1250-1258 and 1321-1340 $cm^{-1}$ in the prepared complexes (**3.2**, **3.3**, **3.4** and **3.6**) and (**3.9**, **3.11** and **3.12**) respectively. This indicates coordination of the sulfur atom. The presence of phenyl group in **3.4** may promote the decrease of C=S due to resonance. In addition, the coordination between **ACbe-H** with Zn(II) ion weaken the C=S bond due to the high electro positivity of the metal center. What is interesting in IR data is the absence of C=S stretching vibration from IR spectra of (**3.1**, **3.5**) and (**3.7**, **3.8**, **3.10**) and this result supports the enol form of **ACbe** and **ACTM** respectively in these complexes.

In all perchlorate complexes (**3.1**-**3.4**), the presence of two characteristic unsplit bands at 1092-1096 and 619-622 $cm^{-1}$ indicates the $T_d$ symmetry of non-coordinating $ClO_4^-$.[51, 52] All of these features are consistent with the X-ray crystal structures and $^1H$,$^{13}C$ NMR spectra for all complexes.

**Table 3.1:** Infrared spectral assignments ($cm^{-1}$) for ACbe-H and ACTM-H thiosemicarbazones ligands and Cu(II) Ni(II) and Zn(II) complexes (**3.1**-**3.12**).

| Compound | ν (N-H) | ν (C=O) | ν (C=S) | ν (Cl-O) |
|---|---|---|---|---|
| **ACbe-H** | 3391 | 1663 | 1332 | - |
| **3.1** | 3429 | 1660 | - | 1092, 621 |
| **3.2** | 3410 | 1662 | 1258 | 1096, 621 |
| **3.3** | 3350 | 1660 | 1252 | 1093,622 |
| **3.4** | 3366 | 1663 | 1250 | 1096, 619 |
| **3.5** | 3310 | 1664 | - | - |
| **3.6** | 3279 | 1663 | 1270 | - |
| **ACTM-H** | 3298 | 1672 | 1371 | - |
| **3.7** | 3333 | 1710(DMF) | - | - |
| **3.8** | 3335 | 1707(DMF)<br>1670 | - | - |
| **3.9** | 3329 | 1669 | 1330 | - |
| **3.10** | 3314 | 1671 | - | - |
| **3.11** | 3170 | - | 1321 | - |
| **3.12** | 3167 | 1670 | 1340 | - |

## 3.3.3.3 Electronic absorption spectra

The electronic spectra of the ligands **ACbe-H** and **ACTM-H** and their complexes with Cu(II), Ni(II) and Zn(II) ions were recorded in DMF solution at room

temperature and electronic bands are listed in the experimental section. The intense absorption maxima in the region 287(14,500) and 345 nm(10,800 $M^{-1}$ $cm^{-1}$) in **ACbe-H** and 270(21,800) and 337 nm (23,350 $M^{-1}$ $cm^{-1}$) in **ACTM-H** are assigned to $\pi \rightarrow \pi^*$ and $n \rightarrow \pi^*$ respectively. The Zn(II) complexes are diamagnetic and do not show any *d-d* transition bands due to a complete d shell. The UV–vis. peaks of the Zn(II) complexes **3.4**, **3.6**, **3.11** and **3.12** are attributed to π–π* and n–π* transitions of aryl, pyridyl and carbonyl groups in the **ACbe-H** and **ACTM-H** ligands. These peaks for **3.4** and **3.6** complexes are shifted to a longer wavelength (lower frequency) due to the conjugation of the carbonyl group with double bond in the phenyl group shifts both n → π* and π → π* transitions to longer wavelengths. In addition to, the coordination between **ACbe** and Zn(II) ion weaken double bonds due to the high electro positivity of Zn(II) ions. **3.11** and **3.12** are shifted to a lower wavelength (higher frequency) as compared with the corresponding their free ligands due to the absence of the phenyl group.

The electronic spectra of Cu(II) complexes **3.1**, **3.2**, **3.7**, **3.8** and **3.9** show a shift towards shorter wavelength for π–π* and n–π* transitions as compared to their corresponding free ligands. This is due to the electropositive charge of Cu(II) ion which withdraws electrons towards it and decreases the conjugation between the carbonyl and the phenyl groups. The MLCT observed in Cu(II) complexes occurs at 421 (2,600), 455 (2,550) in **3.1**, 441 (7,600), 457 (2,300) in **3.2**, 414 (6,150) in **3.7**, 393 (4,650) in **3.8** and 412(4,200) in **3.9**, see **Table 3.2**. The new peak observed in **3.1** at $\lambda_{nm}(cm^{-1})$ 620 (16,129), **Figure 3.6**, is assigned to a *d-d* transition. The complex $[Cu(HBz4E)Cl_2]$ ($HB_Z4E$= 2-benzoyl pyridine-$^4$N-ethyl amine thiosemicarbazone) reported by West *et al*,[53] also exhibited square bipyramidal environment around the Cu(II) centre and has a similar UV-vis. spectrum: $\lambda_{nm}(cm^{-1})$ 322 (31,060), 368 (27,170), 437 (22,870) and 468 (21,370) 661 (15,130 *d-d* ). The Jahn-Teller distorted[54] octahedral complexes **3.2** and **3.9** show *d-d* transitions centred at 634 and 594 nm respectively. The new peaks which are observed in **3.7** and **3.8** at $\lambda_{nm}(cm^{-1})$ 611 (16,367) and 588 (17,007) respectively are assigned to *d-d* transition, (**Figure 3.7**). However, it is very similar to the complex $[Cu(SBCM)_2]$ (SBCM=N-[1-(2-Oxo-2H-Chromen-3-yl)-ethylidene]

hydrazinecarbodithioc acid benzylester) reported by Low *et al.* which has similar square planar environment and *d-d* transition at 606 nm.[55]

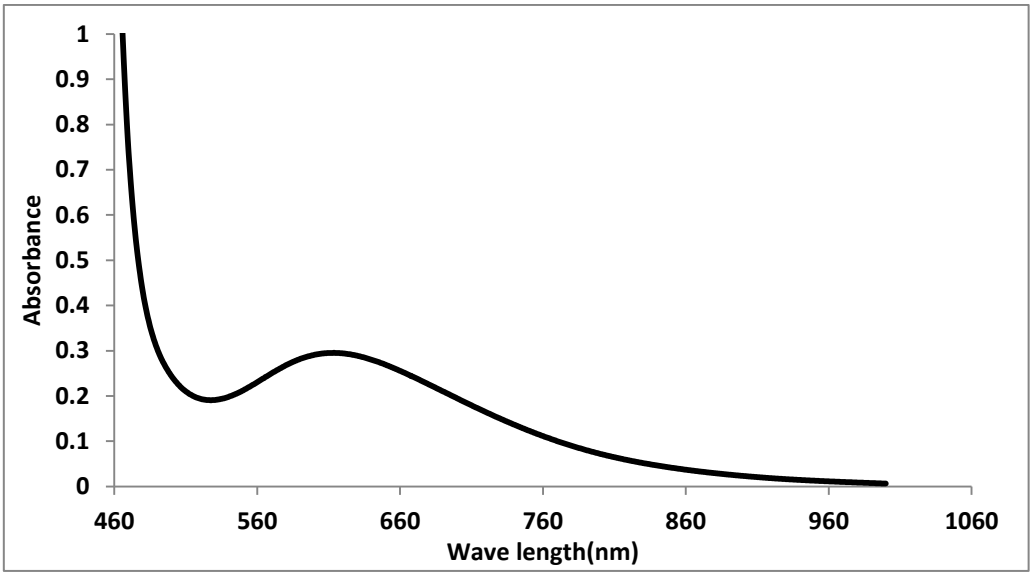


**Figure 3.6:** The electronic spectra of square bipyramidal Cu(II) **3.1**.

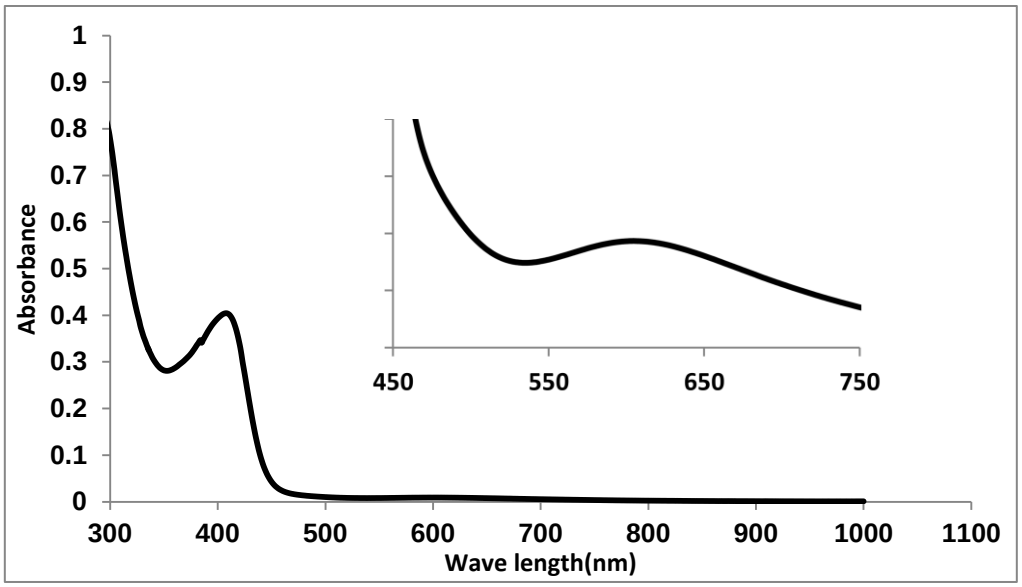


**Figure 3.7:** The electronic spectra of square planar Cu(II) **3.7**

The Ni(II) complex, **3.3** shows the π–π* and n–π* intraligand transitions which are shifted to lower wavelength (higher frequency) and observed at 267 and 296 nm and this is due to the coordination between **ACbe-H** and Ni(II) ion and the presence of MLCT which promote the double bonds. The bands observed at 448

and 476 nm are assigned to Ni(II)→S charge transfer. The appearance of MLCT bands is good evidence to the coordination between Ni(II) ion with the thiolate sulfur atom. The electronic spectrum of complex **3.3** shows only one *d-d* band at 816 nm (12,255 $cm^{-1}$) but octahedral Ni(II) complexes are expected to show three bands ($^3A_{2g}\rightarrow{}^3T_{2g}$, $^3A_{2g}\rightarrow{}^3T_{1g}$(F) and $^3A_{2g}\rightarrow{}^3T_{1g}$(P)) transitions. This is due to the high energy transitions being hidden by the charge transfer absorptions.[56] The octahedral complex [$Ni(L)_2$] (L= S-allyl-3-[(2-pyridyl-methylene)] dithiocarbazate), published by Takjoo *et al.*[57] also showed one *d-d* band at 818 nm (12,225 $cm^{-1}$), similar to complex **3.3**.

The electronic spectra of Ni(II) complexes **3.5** and **3.10** exhibited one absorption band at 609 (16,420) and 607 nm (16,474 $cm^{-1}$) respectively, which may be attributed to a *d-d* transition, characteristic of square planar geometry around Ni(II) ion, **Figure 3.8**.[58] The bands at 281 and 300 nm in **3.5** and at 266 and 303 nm in **3.10** are assigned to π–π* and n–π* intraligand transitions. These transitions were shifted to lower wavelength (higher frequency) as compared with their free ligands **ACbe-H** and **ACTM-H**. This is due to the electropositive charge on the metal centre, which withdrew electrons towards it and decreases the conjugation of the phenyl with the carbonyl group and also perturbs the conjugation between the imine and the pyridyl ring. The other bands observed at 382 (5,500), 490 (1,300) and 381 (12,300), 482 nm (2,000 $M^{-1}cm^{-1}$) in **3.5** and **3.10** respectively, are assigned to metal-ligand charge transfer. This is in good agreement with the square planar complex [Ni(Ampip)(OAc)] (Ampip= 2-pyridineformamide 3-piperidylthiosemicarbazone) reported by Ketcham *et al.* which shows peaks at 317 ($\pi\rightarrow\pi^*$), 350 nm ($n\rightarrow\pi^*$), 480 nm (MLCT) and, 591 nm (*d-d*).[59] The planarity of complexes **3.5** and **3.10**, which are diamagnetic, is confirmed by their crystal structures. The *d−d* spectra showed no bands above 10,000 $cm^{-1}$, which is consistent with a diamagnetic, planar Ni(II) complexes**.**[60]

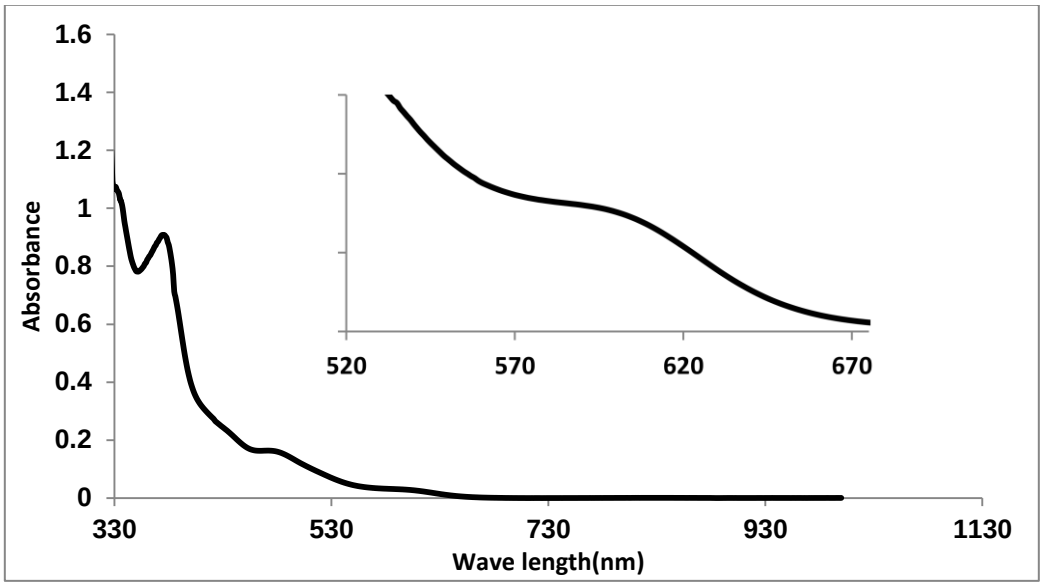


**Figure 3.8:** The electronic spectra of square planar Ni(II) complex **3.10**

**Table 3.2:** Electronic spectral assignment for Cu(II) and Ni(II) complexes of **ACbe-H** and **ACTM-H**.

| Compound | MLCT $\lambda_{max}$ nm, ($\varepsilon$, $M^{-1}cm^{-1}$) | d-d transition $\lambda_{max}$ nm, ($\varepsilon$, $M^{-1}$ $cm^{-1}$) | |
|---|---|---|---|
| | | $d_{xy} \rightarrow d_{x^2-y^2}$ | $^3A_2g \rightarrow {}^3T_1g(P)$ ($\nu_3$) |
| **3.1** | 421(2,600)<br>455(2,550) | 620(47) | - |
| **3.2** | 441(7,600)<br>457(2,300) | 634(25) | - |
| **3.3** | 448(7,300)<br>476(1,300) | - | 816(23) |
| **3.5** | 382(5,500)<br>490(1,300) | 609(59) | - |
| **3.7** | 414(6,150) | 611(19) | - |
| **3.8** | 393(4,650) | 588(23) | - |
| **3.9** | 412(4,200) | 594(11) | - |
| **3.10** | 381(12,300)<br>482(2,000) | 607(55) | - |

## 3.3.4 Magnetic susceptibility measurements

**Table 3.3** shows the magnetic data which includes mass magnetic susceptibility $\chi_{mass}$, molar magnetic susceptibility $\chi_M$ and magnetic moments $\mu_{eff.}$ for Cu(II) and octahedral Ni(II) complexes of **ACbe-H** and **ACTM-H**. Magnetic susceptibility measurements were carried out at room temperature using the Evans method.[49] The observed magnetic moments of Ni(II) complexes **3.5** and **3.10** are zero confirming the diamagnetic properties of the square-planar complexes. The magnetic moment for the Ni(II) complex **3.3** is 3.32 B.M. corresponding to two unpaired electrons consistent with an octahedral geometry around the Ni(II) complex. The magnetic moments of the Cu(II) complexes **3.7** and **3.8** are 1.84 and 1.76 B.M. which correspond to one unpaired electron and indicate that these complexes are paramagnetic and contain the Cu(II) ion. The Cu(II) complexes **3.2** and **3.9** show paramagnetic properties and their magnetic moment values are 2.01 and 2.15 B.M. respectively. The magnetic moment of **3.1** is 1.92 B.M. again confirming the presence of Cu(II). Finally, measurements confirmed the Zn(II) complexes were diamagnetic, as expected.

**Table 3.3:** Magnetic data of Cu(II) and octahedral Ni(II) complexes of **ACbe-H** and **ACTM-H**.

| Complex | $\chi_{mass}$ x10$^{-6}$ | $\chi_{molar}$ x10$^{-6}$ | $\mu_{obs}$B.M. experimental |
|---|---|---|---|
| **3.1** | 2.986 | 1551.06 | 1.92 |
| **3.2** | 1.979 | 1700.77 | 2.01 |
| **3.3** | 5.462 | 4666.34 | 3.32 |
| **3.4** | - | - | zero (diamagnetic) |
| **3.5** | - | - | zero (diamagnetic) |
| **3.6** | - | - | zero (diamagnetic) |
| **3.7** | 3.412 | 1421.85 | 1.84 |
| **3.8** | 2.584 | 1291.84 | 1.76 |
| **3.9** | 2.466 | 1957.60 | 2.15 |
| **3.10** | - | - | zero (diamagnetic) |
| **3.11** | - | - | zero (diamagnetic) |
| **3.12** | - | - | zero (diamagnetic) |

## 3.3.5 Electrochemical studies of Cu(II) and Ni(II) complexes

The electrochemical data for Cu(II) and Ni(II) complexes were measured in acetonitrile solution using $[Bu_4N][PF_6]$ (0.1 M) as supporting electrolyte. The data is summarized for Cu(II) complexes in **Table 3.4** and for Ni(II) complexes in **Table 3.5**. The cyclic voltammogram of all the Cu(II) complexes is very similar, with **Figures 3.9 and 3.10** showing representative cyclic voltammograms of the reductive region for **3.1** and **3.7** respectively. Typically a quasi-reversible process is observed between -1.03 to -1.39 V (vs $Fc/Fc^+$), with very large peak to peak separations being observed (250-600 mV); see **Table 3.4**. The peak to peak separations, being much greater than those observed with the ferrocene internal standard, suggest a quasi-reversible nature. Furthermore, the ratio of $i_{pc}$ to $i_{pa}$ is less than 1, which also supports the idea that the couple is quasi-reversible. The voltammogram of the Cu(II) complexes is in a good agreement with work reported by Kumbhar *et al.* for the Cu(II) complexes $[Cu(L^1)Cl]$ and $[Cu(L^2)Cl]$ (where $L^1$=(2-acetylpyridine-3-piperidinyl thiosemicarbazone), $L^2$=(2-acetylpyridine-3-hexamethyl eneiminyl thiosemicarbazone) which show one quasi-reversible peak -0.525V (vs Ag/AgCl) (-1.03V vs $Fc/Fc^+$), and at -0.500V (vs Ag/AgCl) (-1.00 V vs $Fc/Fc^+$) respectively which is attributed to a Cu(II) to Cu(I) reduction process.[61] The potential of Cu(II)/Cu(I) couple for the Cu(II) complex with thiourea (**2.20**) in chapter two is observed at –0.39 V while Cu(I) complexes **2.1**, **2.6**, **2.11**, **2.12**, **2.15**, **2.16**, **2.19**, **2.24** and **2.25** showed quasi-reversible process of Cu(I)/Cu(II) between -0.20 to -0.30 V (vs $Fc/Fc^+$).

Although the potential observed for the Cu(II) complexes **3.1**, **3.2**, **3.7**, **3.8** and **3.9** is similar to the potential of the clearly state the complex, further investigation is required to assign the exact nature of this feature. All Cu(II) complexes show an irreversible oxidative process and this peak is centred between +0.41 to +0.57V.

The cyclic voltammogram of Ni(II) complexes **3.3**, **3.5** and **3.10** reveal two irreversible oxidative peaks in the anodic region in the range + 0.33 to +0.62V (vs $Fc/Fc^+$) and +0.698 to +0.909V (vs $Fc/Fc^+$) respectively. The cyclic voltammograms of **3.3** and **3.5** are shown in **Figures 3.11 and 3.12** as representative examples.

Similar behaviour has been reported by Saswati[62] for the complex [{Ni($L^3$)}$_2$(μ-4,4′-byp)]·2DMSO, $L^3$= 4-(p-methoxyphenyl) salicylaldehyde thiosemicarbazone which shows two similar irreversible oxidative processes at +0.674 and +0.980V assigned to Ni(II)/Ni(III) process. Reguig *et al*. reported the Ni(II) complex [Ni($HL^1$)$_2$], $L^1$= N-(2-hydroxybenzylidene) benzene sulfonohydrazide) which show two similar irreversible oxidative processes at +0.58 V and +1.22 V.[63] Without further investigate, it is impossible to unequivocally assign these processes.

**Table 3.4:** Electrochemical parameters for the **irreversible oxidation** and **quasi-reversible** processes exhibited by Cu(II) complexes **3.1**, **3.2**, **3.7**, **3.8** and **3.9** in acetonitrile solution, supporting electrolyte [$Bu_4N$][$PF_6$] (0.1 M), t =25º C measured at 100 mv/sec.

| **Complex** | ***Irreversible oxidation*** | ***Quasi reversible* vs Fc/Fc$^+$** | | |
|---|---|---|---|---|
| | **$E_P$/V vs Fc/Fc$^+$** | **$E_{Pa}$ V** | **$\Delta E_P$ mv** | **$I_{pc}/I_{Pa}$** |
| **3.1** | +0.405 | -1.242 | 543 | 0.353 |
| **3.2** | +0.543 | -1.034 | 428 | 0.295 |
| **3.7** | +0.571 | -1.065 | 254 | 0.685 |
| **3.8** | +0.417 | -1.118 | 596 | 0.284 |
| **3.9** | +0.556 | -1.388 | 431 | 0.391 |

**Table 3.5:** Electrochemical parameters for the **irreversible oxidation** processes exhibited by Ni(II) complexes **3, 5** and **10** in acetonitrile solution, supporting electrolyte [$Bu_4N$][$PF_6$] (0.1 M), t =25º C measured at 100 mv/sec.

| **Complex** | **$E_P$/V vs Fc/Fc$^+$** | |
|---|---|---|
| | ***Irreversible oxidation*** | |
| **3.3** | +0.331 | +0.698 |
| **3.5** | +0.615 | +0.909 |
| **3.10** | +0.583 | +0.828 |

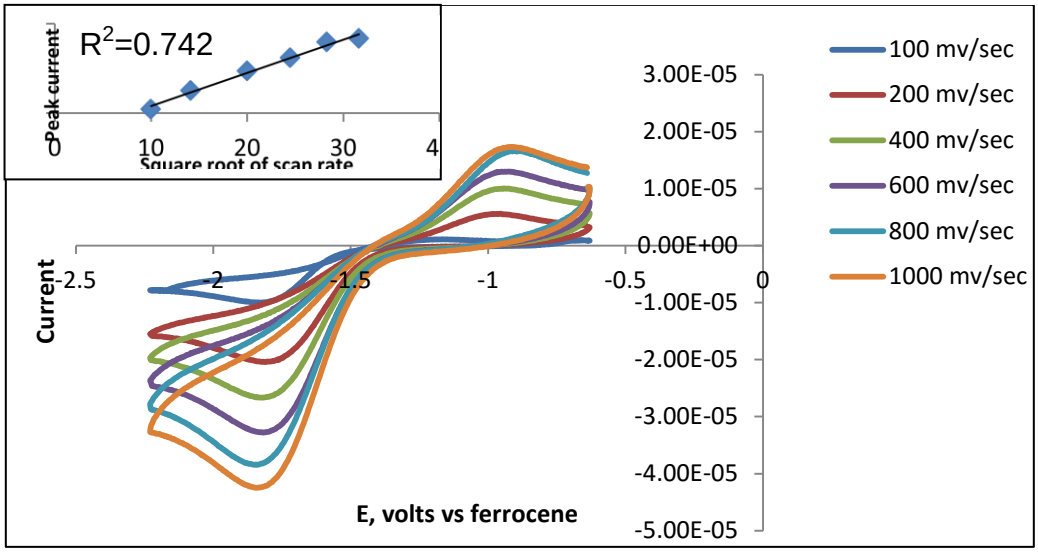


**Figure 3.9**: Cyclic voltammogram of complex **3.1** shows quasi-reversible process.

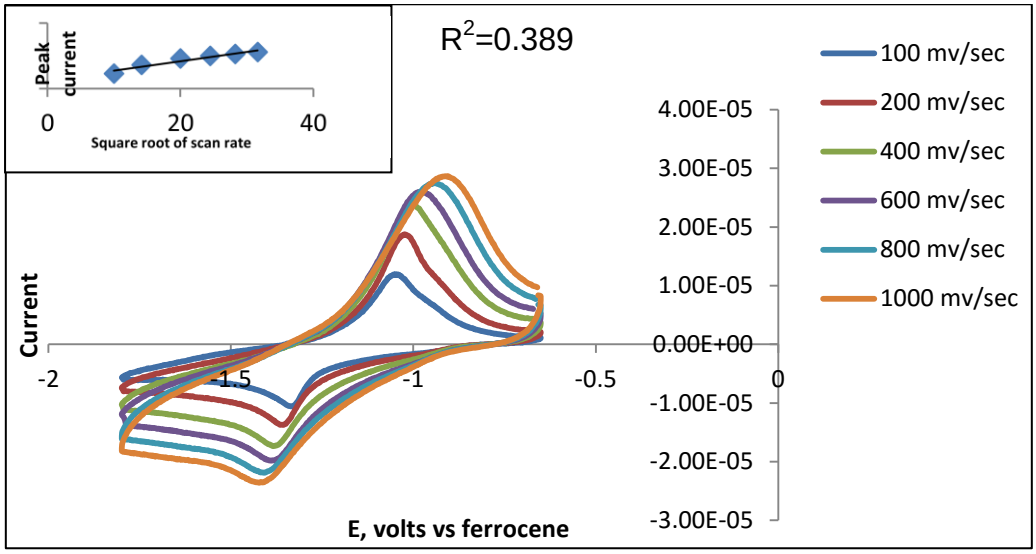


**Figure 3.10**: Cyclic voltammogram of complex **3.7** shows quasi-reversible process.

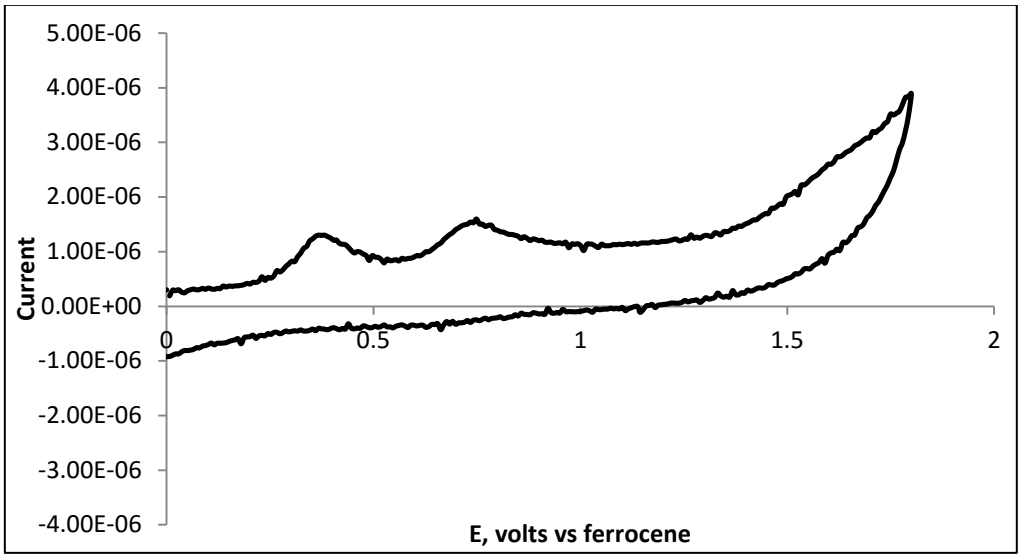


**Figure 3.11**: Cyclic voltammogram of complex **3.3** show irreversible oxidative process at 100 mv.sec$^{-1}$.

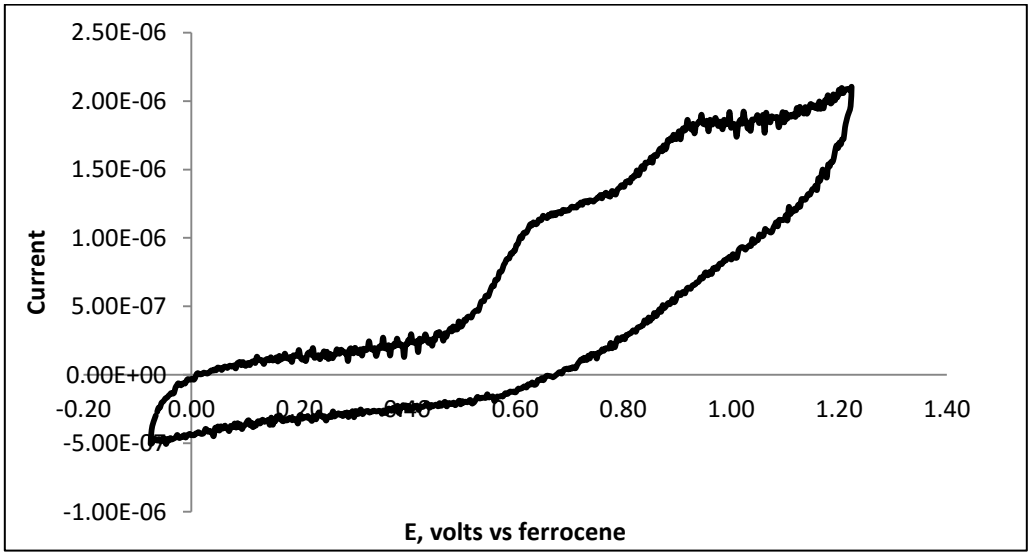


**Figure 3.12**: Cyclic voltammogram of complex **3.5** show irreversible oxidative process at 100 mv.sec$^{-1}$.

## 3.3.6 Crystallographic studies

Crystal parameters, details of the data collection and structural refinements of **3.1**, **3.5**, **3.6**, **3.7** are presented in **Table 3.11** while **3.8** and **3.10** and **3.11** are presented in **Tables 3.12**. Structure solution was refined by full-matrix least-squares on $F^2$.[64] Relevant crystal data are given for all structures in **Tables 3.6-3.10** along with relevant bond lengths and angles.

### 3.3.6.1 Crystal structure of $[Cu^{II}(ACbe)(CH_3CN)(H_2O)]\ ClO_4$ (3.1)

Green crystals of **3.1** were obtained by vapour diffusion of diethyl ether into an acetonitrile solution of the complex. The copper compound crystallises in the monoclinic space group $P2_1/n$ and contains two structurally similar complexes. Just one of them is discussed. Selected bond distances and bond angles are given in **Table 3.6**. **Figure 3.13** shows the complex with atomic numbering scheme for the coordinating sites. The metal centre is 5-coordinate and is coordinated by a tridentate **ACbe-H** ligand, the nitrogen atom of an acetonitrile and the oxygen atom of $H_2O$. **ACbe-H** through nitrogen atom of the pyridyl ring, and the nitrogen and sulfur atoms in the thiosemicarbazone. The coordination around the Cu(II) centre atom is almost square pyramidal with based bond angles ranging from 80.77(7)º to 101.71(4). The C8–S1 bond length [1.726(2) Å], is intermediate between a C–S single bond [1.82 Å] and C=S double bond [1.62 Å] meaning it has partial double bond character, indicating delocalization over the C-S-N-N-C chain. The **ACbe-H** ligand is in its deprotonated form, common for coordinated thiosemicarbazone ligands. According to the CCDC, there are 40 crystal structures of Cu(II) thiosemicarbazone complexes that have three nitrogen, one oxygen and one sulfur atom around Cu(II) ion and all possess 5-coordinate square pyramidal geometry. In particular, only ten of them were derivatives of pyridyl thiosemicarbazone and show coordination as a tridentate ligand, similar to **3.1** with the Cu(II) ion.[65-68]

The related complex $[Cu(L^4)(sac)(H_2O)]$. Hsac ($L^4$=N-methyl-2-(1-(5-methylpyridin-2-yl)ethylidene)hydrazine-1-carbimidothioic acid, sac= saccharinate), **Figure 3.14**, which was reported by Omar *et al.,*[69] also exhibits a square pyramidal geometry and the tridentate NNS ligand is coordinated to Cu(II) ion through pyridine nitrogen,

azomethine nitrogen and thiolate sulfur atoms, while the fourth and fifth coordination positions are occupied by the N-bonded saccharinate anion and a water ligand, respectively. The bond lengths and angles in this complex are very close to **3.1**, (bond lengths: Cu1–N 1.968-2.010 Å, Cu1–S1 2.274 Å and Cu1–O1 2.361 Å).

In addition, there are two intramolecular hydrogen bonds within the thiourea, first between the oxygen of the water molecule with N-H, N4–H4A···O21$^{i}$ and the other between the hydrogen of the water molecule with the nitrogen thiourea atom O21–H21A···N3$^{i}$. Finally, there is an intermolecular hydrogen bond O21–H21B···O73$^{iii}$ between the $H_2O$ hydrogen atom and the oxygen perchlorate ion, **Figure 3.13**. The Cu(II) complex, **3.1** did not show the common hydrogen bond attached to N-carbonyl thiourea derivative such as (**2.1**, **2.6**, **2.15**, **2.16**, **2.24** in chapter two). This is due to the deprotonation of H3-atom of N3-H3 bond in the ligand **ACbe** after complexation to form **3.1**.

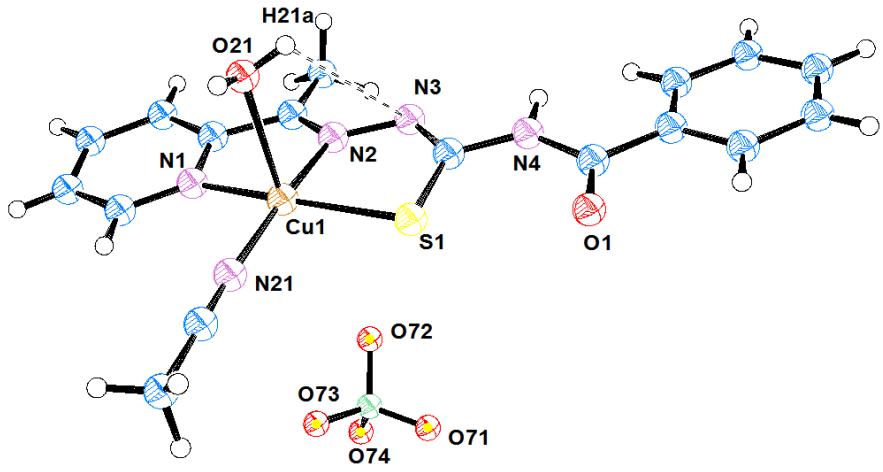


**Figure 3.13:** ORTEP diagram of complex **3.1** showing partial atomic numbering scheme.

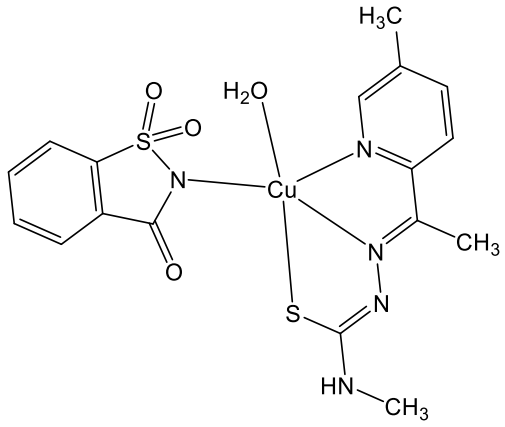


**Figure 3.14:** Chemical structure of the complex [Cu($L^4$)(sac)($H_2O$)]

**Table 3.6:** Selected bond lengths (Å) and bond angles ($^o$) for complex **3.1**.

| | | | |
|---|---|---|---|
| **Bond lengths (Å)** | | | |
| Cu1–N2 | 1.9497(16) | Cu1–S1 | 2.2824(5) |
| Cu1–N21 | 1.9536(17) | Cu1–O21 | 2.3873(14) |
| Cu1–N1 | 2.0362(17) | | |
| **Bond Angles ($^o$)** | | | |
| N2–Cu1–N21 | 175.00(7) | N1–Cu1–S1 | 162.03(5) |
| N2–Cu1–N1 | 80.77(7) | N2–Cu1–O21 | 89.48(6) |
| N21–Cu1–N1 | 99.00(7) | N21–Cu1–O21 | 95.51(6) |
| N2–Cu1–S1 | 84.59(5) | N1–Cu1–O21 | 88.57(6) |
| N21–Cu1–S1 | 94.68(5) | S1–Cu1–O21 | 101.71(4) |

### 3.3.6.2 Crystal structures of [Ni(ACbe)Cl].DMF (3.5) and [Ni(ACTM)Cl] (3.10)

Triclinic red plates with the space group *P-1* of **3.5** and monoclinic orange crystals with space group *$P2_1/m$* of **3.10**, were obtained by vapor diffusion of diethyl ether into a DMF and an acetonitrile solution of **3.5** and **3.10** respectively. **Table 3.7** shows selected bond lengths and angles for complexes **3.5** and **3.10**. The metal centre has a four coordinate distorted square planar geometry and is surrounded by Cl1 atom and N1, N2, S1 atoms for a tridentate thiosemicarbazone ligand. The **ACbe-H** and **ACTM-H** ligands coordinate to the Ni(II) ion as deprotonated

thiosemicarbazone ligand similar to **ACbe-H** behavior in the Cu(II) complex, **3.1**. The C8-S1 bond length in **3.5** [1.7406(18) Å] and in **3.10** [1.740(4) Å] exhibits similar bond lengths in **3.1** with it retains partial double bond character. The two nitrogen bonds are 1.8374(15) and 1.9341(15) Å in **3.5** and1.842(4) and 1.939(4) Å in **3.10**. The chloro bond Ni-Cl at 2.1588(5) in **3.5** and 2.1720(12) Å in **3.10** is significantly longer than Ni-N and Ni-S, (see **Table 3.7**), but is in the typically observed range.[73]. **Figure 3.15** shows a single Ni(II) complex within the asymmetric unit (asu). Bond angles about the metal centre range from 83.33(6)-97.64(5) for idealised 90º angle as well as angles of 170.50(5) and 179.00(4) degrees for the trans angles. The bond angles N2–Ni1–N1 and N2–Ni1–S1 are less than N1–Ni1–Cl1 and S1–Ni1–Cl1 and a large deviation from the perfect square planar bond angle is observed for N2–Ni1–N1 83.33(6) and N1–Ni1–S1 170.50(5). This distortion is due to the restricted bite angles of the thiosemicarbazone ligands **ACbe** and **ACTM** rather than the bulkiness of the chlorine atom.

There are ten published crystal structures of the square planar Ni(II) complexes of pyridyl thiosemicarbazone derivatives. Ni(II) ion coordinates with one chloro atom and one tridentate ligand through a pyridyl nitrogen, azomethine nitrogen and sulfur atoms.[70-72]

The bond lengths and angles data in complex **3.5** agree very well with those in the four coordinate distorted square planar complex [Ni($^4$N-DMACPYTSC)Cl] ($^4$N-DMACPY TSC)=$^4$N-dimethyl-2-acetylpyridine thiosemicarbazone), **Figure 3.17**, (Ni-N(2) 1.849(3), Ni-N(1) 1.924(3), Ni-S 2.146(3) and Ni-Cl 2.174, N(1)–Ni–N(2) 83.7(1), N(2)–Ni–S 87.0(1), N(1)–Ni–S 170.6(1), N(2)–Ni–Cl 178.4(1), N(1)–Ni–Cl 96.9(1) and S–Ni–Cl 92.4(1)), reported by Murugkar *et al.*[73] A strong intermolecular hydrogen bond, N4–H4···O21$^{i}$, is observed between the DMF oxygen atom and the hydrogen of the thiosemicarbazone, N-H, at 1.98 Å in **3.5**. Complex **3.10**, **Figure 3.16** has an almost identical co-ordination sphere to **3.5**. An intermolecular hydrogen bond, N4–H4···Cl1$^{ii}$, is observed in **3.10** at 2.62 Å and it is longer than the hydrogen bond N4–H4···O21$^{i}$ in **3.5** (1.98 Å) and this is due the presence of lone pair of electron in oxygen atom is attracted to the high

electropositive N-H proton. This causes compress the hydrogen bond N4–H4···O21$^{i}$. In addition, the atomic size of chloride atom is bigger than oxygen atom.

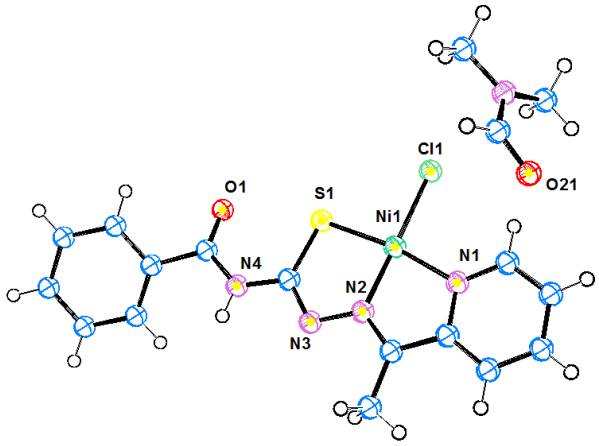


**Figure 3.15:** ORTEP diagram of complex **3.5** showing partial atomic numbering scheme.

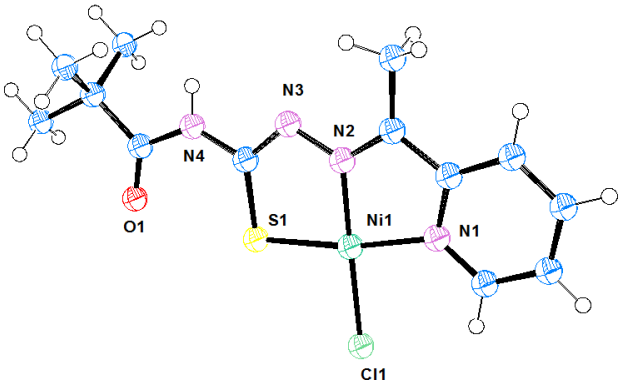


**Figure 3.16:** ORTEP diagram of complex **3.10** showing partial atomic numbering scheme.

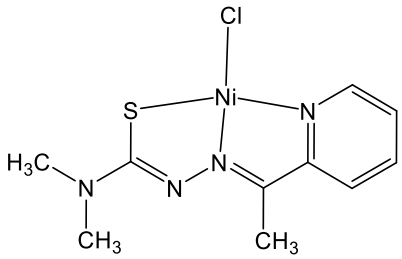


**Figure 3.17:** Chemical structure of the complex [Ni($^{4}$N-DMACPYTSC)Cl].

**Table 3.7:** Selected bond lengths (Å) and bond angles ($^{o}$) for complexes **3.5** and **3.10**.

| **Bond lengths(Å)** | **3.5** | **3.10** |
|---|---|---|
| Ni1–N2 | 1.8374(15) | 1.842(4) |
| Ni1–N1 | 1.9341(15) | 1.939(4) |
| Ni1–S1 | 2.1473(5) | 2.1606(11) |
| Ni1–Cl1 | 2.1588(5) | 2.1720(12) |
| C8-S1 | 1.7406(18) | 1.740(4) |
| **Bond Angles ($^{o}$)** | | |
| N2–Ni1–N1 | 83.33(6) | 83.00(15) |
| N2–Ni1–S1 | 87.26(5) | 87.39(11) |
| N1–Ni1–S1 | 170.50(5) | 170.38(11) |
| N2–Ni1–Cl1 | 179.00(4) | 178.89(11) |
| N1–Ni1–Cl1 | 97.64(5) | 95.90(11) |
| S1–Ni1–Cl1 | 91.765(18) | 93.72(4) |

### 3.3.6.3 Crystal structure of [Zn(ACbe-H)$Cl_2$] (3.6)

For the zinc compound **3.6**, the crystallographic data and the final refinement details are listed in **Table 3.11** and selected bond lengths and bond angles are given in **Table 3.8**. The light yellow crystals of the zinc compound crystallise in the monoclinic space group $P2_1/c$ and contain one complex within the asu, **Figure 3.18**. The geometrical parameter $\tau$, i.e. $\tau = (\beta-\alpha)/60$,[74] where β and α are N1–Zn1–S1 and N2–Zn1–Cl2 bond angles, respectively, has a value of 0.013. This suggests that the Zn(II) complex **3.6** has a square pyramidal geometry with a 1.3% distortion towards a trigonal bipyramid.

The Zn(II) ion is surrounded by five donor atoms (two nitrogen atoms (the nitrogen of the pyridine ring and in C=N group), and the sulfur atom from the thiosemicarbazone ligand and two chloride ions). Bond angles around the metal centre range from 72.86(5)-111.292(17),143.12(4) and 143.89(4) degrees. The more acute of these angles is associated with the bond angles between the three

donors of the tridentate ligand. The Zn-S bond length at 2.5209(5) Å, is longer than the other coordinative bond lengths which vary from 2.1396(14) to 2.2889(5) Å. The bond length of C8-S1 [1.6788(17) Å] in **3.6** exhibits full double bond character C=S due to the protonated form of **ACbe-H** in its complex and this is in contrast to the bond length of C8-S1 in **3.1**, **3.5** and **3.10** which contain the deprotonated form of the ligands. The bond lengths and angles and the geometry of **3.6** are similar compared to those of related compounds. For instance, the complex [$ZnCl_2$(HATtsc)], HATtsc = 2-acetyl-2-thiazoline thiosemicarbazone, **Figure 3.19**, has the zinc ion surrounded by five atoms ($N_2$, S and $Cl_2$) with a similar square pyramidal geometry[75] and exhibits coordinative bond lengths (Zn–N1 2.140(2), Zn–N2 2.214(2), Zn–Cl1 2.267(1), Zn–Cl2 2.284(1) and Zn–S1 2.491(1)).Typical for N-carbonyl thiourea ligand, there is intramolecular hydrogen bonding of N3–H3···O1 in complex **3.6** (1.87 Å), formed between the N-H hydrogen atom within thiourea group and the oxygen carbonyl group. This hydrogen bond (N3–H3···O1) is present because **ACbe-H** coordinates as neutral ligand (there is no deprotonation of ligand after complaxation). The hydrogen bond N3–H3···O1 in **3.6** is very similar to those in N-carbonyl thiourea complexes in chapter two (**2.1**, **2.6**, **2.15**, **2.16** and **2.24**). The intermolecular hydrogen bond N4–H4···Cl1$^{i}$, at 2.74 Å, is similar to hydrogen bond in the Ni(II) complex **3.10** (2.62 Å).

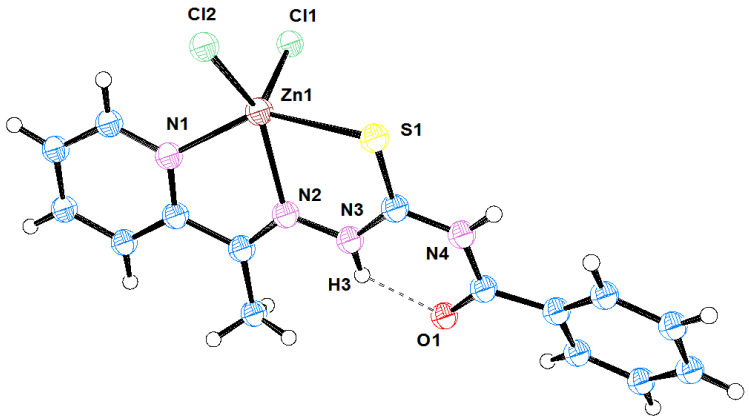


**Figure 3.18:** ORTEP diagram of complex **3.6** showing partial atomic numbering scheme

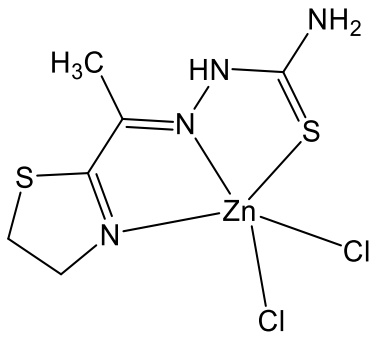


**Figure 3.19:** Chemical structure of the complex [$ZnCl_2$(HATtsc)].

**Table 3.8:** Selected bond lengths (Å) and bond angles ($^o$) for complex **3.6.**

| | | | |
|---|---|---|---|
| **Bond lengths (Å)** | | | |
| Zn1–N1 | 2.1396(14) | Zn1–Cl1 | 2.2889(5) |
| Zn1–N2 | 2.1944(14) | Zn1–S1 | 2.5209(5) |
| Zn1–Cl2 | 2.2701(4) | C8-S1 | 1.6788(17) |
| **Bond Angles ($^o$)** | | | |
| N1–Zn1–N2 | 72.86(5) | Cl2–Zn1–Cl1 | 111.292(17) |
| N1–Zn1–Cl2 | 96.74(4) | N1–Zn1–S1 | 143.89(4) |
| N2–Zn1–Cl2 | 143.12(4) | N2–Zn1–S1 | 76.42(4) |
| N1–Zn1–Cl1 | 101.33(4) | Cl2–Zn1–S1 | 96.520(16) |
| N2–Zn1–Cl1 | 105.48(4) | Cl1–Zn1–S1 | 104.800(16) |

### 3.3.6.4 Crystal structure of [$Cu^{II}$(ACTM$^*$)(DMF)]($BF_4$).2DMF (3.7), [$Cu^{II}$(ACTM)(DMF)]($BF_4$).1.5 DMF (3.8)

Dark green crystals of **3.7** and **3.8** were obtained by vapour diffusion of diethyl ether into a DMF solution of the complex. The copper compounds **3.7** and **3.8** crystallise in the monoclinic space group *$P2_1/c$* and *$P2_1/n$* respectively and contain one complex within the asu of **3.7** and two similar complexes of **3.8**, **Figures 3.20** and **3.21**. Selected bond lengths and bond angles are given in **Table 3.9**. The molecular structure of **3.7** shown in **Figure 3.20** shows the Cu(II) complex is four coordinate. One thiosemicarbazone ligand and one DMF molecule are coordinated

to the central Cu(II) ion through N3, N4, S1 and O11 atoms. The Cu(II) complex is clearly square planar, **Figure 3.20**, with bond angles about the metal centre ranging from 80.98(16)-100.47(10), with trans angles of 157.76(11) and 169.37(14) degrees. The bond angles N3–Cu1–N4 and N3–Cu1–S1 are less than O11–Cu1–N4 and O11–Cu1–S1 in **3.7** and the largest deviations from the idealised bond angles is observed for N3–Cu1–N4 80.98(16) and N4–Cu1–S1 157.76(11). These distortions are due to the fixed bite angles of the rigid thiosemicarbazone **ACTM** ligand.

The bond lengths C1-S1 [1.772(5) Å] in **3.7** and C8-S1 [1.741(3) Å] in **3.8** suggest a partial double bond character similar to that in **3.1**, **3.5** and **3.10** and contrast that in **3.6**. This is due to the deprotonated form of **ACbe** in **3.1** and **3.5** and, **ACTM** in **3.7**, **3.8** and **3.10**. The Cu-N and Cu-O coordinative bond lengths range from 1.957(3)- 2.028(4) Å, and the Cu-S bond length is significantly longer at 2.2870(13) Å. These bond lengths in complex **3.7** are in good agreement with those in the square planar complex [Cu(Ap44mT)(OAc)].3H2O (HAp44mT: 2-acetyl pyridine 4,4-dimethyl-3-thiosemicarbazone, OAC: acetate), **Figure 3.22** Cu-O1 1.954(2), Cu-N2 1.943(3), Cu-N1 2.014(3) and Cu-S1 2.253(1), reported by Jansson *et al.*[76] There are three strong intermolecular hydrogen bonds. One of these interactions is N1–H1B···O21$^{ii}$ which occurs between a DMF oxygen atom and the thiosemicarbazone hydrogen atom in $NH_2$ group (1.96 Å). The other interactions N1–H1A···F2$^{iii}$ and N1–H1A···F1A$^{iii}$ are observed between $BF_4$ fluoride atom and the two hydrogen thiosemicarbazone atoms in $NH_2$ group at 2.19 and 2.11 Å respectively. Complex **3.8** (**Table 3.9** and **Figure 3.21**) differs from **3.7** by the presence of a *t*-butyl group. **3.7** and **3.8** have an almost identical coordination sphere.

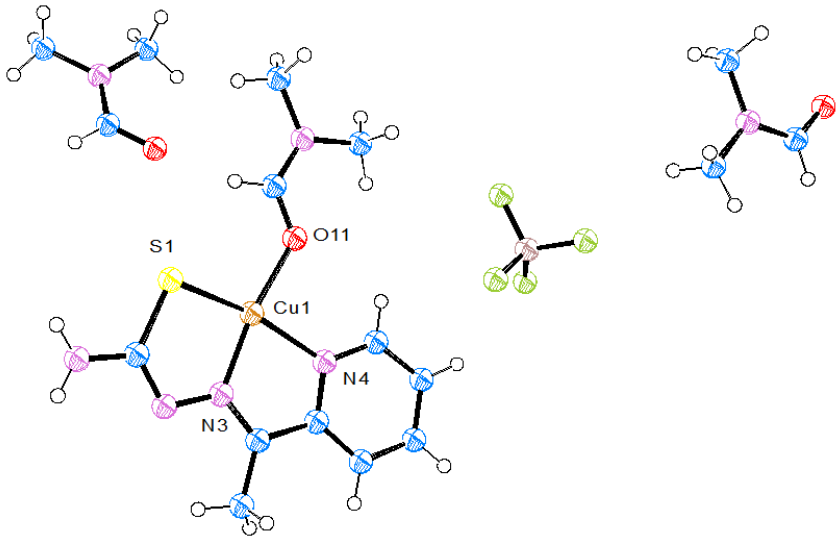


**Figure 3.20**: ORTEP diagram of complex **3.7** showing partial atomic numbering scheme.

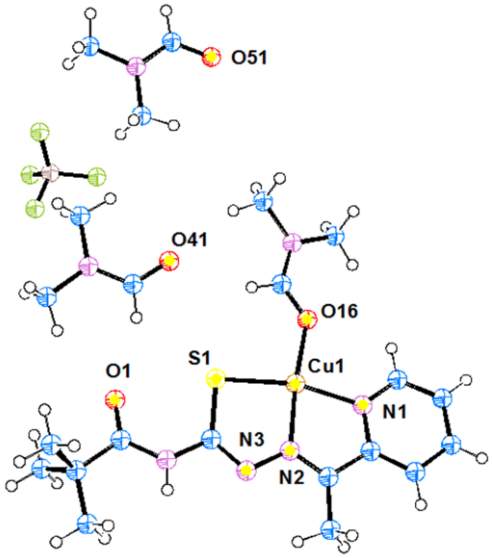


**Figure 3.21**: ORTEP diagram of complex **3.8** showing partial atomic numbering scheme.

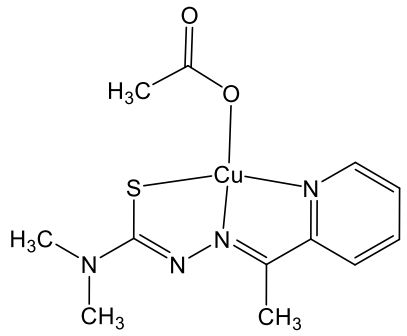


**Figure 3.22:** Chemical structure of the complex [Cu(Ap44mT)(OAc)]

**Table 3.9:** Selected bond lengths (Å) and bond angles ($^{o}$) for complexes **3.7** and **3.8.**

| **Bond lengths (Å)** | **3.7** | **3.8** | |
|---|---|---|---|
| Cu1–O11, O16 | 1.957(3) | 1.940(2) | |
| Cu1–N3, N2 | 1.959(4) | 1.946(3) | |
| Cu1–N4, N1 | 2.028(4) | 2.011(3) | |
| Cu1–S1 | 2.2870(13) | 2.2583(9) | |
| **Bond Angles ($^{o}$)** | **3.7** | **3.8** | |
| O11–Cu1–N3 | 169.37(14) | O16–Cu1–N2 | 174.30(11) |
| O11–Cu1–N4 | 91.87(14) | O16–Cu1–N1 | 93.88(11) |
| N3–Cu1–N4 | 80.98(16) | N2–Cu1–N1 | 80.49(11) |
| O11–Cu1–S1 | 100.47(10) | O16–Cu1–S1 | 100.14(7) |
| N3–Cu1–S1 | 83.97(12) | N2–Cu1–S1 | 85.44(9) |
| N4–Cu1–S1 | 157.76(11) | N1–Cu1–S1 | 165.62(9) |

### 3.3.6.5 Crystal structures of [Zn(ACTM*-H)$Cl_2$].DMF (3.11) and [Zn(ACTM-H)$Cl_2$] (3.12)

Yellow plates of **3.11** and **3.12** were obtained by vapour diffusion of diethyl ether into a DMF solution of the complex. The zinc compound crystallises in the space group *P-1* and $P2_1/c$ in **3.11** and **3.12** respectively. Each contains a single complex within the asu, **Figures 3.23** and **3.24** respectively. In the complex **3.11** the cleavage ligand, **ACTM*-H**, behaves as a tridentate donor, complexing via the azomethine nitrogen N3, the sulfur atom S1 and pyridyl nitrogen N4. Two chloride

atoms Cl1 and Cl2 occupy the fourth and fifth positions. The geometrical parameter *τ*, i.e. $\tau = (\beta - \alpha) / 60$,[74] where β and α are N4–Zn1–S1 and N3–Zn1–Cl2 bond angles, respectively, has a value of 0.28. This suggests that the Zn(II) complex **3.11** has a square pyramidal geometry with a 28% distortion towards a trigonal bipyramid.

The metal-donor bond lengths are typical and range from 2.148(7)-2.291(2) Å. The Zn-sulfur bond is significantly longer at 2.452(2) Å, see **Table 3.10**. These bond lengths are similar in comparison to those of related compounds. For instance, the square pyramidal complex [Zn(Triapine)$Cl_2$], **Figure 3.25** (Triapine= 3-aminopyridine-2-carbox aldehyde thio semicarbazone) reported by Kowol *el al.*, exhibits coordinative bond lengths Zn–Cl1, 2.2657(5); Zn–Cl2, 2.3038(5); Zn–S, 2.5016(5); Zn–N1, 2.1486(16); Zn–N3, 2.1378(15).[77] According to the CCDC, there are seven published crystal structures of Zn(II) with thiosemicarbazone based ligands, all of which have two nitrogen, sulfur atom and two chloride atoms around the Zn(II) ion in a square pyramidal geometry. Five of these structures are for pyridyl thiosemicarbazone.[78,79] Complex **3.12** (**Figure 3.24**) contains a *t*-butyl group which has been lost in **3.11**, but **3.11** and **3.12** have an almost identical coordination sphere. The Zn(II) complex **3.12** has a square pyramidal geometry with a 12% distortion towards a trigonal bipyramid. Complexes **3.11** and **3.12** exhibit a similar C=S bond length: C1-S1 [1.700(8) Å] and C7-S1 [1.6789(15) Å] respectively confirming the double bond character of the protonated form of **ACTM-H**.

Furthermore, in **3.11**, an intermolecular hydrogen bond, N1–H1B···O11$^{ii}$, occurs between the DMF oxygen atom and thiosemicarbazone hydrogen atom in $NH_2$ group. Finally, two chlorides atoms are hydrogen bonded to the thiourea hydrogen atom, N1–H1A···Cl1$^{i}$ and N2–H2···Cl2$^{i}$, (2.43 and 2.71 Å respectively). The hydrogen bonds with chloride atoms are similar to **3.6** and **3.10**, they are observed at 2.74 and 2.62 Å respectively. Complex **3.12** shows an intramolecular hydrogen bond (N3–H3…O1) 1.84 Å similar to that in **3.6** and the carbonyl thiourea complexes in chapter two.

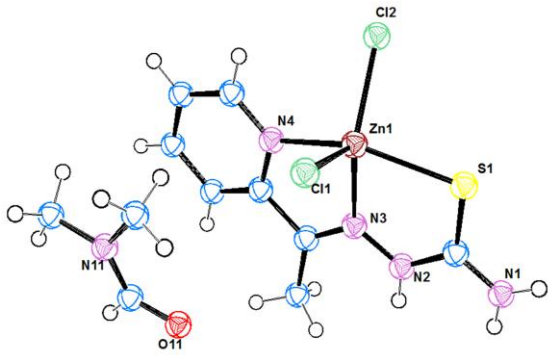


**Figure 3.23:** ORTEP diagram of complex **3.11** showing partial atomic numbering scheme.

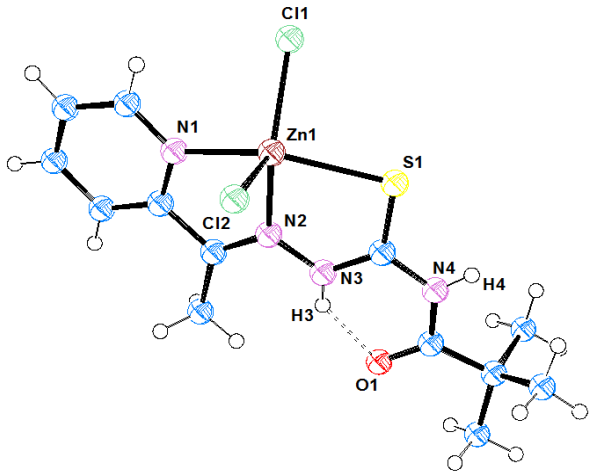


**Figure 3.24:** ORTEP diagram of complex **3.12** showing partial atomic numbering scheme.

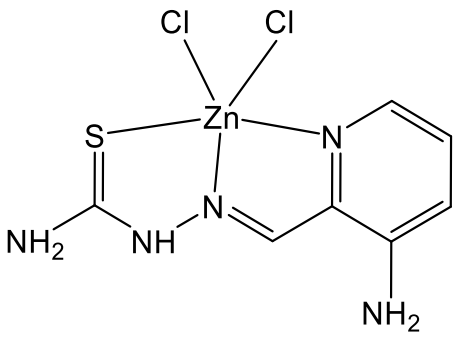


**Figure 3.25:** Chemical structure of the complex [Zn(Triapine)$Cl_2$]

**Table 3.10:** Selected bond lengths (Å) and bond angles ($^{o}$) for **3.11** and **3.12**

| **Bond lengths (Å)** | **3.11** | **3.12** |
|---|---|---|
| Zn1–N4/N1 | 2.148(7) | 2.1728(13) |
| Zn1–N3/N2 | 2.163(7) | 2.1885(13) |
| Zn1–Cl1 | 2.284(2) | 2.2690(4) |
| Zn1–Cl2 | 2.291(2) | 2.2714(4) |
| Zn1–S1 | 2.452(2) | 2.4948(4) |
| **Bond Angles ($^{o}$)** | | |
| N4/N1–Zn1–N3/N2 | 73.5(3) | 72.37(5) |
| N4/N1–Zn1–Cl1 | 96.44(19) | 96.57(4) |
| N3/N2–Zn1–Cl1 | 110.08(19) | 138.44(3) |
| N4/N1–Zn1–Cl2 | 93.8(2) | 97.78(4) |
| Cl1–Zn1–S1 | 101.79(8) | 95.089(16) |
| Cl2–Zn1–S1 | 98.68(8) | 105.566(16) |
| N3/N2–Zn1–Cl2 | 133.95(19) | 104.75(3) |
| Cl1–Zn1–Cl2 | 115.31(8) | 116.537(16) |
| N4/N1–Zn1–S1 | 150.80(19) | 145.69(4) |
| N3/N2–Zn1–S1 | 78.91(19) | 77.53(3) |

**Table 3.11:** Crystallographic data for $[Cu^{II}(ACbe)(CH_3CN)(H_2O)]ClO_4$ **(3.1)**, [Ni(ACbe)Cl].DMF **(3.5)**, $[Zn(ACbe\text{-}H)Cl_2]$ **(3.6)** and $[Cu^{II}(ACTM^{*})DMF](BF_4).2DMF$ **(3.7)**

| **Compound** | **3.1** | **3.5** | **3.6** | **3.7** |
|---|---|---|---|---|
| **Chemical Formula** | $CuC_{17}H_{18}ClN_5O_6S$ | $NiC_{18}H_{20}ClN_5O_2S$ | $ZnC_{15}H_{14}Cl_2N_4OS$ | $CuC_{17}H_{30}BF_4N_7O_3S$ |
| **Mr. g.mol$^{-1}$** | 519.41 | 464.61 | 434.63 | 562.89 |
| **Crystal system** | Monoclinic | Triclinic | Monoclinic | Monoclinic |
| **Space group** | $P2_1/n$ | $P\bar{1}$ | $P2_1/c$ | $P2_1/c$ |
| **T(K)** | 100(2) | 100(2) | 100(2) | 100(2) |
| **a, Å** | 15.1334(11) | 9.5241(7) | 11.6644(8) | 14.2666(8) |
| **b, Å** | 15.1835(11) | 10.0471(7) | 18.0850(13) | 23.4497(14) |
| **c, Å** | 18.4555(13) | 11.4096(8) | 8.5461(5) | 7.5245(4) |
| **α, degree** | 90° | 111.950(5)° | 90° | 90° |
| **β, degree** | 107.0550(10)° | 91.708(4)° | 110.381(2)° | 101.593(6)° |
| **γ, degree** | 90° | 105.199(5)° | 90° | 90° |
| **Z** | 8 | 2 | 4 | 4 |
| **Dc. Mg/m$^3$** | 1.702 | 1.595 | 1.708 | 1.516 |
| **μ($M_O$ K α), mm$^{-1}$** | 1.360 | 1.274 | 1.903 | 1.034 |
| **Reflections collected** | 53507 | 17855 | 20193 | 27241 |
| **Unique reflections** | 9272 | 4444 | 3842 | 5630 |
| **$R_{int}$** | 0.0453 | 0.0629 | 0.0462 | 0.0792 |
| **R1[I>2σ<(I)]** | 0.0342 | 0.0350 | 0.0255 | 0.0769 |
| **wR2(all data)** | 0.0947 | 0.0911 | 0.0681 | 0.1814 |

**Table 3.12:** Crystallographic data for [$Cu^{II}$(ACTM).DMF]($BF_4$).1.5 DMF **(3.8)**, [Ni(ACTM)Cl] **(3.10)**, [Zn($ACTM^*$-H)$Cl_2$].DMF **(3.11)** and [Zn(ACTM-H)$Cl_2$] **(3.12)**.

| **Compound** | **3.8** | **3.10** | **3.11** | **3.12** |
|---|---|---|---|---|
| **Chemical Formula** | $CuC_{20.50}H_{34.50}BF_4N_{6.50}O_{3.50}S$ | $NiC_{13}H_{17}ClN_4OS$ | $ZnC_{11}H_{17}Cl_2N_5OS$ | $ZnC_{13}H_{18}Cl_2N_4OS$ |
| **Mr. g.mol$^{-1}$** | 610.45 | 371.52 | 403.62 | 414.64 |
| **Crystal system** | Monoclinic | Monoclinic | Triclinic | Monoclinic |
| **Space group** | $P2_1/n$ | $P2_1/m$ | $P-1$ | $P2_1/c$ |
| **T(K)** | 100(2) | 100(2) | 100(2) | 100(2) |
| **a, Å** | 6.59390(10) | 8.5126(5) | 7.4133(6) | 10.9082(8) |
| **b, Å** | 25.9958(5) | 6.7302(5) | 9.2268(8) | 8.5805(5) |
| **c, Å** | 31.1516(5) | 13.6860(10) | 11.9719(11) | 18.5869(13) |
| **α, degree** | 90° | 90° | 101.623(7)° | 90° |
| **β, degree** | 91.328(2)° | 102.009(3)° | 95.663(7)° | 101.553(2)° |
| **γ, degree** | 90° | 90° | 91.170(7)° | 90° |
| **Z** | 8 | 2 | 2 | 4 |
| **Dc. Mg/m$^3$** | 1.519 | 1.609 | 1.681 | 1.616 |
| **μ($M_O$ K α), mm$^{-1}$** | 0.963 | 1.578 | 2.010 | 1.882 |
| **Reflections collected** | 13725 | 8271 | 9733 | 23535 |
| **Unique reflections** | 13725 | 1893 | 9733 | 3882 |
| **$R_{int}$** | - | 0.0705 | - | 0.0376 |
| **R1[I>2σ<(I)]** | 0.0553 | 0.0536 | 0.0861 | 0.0221 |
| **wR2(all data)** | 0.1183 | 0.1464 | 0.2476 | 0.0549 |

## 3.4 Conclusion

Cu(II), Ni(II) and Zn(II) complexes with thiosemicarbazone derivatives **ACbe-H** and **ACTM-H** have been synthesized and characterized. Within the series **3.1**, **3.5**, **3.6**, **3.7**, **3.8**, **3.10**, **3.11** and **3.12** complexes have been characterized using X-ray crystallography. The redox behaviour of copper and nickel species have been probed via cyclic voltammetry and shows one quasi-reversible process in the Cu(II) complexes and two irreversible oxidative processes in the Ni(II) complexes. The single crystal X-ray structures of **3.1**, **3.5**, **3.6**, **3.7**, **3.8, 3.10**, **3.11** and **3.12** were determined. It was found that the Cu(II) centre of **3.1** had a 5-coordinate square pyramidal structure, the Cu(II) centre of **3.7** and **3.8** had a 4-coordinate square planar structure, the Ni(II) centre of **3.5** and **3.10** had a 4-coordinate square planar and the Zn(II) centre of **3.6**, **3.11** and **3.12** had a 5-coordinate square pyramidal. The X-ray crystal structures showed deprotonated ligand form **ACbe** in **3.1** and **3.5**, deprotonated ligand **ACTM** in **3.7**, **3.8, 3.10**, protonated **ACbe-H** and **ACTM-H** ligands in **3.6** and (**3.11**, **3.12**) respectively. The thiosemicarbazone ligands (**Acbe-H** and **ACTM-H**) have been found to act as tridentate ligands through sulfur atom in C=S, nitrogen atom in azomethine and nitrogen atom in pyridyl group. This tridentate behaviour for **ACbe** and **ACTM** ligands is expected due to the presence of three donor atoms, two nitrogen and one sulfur atoms. The Zn(II) complexes **3.6** and **3.12** has an intramolecular, strong and short hydrogen bond between the C=O and N-H to form six member ring. The IR data showed absence of C=S stretching vibration in **3.1**, **3.5**, **3.7**, **3.8** and **3.10** confirming the deprotonated form of their corresponding free ligands.

We can conclude from the syntheses that the **Acbe-H** ligand was more stable at high temperatures than **ACTM-H**. Pivaloyl group cleavage from amide group in complexes **3.7** and **3.11** occurs at higher temperature (50ºC) and protic solvents appear to promote the cleavage process. The understanding of the cleavage process may have future application in the controlled delivery of therapeutic agents in a biological context. The Ni(II) complex of the perchlorate anion **3.3** show protonated **ACbe-H** behaviour while the same ligand behaves as deprotonated in the chloride anion complex **3.5**. The Cu(II) complexes with perchlorate anion **3.1** and hexa flouro borate anion **3.7** and **3.8** exhibit

deprotonated behaviour of **ACbe-H** and **ACTM-H** ligands when **3.2** and **3.9** show protonated behaviour of the same ligands. While all the Zn(II) complexes of perchlorate anion **3.4** or chloride anion **3.6**, **3.11** and **3.12** show protonated behaviour of **ACbe-H** and **ACTM-H** ligands due to the Lewis acid property of Zn(II) ions.

## 3.5 References:


**(1)** D. Hamre, J. Bernstein and R. Donovick, *Proc. Soc. Exp. Biol. Med.*, **1950**, 73, 275-278.

**(2)** C. Shipman, S. H. Smith, J. C. Drach and D. L. Klayman, *Antiviral Res.*, **1986**, 6, 197–222.

**(3)** P. T. Sah and T. C. Daniels. *Rec. Trav. Chim.*, **1950**, 69, 1545.

**(4)** B. A. Gingras, R. W. Hornal and C. H. Bayley, *Can. J. Chem.*, **1960**, 38(*5618*), 712-719.

**(5)** D. X. West, Y. Yang, T. L. Klein, K. I. Goldberg, A. E. Liberta, J. Valdes-Martinez and R. A. Toscano, *Polyhedron*, **1995**, 14(*12*), 1681–1693.

**(6)** R. H. Dodd, C. Ouannès, M. Robert-Gèro and P. Potier, *J. Med. Chem.*, **1989,** 32(*6*),1272–1276.

**(7)** S. Chandra and L. K. Gupta, *Spectrochim. Acta - Part A*, **2005**, 62, 1089–1094.

**(8)** M. Belicchi, G. Gasparri, E. Leporati, G. Pelosi, R. Rossi, P. Tarasconi, R. Albertini, A. Bonati, P. Lunghi and S. Pinelli, *J. Inorg. Biochem.*,**1998**, 70, 145-154.

**(9)** M. B. Ferrari, S. Capacchi, G. Reffo, G. Pelosi, P. Tarasconi, R. Albertini, S. Pinelli and P. Lunghi, *J. Inorg. Biochem.*, **2000**, 81, 89–97.

**(10)** E. M. Jouad, G. Larcher, M. Allain, A. Riou, G. M. Bouet, M. A. Khan and X. D. Thanh, *J. Inorg. Biochem.*, **2001**, 86, 565–571.

**(11)** S. A. Patil, V. H. Naik, A. D. Kulkarni and P. S. Badami, *Spectrochim. Acta - Part A,* **2010**, 75, 347–354.

**(12)** P. Tarasconi, S. Capacchi, G. Pelosi, M. Cornia, R. Albertini, A. Bonati, P. P. Dall'Aglio, P. Lunghi and S. Pinelli, *Bioorg. Med. Chem.*, **2000**, 8, 157–162.

**(13)** H. Beraldo, *Quim. Nova*, **2004**, 27, 461.

**(14)** D. Kovala-Demertzi, J. R. Miller, N. Kourkoumelis, S. K. Hadjikakou and M. A. Demertzis, *Polyhedron*, **1999**, 18, 1005–1013.

**(15)** R. W. Byrnes, M. Mohan, W. E. Antholine, R. X. Xu and D. H. Petering, *Biochemistry*, **1990**, 29(*30*), 7046–7053.

**(16)** M. B. Ferrari, F. Bisceglie, G. Pelosi, P. Tarasconi, R. Albertini and S. Pinelli, *J. Inorg. Biochem.*, **2001**, 87, 137–147.

**(17)** D. L. Klayman, J. P. Scovill, J. F. Bartosevich and C. J. Mason, *J. Med. Chem.*,**1979**, 22(*11*), 1367–1373.

**(18)** J. P. Scovill, D. L. Klayman and C. F. Franchino, *J. Med. Chem.*, **1982**, 25(*10*), 1261–1264.
**(19)** H. Beraldo and L. Tosi, *Inorg.Chim*. *Acta*, **1983**, 75, 249-257.
**(20)** J. Easmon, G. Pürstinger, G. Heinisch, T. Roth, H. H. Fiebig, W. Holzer, W. Jäger, M. Jenny and J. Hofmann, *J. Med. Chem.*, **2001**, 44(*13*), 2164–2171.
**(21)** D. X. West, A. E. Liberta, K.G. Rajendran and I. H. Hall, *Anti-cancer Drugs,* **1993**, 4, 241-249.
**(22)** C. Shipman, S. H. Smith, J. C. Drach and D. L. Klayman, *Antimicrob. Agents Chemother.*,**1981**, 19(*4*), 682–685.
**(23)** D. L. Klayman, A. J. Lin, J. M. Hoch, J. P. Scovill, C. Lambros and A. S. Dobek, *J. Pharma. Sci.*, **1984**, 73(*12*), 1763-1767.
**(24)** D. K. Demertzi, M. A. Demertzis, J. R. Miller, C. Papadopoulou, C. Dodorou and G. Filousis, *J. Inorg. Biochem.*, **2001**, 86, 555–563.
**(25)** L. Otero, M. Vieites, L. Boiani, A. Denicola, C. Rigol, L. Opazo, C. Olea-Azar, J. D. Maya, A. Morello, R. L. Krauth-Siegel, O. E. Piro, E. Castellano, M. González, D. Gambino and H. Cerecetto, *J. Med. Chem.*, **2006**, 49(*11*), 3322–3331.
**(26)** D. K. Demertzi, A. Domopoulou, M. A. Demertzis, A. Papageorgieou and D. X. West, *Polyhedron*, **1997**, 16(*20*), 3625-3633.
**(27)** S. Sharma, F. Athar, M. R. Maurya, F. Naqvi and A. Azam, *Eur. J. Med. Chem.*, **2005**, 40, 557–562.
**(28)** S. Sharma, F. Athar, M. R. Maurya and A. Azam, *Eur. J. Med. Chem.*, **2005**, 40, 1414–1419.
**(29)** R. B. Singh, B. S. Garg and R. P. Singh, *Talanta*, **1978**, 25, 619-632.
**(30)** M. Y. Khuhawar, Z. P. Memon and S. N. Lanjwani, *Chromatographia*, **1995**, 41(*3*), 236-237.
**(31)** W. Hernández, J. Paz, F. Carrasco, A. Vaisberg, E. Spodine, J. Manzur, L. Hennig, J. Sieler, S. Blaurock and L. Beyer, *Bioinorg. Chem. Appl.*, **2013**, 2013, 1-12.
**(32)** K. A. Ketcham, J. K. Swearingen, A. Castineiras, I. Garcia, E. Bermejo and D. X. West, *Polyhedron*, **2001**, 20, 3265–3273.
**(33)** M. C. Argüelles, M. B. Ferrari, G. G. Fava, C. Pelizzi, P. Tarasconi, R. Albertini, P. Paolo, D. Aglio, P. Lunghi and S. Pinelli, *J. Inorg. Biochem.*, **1995**, 58, 157–175.
**(34)** A. Castiñeiras, R. Carballo and T. Pe´rez, *Polyhedron*, **2001**, 20, 441–448.
**(35)** V. Jevtović, S. Ivković, S. Kaisarević and R. Kovacević, *Contemporary Materials*, **2010**, 2(*1*), 133–137.
**(36)** V. Jevtović, *Res. Cancer Tumor*, **2014**, 3(*1*), 1-5.
**(37)** I. C. Mendes, J. P. Moreira, N. L. Speziali, A. S. Mangrich, J. A. Takahashi and H. Beraldo, *J. Braz. Chem. Soc.*, **2006**, 17(*8*), 1571–1577.
**(38)** T. S. Lobana, R. J. Butcher, A. Castineiras, E. Bermejo and P. V. Bharatam, *Inorg. Chem.*, **2006**, 45(*4*),1535–1542.
**(39)** L. S. Vojinović-ješić, V. M. Leovac, M. M. Lalović, V. I. Češljević, L. S. Jovanović, M. V. Rodić and V. Divjaković, *J. Serbian Chem. Soc.*, **2011**, 76(*6*), 865–877.

**(40)** M. Cindrić, M. Rubčić, I. Đilović, G. Giester and B. Kamenar, *Croat. Chem. Acta*, **2007**, 80(*3–4*), 583–590.
**(41)** A. I. Matesanz, J. M. Perez, P. Navarro, J. M. Moreno, E. Colacio and P. Souza, *J. Inorg. Biochem.*, **1999**, 76, 29–37.
**(42)** E. Labisbal, A. Sousa, A. Castineiras, J. A. Garcia-Vazquez, J. Romero and D. X. West, *Polyhedron*, **2000**, 19, 1255–1262.
**(43)** S. G. Teoh, S. H. Ang, H. K. Fun and C. W. Ong, *J. Organomet. Chem.*, **1999**, 580, 17–21.
**(44)** D. K. Demertzi, P. N. Yadav, M. A. Demertzis and M. Coluccia, *J. Inorg. Biochem.*, **2000**, 78, 347–354.
**(45)** A. Castiñeiras, I. Garcia, E. Bermejo and D. X. West, *Polyhedron*, **2000**,19, 1873–1880.
**(46)** I. Garcıa, E. Bermejo, A. K. El Sawaf, A. Castin˜eiras and D. X. West, *Polyhedron*, **2002**, 21, 729-737.
**(47)** W. Kaminsky, K. I. Goldberg and D. X. West, *J. Mol. Struct.*, **2002**, 605, 9–15.
**(48)** T. S. Gardner, F. A Smith, E. Wenis and J. Lee, *J. Org. Chem.*, **1956**, 21, 530-533.
**(49)** D. F. Evans, *J.Chem.Soc.*, **1959**, 2003-2005.
**(50)** J. Coates,**"Interpretation of Infrared Spectra, A Practical Approach",** *Encyclopedia of Analytical Chemistry,* R.A. Meyers (Ed.) ©John Wiley & Sons Ltd, Chichester, **2000**, 10815–10837.
**(51)** C. Lodeiro, J. L. Capelo, E. Bértolo and R. Bastida, *Z. Anorg. Allg. Chem.,* **2004**, 630(*7*), 1110–1115.
**(52)** B. J. Hathaway, *Proc. Chem. Soc.,* **1958,** 344.
**(53)** D. X. West, J. S. Ives, J. Krejci, M. M. Salberg, T. L. Zumbahlen, G. A. Bain, A. E. Liberta, J. V. Martinez, S. H. Ortiz and R. A. Toscano, *Polyhedron,***1995**, 14(15), 2189-2200.
**(54)** M. S. Nair and R. S. Joseyphus, *Spectrochim. Acta - Part A,* **2008**, 70 (*4*), 749–753.
**(55)** M. L. Low, G. Paulus, P. Dorlet, R. Guillot, R. Rosli, N. Delsuc, K. A. Crouse and C. Policar, *BioMetals*, **2015**, 28, 553–566.
**(56)** S. S. Konstantinović, B. C. Radovanović and A. Krklješ, *J. Therm. Anal.*, **2007**, 90, 525–531.
**(57)** R. Takjoo, R. Centore, M. Hakimi, S. A. Beyramabadi and A. Morsali, *Inorganica Chim. Acta*, **2011**, 371(*1*), 36–41.
**(58)** A. B. P. Lever, *INORGANIC ELECTRONIC SPECTROSCOPY*, second eddition, (Amsterdam: Elsevier), **1986**, 534.
**(59)** K. A. Ketcham, I. Garcia, J. K. Swearingen, A. K. El-sawaf, E. Bermejo, A. Castin and D. X. West, **2002**, 21, 859–865.
**(60)** L. D. Dave and P. Francis, *Indian J. Chem.*, **1983**, 22(*5*), 422-424.
**(61)** A. S. Kumbhar and S. B. Padhye, *Transition. Met. Chem.*, **1992**, 17, 247-249.
**(62)** Saswati, “Thiosemicarbazone complexes of transition metals: Synthesis, characterization and study of reactivity. PhD thesis, Department of Chemistry, National Institute of Technology, Rourkela, India, **2015**.
**(63)** A. Reguig, M. M. Mostafa, L. Larabi and Y. Harek, *J. Applied Sci.*, **2008**, 8(*18*), 3191-3198.

**(64)** G. M. Sheldrick, SHELXL-97, University of Göttingen, Germany, **1997**.
**(65)** T. B. Ravoof, K. A. Crouse, M. I. Tahir, A. R. Cowley and M. A. Ali, *Polyhedron*, **2004**, 23(*16*), 2491-2498.
**(66)** E. W. Ainscough, E. N. Baker, A. M. Brodie, R. J. Cresswell, J. D. Ranford and J. M. Waters, *Inorg. Chim. Acta.*, **1990**, 172(*2*), 185-190.
**(67)** M. A. Ali, A. H. Mirza, T. B. Ravoof and P. V. Bernhardt, *Polyhedron*, **2004**, 23(*11*), 2031-2036.
**(68)** M. A. Ali, A. H. Mirza, R. J. Butcher, P. V. Bernhardt and M. R. Karim, *Polyhedron*, **2011**, 30(*9*), 1478-1486.
**(69)** S. A. Omar, T. B. Ravoof, M. I. Tahir and K. A. Crouse, *Transition Met. Chem.*, **2014**, 39(*1*), 119-126.
**(70)** V. Philip, V. Suni, M. R. Kurup and M. Nethaji, *Polyhedron*, **2004**, 23(*7*), 1225-1233.
**(71)** D. X. West, M. A. Lockwood, A. E. Liberta, X. Chen and R. D. Willett, *Trasnsition Met. Chem.*, **1993**, 18(2), 221-227.
**(72)** J. K. Swearingen and D. X. West, *Transition Met. Chem.,* **2001**, 26(*3*), 252-260.
**(73)** A. Murugkar, R. Bendre, S. Padhye and T. Groy, *Indian J. Chem.*, **1999**, 38A, 981-984.
**(74)** A. W. Addison, T. N. Rao, J. Reedijk, J. V. Rijn and G. C. Verschoor, *J. Chem. Soc. Dalton Trans.*, **1984**, 1349-1356.
**(75)** E. Zahinos, F. Giles, P. Garcia and M. Calderon, *Eur. J. Med. Chem.*, **2011**, 46(*1*), 150-159.
**(76)** P. J. Jansson, P. C. Sharpe, P. V. Bernhardt and D. R. Richardson, *J. Med. Chem.*, **2010**, 53(*15*), 5759–5769.
**(77)** C. R. Kowol, R. Trondl, V. B. Arion, M. A. Jakupec, I. Lichtscheidl and B. K. Keppler, *Dalton Trans.*, **2010**, 39, 704-706.
**(78)** D. Demertzi, P. N. Yadav, J. Wiecek, J. Skoulika, T. Varadinova and M. A. Demertzi, *J. Inorg. Biochem.*, **2006**, 100(*9*), 1558-1567.
**(79)** J. Shao, Z. Ma, A. Li, Y. Liu, C. Xie, Z. Qiang and J. Xu, *J. Inorg. Biochem.*, **2014**, 136, 13-23.

# Chapter Four

## Spectral, magnetic and electrochemical studies of Cu(I), Cu(II) and Ni(II) complexes with N-((6-benzamido or pivalamido pyridin-2-yl)carbamothioyl benzamide or pivalamide derivatives ($L^{5}$-$L^{7A}$).

# 4.1 Introduction

Although there has been much research concerning the coordination chemistry of carbonyl thiourea derivatives,[1-10] according to the Cambridge Crystallographic Data Center (CCDC) and, Scifinder database, the derivatives of N-(6-pyridin-2-yl)carbamothioyl amide have not been reported (R and R' are alkyl, aryl or different groups, **Figure 4.1**). Therefore, and logically, the coordination chemistry of Cu(I), Cu(II) and Ni(II) ions with these derivatives has not been studied, and this was the motivation for the present study.

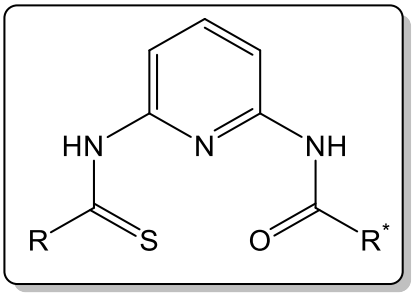


**Figure 4.1**: General form of N-(6-pyridin-2-yl)carbamothioyl amide derivatives.

To understand the coordination chemistry of the metal complexes for the ligands under study, (N-(6-pyridin-2-yl)carbamothioyl amide derivatives), we will consider the coordination chemistry of ligands with similar functional groups. The most significant example for these ligands are 2,6-dicarbonyl amido pyridyl (DAP) derivatives, **Figure 4.2**. There has been much interest over the last 30 years in the investigation of the coordination chemistry of tridentate DAP ligands. In 1980, El-Shazly *et al.* prepared Cu(II) complexes [Cu(daapH)$X_2$] and [Cu(dbapH)$X_2$], (daapH)= 2,6 [(N,N'-diacetyl) diamino pyridine], (dbapH)=2,6 [(N,N'-dibenzoyl) diamino pyridine] and X=Cl, Br, $NO_3$,[11] (**Figure 4.3**). They reported that the Cu(II) complexes formed five coordinate square-based pyramidal compounds.

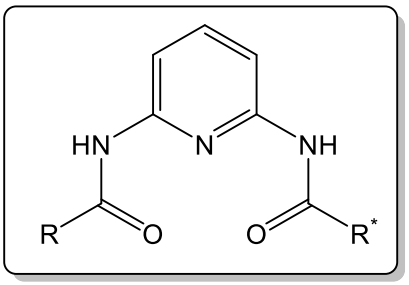


**Figure 4.2**: General structure of 2,6-dicarbonyl amido pyridyl derivatives.

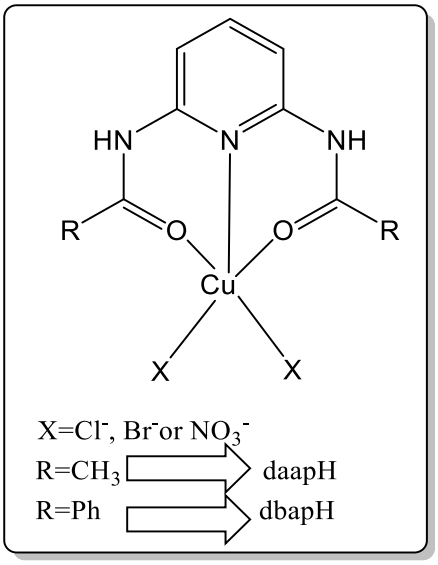


**Figure 4.3**: Structures of [Cu(daapH)$X_2$] and [Cu(dbapH)$X_2$] complexes.

Octahedral [Fe($H_2$daap)$_2$](OTf)$_2$ and [Fe($H_2$daap)($H_2$O)(OTf)($CH_3$CN)](OTf) complexes were reported by McMoran *et al.*, who prepared these complexes in 2:1 and 1:1 ligand to metal ratios, **Figure 4.4**. They also prepared [Cu($H_2$daap)(OTf)$_2$($CH_3$CN], $H_2$daap=N,N'-2,6-diacetamidopyridine, where the Cu(II) complex showed a tetragonally elongated structure due to a Jahn-Teller distortion from the $d^9$ electronic configuration of Cu(II) and the weaker interactions between Cu(II) ion centre and the triflate ligands.[12]

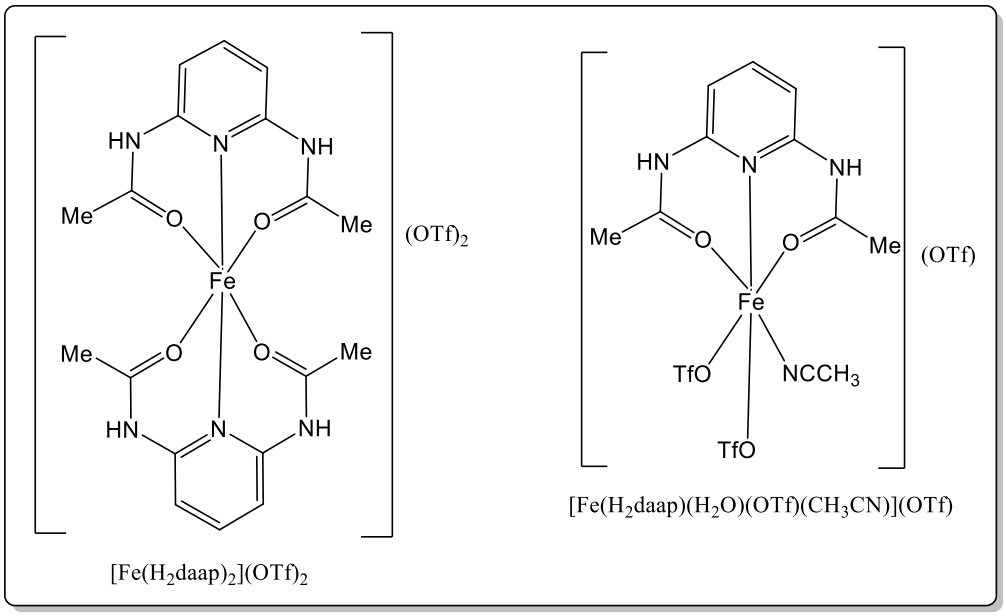


**Figure 4.4**: Structures of $[Fe(H_2daap)_2](OTf)_2$ and $[Fe(H_2daap)(H_2O)(OTf)(CH_3CN)](OTf)$ complexes.

Another substitution derivative of dicarbonyl amido pyridyl is pyridine-2,6-dicarboxamide. Octahedral Ni(II) complex, $[Ni(L^1)_2(mip)_2(H_2O)].2H_2O$, ($L^1$= N,N'-bis(pyridine-3-yl)pyridine-2,6-dicarboxamide, mip= 5-methylisophthalic acid), (**Figure 4.5**) have been reported by Wang *et al*. The Ni(II) ion shows an octahedral coordination geometry, coordinated by two nitrogen atoms from two molecules of $L^1$, three oxygen atoms from two carboxylic groups of different mip anions, the sixth site occupied by one oxygen atom of a coordinated water molecule.[13] The Cu(II), Cu(I), Co(II) and Ni(II) complexes of 2,6-bis(carbonylamino) pyridine 2,6-pyridinedicarboxamide and pyridine-2,6-dicarboxamide derivatives were prepared and their coordination chemistry was investigated.[14-20]

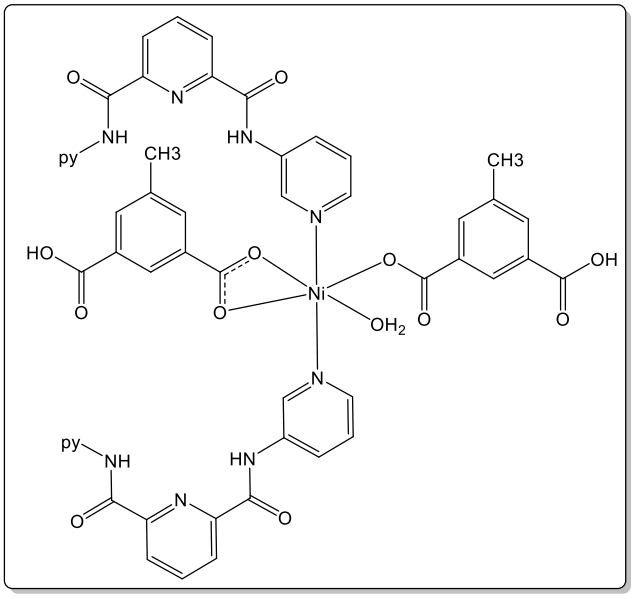


**Figure 4.5**: Structure of $[Ni(L^1)_2(mip)_2(H_2O)]$ complex.

In this chapter, an investigation into the preparation of the N-(6-amido-pyridin-2-yl)carbamothioyl amide ligand derivatives trifunctionalised with benzoyl and pivaloylthiourea groups was explored. The synthesis of these new ligand derivatives may lead to different chemistry to the 2, 6-dicarbonyl amido pyridyl (DAP) based structures. This is due to the new ligands being differentiated by the presence of a sulfur atom instead of oxygen atom in the DAP derivatives. In addition, it is expected that the benzoyl and pivaloyl thiourea will cyclise through intramolecular hydrogen bonding, with the sulfur atoms in the thiourea group available for the coordination to the metal centre, **Figure 4.6**.

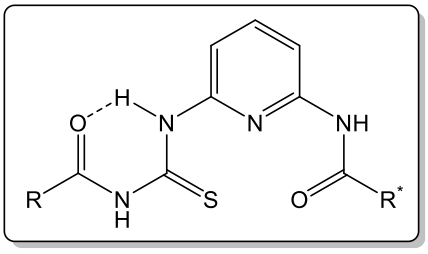


**Figure 4.6**: Structure of N-(6-amido-pyridin-2-yl)carbamothioyl) amide ligand derivatives.

In this chapter, the synthesis, characterization, electrochemistry and X-ray crystal structures of Cu(I), Cu(II) and Ni(II) complexes are discussed.

# 4.2 Experimental

## 4.2.1 Instrumentation

The details regarding of mass spectrometry, NMR, Infrared, UV-vis., elemental analyses, magnetic susceptibilities[21] and electrochemical measurements is similar to that shown in previous chapters.

## 4.2.2 Synthesis of ligands ($L^5$-$L^{7A}$)

### 4.2.2.1 Synthesis of N-((6-benzamidopyridin-2-yl)carbamothioyl) benzamide $L^5$

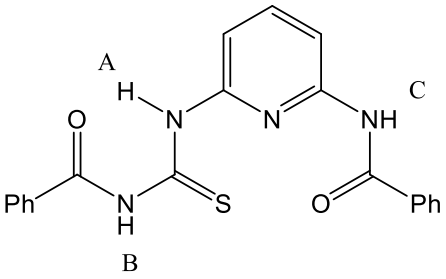


The starting material N-(6-aminopyridin-2-yl)benzamide **$L^4$** was prepared as described before.[22,23] A mixture of **$L^4$** (0.5 g, 2.3 mmol) in acetonitrile (20 $cm^3$) and benzoyl isothiocyanate (0.38 g, 2.3 mmol) in acetonitrile (5 $cm^3$ ) was refluxed with stirring for 3 hours. White crystals were formed, filtered and washed with acetonitrile (10 $cm^3$). Dry it under vacuum. Yield: (0.45 g, 91%); m.p: 193-194$^o$C; white crystals; ESI-MS (m/z)(%): 375.14 [M-H] (100%); Mass: 375.0913, Calc. Mass: 375.0916; FT-IR ($cm^{-1}$): ν(N-H) 3428, 3341, ν(C=O) 1670, ν(C=S) 1333; UV-vis. spectrum, $\lambda_{max}$ nm (εM, $M^{-1}cm^{-1}$): 277(25150), 322(16400); $^1$H NMR (250 MHz, $CDCl_3$), δ(ppm): 13.00 (1H, s, N-$H_A$), 9.06 (1H, s, N-$H_B$), 8.59 (1H, d, Py $J_{HH}$ =7.5 Hz), 8.49 (1H, s, N-$H_C$), 8.22 (1H, d, Py $J_{HH}$ =10 Hz), 7.94 –7.47 (11H, m, (10 H, Ar + 1H, Py); $^{13}$C NMR (100 MHz, $CDCl_3$), δ(ppm): 176.86 (C=S), 166.75 (C=O), 165.84 (C=O), 150.39, 149.53, 140.59, 134.18, 134.08, 132.59, 131.69, 129.46, 129.07, 127.75, 127.44, 111.82, 111.72.

### 4.2.2.2 Synthesis of N-((6-benzamidopyridin-2-yl)carbamothioyl) pivalamide $L^{5A}$

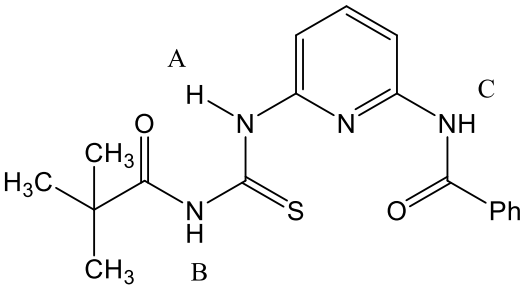


The starting material N-(6-aminopyridin-2-yl)benzamide **$L^4$** was prepared as described before.[22,23] To a suspension of potassium thiocyanate (0.23 g, 2.3 mmol) in acetonitrile (10 $cm^3$) was added dropwise the solution of trimethyl acetyl chloride (0.28 g, 2.3 mmol) in acetonitrile (15 $cm^3$). The reaction mixture was refluxed for 3 hours. The mixture was yellow solution with white precipitate. The mixture was filtered to remove the white precipitate (KCl). The yellow solution was added to a solution of **$L^4$** (0.5 g, 2.3 mmol) in acetonitrile (10 $cm^3$) and refluxed with stirring for 15 hours. The yellow solution was left in fridge to cool. The White crystals were formed, filtered, washed with acetonitrile (5 $cm^3$) and dried under vacuum. Yield: (0.37, 75%); m.p: 148-150$^oC$; white crystals; ESI-MS (m/z)(%): 355.17 [M-H] (100%); Mass: 355.1225, Calc Mass: 355.1229; FT-IR ($cm^{-1}$): ν(N-H) 3429, 3391, ν(C=O) 1690, 1672, ν(C=S) 1321; UV-vis. spectrum, $\lambda_{max}$ nm (εM, $M^{-1}cm^{-1}$): 268(14400), 316(14800); $^1H$ NMR (250 MHz, $CDCl_3$), δ(ppm): 12.94 (1H, s, N-$H_A$), 8.55 (1H, d, Py 7.5 Hz), 8.49 (1H, s, N-$H_B$), 8.42 (1H, s, N-$H_C$), 8.21 (1H, d, Py $J_{HH}$ =7.5 Hz), 7.89 (2H, d, Ar $J_{HH}$ =7.5 Hz ), 7.81 (1H, t, py $J_{HH}$ =10 Hz), 7.59-7.46 (3H, m, Ar), 1.31 (9H, s, $3CH_3$); $^{13}C$ NMR (100 MHz, $CDCl_3$), δ(ppm): 179.34 (C=S), 177.05 (C=O), 165.71 (C=O), 150.33, 149.53, 140.57, 134,16, 132.49, 129.10, 127.19, 111.79, 40.15, 27.22 ($3CH_3$).

### 4.2.2.3 Synthesis of N-((6-pivalamidopyridin-2-yl)carbamothioyl) benzamide $L^7$:

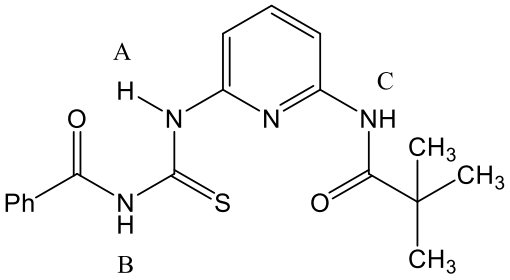


The starting material N-(6-aminopyridin-2-yl)pivalamide **$L^6$** was prepared as described before.[22,23] A mixture of **$L^6$** (0.5 g, 2.6 mmol) in acetonitrile (10 $cm^3$) and benzoyl isothiocyanate (0.42 g, 2.6 mmol) in acetonitrile (15 $cm^3$) was

refluxed with stirring for 3 hours. The yellow solution was left in fridge to cool. The White crystals were formed, Filtered, washed with acetonitrile (5 $cm^3$) and dried under vacuum. Yield: (0.4, 80%); m.p: 176-177$^oC$ white crystals; ESI-MS (m/z)(%): 356.10 [M+H] (100%); Mass: 355.1226, Calc. Mass: 355.1229; FT-IR ($cm^{-1}$): ν(N-H) 3427, 3402, ν(C=O) 1678, ν(C=S) 1331; UV-vis. spectrum, $\lambda_{max}$ nm (εM, $M^{-1}cm^{-1}$): 274(13650), 299(12400), 322(11000); $^1$H NMR (250 MHz, $CDCl_3$), δ(ppm): 12.92 (1H, s, N-$H_A$), 9.04 (1H, s, N-$H_B$ ), 8.53 (1H, d, py $J_{HH}$ =7.5 Hz), 8.09 (1H, d, py $J_{HH}$ =7.5 Hz ), 7.91 (1H, s, N-$H_C$), 7.88 (2H, d, Ar $J_{HH}$ =2.5 Hz), 7.76 (1H, t, py $J_{HH}$ =7.5 Hz), 7.65 (1H, t, Ar $J_{HH}$ =7.5 Hz), 7.54 (2H, t, Ar $J_{HH}$ =5 Hz), 1.31 (9H, s, $3CH_3$); $^{13}$C NMR (100 MHz, $CDCl_3$), δ(ppm): 177.32 (C=S), 176.87 (C=O), 166.75 (C=O), 150.32, 149.35, 140.72, 133.89, 131.99, 129.70, 127.73, 111.82, 111.53, 39.66, 27.67 ($3CH_3$).

## 4.2.2.4 Synthesis of N-((6-pivalamidopyridin-2-yl)carbamothioyl) pivalamide $L^{7A}$

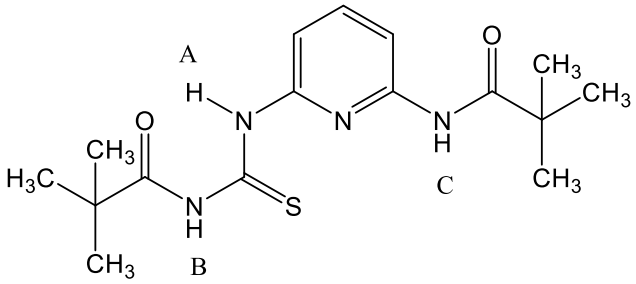


The starting material N-(6-aminopyridin-2-yl)pivalamide **$L^6$** was prepared as described before.[22,23] To a suspension of potassium thiocyanate (0.25 g, 2.6 mmol) in acetonitrile (10 $cm^3$) was added dropwise the solution of trimethyl acetyl chloride (0.31 g, 2.6 mmol) in acetonitrile (15 $cm^3$). The reaction mixture was refluxed for 3 hours. The mixture was yellow solution with white precipitate. The mixture was filtered to remove the white precipitate (KCl). A mixture of the yellow solution and **$L^6$** (0.5 gm, 2.6 mmol) in acetonitrile (10 $cm^3$) was refluxed with stirring for 15 hours. The mixture of reaction was kept in fridge. White crystals were formed, Filtered, washed with acetonitrile (10 $cm^3$) and dried under vacuum. Yield:(0.36, 72%); m.p: 185-186$^oC$; white crystals; ESI-MS (m/z)(%): 336.13 [M+H] (100%); Mass: 335.1535, calc. Mass: 335.1542; FT-IR ($cm^{-1}$): ν(N-H) 3428, ν(C=O) 1682,1663, ν(C=S) 1323; UV-vis. spectrum, $\lambda_{max}$ nm (εM, $M^{-1}cm^{-1}$): 266(43300), 297(37500), 315(53100); $^1$H NMR (250 MHz, $CDCl_3$), δ(ppm): 12.85 (1H, s, N-$H_A$), 8.51 (1H, d, Py $J_{HH}$ =7.5 Hz), 8.48 (1H, s, N-$H_B$), 8.05 (1H, d, Py $J_{HH}$ =7.5 Hz),

7.85 (1H, s, N-$H_C$), 7.73 (1H, t, Py $J_{HH}$ =7.5 Hz), 1.29 (18H, s, 6$CH_3$); $^{13}$C NMR (100 MHz, $CDCl_3$), δ(ppm): 179.32 (C=S), 177.28 (C=O), 177.02 (C=O), 150.41, 149.34, 140.42, 111.51, 111.42, 40.32, 40.01, 27.65 (3$CH_3$), 27.14 (3$CH_3$).

## 4.2.3 Synthesis of complexes (4.1-4.13)

***CAUTION***: Perchlorate compounds of metal ions are potentially explosive especially in presence of organic ligands. Only a small amount of material should be prepared and handled with care.

### 4.2.3.1 Synthesis of $[Cu^I(L^5)_2](BF_4)$ (4.1)

A solution of $Cu(BF_4)_2.6H_2O$ (0.12 g, 0.5 mmol) in methanol (3 $cm^3$) was added to a solution of **$L^5$** (0.38 g, 1 mmol) in $CHCl_3$ (5 $cm^3$). The mixture was allowed to stirring at room temperature for 6 hours. The colorless solution turned to brown. The yellow precipitate formed was filtered, washed with $CHCl_3$ (3 $cm^3$) to remove unreacted $L^5$ and dried under vacuum.

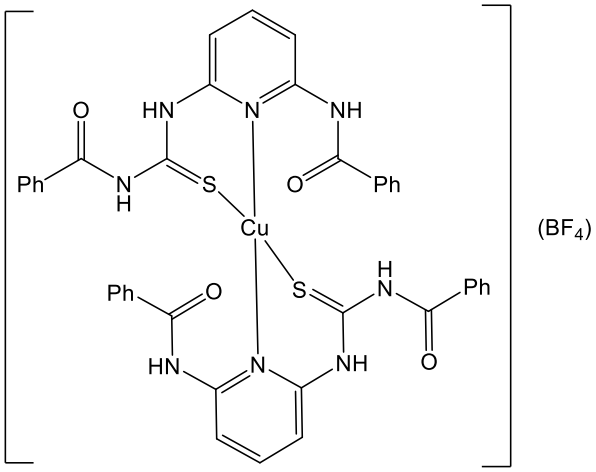


Yield: (0.27 g, 72%); yellow powder; ESI-MS (m/z)(%): 815.13 [M+] (100%); Mass: 815.1284 Calc. Mass: 815.1284; FT-IR ($cm^{-1}$): ν(N-H) 3314, ν(C=O) 1663, ν(C=S) 1298; UV-vis. spectrum, $\lambda_{max}$ nm, (εM, $M^{-1}$ $cm^{-1}$): 275(23250), 316(20900), 400(7700); $^1$H NMR (300 MHz, DMSO-$d^6$), δ(ppm): 13.23 (2H, s, 2N-$H_A$), 11.78 (2H, s, 2N-$H_B$), 10.88 (1H, s, N-$H_C$), 8.22 (2H, d, 2H Py $J_{HH}$ =7.5 Hz), 8.10 (2H, d, 2H Py $J_{HH}$ =10 Hz), 8.01 –7.51 (22H, m, (20 H Ar + 2H Py); $^{13}$C NMR (100 MHz, DMSO-$d^6$), δ(ppm): 177.32 (C=S), 166.79 (C=O), 166.40 (C=O), 151.46, 149.99, 140.56, 134.29, 133.45, 133.22, 132.55, 129.32, 129.20, 129.00, 128.81, 128.75, 128.49, 128.34, 128.09, 116.47, 114.02. Anal. Calcd. for **$C_{40}H_{32}BCuF_4N_8O_4S_2$**: C, 53.19; H, 3.57; N,12.41. Found: C, 52.88; H, 3.30; N, 12.24.

### 4.2.3.2 Synthesis of $[Cu^{II}L^5(H_2O)](BF_4)_2$ (4.2)

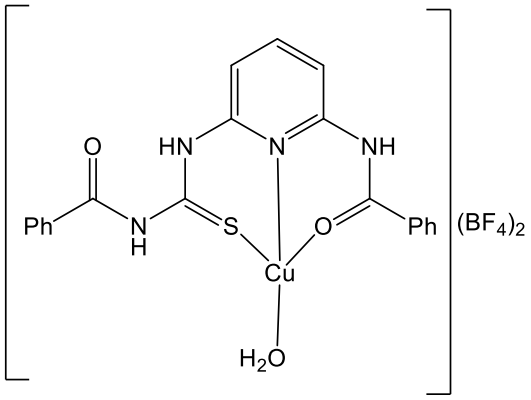


Using the same procedure as described for **4.1** was followed by using: $Cu(BF_4)_2.6H_2O$ (0.24 g, 1 mmol), $\mathbf{L^5}$ (0.38 g, 1 mmol). Yield: (0.3 g, 80%); green powder; ESI-MS *(m/z)*(%): 456.07 [M-H] (100%); FT-IR ($cm^{-1}$): ν(N-H) 3310, ν(C=O) 1666, ν(C=S) 1275; UV-vis. spectrum, $\lambda_{max}$ nm, (εM, $M^{-1}$ $cm^{-1}$): 269(14600), 299(11150), 762(24); Anal. Calcd. for $\mathbf{C_{20}H_{18}B_2CuF_8N_4O_3S}$ (%): C,38.03; H, 2.87; N,8.87. Found (%): C, 38.42; H, 3.00; N, 8.94.

### 4.2.3.3 Synthesis of $[Ni(L^5)_2](ClO_4)_2$ (4.3)

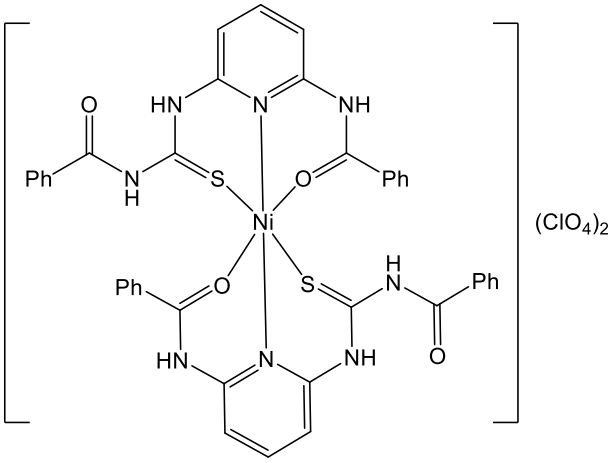


A methanolic solution (5 $cm^3$) of $Ni(ClO_4)_2.6H_2O$ (0.18 g, 0.5 mmol) was added drop wise to a solution of $\mathbf{L^5}$ ( 0.38 g, 1 mmol) in $CHCl_3$ (10 $cm^3$). The mixture was stirred at 50°C for 8 hours. The green precipitate formed was filtered, washed with $CHCl_3$ (10 $cm^3$) to remove the unreacted ligand and dried under vaccum. Yield: (0.31 g, 82%); green powder; ESI-MS *(m/z)*(%): 809.13 [M-H] (100%); Mass: 809.1263 Calc. Mass: 809.1263; FT-IR ($cm^{-1}$): ν(N-H) 3304, ν(C=O) 1662, ν(C=S) 1267; ν(Cl-O) 1094, 621; UV-vis. spectrum, $\lambda_{max}$ nm, (εM, $M^{-1}$ $cm^{-1}$): 245(27500), 306(18450), 395(1910), 600(15), 972(19); Anal. Calcd. for $\mathbf{C_{40}H_{32}Cl_2N_8NiO_{12}S_2}$ (%): C, 47.55; H, 3.19; N, 11.09. Found (%): C, 47.25; H, 3.49; N, 11.02.

### 4.2.3.4 Synthesis of $[Cu^{I}(L^{5A})_2](BF_4)$ (4.4)

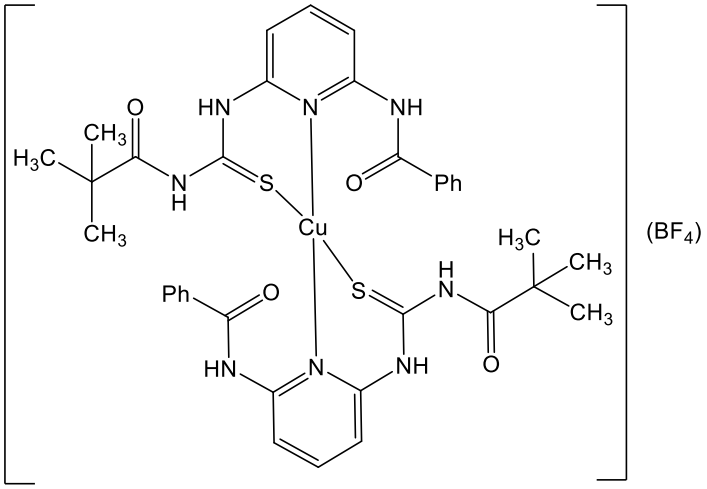

Using the same procedure as described for **4.1** was followed by using: $Cu(BF_4)_2.6H_2O$ (0.12 g, 0.5 mmol), $\mathbf{L^{5A}}$ (0.36 g, 1 mmol). Orange crystals of **4.4** were grown at room temperature by the diffusion of diethyl ether vapor into an ethanol:DCM (1:1) solution. Yield: (0.24 g, 69%); Orange crystals; ESI-MS *(m/z)* (%): 775.19 [M+] (100%); Mass: 775.1923 Calc. Mass: 775.1910, FT-IR ($cm^{-1}$): ν(N-H) 3294, ν(C=O) 1688,1615, ν(C=S) 1265; UV-vis. spectrum, $\lambda_{max}$ nm, (εM, $M^{-1}$ $cm^{-1}$): 266(17000), 308(16500), 396(2000); $^1$H NMR (400 MHz, DMSO-$d^6$), δ(ppm): 13.19 (2H, s, 2N-$H_A$), 10.82 (2H, s, 2N-$H_B$), 10.76 (2H, s, 2N-$H_C$), 8.29 (2H, d, 2H py $J_{HH}$ =5 Hz), 8.05 (2H, d, 2H py $J_{HH}$ =5 Hz), 7.99 (4H, d, H Ar $J_{HH}$ =5 Hz), 7.93 (2H, t, 2H Ar $J_{HH}$ =7.5 Hz), 7.58 (2H, t, 2H py $J_{HH}$ =5 Hz), 7.49 (4H, t, 4H Ar $J_{HH}$ =5 Hz), 1.23 (18H, s, $6CH_3$); $^{13}$C NMR (100 MHz, DMSO-$d^6$), δ(ppm): 188.05 (C=S), 181.37 (C=O), 166.47 (C=O), 151.12, 149.49, 140.87, 132.64, 129.29,128.83, 128.37, 116.68, 114.93, 39.12, 26.43 ($CH_3$). Anal. Calcd. for $\mathbf{C_{36}H_{40}BCuF_4N_8O_4S_2.2CHCl_3.2H_2O}$ (%): C, 40.11; H, 4.07; N, 9.85. Found (%): C, 40.11; H, 4.12; N, 10.12.

### 4.2.3.5 Synthesis of $[Cu^{II}L^{5A}(H_2O)](BF_4)_2$ (4.5)

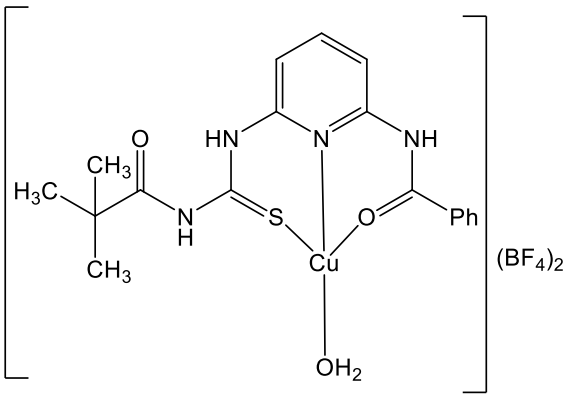

Using the same procedure as described for **4.1** was followed by using: $Cu(BF_4)_2.6H_2O$ (0.24 g,1 mmol), $\mathbf{L^{5A}}$ (0.36 g, 1 mmol). Yield: (0.27 g, 77%); green powder; ESI-MS *(m/z)*(%): 436.12 [M-H] (100%); FT-IR ($cm^{-1}$): ν(N-H) 3318, ν(C=O) 1682, 1613, ν(C=S) 1273; UV-vis. spectrum, $\lambda_{max}$ nm, (εM, $M^{-1}$ $cm^{-1}$): 266(14100), 306(13300),

779(20); Anal. Calcd. for **$C_{18}H_{22}B_2CuF_8N_4O_3S$** (%) : C, 35.35; H, 3.63; N, 9.16. Found (%): C, 35.66; H, 3.74; N, 9.28.

### 4.2.3.6 Synthesis of $[Ni(L^{5A})_2](ClO_4)_2$ (4.6)

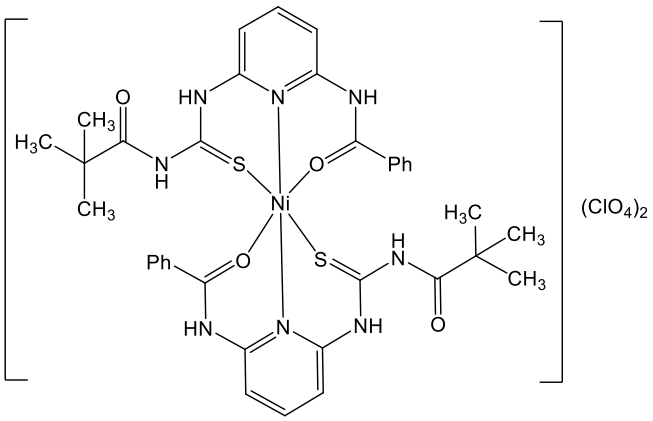

Using the same procedure as described for **4.3** was followed by using: $Ni(ClO_4)_2.6H_2O$ (0.18 g, 0.5 mmol), **$L^{5A}$** (0.36 g, 1 mmol)**.** Pale green crystals of **4.6** were grown at room temperature by the diffusion of diethyl ether vapor into an acetone solution. Yield: (0.25 g, 71%); ESI-MS *(m/z)*(%): 769.19 [M-H] (100%); Mass: 769.1873 Calc. Mass: 769.1889; FT-IR ($cm^{-1}$): ν(N-H) 3312, ν(C=O) 1686, 1637, ν(C=S) 1267; ν(Cl-O) 1096, 621; UV-vis. spectrum, $\lambda_{max}$ nm, (εM, $M^{-1}$ $cm^{-1}$): 250(29000), 305(25300), 374(2520), 605(16), 967(22); Anal. Calcd. for **$C_{36}H_{40}Cl_2N_8NiO_{12}S_2.CH_2Cl_2$** (%): C, 42.11; H, 4.01; N, 10.62. Found (%): C, 42.19; H, 3.87; N, 10.76.

### 4.2.3.7 Synthesis of $[Ni(L^{5A*})_2](ClO_4)_2$ (4.7)

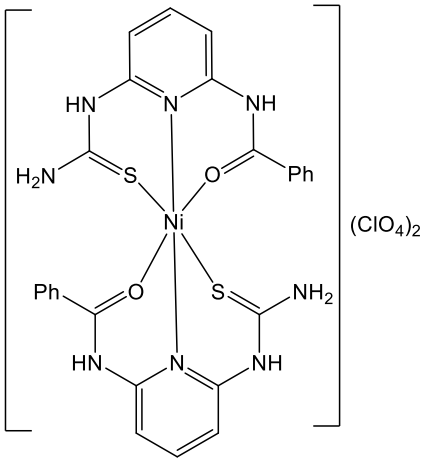

Using the same procedure as described for **4.3** was followed by using: $Ni(ClO_4)_2.6H_2O$ (0.18 g, 0.5 mmol), **$L^{5A}$** (0.36 g, 1 mmol) by refluxing the mixture at 75°C instead of 50°C. Light green crystals of **4.7** were grown at room temperature by the diffusion of diethyl ether vapor into a mixture of ethanol:DCM(1:3) solution.Yield: (0.23 g, 66%); ESI-MS *(m/z)*(%): 601.1 [M-H] (100%); Mass: 601.0732 Calc. Mass: 601.0739; FT-IR ($cm^{-1}$): ν(N-H) 3321, ν(C=O) 1636, ν(C=S) 1266; ν(Cl-O) 1103, 619; UV-vis. spectrum, $\lambda_{max}$ nm, (εM, $M^{-1}$ $cm^{-1}$): 254(24750), 308(30100), 393(1920), 589(13), 947(14); Anal. Calcd. for **$C_{26}H_{24}Cl_2N_8NiO_{10}S_2$**: C,38.93; H, 3.02; N,13.97. Found: C, 39.08; H, 3.15; N, 13.90.

### 4.2.3.8 Synthesis of $[Cu^{I}(L^{7})_2](BF_4)$ (4.8)

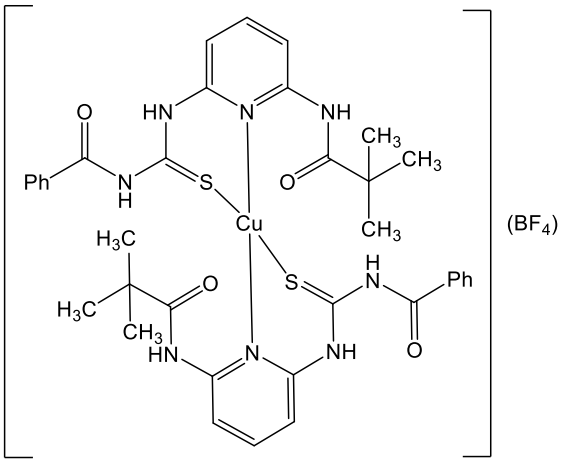

Using the same procedure as described for **4.1** was followed by using: $Cu(BF_4)_2.6H_2O$ (0.12 g, 0.5 mmol), $\mathbf{L^7}$ (0.36 g, 1 mmol). Yield: (0.3 g, 84%); yellow powder; ESI-MS *(m/z)*(%): 775.19 [M+] (100%); Mass: 775.1915 Calc. Mass: 775.1910, FT-IR ($cm^{-1}$): ν(N-H) 3304, ν(C=O) 1678,1601, ν(C=S) 1260; UV-vis. spectrum, $\lambda_{max}$ nm, (εM, $M^{-1}$ $cm^{-1}$): 267(26000), 302(25800), 390(4900); $^1$H NMR (400 MHz, DMSO-$d^6$), δ(ppm): 13.16 (2H, s, 2N-$H_A$), 11.74 (2H, s, 2N-$H_B$), 9.89 (2H, s, 2N-$H_C$), 8.44 (4H, d, 4H py $J_{HH}$ =5 Hz), 7.98 (4H, d, 4H Ar $J_{HH}$ =5 Hz), 7.88 (2H, t, 2H Ar $J_{HH}$ =5 Hz), 7.67 (2H, t, 2H py $J_{HH}$ =2.5 Hz), 7.54 (4H, t, 4H Ar $J_{HH}$ =5 Hz), 1.23 (18H, s, 6$CH_3$); $^{13}$C NMR (100 MHz, DMSO-$d^6$), δ(ppm): 177.80 (C=S), 177.34 (C=O), 168.93 (C=O), 151.63, 149.79, 140.43, 133.80, 133.21, 129.21, 128.99, 116.46, 114.68, 39.15, 27.59 ($CH_3$). Anal. Calcd. for $\mathbf{C_{36}H_{40}BCuF_4N_8O_4S_2}$ (%): C, 50.09; H, 4.67; N, 12.98. Found (%): C, 50.62; H, 4.36; N, 13.27.

### 4.2.3.9 Synthesis of $[Cu^{II}L^{7}(H_2O)](ClO_4)_2$ (4.9)

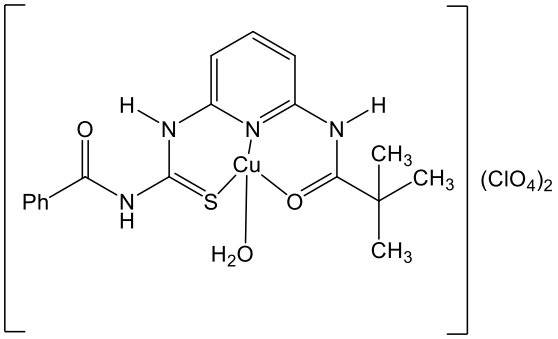

Using the same procedure as described for **4.1** was followed by using: $Cu(ClO_4)_2.6H_2O$ (0.37 g, 1 mmol), $\mathbf{L^7}$ (0.36 g, 1 mmol). Pale green crystals of **4.9** were grown at room temperature by the diffusion of diethyl ether vapor into an acetone solution. Yield: (0.28 g, 79%); ESI-MS *(m/z)*(%): 436.16 [M-H] (100%); FT-IR ($cm^{-1}$): ν(N-H) 3318, ν(C=O) 1676, 1618, ν(C=S) 1283, ν($ClO_4$) 1089, 621; UV-vis. spectrum, $\lambda_{max}$ nm, (εM, $M^{-1}$ $cm^{-1}$): 268(8750), 302(9500), 776(27); Anal. Calcd. for $\mathbf{C_{18}H_{22}Cl_2CuN_4O_{11}S}$: C,33.95; H, 3.48; N,8.80. Found: C, 33.88; H, 3.57; N, 8.72.

### 4.2.3.10 Synthesis of $[Ni(L^7)_2](ClO_4)_2$ (4.10)

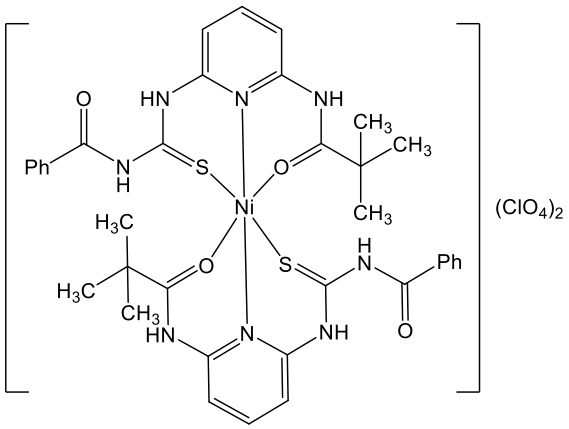

Using the same procedure as described for **4.3** was followed by using: $Ni(ClO_4)_2.6H_2O$ (0.18 g, 0.5 mmol), $\mathbf{L^7}$ (0.36 g, 1 mmol)**.** Yield:(0.3 g, 84%); green powder; ESI-MS *(m/z)*(%): 769.19 [M-H] (100%); Mass: 769.1864 Calc. Mass: 769.1889; FT-IR ($cm^{-1}$): ν(N-H) 3318, ν(C=O) 1676, 1610, ν(C=S) 1271; ν(Cl-O) 1092, 619; UV-vis. spectrum, $\lambda_{max}$ nm, (εM, $M^{-1}$ $cm^{-1}$): 238(32900), 293(19950),397(1850), 588(18), 952(20); Anal. Calcd. for **$C_{36}H_{40}Cl_2N_8NiO_{12}S_2$ (%):** C, 44.56; H, 4.15; N, 11.55. Found (%): C, 44.45; H, 4.15; N, 11.43.

### 4.2.3.11 Synthesis of $[Cu^I(L^{7A})_2](BF_4)$ (4.11)

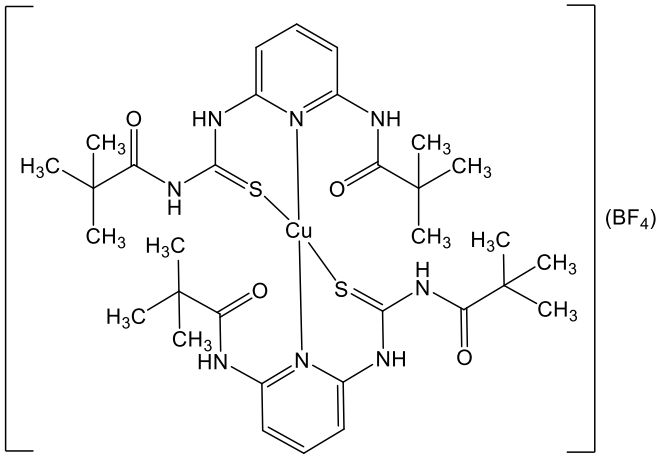

Using the same procedure as described for **4.1** was followed by using: $Cu(BF_4)_2.6H_2O$ (0.12 g, 0.5 mmol), $\mathbf{L^{7A}}$ (0.34 g, 1 mmol). Yield: (0.23 g, 68%); orange powder; ESI-MS *(m/z)*(%): 735.24 [M+] (100%); Mass: 735.2536 Calc. Mass: 735.2536, FT-IR ($cm^{-1}$): ν(N-H) 3327, ν(C=O) 1683,1625, ν(C=S) 1283; UV-vis. spectrum, $\lambda_{max}$ nm, (εM, $M^{-1}$ $cm^{-1}$): 266(16400), 321(18200), 385(3100); $^1$H NMR (400 MHz, DMSO-$d^6$), δ(ppm): 13.14 (2H, s, 2N-$H_A$), 10.80 (2H, s, 2N-$H_B$), 9.76 (2H, s, 2N-$H_C$), 8.17 (2H, t, 2H Py $J_{HH}$ =5 Hz), 7.78 (2H, d, 2H Py $J_{HH}$ =7.5 Hz), 7.30 (2H, d, 2H Py $J_{HH}$ =7.5 Hz), 1.32 (9H, s, $3CH_3$), 1.27 (9H, s, $3CH_3$), 1.24 (9H, s, $3CH_3$),1.22 (9H, s, $3CH_3$); $^{13}$C NMR (100 MHz, DMSO-$d^6$), δ(ppm): 189.22 (C=S), 181.33 (C=O), 177.77 (C=O), 151.35, 150.11, 141.11, 116.70, 115.17, 39.76, 39.00, 27.65 ($CH_3$), 27.25 ($CH_3$). Anal. Calcd. for

**$C_{32}H_{48}BCuF_4N_8O_4S_2$** (%): C, 46.69; H, 5.88; N, 13.61. Found (%): C, 46.13; H, 5.52; N, 13.19.

### 4.2.3.12 Synthesis of $[Cu^{II}L^{7A}(H_2O)](ClO_4)_2$ (4.12)

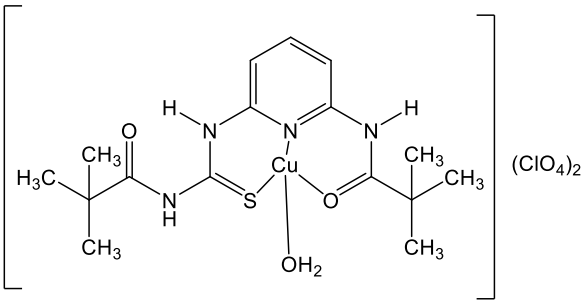

Using the same procedure as described for **4.1** was followed by using: $Cu(ClO_4)_2.6H_2O$ (0.37 g, 1 mmol), **$L^{7A}$** (0.34 g, 1 mmol). Yield: (0.22 g, 65%); green powder; ESI-MS *(m/z)*(%): 415.99 [M-H] (100%); FT-IR ($cm^{-1}$): ν(N-H) 3314, ν(C=O) 1684, 1616, ν(C=S) 1275, ν($ClO_4$) 1090, 617 ; UV-vis. spectrum, $\lambda_{max}$ nm, (εM, $M^{-1}$ $cm^{-1}$): 264(5950), 309(7300), 792(33); Anal. Calcd. for **$C_{16}H_{26}Cl_2CuN_4O_{11}S$** (%): C, 31.15; H, 4.25; N, 9.08. Found (%): C, 31.04; H, 4.36; N, 8.79.

### 4.2.3.13 Synthesis of $[Ni(L^{7A})_2](ClO_4)_2$ (4.13)

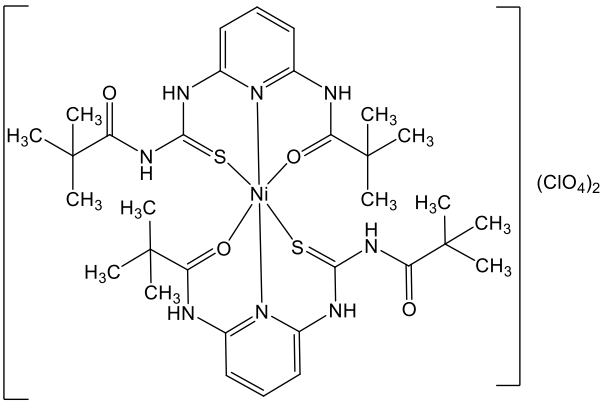

Using the same procedure as described for **4.3** was followed by using: $Ni(ClO_4)_2.6H_2O$ (0.18 g, 0.5 mmol), **$L^{7A}$** (0.34 g, 1 mmol)**.** Green crystals of **4.13** were grown at room temperature by the diffusion of diethyl ether vapor into an $CHCl_3$ solution. Yield: (0.24 g, 72%); ESI-MS *(m/z)*(%): 729.25 [M-H] (100%); Mass: 729.2515 Calc. Mass: 729.2515; FT-IR ($cm^{-1}$): ν(N-H) 3306, ν(C=O) 1681, 1614, ν(C=S) 1265; ν(Cl-O) 1094, 617; UV-vis. spectrum, $\lambda_{max}$ nm, (εM, $M^{-1}$ $cm^{-1}$): 229(33900), 306(24000), 414(3280), 607(15), 946(18); Anal. Calcd. for **$C_{32}H_{48}Cl_2N_8NiO_{12}S_2$** (%): C, 41.31; H, 5.20; N, 12.04. Found (%): C, 41.21; H, 5.27; N, 11.98.

# 4.3 Results and discussion

## 4.3.1 Synthesis of ligands ($L^5$-$L^{7A}$)

The N,N′-substituted thioureas (**$L^5$-$L^{7A}$**) were synthesized by a modification of the method described by Kaminsky *et al.*[22] The synthesis of N,N′-substituted thioureas (**$L^5$-$L^{7A}$**) was achieved in three steps. First, synthesis of N-(6-aminopyridin-2-yl)benzamide **$L^4$** and N-(6-aminopyridin-2-yl)pivalamide **$L^6$** ligands as described previously[23] by stirring at room temperature for 17 hours a mixture of 2,6-diaminopyridine and benzoyl chloride or (pivaloyl chloride) in dry THF solution. Then, the mixture of an equimolar ratio of pivaloyl chloride with potassium thiocyanate in acetonitrile was heated to reflux for 3 hours to obtain the pivaloyl isothiocyanate. Finally, the benzoyl isothiocyanate was heated to reflux with **$L^4$** or **$L^6$** for 3 hours to yield the final thiourea ligands **$L^5$** and **$L^7$** respectively. Pivaloyl isothiocyanate was heated with **$L^4$** or **$L^6$** for 15 hours to give **$L^{5A}$** and **$L^{7A}$** respectively. These crude compounds of **$L^5$**- **$L^{7A}$** were washed and recrystallized from acetonitrile to obtain white crystals of **$L^5$** - **$L^{7A}$** in good yields (72-91%). The synthetic route to **$L^5$-$L^{7A}$** is shown in **Scheme 4.1**. **$L^5$** - **$L^{7A}$** were soluble in DMF and DMSO. **$L^5$** was soluble in $CHCl_3$ and insoluble in acetone, acetonitrile, ethyl acetate and alcohol. **$L^{5A}$** and **$L^7$** were soluble in $CHCl_3$ and partially soluble in acetone, acetonitrile, ethyl acetate and alcohol. **$L^{7A}$** was soluble in $CHCl_3$, acetone, acetonitrile, ethyl acetate, alcohol. **$L^5$-$L^{7A}$** are insoluble in n-hexane.

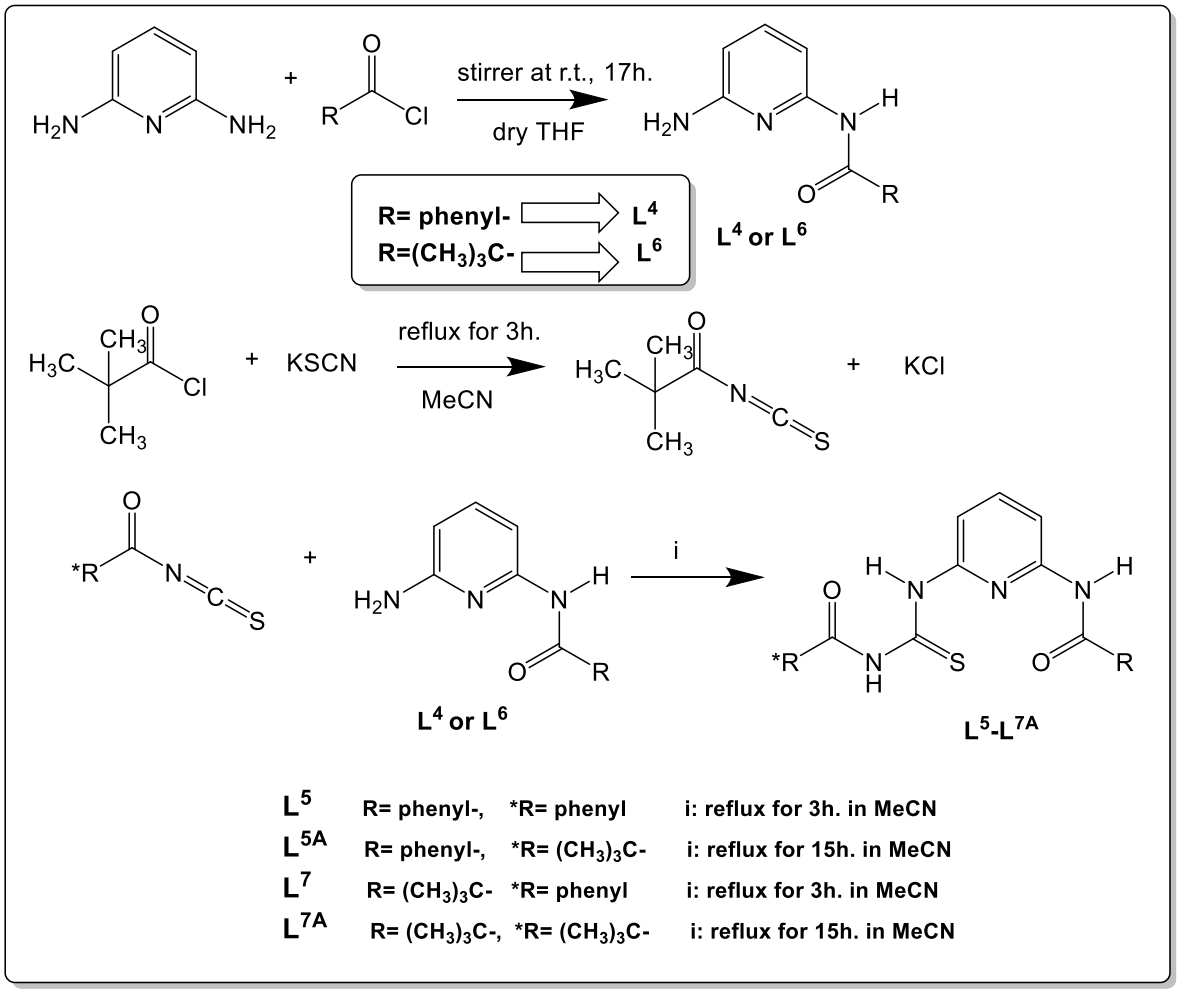


**Scheme 4.1:** Synthesis of the ligands $L^5$-$L^{7A}$. (reaction conditions and reagents).

## 4.3.2 Synthesis of complexes (4.1- 4.13)

The reaction between **$L^5$-$L^{7A}$** with $Cu(BF_4)_2.6H_2O$ or $Cu(ClO_4)_2.6H_2O$ in a 2:1 and 1:1 stoichiometry was carried out in a $CHCl_3$/MeOH solution by stirring the mixture at room temperature for a few hours. Analytical, spectral and crystallographic data indicated the formation of $[Cu^{I}(L)_2](X)$ and $[Cu^{II}(L)(H_2O)](X)_2$ (X = $BF_4$ or $ClO_4$), **Scheme 4.2**. Recently, it has been shown that the preparation of complexes of Cu(I) with some thiourea derivatives can be simply accomplished by mixing the solution of ligand and the corresponding Cu(II) salts.

It has been reported that in such case the thiourea is also acting as reducing agent.[24-26] Cu(I) complexes **4.1**, **4.4**, **4.8** and **4.11** were obtained from the reaction of **$L^5$-$L^{7A}$** with $Cu(ClO_4)_2.6H_2O$ or $Cu(BF_4)_2.6H_2O$ in a 2:1 molar ratio respectively,

while Cu(II) complexes **4.2**, **4.5**, **4.9** and **4.12** formed when the same reaction was carried out in 1:1 molar ratio. At first glance, this observation suggests that one mole of the free ligand, **$L^5$-$L^{7A}$** is not able to reduce Cu(II) to Cu(I) and this observation support the happening of the reduction process. However in our experiments thiourea role as reducing agent appears unlikely due to the stoichiometry of the reaction. Although, many researches of Cu(I) complexes have been accomplished by the reaction between thiourea and the Cu(II) salts, the precise mechanism of the conversion of Cu(II) to Cu(I) by using thiourea derivatives has not been reported. The stable and unchanged structure for the thiourea ligand in its Cu(I) complexes here in this chapter lead us to suggest that if the ligand is oxidized it then returns again to its normal oxidation state. In addition, it is possible that the solvents in the reaction may be have any role in the reduction process of Cu(II) to Cu(I).

The Cu(I) complexes **4.1**, **4.4**, **4.8** and **4.11** were isolated as yellow or orange solids, which were stable at room temperature and completely soluble in DMF or DMSO. They are partially soluble in acetone, acetonitrile, alcohol, ethyl acetate but insoluble in $CHCl_3$, DCM and n-hexane. Cu(II) complexes **4.2**, **4.5**, **4.9** and **4.12** were isolated as green solids which were stable at room temperature and soluble in DMF, DMSO, acetone, acetonitrile, alcohol and ethyl acetate, but insoluble in $CHCl_3$, DCM or n-hexane.

Ni(II) perchlorate complexes **4.3**, **4.6**, **4.7**, **4.10** and **4.13** were prepared by the reaction of **$L^5$-$L^{7A}$** with $Ni(ClO_4)_2.6H_2O$ in a mixture of $CHCl_3$ and methanol (2:1) to ensure complete solubility of the reactants. The synthesis of the Ni(II) complexes was carried out at 75°C and 50°C. Ni(II) complexes prepared by heating the mixture solution at 75°C showed cleavage of two pivaloyl groups (**4.7**). These results led to carry out the preparation of the complexes by heating the mixture solution to lower temperatures (50°C) to form complexes without cleavage of the acyl (benzoyl or pivaloyl) group. Attempts to prepare complexes between **$L^5$- $L^{7A}$** and $Ni(ClO_4)_2.6H_2O$ in 1:1 and 2:1 ratios formed complexes with the same general formula, $[Ni(\mathbf{L})_2](ClO_4)_2$, **Scheme 4.2**. The Ni(II) complexes were stable at room temperature and were collected as green solids and were soluble in acetone,

acetonitrile, alcohol, $CHCl_3$, DCM, DMF and DMSO but insoluble in n-hexane. Unfortunately, we could not prepare the Zn(II) complexes between **$L^5$- $L^{7A}$** and $Zn(ClO_4)_2.6H_2O$ or $ZnCl_2$ in 1:1 and 2:1 ratios in spite of many attempts at different temperatures. Each time, the NMR spectra of the reaction mixture were exactly the same as the starting ligands.

The purification of the Cu(I), Cu(II) and Ni(II) complexes was achieved by washing the resulting precipitates with the same solvents used in their synthesis, and then recrystallization of **4.4** and **4.7** in DCM:EtOH, **4.6** and **4.9** in acetone and **4.13** in $CHCl_3$ solutions. The yields of these prepared complexes were moderate to good (65-84%). Experimental observations on the reactivity of the ligands can be summarized:

i) ligands **$L^5$- $L^{7A}$** are stable (without cleavage of the carbonyl group) in a mixture of $CHCl_3$:methanol:$H_2O$ (3:3:0.5ml) at different temperatures (25, 37, 50 and 75°C); ii) all prepared Cu(I) and Cu(II) complexes are stable (without cleavage of the carbonyl group) in a mixture of $CHCl_3$:methanol:$H_2O$ (3:3:0.5ml) at (25, 37, 50 and 75°C); iii) all the prepared Ni(II) complexes are stable (without cleavage of the carbonyl group) in the mixture of $CHCl_3$:methanol:$H_2O$ (3:3:0.5ml) at different temperatures (25, 37 and 50°C) but suffer from cleavage of carbonyl group at 75°C.

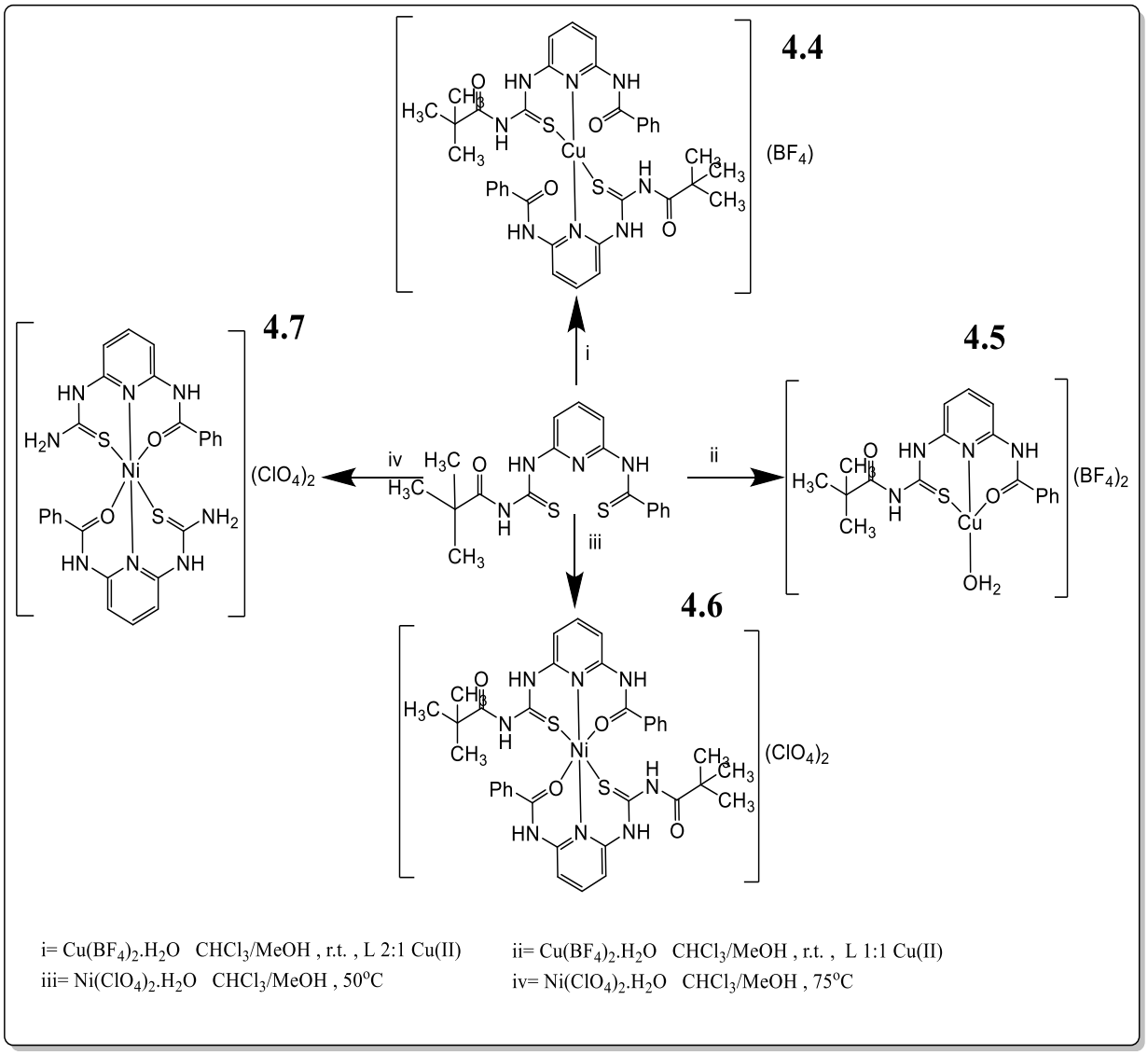


**Scheme 4.2:** Synthesis of the Cu(I), Cu(II) and Ni(II) complexes of $L^{5A}$(**4.4**-**4.7**).

## 4.3.3 Spectroscopic studies of ligands ($L^5$-$L^{7A}$) and their complexes (4.1-4.13)

### 4.3.3.1 $^1$H and $^{13}$C-NMR spectra

The $^1$H and $^{13}$C NMR spectroscopic characterization for the investigated ligands (**$L^5$-$L^{7A}$**) and their Cu(I) complexes (**4.1**, **4.4**, **4.8** and **4.11**) are listed in the experimental section. The $^1$H NMR data for the ligands **$L^5$-$L^{7A}$** show that the *N-H* resonates ($CONH_1$, $CONH_2$ and CSNH) considerably downfield in the spectra when compared with the other peaks. The proton chemical shifts for two free and

one hydrogen bonded *N-H* ($CONH_1$, $CONH_2$ and CSNH respectively) are found around 7.85–8.49, 8.48-9.06 and 12.85-13.00 ppm respectively, whilst the aromatic protons appear between 7.46- 8.59 ppm. The $^{13}C$ NMR spectra of **$L^5$-$L^{7A}$** show the expected number of resonances. The signals observed in the range 111.42-150.41 ppm were assigned to the aromatic carbons. The resonances due to the C=O ($C=O_1$, $C=O_2$) and C=S groups in the ligands **$L^5$-$L^{7A}$** appear in the regions of 165.71-177.02, 166.75-177.28 and 176.86-179.34 ppm, respectively.

$^1H$ NMR data for the Cu(I) complexes **4.1**, **4.4**, **4.8** and **4.11** show the existence of aromatic protons in the range 7.30-8.44 ppm. The proton chemical shifts for the N-H ($CONH_1$, $CONH_2$ and CSNH) groups in the Cu(I) complexes were found around 9.76-10.88, 10.80-11.78 and 13.14-13.23 ppm respectively. In addition, Cu(I) complexes **4.4** and **4.8** show a singlet peak at 1.23 ppm and for **4.11** at 1.22-1.32 ppm which have been assigned to the methyl group in t-butyl groups. The $^{13}C$ NMR spectra of Cu(I) complexes **4.1**, **4.4**, **4.8** and **4.11** show the expected number of resonances. Signals observed in the range 114.02-151.63 ppm were assigned to the aromatic carbons. The$^{13}C$ NMR peaks of C=O ($C=O_1$, $C=O_2$) and C=S of Cu(I) complexes appeared in the regions of 166.40-177.77, 166.79-181.37 and 177.32-189.22 ppm respectively. Unfortunately and logically, it is not possible to directly compare the $^1H$ and $^{13}C$ NMR spectra for the Cu(I) complexes with their corresponding free ligands due to the use of different deuterated solvents. $CDCl_3$ was used as NMR solvent in (**$L^5$-$L^{7A}$**) ligands while DMSO-$d^6$ was used to measure NMR spectra for the Cu(I) complexes **4.1**, **4.4**, **4.8** and **4.11.**

## 4.3.3.2 Infrared spectra

The main vibrational bands of ligands (**$L^5$-$L^{7A}$**) and their complexes (**4.1-4.13**) are given in the experimental section and listed in **Table 4.1**. The IR spectra of free ligands (**$L^5$-$L^{7A}$**) show characteristic absorption bands at $\nu_{max}$ ($cm^{-1}$) 3341-3429 (N-H), 1670-1690 (C=O) and 1321-1333 (C=S). The IR spectra of thiourea complexes (**4.1-4.13**) show these absorption bands at $\nu_{max}$ ($cm^{-1}$) 3294-3327 (N-H), 1661-1688 (C=O) and 1260-1298 (C=S). According to the literature, the amide carbonyl stretch appears at ~ 1640-1690 $cm^{-1}$.[27] The Cu(I) complexes **4.1**, **4.4**, **4.8** and **4.11** show little change in C=O stretching frequency indicating the

oxygen carbonyl group does not coordinate to the metal center. The FT-IR spectra of Cu(II) complexes **4.2, 4.5, 4.9** and **4.12** and Ni(II) complexes **4.3, 4.6, 4.7, 4.10** and **4.13** show considerable changes of the C=O stretching frequency position by shifting to lower energy when compared with their corresponding free ligands, suggesting the coordination with the metal centre through the carbonyl group.[28,29] This red shift (lower wavenumber) may be due to the electrons donating behaviour of the oxygen atom in C=O group to the electropositive metal centre which cause the reducing of the double bond property in C=O bond and weakens it. This weakens the bond and causes it to be observed at lower wavenumber. In addition, the formation of a strong intramolecular hydrogen bond within the thiourea (C=O…H-N) may cause this shift of C=O to lower energy by weakens the bond through electrons donating behaviour of the oxygen atom in C=O group to the hydrogen N-H bond.

A strong peak at 1321-1333 $cm^{-1}$, assigned to C=S in the ligands **$L^5$-$L^{7A}$,** also shifted to lower energy at 1260-1298 $cm^{-1}$ in all prepared complexes (**4.1-4.13**). This indicates coordination of the C=S group to the metal centre, reducing the bond order because electrons are donated to metal from sulfur atom and this weakens the C=S bond. In all perchlorate complexes, the presence of two characteristic unsplit IR active bands at 1089-1103 $cm^{-1}$ and 617-621 $cm^{-1}$ indicates that the $T_d$ symmetry of $ClO_4$ is maintained in all its complexes and therefore outside the coordination sphere.[30,31]

**Table 4.1:** IR data ($\nu_{max}$, $cm^{-1}$) for the ligands (**$L^5$**- **$L^{7A}$**) and their complexes (**4.1**- **4.13**).

| Compound | ν (N-H) | ν (C=O) | ν (C=S) | ν (Cl-O) |
|---|---|---|---|---|
| **$L^5$** | 3428,3341 | 1670 | 1333 | - |
| **4.1** | 3314 | 1668 | 1298 | - |
| **4.2** | 3310 | 1661 | 1275 | - |
| **4.3** | 3304 | 1662 | 1267 | 1094, 621 |
| **$L^{5A}$** | 3429,3391 | 1690 | 1321 | - |
| **4.4** | 3294 | 1688 | 1265 | - |
| **4.5** | 3318 | 1682 | 1273 | - |
| **4.6** | 3312 | 1680 | 1267 | 1096, 621 |
| **4.7** | 3321 | 1676 | 1266 | 1103,619 |
| **$L^7$** | 3427,3402 | 1678 | 1331 | - |
| **4.8** | 3304 | 1678 | 1260 | - |
| **4.9** | 3318 | 1671 | 1283 | 1089, 621 |
| **4.10** | 3318 | 1670 | 1271 | 1092, 619 |
| **$L^{7A}$** | 3428 | 1682 | 1323 | - |
| **4.11** | 3327 | 1683 | 1283 | - |
| **4.12** | 3314 | 1674 | 1275 | 1090, 617 |
| **4.13** | 3306 | 1671 | 1265 | 1094, 617 |

## 4.3.3.3 Electronic spectra

The UV-visible spectra of the ligands **$L^5$-$L^{7A}$** and their complexes **4.1-4.13** were recorded in DMF solution and the data are presented in the experimental section. Electronic spectra of **$L^5$-$L^{7A}$** show π→π* and n→π* transitions at 266-297, and 315 and 322 nm respectively. As expected the Cu(I) complexes **4.1**, **4.4**, **4.8** and **4.11** do not show any *d-d* transitions. The Cu(I) complexes show π→π* and n→π* transitions at $\lambda_{max}$ nm ($\varepsilon$,$M^{-1}cm^{-1}$) 266(16400)-275(23250) and 302(25800)-321(18200) respectively. The absorption bands centred around 385(3100)-

400(7700) $\lambda_{max}$ nm (ε,$M^{-1}cm^{-1}$), are attributed to Cu(I)→L charge transfer (MLCT) of Cu(I) complexes **4.1**, **4.4**, **4.8** and **4.11**.

The electronic spectra of Cu(II) complexes **4.2**, **4.5**, **4.9** and **4.12** show shorter wavelength shifts of π–π* and n–π* transitions as compared to their corresponding free ligands.This is due to the electropositive charge of Cu(II) ion which decrease the double bond character of the intraligand bonds after complexation. As expected, the new peak observed in **4.2**, **4.5**, **4.9** and **4.12** at $\lambda_{nm}$(ε, $M^{-1}cm^{-1}$) 762(24), 779(20), 776 (27) and 792(33) is assigned to a *d-d* transition ($d_{xy}$→$d_{x2-y2}$), **Figure 4.7**, **Table 4.2.** The spin allowed transition generally falls within the ranges 13000-20000 $cm^{-1}$ (770-500 nm) for regular square planar systems.[32]

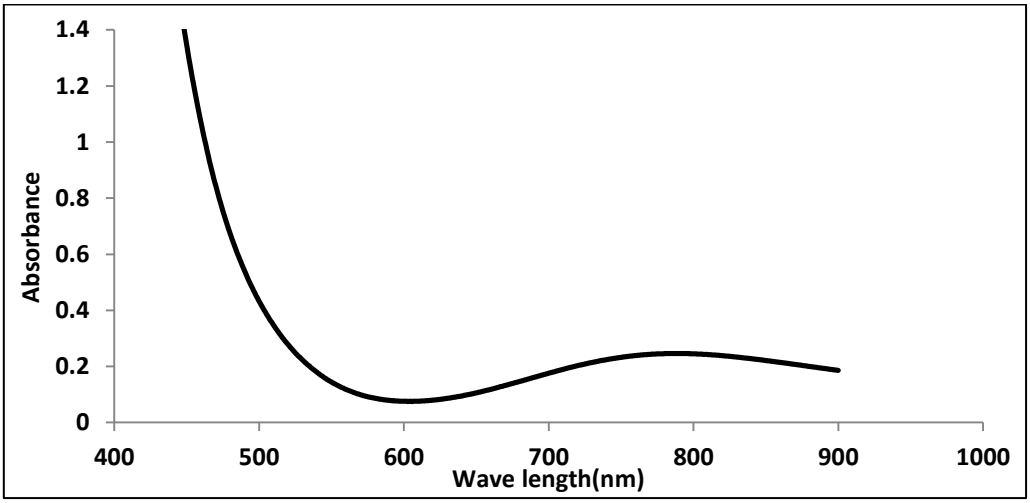


**Figure 4.7:** The electronic spectrum of Cu(II) complex **4.2**.

The Ni(II) complexes, **4.3**, **4.6**, **4.7**, **4.10** and **4.13** show the π–π* and n–π* intraligand transitions which are shifted to lower wavelength (higher frequency) when compared with their free corresponding ligands observe at 229(33900)-254(24750) and 293(19950)-308 nm(30100 $M^{-1}cm^{-1}$) respectively. This shifting is due to the coordination between ligands and Ni(II) ion causing a decreased stabilisation of the HOMO creating a larger HOMO-LUMO gap.

The UV-vis. spectra of octahedral six-coordinate Ni(II) complexes **4.3**, **4.6**, **4.7**, **4.10** and **4.13** show two *d-d* transitions (see **Figure 4.8**, **Table 4.2**) which are attributed to $^3A_{2g}$→$^3T_{2g}$ ($v_1$) and $^3A_{2g}$→$^3T_{1g}$(F) ($v_2$) respectively, The third transition

$^3A_{2g}\rightarrow{}^3T_{1g}(P)$ ($v_3$) has been obscured by the more intense MLCT band at around 374-414 nm. The three spin allowed transitions generally fall within the ranges 1429-769 nm, 909-500 nm and 526-370 nm respectively, for regular octahedral systems.[32] The assignments yields spectrochemical parameters (10Dq, B and *β*) are shown in **Table 4.2**. The related mononuclear octahedral Ni(II) complex, $[Ni^{II}(C_{14}H_{13}N_3OS)_2(CH_3CN)_2](ClO_4)_2$ which was reported by Saad *et al*., has a similar coordination sphere and exhibits the same octahedral six-coordinate environment around the Ni(II) ion and shows three transitions at 948, 589 and 360nm. The bands have been assigned as $^3A_{2g}\rightarrow{}^3T_{2g}$ ($v_1$), $^3A_{2g}\rightarrow{}^3T_{1g}$ (F) ($v_2$) and $^3A_{2g}\rightarrow{}^3T_{1g}$ (P) ($v_3$) respectively, and spectrochemical parameters (10Dq, B and *β*) are 1054.9 $cm^{-1}$, 876,52 $cm^{-1}$ and 0.84.[33] These values are in a good agreement with octahedral Ni(II) complexes **4.3**, **4.6**, **4.7**, **4.10** and **4.13** which have a similar absorption profile and spectrochemical parameters, See **Table 4.2**. The nephelauxetic parameter, β value (0.84) for the example above shows the ionic character of the new coordinate bonds.[34] This ionic character is similar for **4.3**, **4.6**, **4.7**, **4.10** and **4.13** which shows β values 0.7-0.84.

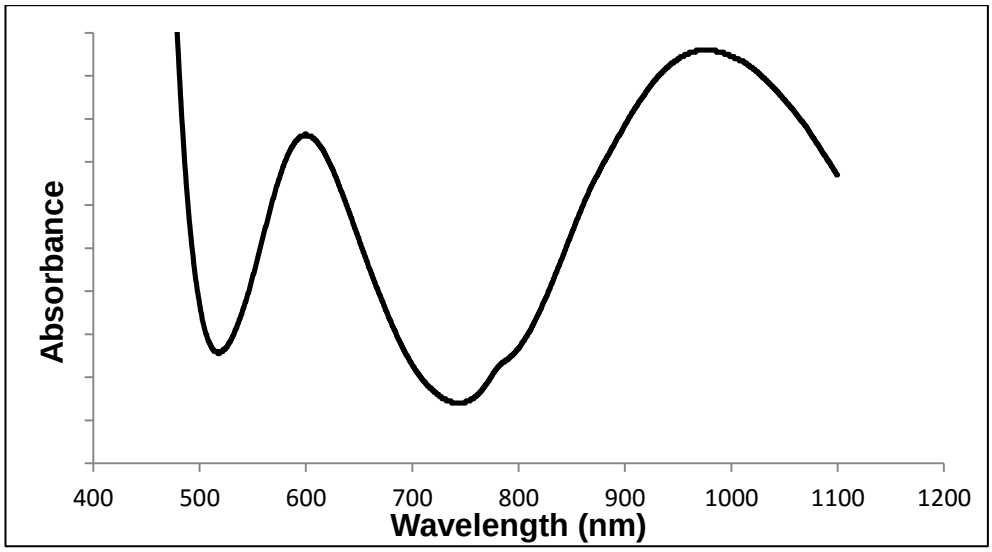


**Figure 4.8:** The electronic spectrum of octahedral Ni(II) complex **4.3**.

**Table 4.2:** Electronic spectral assignment for Cu(II) and Ni(II) complexes of **$L^5$-$L^{7A}$**.

| | MLCT $\lambda_{max}$ nm, ($\varepsilon$, $M^{-1}cm^{-1}$) | d-d transition $\lambda_{max}$ nm, ($\varepsilon$, $M^{-1}$ $cm^{-1}$) | | | Δ ($cm^{-1}$) | B ($cm^{-1}$) | β |
|---|---|---|---|---|---|---|---|
| | | $d_{xy}\rightarrow d_X{}^2\text{-}y^2$ | $^3A_{2g}\rightarrow{}^3T_{1g}$ (F) ($\nu_2$) | $^3A_{2g}\rightarrow{}^3T_{2g}$ ($\nu_1$) | | | |
| **4.2** | - | 762(24) | - | - | | | |
| **4.3** | 395(1910) | - | 600(15) | 972(19) | 1028.8 | 857 | 0.82 |
| **4.5** | - | 779(20) | - | - | | | |
| **4.6** | 374(2520) | - | 605(16) | 967(22) | 1034.1 | 795 | 0.76 |
| **4.7** | 393(1920) | - | 589(13) | 947(14) | 1056.0 | 844 | 0.81 |
| **4.9** | - | 776(27) | - | - | | | |
| **4.10** | 397(1850) | - | 588(18) | 952(20) | 1050.4 | 875 | 0.84 |
| **4.12** | - | 792(33) | - | - | | | |
| **4.13** | 414(3280) | - | 607(15) | 946(18) | 1057.1 | 729 | 0.70 |

## 4.3.4 Magnetic susceptibility measurements

Magnetic susceptibility measurements were carried out at room temperature using the Evans method.[21] The observed magnetic moments of the Ni(II) complexes **4.3**, **4.6**, **4.7**, **4.10** and **4.13** were centred around 2.91-3.05 B.M. and correspond to two unpaired electrons consistent with an octahedral geometry around the Ni(II) ion. The magnetic moments of Cu(II) complexes **4.2**, **4.5** and **4.9** and **4.12** were found around 1.83-1.92 B.M. which correspond to one unpaired electron and are consistent with a $d^9$ configuration. Finally, measurements confirmed Cu(I) complexes **4.1**, **4.4**, **4.8** and **4.11** were diamagnetic, as expected. **Table 4.3** shows the magnetic data which includes mass magnetic susceptibility $\chi_{mass}$, molar magnetic susceptibility, $\chi_M$ , and magnetic moments, $\mu_{eff}$ , for Cu(II) and octahedral Ni(II) complexes of $L^5$-$L^{7A}$.

**Table 4.3:** Magnetic data of Cu(II) and octahedral Ni(II) complexes of (**$L^5$-$L^{7A}$**).

| Complex | $\chi_{mass}$ x$10^{-6}$ | $\chi_{molar}$ x$10^{-6}$ | $\mu_{obs}$B.M. experimental |
|---|---|---|---|
| **4.2** | 2.239 | 1414.15 | 1.83 |
| **4.5** | 2.488 | 1521.73 | 1.90 |
| **4.9** | 2.280 | 1452.13 | 1.84 |
| **4.12** | 2.505 | 1545.18 | 1.92 |
| **4.3** | 3.763 | 3802.42 | 3.00 |
| **4.6** | 3.898 | 3782.89 | 2.97 |
| **4.7** | 4.639 | 3721.59 | 2.91 |
| **4.10** | 3.977 | 3859.56 | 3.02 |
| **4.13** | 4.218 | 3924.81 | 3.05 |

## 4.3.5 Electrochemical studies of Cu(I), Cu(II) and Ni(II) complexes

The electrochemical data for Cu(I), Cu(II) and Ni(II) complexes (**4.1**-**4.13**) were measured in acetonitrile using $[Bu_4N][PF_6]$ (0.1 M) as supporting electrolyte. The data is summarized for Cu(I) and Cu(II) complexes in **Table 4.4** and for Ni(II) complexes in **Table 4.5**. The cyclic voltammogram of Cu(I) complexes **4.1**, **4.4**, **4.8** and **4.11** shows similar cyclic voltammogram Cu(II) complexes **4.2**, **4.5**, **4.9** and **4.12**. **Figures 4.9-4.11** show representative cyclic voltammograms of the reductive region for **4.2, 4.8** and **4.9** respectively. Typically a quasi-reversible process is observed for the Cu(I) complexes **4.1**, **4.4**, **4.8** and **4.11** between -0.32 to -0.33 V (vs $Fc/Fc^+$), with very large peak to peak separations being observed (184-346 mV). A quasi-reversible process too, is observed for the Cu(II) complexes **4.2**, **4.5**, **4.9** and **4.12** between -0.37 to -0.39 V (vs $Fc/Fc^+$), with very large peak to peak separations being observed (188-199 mV) which is typical for a Cu(II)/Cu(I) redox process. See **Table 4.4**. Both Cu(I) and Cu(II) couples have similar CV´s. However the presence of two ligands in the complexes causes the Cu(II)/Cu(I) couple to occur at more +VE potential (The reaction is more facile) meaning we isolate the Cu(I) complex. The converse is true for the 1:1 complexes where a reduction at higher –VE potential indicates that the complex is less will to gain an electron and in this case the Cu(II) complexes are isolated.

The peak to peak separations, being much greater than those observed with the ferrocene internal standard ($\Delta E_P = E_{Pa} - E_{Pc}$ is greater than 59 mV), suggest a quasi-reversible nature. This is possibly due to a structural/geometric rearrangement occurring on the transitions between the Cu(I) and Cu(II) oxidation state. Furthermore, the ratio of $i_{pc}$ to $i_{pa}$ is less than 1, which also supports the quasi-reversible nature of this process. The Cu(II) complex $[CuC_{34}H_{30}N_8O_2S_2]\cdot[ClO_4]_2$ has been reported by Saad *et al.*,[35] and the cyclic voltammogram contains a single wave process at the cathodic potential of −0.379V (vs $Fc/Fc^+$). This is responsible for the Cu(II)/Cu(I) redox couple and in good agreement with the Cu(II) complexes **4.2**, **4.5**, **4.9** and **4.12**. The cyclic voltammogram of Cu(I) complexes **2.1**, **2.6**, **2.11**, **2.12**, **2.15**, **2.16**, **2.19**, **2.24** and **2.25** in chapter two, showed a quasi-reversible process with potential around ~ -0.3 V. This is in a good agreement with the Cu(I)

complexes **4.1**, **4.4**, **4.8** and **4.11**. In addition, the Cu(II) complex, **2.20** in chapter two, showed a quasi-reversible redox process at ~ -0.4 V consistent with the Cu(II) complexes **4.2**, **4.5**, **4.9** and **4.12**.

**Table 4.4:** Electrochemical parameters for the **quasi-reversible** processes exhibited by Cu(I) complexes **4.1**, **4.4**, **4.8** and **4.11** and Cu(II) complexes **4.2**, **4.5**, **4.9** and **4.12** in acetonitrile solution, supporting electrolyte $[Bu_4N][PF_6]$ (0.1 M), t =$25^0$ c measured at 100 mv/sec. Potentials are vs $Fc/Fc^+$.

| **Complex** | ***$E_P$/V Quasi reversible*** | | | | |
|---|---|---|---|---|---|
| | **$E_{Pa}$ V** | **$\Delta E_P$ mv** | **$I_{pa}$ µA** | **$I_{pc}$ µA** | **$I_{pc}/I_{Pa}$** |
| **4.1** | -0.328 | 326 | 9.1 | 5.2 | 0.571 |
| **4.2** | -0.399 | 188 | 4.22 | 1.99 | 0.472 |
| **4.4** | -0.321 | 346 | 7.31 | 2.14 | 0.293 |
| **4.5** | -0.378 | 191 | 4.97 | 2.15 | 0.433 |
| **4.8** | -0.320 | 190 | 6.80 | 3.59 | 0.528 |
| **4.9** | -0.384 | 199 | 7.53 | 4.99 | 0.663 |
| **4.11** | -0.322 | 184 | 4.82 | 1.93 | 0.400 |
| **4.12** | -0.386 | 188 | 6.30 | 3.07 | 0.487 |

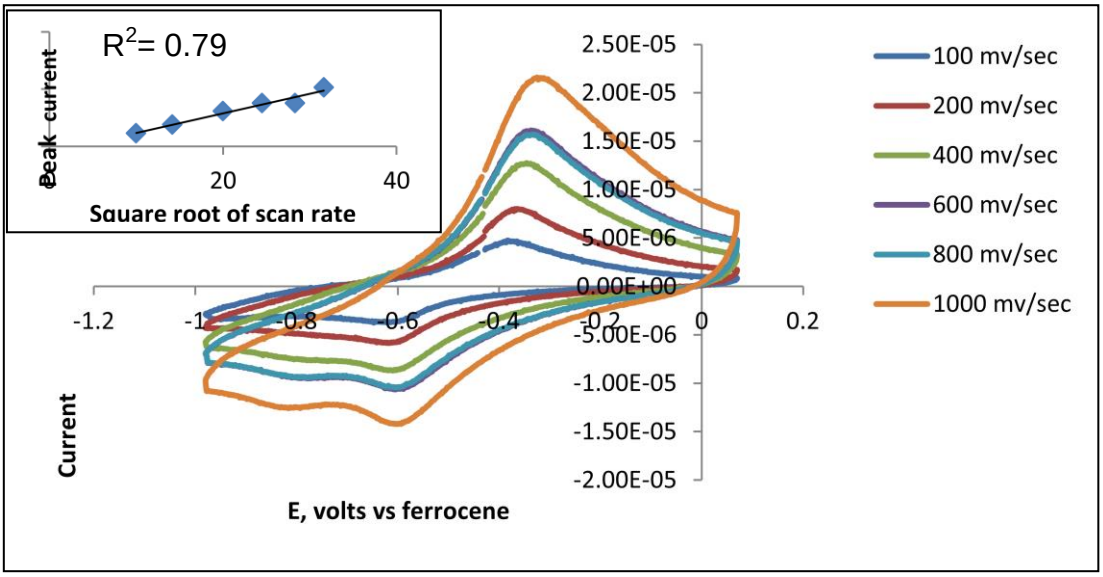


**Figure 4.9**: Cyclic voltammogram of complex **4.2** shows quasi-reversible process

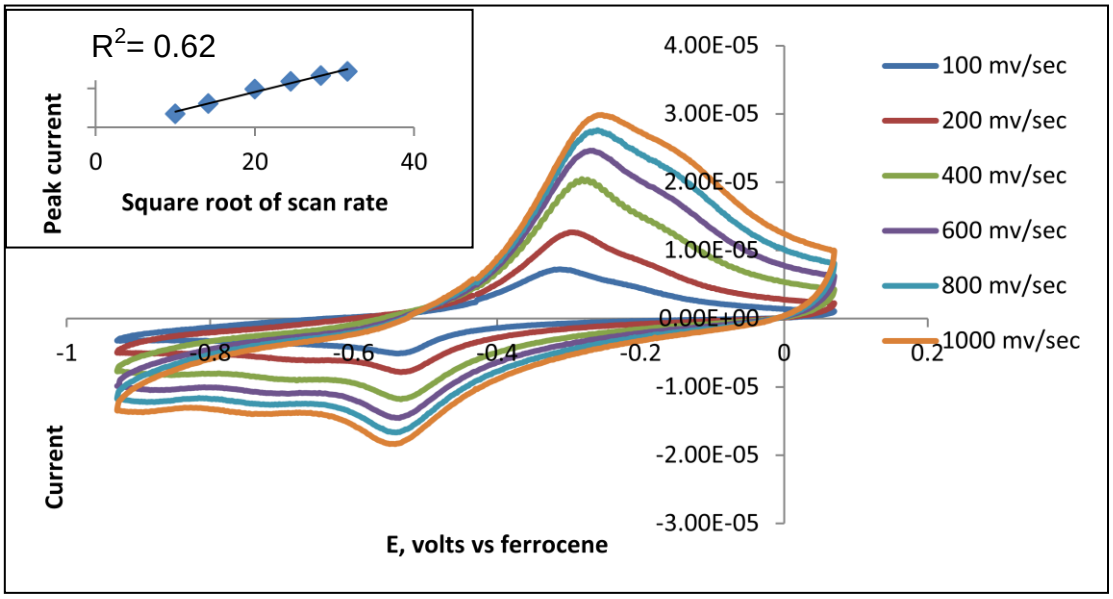


**Figure 4.10**: Cyclic voltammogram of complex **4.8** shows quasi-reversible process

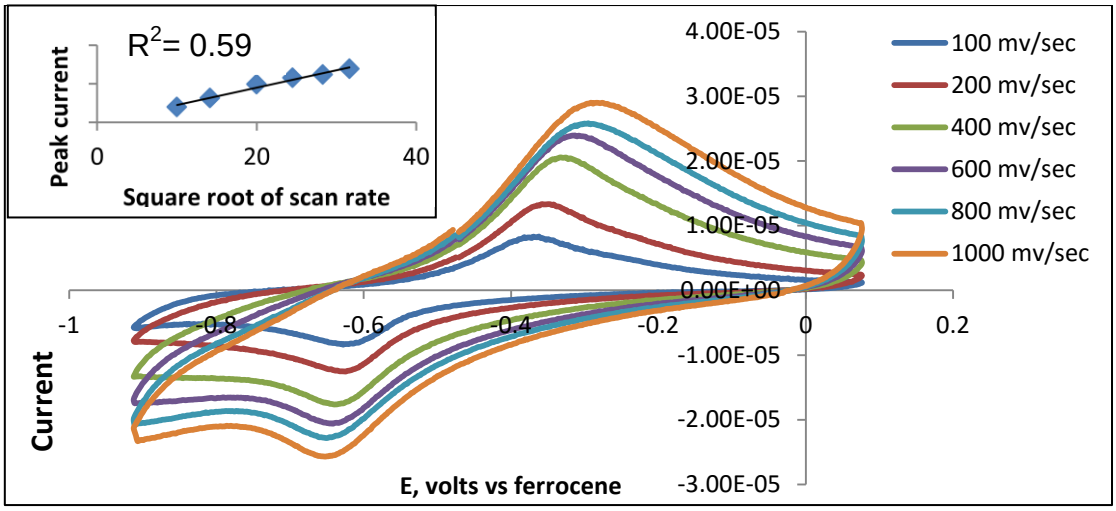


**Figure 4.11**: Cyclic voltammogram of complex **4.9** shows quasi-reversible process

The cyclic voltammogram of the Ni(II) complexes **4.3**, **4.6**, **4.7**, **4.10** and **4.13** reveal two irreversible reductions (-1.20 to -1.30 V vs $Fc/Fc^+$) and (-1.60 to -1.90 V vs $Fc/Fc^+$) respectively, see **Table 4.5**. The cyclic voltammogram of **4.3** and **4.6** are shown in **Figures 4.12** and **4.13** as representative examples. Similar behaviour has been reported for the Ni(II) complex of bis(6-benzoylthiourea-2-pyridylmethyl)(2-pyridylmethyl) amine which shows two similar irreversible reductions at -1.37 V and -1.78 V (vs Fc/Fc+) in acetonitrile solution.[35] It is suggested that the first irreversible reduction may be ligand based. Moreover, the second irreversible reduction process may be attributed to Ni(II) to Ni(I) process. However, without further investigate; it is impossible to unequivocally assign these processes. The cyclic voltammogram of the Ni(II) complexes **2.2**, **2.3**, **2.7**, **2.8**, **2.13**, **2.17**, **2.21**, **2.22** and **2.26** in chapter two, revealed two irreversible reductions too, range (-1.11 to -1.34V vs $Fc/Fc^+$) and (-1.63 to -1.99V vs $Fc/Fc^+$) respectively. This is consistent with the cyclic voltammogram of the Ni(II) complexes **4.3**, **4.6**, **4.7**, **4.10** and **4.13** and with similar potential.

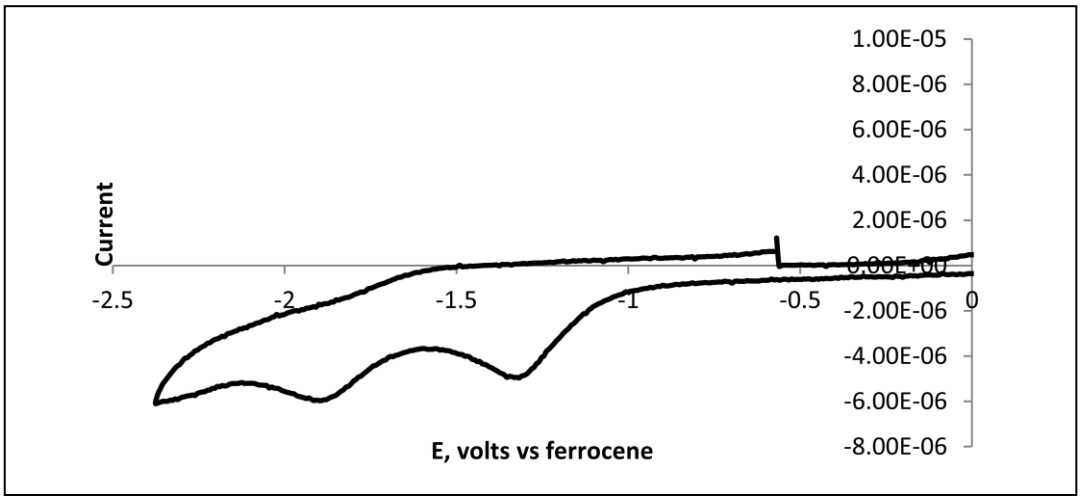


**Figure 4.12**: Cyclic voltammogram of complex **4.3** showing irreversible reductive process at 100 mv.sec$^{-1}$.

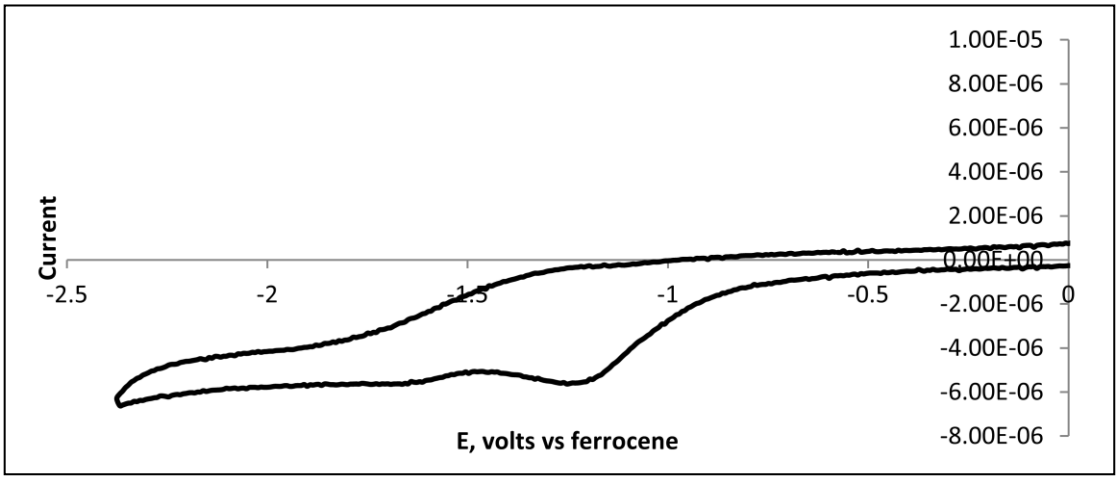


**Figure 4.13**: Cyclic voltammogram of complex **4.6** showing irreversible reductive process at 100 mv.sec$^{-1}$.

**Table 4.5:** Electrochemical parameters for the irreversible reduction processes exhibited by Ni(II) complexes, **4.3, 4.6, 4.7, 4.10 and 4.13** in acetonitrile solution, supporting electrolyte $[Bu_4N][PF_6]$ (0.1 M), t =25º C measured at 100 mv/sec.

| complex | $E_P$/V vs $Fc/Fc^+$ irreversible reductions | |
|---|---|---|
| **4.3** | -1.289 | -1.865 |
| **4.6** | -1.195 | -1.620 |
| **4.7** | -1.274 | -1.692 |
| **4.10** | -1.260 | -1.865 |
| **4.13** | -1.282 | -1.894 |

## 4.3.6 Crystallographic studies

Crystal parameters, details of the data collection and structural refinements of **4.4, 4.6, 4.7, 4.9** and **4.13** are presented in **Tables 4.11-4.12**. Selected bond lengths, angles and hydrogen bonds are given for all crystal structures in **Tables 4.6-4.10**.

### 4.3.6.1 Crystal structure of $[Cu(L^{5A})_2](BF_4)$. $0.17CH_2Cl_2$ (4.4)

Orange, block-like crystals of **4.4** were obtained by vapour diffusion of diethyl ether into an ethanol:DCM solution of the complex. The Cu(I) complex crystallises in the triclinic space group *P*-1 and contains a single complex within the asymmetric unit (asu) (see **Figure 4.14**). Selected bond length and angles are given in **Table 4.6**. **Figure 4.14** shows **4.4**, with the metal centre to be tetrahedrally coordinated by two molecules of $\mathbf{L^{5A}}$ acting as bidentate ligands. Each ligand coordinates by the nitrogen pyridine ring and the sulfur within the thiourea. Bond angles about the metal centre signify a significant distortion when compared with the perfect tetrahedral angle, 109.5º. The large deviation from the perfect tetrahedral bond angle is observed for N21–Cu1–S1 (124.81(5)º) suggestive of greater steric (or van der Waals) repulsion. Similar nature of greater steric repulsion based ligand was

reported in **chapter Two**, in tetrahedral Cu(I) complexes, **2.6**, N3–Cu1–S21 125.51(5), **2.15**, N1–Cu1–S21 116.05(18), tetrahedral Zn(II) complex, **2.4**, N3–Zn1–S11 114.11(14). The $N_2S_2$ donor sites from the bidentate ligands coordinates the Cu(I) centre to form two six membered $C_2N_2SCu$ rings. According to the CCDC, and Scifinder searches this class of polydentate ligand has not been reported before. The Cu–N and Cu–S bond lengths are typical when compared to complexes with similar donor sets; for instance, the tetrahedral complex **2.1**, which contains the $N_2S_2$ site donor (as reported in **Chapter 2**) has very similar coordinative bond lengths to **4.4** (Cu1-N21 2.079(2), Cu1-N1 2.074(2), Cu1-S1 2.2235(7) and Cu1-S21 2.2191(7) Å). It is clear that the Cu–S bond lengths are longer than Cu–N and this is due to the larger size of sulfur than oxygen atom. It is apparent from **Table 4.6** that the bond angles N1-Cu1-S1 and N21-Cu1-S21 are exactly the same ~ 99º as they form identical $C_2N_2SCu$ rings. Typically for N-carbonyl thiourea ligands, there are two intramolecular hydrogen bonds. These interactions N3–H3···O2 and N23–H23···O22 occur between the carbonyl oxygen atom and hydrogen of the amide within the thiourea at 1.84 and 1.83 Å respectively. An intermolecular hydrogen bond N24–H24···F24 at 2.04 Å was observed in **4.4** between the hydrogen of the amide and fluorine atom in the $BF_4$ counter ion (**Figure 4.14**).

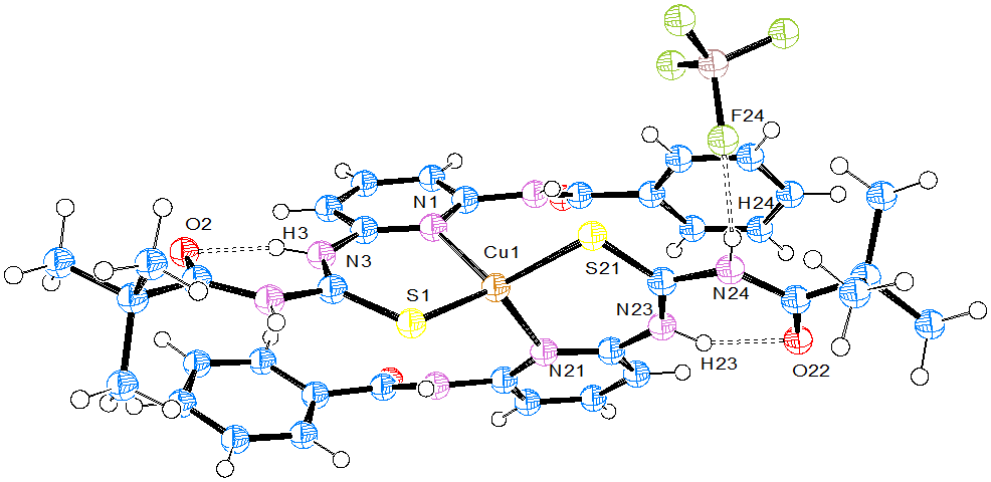


**Figure 4.14:** The asymmetric unit of **4.4** Displacement ellipsoids are shown at 50% probability, solvent of crystallisation omitted for clairty.

**Table 4.6:** Selected bond lengths (Å) and bond angles (º) for **4.4**

| | | | |
|---|---|---|---|
| **Bond length (Å)** | | | |
| Cu1–N21 | 2.0915(17) | Cu1–S1 | 2.2082(6) |
| Cu1–N1 | 2.1087(16) | Cu1–S21 | 2.2261(5) |
| **Bond Angles (º)** | | | |
| N21–Cu1–N1 | 101.45(6) | N21–Cu1–S21 | 99.89(5) |
| N21–Cu1–S1 | 124.81(5) | N1–Cu1–S21 | 118.30(5) |
| N1–Cu1–S1 | 99.24(5) | S1–Cu1–S21 | 113.82(2) |

### 4.3.6.2 Crystal structures of $[Ni(L^{5A})_2](ClO_4)_2$ (4.6) and $[Ni(L^{5A*})_2](ClO_4)_2.(CH_3CH_2)_2O$ (4.7)

Pale green crystals of **4.6** and light green of **4.7** were obtained by vapour diffusion of diethyl ether into an acetone and an ethanol:DCM solution of **4.6** and **4.7** respectively. Selected bond lengths and angles are given in **Tables 4.7** and **4.8**. **Figures 4.15** and **4.16** show ORTEP diagrams of complexes **4.6** and **4.7** respectively with atomic numbering scheme for the coordinating sites. The complex contains two tridentate ligands $\mathbf{L^{5A}}$ or $\mathbf{L^{5A*}}$ with two perchlorate counter ions. The bond lengths and angles show that the coordination sphere around the Ni(II) ion is six-coordinate octahedral with a small distortion. In both complexes, the Ni(II) ion is surrounded by three types of donor atoms: two nitrogen donors (N1 and N21), two sulfur donors (S1 and S21) and two oxygen donors(O1 and O21). The Ni(II) complexes crystallise in the triclinic space group *P*-1 and monoclinic space group *C2/c* respectively and a contain a single complex within the asu. The bond angles about the metal centre range from 84.3(5)-95.6(3) and 175.2(3)-176.5(3) in **4.6** and 85.00(19)-93.85(10) and 174.6(2)-177.84(10)º in **4.7**. Other complexes with the $NiN_2S_2O_2$ core (N= the pyridyl nitrogen) were searched on the CCDC. There were 30 examples and the Ni(II) ion adopted an octahedral geometry in all of them. The bond angles observed in the range 83.873-97.903 and 174.874-180.000 degrees which confirm that the bond angles in **4.6** and **4.7** are common. The Ni-S bonds in **4.6** and **4.7** are significantly longer than the nitrogen and the oxygen bonds with the Ni(II) ion, Ni-N and Ni-O and this is due to the large size of sulfur atom when

compare with the size of the nitrogen and the oxygen atoms. **Table 4.11** shows that R-factor is high (0.1678) and this is may be due to the small size of the crystals of **4.6** sent for X-ray analysis.

Again, typical for N-carbonyl thiourea ligands, **4.6** shows two intramolecular hydrogen bonds, assigned to N3–H3···O2 and N23–H23···O22 at 1.92 and 1.89 Å which occur within the thiourea between the oxygen carbonyl group and the hydrogen amide. This is similar to N-carbonyl thiourea, complexes **2.1**, **2.6**, **2.15**, **2.16** and **2.24** (see **chapter two**) and **3.6** and **3.12** (see **chapter three**) which showed intramolecular hydrogen bonds range 1.83-1.93 Å. Further, there are four intermolecular hydrogen bond between the hydrogen amide and the oxygen perchlorate in the range 2.02-2.33 Å which holds the perchlorate in the cavity, (see **Figure 4.15**). As the acyl groups have been lost, **4.7** does not show any intramolecular hydrogen bond. However, it shows more than one intermolecular hydrogen bond between the hydrogen amides and the oxygen perchlorates in the range 2.06-2.58 Å. The hydrogen bonded perchlorates are disordered. This disorder is due to the high symmetry of the $ClO_4^-$ fragment and to the non-directional ionic forces between the thiourea and the $ClO_4^-$ anion. As is clear in **Figure 5.16**, two possible orientations for the $ClO_4^-$ fragment are presented.

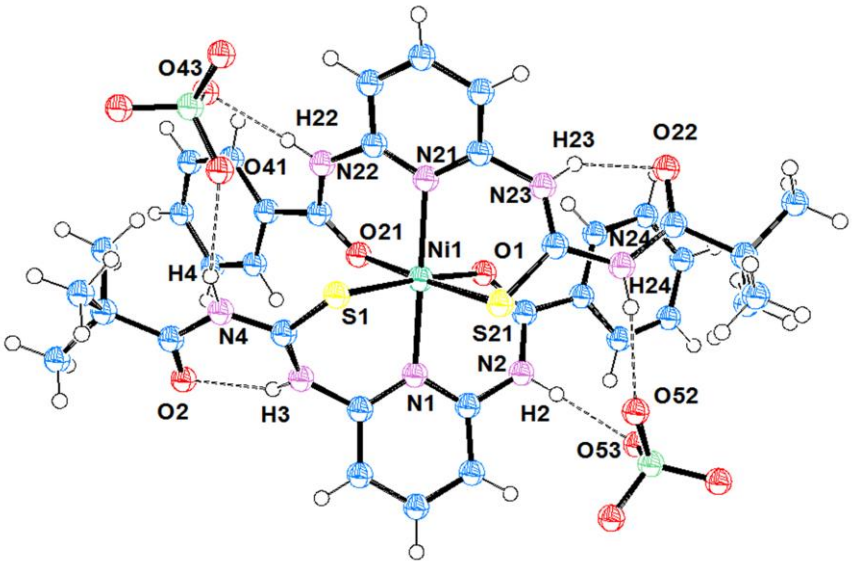


**Figure 4.15:** The asymmetric unit of **4.6.** Displacement ellipsoids are shown at 50% probability.

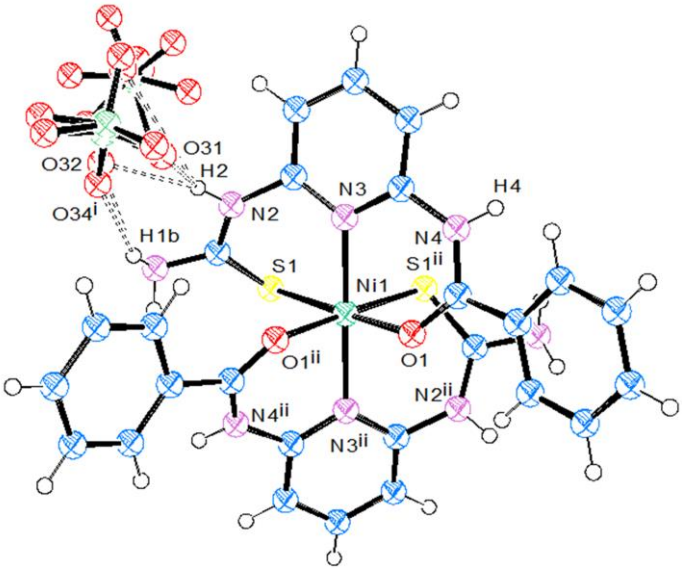


**Figure 4.16:** The asymmetric unit of **4.7.** Displacement ellipsoids are shown at 50% probability.

**Table 4.7:** Selected bond lengths (Å) and angles (º) for **4.6**

| **Bond length (Å)** | |
|---|---|
| Ni1–O21 | 1.993(11) |
| Ni1–O1 | 2.040(9) |
| Ni1–N1 | 2.092(11) |
| Ni1–N21 | 2.110(12) |
| Ni1–S1 | 2.415(4) |
| Ni1–S21 | 2.416(6) |
| **Bond Angles (º)** | |
| O21–Ni1–O1 | 85.4(4) |
| O21–Ni1–N1 | 92.8(5) |
| O1–Ni1–N1 | 85.3(4) |
| O21–Ni1–N21 | 84.3(5) |
| O1–Ni1–N21 | 91.8(4) |
| N1–Ni1–N21 | 176.0(5) |
| O21–Ni1–S1 | 93.5(3) |
| O1–Ni1–S1 | 175.2(3) |
| N1–Ni1–S1 | 90.1(3) |
| N21–Ni1–S1 | 92.8(3) |
| O21–Ni1–S21 | 176.5(3) |
| O1–Ni1–S21 | 95.6(3) |
| N1–Ni1–S21 | 90.6(4) |
| N21–Ni1–S21 | 92.3(4) |
| S1–Ni1–S21 | 85.80(16) |

**Table 4.8:** Selected bond lengths (Å) and angles (º) for **4.7**

| **Bond length (Å)** | |
|---|---|
| Ni1–O1 | 2.027(3) |
| Ni1–O1$^{i}$ | 2.027(3) |
| Ni1–N3$^{i}$ | 2.096(4) |
| Ni1–N3 | 2.096(4) |
| Ni1–S1 | 2.3811(15) |
| Ni1–S1$^{i}$ | 2.3812(15) |
| **Bond Angles (º)** | |
| O1–Ni1–O1$^{i}$ | 85.00(19) |
| O1–Ni1–N3$^{i}$ | 89.87(14) |
| O1$^{i}$–Ni1–N3$^{i}$ | 86.12(14) |
| O1–Ni1–N3 | 86.12(14) |
| O1$^{i}$–Ni1–N3 | 89.87(14) |
| N3$^{i}$–Ni1–N3 | 174.6(2) |
| O1–Ni1–S1 | 177.84(10) |
| O1$^{i}$–Ni1–S1 | 93.84(10) |
| N3$^{i}$–Ni1–S1 | 91.87(11) |
| N3–Ni1–S1 | 92.06(12) |
| O1–Ni1–S1$^{i}$ | 93.85(10) |
| O1$^{i}$–Ni1–S1$^{i}$ | 177.84(10) |
| N3$^{i}$–Ni1–S1$^{i}$ | 92.06(12) |
| N3–Ni1–S1$^{i}$ | 91.87(11) |
| S1–Ni1–S1$^{i}$ | 87.37(8) |

### 4.3.6.3 Crystal structure of $[Cu^{II}L^7(H_2O)](ClO_4)_2.CH_3COCH_3.H_2O$ (4.9)

Triclinic, blade-like and pale green crystals of **4.9** were obtained by vapour diffusion of diethyl ether into an acetone solution of **4.9**. The crystallographic data and the final refinement details are listed in **Table 4.12**. The Cu(II) complex crystallises in the triclinic space group *P*-1 and contains a single complex within the asu, **Figure 4.17**. The geometry of the complex is best considered as slightly distorted square planar with the metal ion coordinated by two oxygen atoms (O2 and O21), one nitrogen atom (N3) and one sulfur atom (S1). The metal centre is coordinated by one tridentate ligand, and one oxygen aqua molecule. The bond angles about the metal centre range from 86.00(12)-95.09(9) and 168.27(9)-174.74(13) degrees (see **Table 4.9**). A more considerable deviation from the perfect square planar bond angle is observed for the O2–Cu1–O21 86.00 (12) and O2–Cu1–S1 168.27(9) although the perfect angles are 90 and 180 degrees. The Cu-O and Cu-N coordinative bond lengths range from 1.921(3) to 1.992(3) Å, and the Cu-S bond length is significantly longer at 2.2593(12) Å. These longer bond lengths of Cu-S than the other bond lengths are quite similar when compared to those of **4.4**, **4.6** and **4.7**. According to the CCDC there are 23 crystal structures of Cu(II) complexes with a Cu(II) ion surrounded by four donor atoms (N, 2O and S) forming a square planar geometry. They exhibit similar Cu-O, Cu-N and Cu-S bond lengths to **4.9** and range (1.909-1.967),(1.970-2.010) and (2.224-2.267 Å) respectively.[36-39]

A single intramolecular strong hydrogen bond N2–H2···O1 was observed at 1.85 Å and this is common with N-carbonyl thiourea derivatives (as shown previously in **chapter two**, **chapter three** and here in **chapter four**). Intermolecular hydrogen bonding is observed between the hydrogen amide and the oxygen perchlorate in the range 2.35-2.52 Å. Finally, a water molecule can be observed hydrogen bonding between the hydrogen aqua molecules with the oxygen perchlorate ion in the range 1.87-2.12Å (**Figure 4.17**).

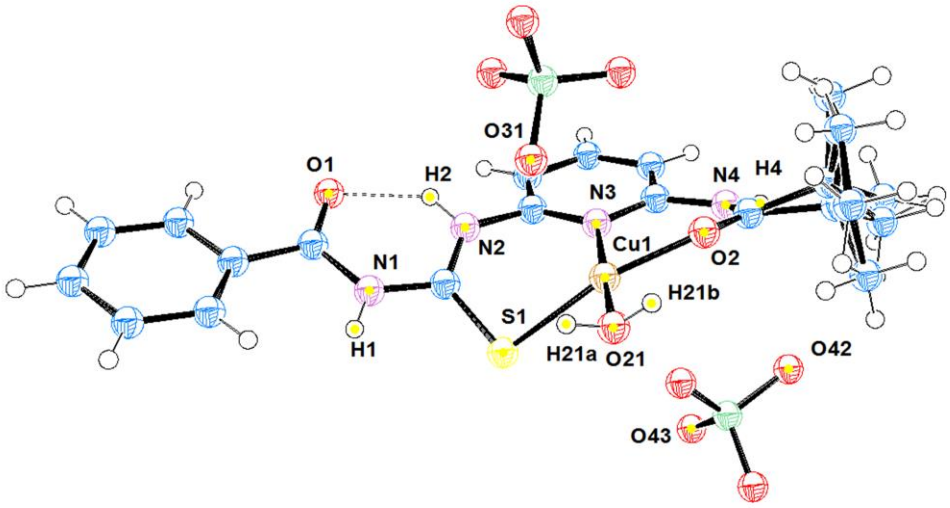


**Figure 4.17:** The asymmetric unit of **4.9.** Displacement ellipsoids are shown at 50% probability.

**Table 4.9:** Selected bond lengths (Å) and angles (º) for **4.9**

| | | | |
|---|---|---|---|
| **Bond length (Å)** | | | |
| Cu1–O2 | 1.921(3) | Cu1–N3 | 1.992(3) |
| Cu1–O21 | 1.969(3) | Cu1–S1 | 2.2593(12) |
| **Bond Angles (º)** | | | |
| O2–Cu1–O21 | 86.00(12) | O2–Cu1–S1 | 168.27(9) |
| O2–Cu1–N3 | 91.70(11) | O21–Cu1–S1 | 87.98(10) |
| O21–Cu1–N3 | 174.74(13) | N3–Cu1–S1 | 95.09(9) |

### 4.3.6.4 Crystal structure of $[Ni(L^{7A})_2](ClO_4)_2$ (4.13)

Monoclinic, blade green crystals of **4.13** were obtained by vapour diffusion of diethyl ether into a $CHCl_3$ solution of the complex. The complex crystallises in the monoclinic space group $P2_1/n$ and contains one complex within the asu (**Figure 4.18**). The Ni(II) cation lies at the centre of a slightly distorted octahedral geometry (**Table 4.10**). There are two nitrogen pyridyl donors, two sulfur (C=S) donors and two oxygen carbonyl groups. The coordinative bond lengths are typical for oxygen carbonyl donors (2.019(8) and 2.029(7) Å), nitrogen pyridyl donors (2.089(8) and 2.104(7) Å) and sulfur (C=S) donors (2.425(3) and 2.443(3) Å), **Table 4.10**. This is

very similar to the octahedral Ni(II) complexes **4.6** and **4.7** reported in this chapter, which range for oxygen carbonyl donors form 1.993(11)-2.040(9) Å, nitrogen donors 2.092(11)-2.110(12) Å and sulfur (C=S) donors 2.3811(15)- 2.416(6) Å, see **Tables 4.7** and **4.8**. The Ni(II) complex is clearly octahedral with bond angles about the metal centre ranging from 83.4(3)-96.2(3), 166.2(3) and 168.32(13) degrees. The N,S donor sites from the tridentate ligands coordinate the Ni(II) centre to form four six membered rings; two as $C_2N_2SNi$ and the other as $C_2N_2ONi$ rings. Interestingly, the steric arrangement of these rings, cause the ligands to bind in a facial manner. The two sulfur donors are trans to each other. While the R-factor is high (0.1508) (see **Table 4.12**), caused in part by disorder in the crystal, the error associated with coordination sphere of the metal is small and hence discussions of the general geometries and M-L bond lengths are valid in this context.

As in all structurally characterized complexes of N-carbonyl thiourea, there are two intramolecular hydrogen bonds between the amide and the carbonyl N3–H3···O2 and N23–H23···O22 (1.83 and 1.86 Å) respectively, **Figure 4.18**. The same class of hydrogen bonding appears in **4.4**, **4.6** and **4.9** in the range 1.83-1.92 Å. In **4.13**, the other strong hydrogen bonds are intermolecular which occur between the oxygen perchlorate with the thiourea hydrogen amide atoms at 2.00-2.48 Å. The same hydrogen bonds appeared in **4.6**, **4.7** and **4.9** in 2.02-2.58 Å and this is similar to **4.13**.

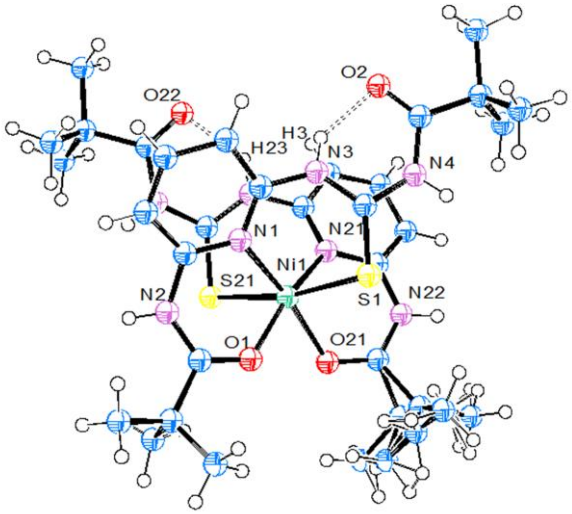


**Figure 4.18:** The asymmetric unit of **4.13** as anion to make it more clarity**.**

**Table 4.10:** Selected bond lengths (Å) and angles (º) for **4.13**

| | | | |
|---|---|---|---|
| **Bond length (Å)** | | | |
| Ni1–O21 | 2.019(8) | Ni1–N1 | 2.104(7) |
| Ni1–O1 | 2.029(7) | Ni1–S21 | 2.425(3) |
| Ni1–N21 | 2.089(8) | Ni1–S1 | 2.443(3) |
| **Bond Angles (º)** | | | |
| O21–Ni1–O1 | 83.4(3) | N21–Ni1–S21 | 83.9(2) |
| O21–Ni1–N21 | 84.6(3) | N1–Ni1–S21 | 88.7(2) |
| O1–Ni1–N21 | 167.0(3) | O21–Ni1–S1 | 92.8(3) |
| O21–Ni1–N1 | 166.2(3) | O1–Ni1–S1 | 96.2(3) |
| O1–Ni1–N1 | 83.5(3) | N21–Ni1–S1 | 89.3(2) |
| N21–Ni1–N1 | 108.8(3) | N1–Ni1–S1 | 84.4(2) |
| O21–Ni1–S21 | 96.1(3) | S21–Ni1–S1 | 168.32(13) |
| O1–Ni1–S21 | 92.3(3) | | |

**Table 4.11:** Crystallographic data for $[Cu^{I}(L^{5A})_2](BF_4).0.17CH_2Cl_2$ **(4.4)**, and $[Ni(L^{5A})_2](ClO_4)_2$ **(4.6)** and $[Ni(L^{5A*})_2](ClO_4)_2.(CH_3CH_2)_2O$ **(4.7)**

| **Compound** | **4.4** | **4.6** | **4.7** |
|---|---|---|---|
| **Chemical Formula** | $C_{36.17}H_{40.33}BCl_{0.33}CuF_4N_8O_4S_2$ | $C_{36}H_{40}Cl_2N_8NiO_{12}S_2$ | $C_{30}H_{34}Cl_2N_8NiO_{11}S_2$ |
| **Mr. g.mol$^{-1}$** | 877.38 | 970.49 | 876.38 |
| **Crystal system** | Triclinic | Triclinic | Monoclinic |
| **Space group** | *P*–1 | *P*–1 | *C*2/*c* |
| **T(K)** | 100(2) | 100(2) | 100(2) |
| **a, Å** | 18.1001(2) | 12.902(3) | 12.6740(9) |
| **b, Å** | 18.1085(2) | 15.043(3) | 23.9734(15) |
| **c, Å** | 18.2115(2) | 15.061(3) | 12.1220(9) |
| **α, degree** | 91.9450(10) | 70.747(18) | 90° |
| **β, degree** | 93.0850(10) | 74.247(18) | 103.616(7)° |
| **γ, degree** | 90.1550(10) | 84.912(16) | 90° |
| **Z** | 6 | 2 | 4 |
| **Dc. Mg/m$^3$** | 1.467 | 1.213 | 1.626 |
| **μ($M_O$ K α), mm$^{-1}$** | 0.746 | 0.601 | 0.879 |
| **Reflections collected** | 106128 | 25357 | 22195 |
| **Unique reflections** | 27419 | 8915 | 4108 |
| **$R_{int}$** | 0.0261 | 0.1940 | 0.0733 |
| **R1[I>2σ<(I)]** | 0.0387 | 0.1678 | 0.0800 |
| **wR2(all data)** | 0.0992 | 0.4479 | 0.2266 |

**Table 4.12:** Crystallographic data for $[Cu^{II}L^7(H_2O)](ClO_4)_2.CH_3COCH_3.H_2O$ **(4.9)** and $[Ni(L^{7A})_2](ClO_4)_2$ **(4.13)**

| **Compound** | **4.9** | **4.13** |
|---|---|---|
| **Chemical Formula** | $C_{22}H_{32}Cl_2CuN_4O_{12}S$ | $C_{32}H_{48}Cl_2N_8NiO_{12}S_2$ |
| **Mr. g.mol$^{-1}$** | 711.01 | 930.51 |
| **Crystal system** | Triclinic | Monoclinic |
| **Space group** | *P*–1 | $P2_1/n$ |
| **T(K)** | 100(2) | 100(2) |
| **a, Å** | 7.7655(5) | 12.4984(5) |
| **b, Å** | 13.5019(10) | 16.4192(7) |
| **c, Å** | 14.3687(11) | 25.5823(17) |
| **α, degree** | 78.858(7) | 90° |
| **β, degree** | 87.457(8) | 103.963(5)° |
| **γ, degree** | 87.924(8) | 90° |
| **Z** | 2 | 4 |
| **Dc. Mg/m$^3$** | 1.600 | 1.213 |
| **μ($M_O$ K α), mm$^{-1}$** | 1.058 | 0.623 |
| **Reflections collected** | 21866 | 63663 |
| **Unique reflections** | 6724 | 11858 |
| **$R_{int}$** | 0.0962 | 0.1133 |
| **R1[I>2σ<(I)]** | 0.0715 | 0.1508 |
| **wR2(all data)** | 0.1980 | 0.4425 |

## 4.4 Conclusion

A new series of Cu(I), Cu(II) and Ni(II) complexes (**4.1**-**4.13**) of new class thiourea derivatives, N-((6-benzamido or pivalamido pyridin-2-yl) carbamothioyl benzamide or pivalamide derivatives (**$L^5$-$L^{7A}$**) have been successfully synthesized and fully characterised. The complexes **4.4**, **4.6**, **4.7**, **4.9** and **4.13** have been characterized using X-ray crystallography. The single crystal X-ray structures revealed that the Cu(I) centre of **4.4** had a 4-coordinate tetrahedral structure, the Ni(II) centre of **4.6**, **4.7** and **4.13** had a 6-coordinate octahedral structures, the Cu(II) centre of **4.9** had a 4-coordinate square planar. The more surprising result is the different Cu oxidation states, Cu(I) and Cu(II) complexes were discovered and synthesized by changing the molar ratio of the reactants. Cu(I) complexes **4.1**, **4.4**, **4.8** and **4.11** were obtained from the reaction **$L^5$-$L^{7A}$** with $Cu(ClO_4)_2.6H_2O$ or $Cu(BF_4)_2.6H_2O$ in a 2:1 molar ratio respectively, while Cu(II) complexes **4.2**, **4.5**, **4.9** and **4.12** formed when the same reaction was carried out in 1:1 molar ratio. At first glance, this observation suggests that one mole of the free ligand, **$L^5$-$L^{7A}$** is not able to reduce Cu(II) to Cu(I) and this observation support the happening of the reduction process. However in our experiments thiourea role as reducing agent appears unlikely due to the stoichiometry of the reaction. The stable and unchanged structure for the thiourea ligand in its Cu(I) complexes here in this chapter lead us to suggest that if the ligand is oxidized it then returns again to its normal oxidation state. In addition, it is possible that the solvents in the reaction may be have any role in the reduction process of Cu(II) to Cu(I).

Electrochemical studies were carried out via cyclic voltammetry and show a single quasi-reversible peak at ~ – 0.3V (vs $Fc/Fc^+$) for Cu(I) complexes **4.1**, **4.4**, **4.8** and **4.11** which attributed to Cu(II)/Cu(I) redox process while Cu(II) complexes **4.2**, **4.5**, **4.9** and **4.12** show the same process at ~ – 0.4V (vs $Fc/Fc^+$). In addition, the Ni(II) complexes **4.3**, **4.6**, **4.7**, **4.10** and **4.13** exhibit two irreversible reductive processes range (-1.20 to -1.30 V vs $Fc/Fc^+$) and (-1.60 to -1.90 V vs $Fc/Fc^+$). Two classes of hydrogen bonding are observed in the prepared complexes, first, intramolecular hydrogen bond between the hydrogen amide and the oxygen carbonyl (N-H…O) which consider as a special signal of N-carbonyl thioura derivatives. It is observed

for **4.4**, **4.6**, **4.9** and **4.13** ranges 1.83-1.92 Å. Second, **4.4**, **4.6**, **4.7**, **4.9** and **4.13** show intermolecular hydrogen bonds between the hydrogen amide thiourea and specific atom from a counter ion such as the F-atom of $BF_4$ (N-H…F) at 2.04 Å or the O-atom of $ClO_4$ (N-H…O) and range 2.03-2.58 Å.

## 4.5 References:


**(1)** W. Hernàndez, E. Spodine, L. Beyer, U. Schröder, R. Richter, J. Ferreira and M. Pavani, *J. Bioinorg. Chem. Applic.*, **2005**, 3(*3*), 299-317.

**(2)** M. K. Rauf, I. U. Din, A. Badshah, M. Gielen, M. Ebihara, D. D. Vos and S. Ahmed, *J. Inorg. Biochem.*, **2009**,103, 1135–1144.

**(3)** N. Gunasekaran, N. Remya, S. Radhakrishnan and R. Karvembu, *J. Coord. Chem.*, **2011**, 64(*3*), 491–501.

**(4)** J. Xie, Z. Cheng, W. Yang, H. Liu, W. Zhou, M. Li and Y. Xu, *Appl. Organometal. Chem.*, **2015**, 29, 157-164.

**(5)** S. Yaseen, M. K. Rauf, S. Zaib, A. Badshah , M. N. Tahir, M. I. Ali, I. U. Din, M. Shahid and J. Iqbal, *Inorganica Chimica Acta*, **2016**, 443, 69-77.

**(6)** M. Amini, A. Bayrami, M. N. Marashi, A. Arab, A. Ellern and L. K. Woo, *Inorganica Chimica Acta,* **2016**, 443, 22-27.

**(7)** O. H. Al-obaidi, *Open J. Inorg. Non-metal. Mat.*, **2012**, 2, 59-64.

**(8)** N. K. Singh, S. B. Singh, A. Shrivastav and S. M. Singh, *Proc. Indian Acad. Sci.*, **2001**, 113(*4*), 257–273.

**(9)** A. M. Plutín, A. Alvarez, R. Mocelo, R. Ramos, E. E. Castellano, M. M. da Silva, L. C. Vegas, F. R. Pavan and A. A. Batista, *Inorganic Chemistry Communications*, **2016**, 63, 74-80.

**(10)** S. Xu, W. Ting-Bin, L. Qiu-Tian, H. Xiao-Ying, K. Bei-Sheng, W. Xiao-Lin, H. Zhi-Shu and G. Lian-Quan, *Polyhedron*, **1997**, 16(*15*), 2605–2611.

**(11)** M. F. El-Shazly, A. El-dissowky, T. Salem and M. Osman, *Inorganica Chimica Acta,* **1980**, 40, 1-6.

**(12)** E. P. McMoran, J. A. Goodner, D. R. Powell and L. Yang, *Inorganica Chimica. Acta*, **2014,** 421, 465–472.

**(13)** X. Wang, N. Chen, G. Liu, H. Lin and J. Zhang, *Inorganica Chim. Acta*, **2014**, 421, 473–480.

**(14)** M. Yamada, K. Araki and S. Shiraishi, *Bull. Chem. Soc. Jpn.,* **1987**, 60, 3149-3155.

**(15)** T. Kojima, H. Kitaguchi, Y. Tachi, M. Yasutake, Y. Naruta and Y. Matsuda, *Inorganica Chim. Acta*, **2005,** 358, 3592–3600.

**(16)** N. M. Hosny and M. M. Mostafa, *J. Incl. Phenom. Macrocycl. Chem.*, **2010**, 67, 85–90.

**(17)** V. Maurizot, G. Linti and I. Huc, *Chem Commun.,* **2004**, 33, 924–925.

**(18)** J. D. Epperson, L. J. Ming, B. D. Woosley, G. R. Baker and G. R. Newkome, *Inorg. Chem.*, **1999**, 38(*20*), 4498–4502.

**(19)** W. B. Blanton, S. W. Gordon-Wylie, G. R. Clark, K. D. Jordan, J. T. Wood, U. Geiser and T. J. Collins, *J. Am. Chem. Soc.*, **1999**,12(*14*), 3551–3552.

**(20)** C. Glotzbach, U. Kauscher, J. Voskuhl, N. S. Kehr, M. C. A. Stuart, R. Fröhlich, H. J. Galla, B. J. Ravoo, K. Nagura, S. Saito, S. Yamaguchi and E. Würthwein, *J. Org. Chem.*, **2013**, 78, 4410−4418.

**(21)** D. F. Evans, *J. Chem. Soc.*, **1959**, 2003–2005.

**(22)** W. Kaminsky, K. I. Goldberg and D. X. West, *J. Mol. Struct.*, **2002**, 605, 9–15.

**(23)** J. M. McGrath and M. D. Pluth, *J. Org. Chem.*, **2014**, 79, 711–719.

**(24)** M. Zhao, X. Dong, G. Li and X. Yang, *Asian Journal of Chemistry,* **2014**, 26(*1*), 277-279

**(25)** S. Xu, W. Ting-Bin, L. Qiu-Tian, H. Xiao-Ying, K. Bei-Sheng, W. Xiao-Lin, H. Zhi-Shu and G. Lian-Quan, *Polyhedron*, **1997**, 16(*15*), 2605–2611.

**(26)** Y. M. Zhang, L. Xian and T. B. Wei, *Acta Crystallogr. Sect. C Cryst. Struct. Commun.*, **2003**, 59(*11*), m473–m474.

**(27)** R. M. Silverstein, G. C. Bassler and T.C. Morrill, *Spectrometric Identification of Organic Compounds.* 4th ed. New York: John Wiley and Sons, **1981**.

**(28)** S. Saeed and R. Hussain, *Turkish J. Chem.*, **2014**, 38, 413–422.

**(29)** M. Jamil, M. Zubair, M. A. Farid, U. Rashid, N. Rasool and S. Islam, *J. Chem.*, **2013**, 2013, 1–8.

**(30)** C. Lodeiro, J. L. Capelo, E. Bértolo and R. Bastida, *Z. Anorg. Allg. Chem.,* **2004**, 630(*7*), 1110–1115.

**(31)** Hathaway, *Proc. Chem. Soc.,* **1958,** 344.

**(32)** A.B.P. Lever, INORGANIC ELECTRONIC SPECTROSCOPY, second eddition, (Amsterdam: Elsevier), **1986**, 534.

**(33)** F. A. Saad, *Spectrochim. Acta - Part A Mol. Biomol. Spectrosc.*, **2014**, 128, 386–392.

**(34)** N. M. El-Metwaly and M. S. Refat, *Spectrochim. Acta Part A*, **2011**, 78, 196–204.

**(35)** F. A.Saad, N. J. Buurma, A. J. Amoroso, J. C. Knight and B. Kariuki, *Dalton Trans*., **2012**, 41, 4608–4617.

**(36)** M. B. Ferrari, S. Capacchi, G. Pelosi, G. Reffo, P. Tarasconi, R. Albertini, S. Pinelli and P. Lunghi, *Inorg. Chim. Acta*, **1999**, 286(*2*), 134-141.

**(37)** Y. Wang, Z. Liu and J. Y. Gao**,** *Acta Cryst.*, **2008**, E64, 633-634.

**(38)** Z. C. Liu, B. D. Wang, Z. Y. Yang, Y. Li, D. D. Qin and T. R. Li, *Euro. J. Med. Chem.*, **2009**, 44(*11*), 4477-4484.

**(39)** D. C. Ilies, E. Pahontu, S. Shova, R. Georgescu, N. Stanica, R. Olar, A. Gulea and T. Rosu, *Polyhedron*, **2014**, 81,123-131.

# Chapter Five

## Cr(III) complexes with 8-Hydroxyquinoline derivatives: Spectroscopic, Electrochemical behaviour and Photoluminescence studies.

# 5.1 Introduction

8-Hydroxyquinoline (HQ) or oxine, is a bicyclic aromatic compound, **Figure 5.1**. Compounds containing the HQ moiety are important ingredients in a variety of pharmaceutically important compounds and are observed in many biologically active natural products due to their unique chemical and biological properties. HQ derivatives are used among a wide range of pathologies, including neurodegenerative diseases, as the source for many prescribed drugs.[1,2] HQ derivatives are used for their antipsychotic, antibacterial, antifungal,[3] antiamoebic, anticonvulsant, anthelmintic, cytotoxic, antiprotozoal and antimalarial activities.[4,5] HQ is also an important analytical reagent and used for the preparation of mixed ligand complexes, forming stable complexes in combination with other ligands. This is due to its high chelating ability as a bidentate ligand through the phenolic oxygen and the ring nitrogen.[6,7] Metal complexes of HQ can also exhibit biological activity.[8,9]

The coordination chemistry in this chapter focuses upon the interaction of HQ derivatives with Cr(III). Chromium is the sixth most abundant element in the earth's crust. According to the Cambridge crystallographic data centre (CCDC) in 17/02/2016, there are 4589 crystal structures of general octahedral Cr(III) complexes and 13 crystal structures had the general form $[Cr(Q)X_4]$ (Q= 8-quinolinato, X = any atom from ligands such as an oxygen, nitrogen and chloride atoms).

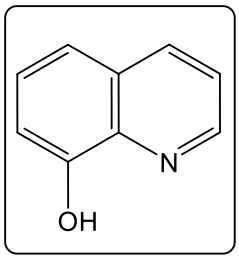


**Figure 5.1:** Chemical structure of 8-Hydroxyquinoline.

In 2014, Elmas *et al.* prepared the chromium(III) complex [Cr(babhq)$OAc^{F-}$(DMF)], babhq = 2,2'-(butylimino)diquinolin-8-olato, ($OAc^{F-}$ = $CF_3CO_2^-$), **Figure 5.2** and used it as the catalyst in the reaction of $CO_2$ with epoxides.[10]

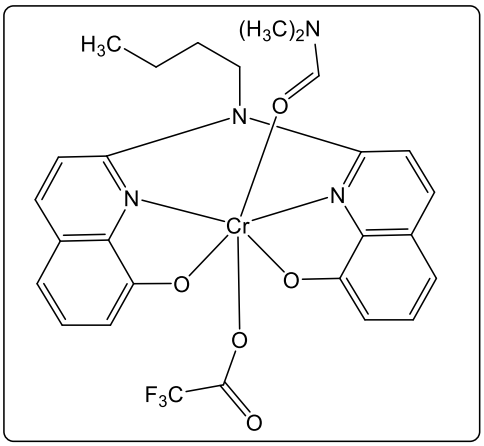


**Figure 5.2:** Chemical structure of [Cr(babhq)$OAc^{F-}$(DMF)]

Chen *et al.* prepared [$CrLCl_3$], L=[8-((pyridin-2-yl)methoxy) quinoline], **Figure 5.3** and the ethylene polymerisation experiments suggest moderately active catalysis for ethylene polymerisation with activation with methylaluminoxane (MAO).[11]

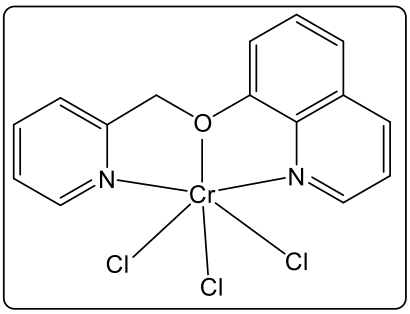


**Figure 5.3:** Chemical structure of [$CrLCl_3$]

The complex [$Cr_2(Q)_2Cl_4(H_2O)_2$]·$2Me_2CO$ (HQ= 8-hydroxyquinoline), **Figure 5.4**, was prepared by Lu *et al.* and constructed by two monomeric units [$Cr(Q)Cl_2(H_2O)$] as a dimer. It contains a bridged oxygen atom of phenoxide group and the two six-coordinated Cr(III) atoms exhibit an octahedral coordination geometry.[12]

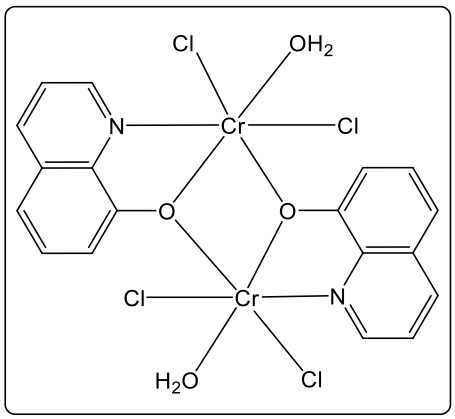


**Figure 5.4:** Chemical structure of $[Cr_2(Q)_2Cl_4(H_2O)_2]\cdot$

According to the CCDC in 17/02/2016, there are 154 and 112 published crystal structures of 2,2′-bipyridine (bpy) and 1,10-phenanthroline (phen) octahedral Cr(III) complexes in the general form $[Cr(bpy)X_4]$[13-17] and $[Cr(phen)X_4]$[18-22] respectively, (bpy= 2,2′-bipyridine, phen= 1,10-phenanthroline, X= any atom from ligands such as an oxygen, nitrogen and Cl atoms). In 1999, Grant *et al.* [23] prepared the six coordinate Cr(III) complex $[CrLCl_2]Cl$, L = 1,2-bis(2,2'-bipyridyl-6-yl)ethane by the reaction of $CrCl_3.6H_2O$ with L in refluxing MeOH to give a mononuclear trans form isomer with the ligand L coordinated equatorially. The cation consists of a six-coordinate Cr(III) ion bound to four N donor atoms from L and two $Cl^-$ ions that are trans to one another, **Figure 5.5**.

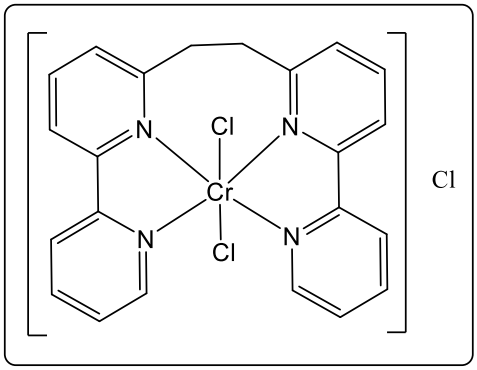


**Figure 5.5:** Chemical structure of $[CrLCl_2]Cl$

The complexes *cis*- and *trans*-$[Cr(mal)(bpy)(H_2O)_2][NO_3]$, **Figure 5.6**, ($H_2$mal= malonic acid, bpy=2,2′-bipyridine) were prepared by Molina *et al*. The single crystal

X-ray structures revealed an octahedral geometry around the Cr(III) ion and *cis*-compound reveals that the cations and anions, as well as between the complex cations are linked into hydrogen-bonded chains.[24]

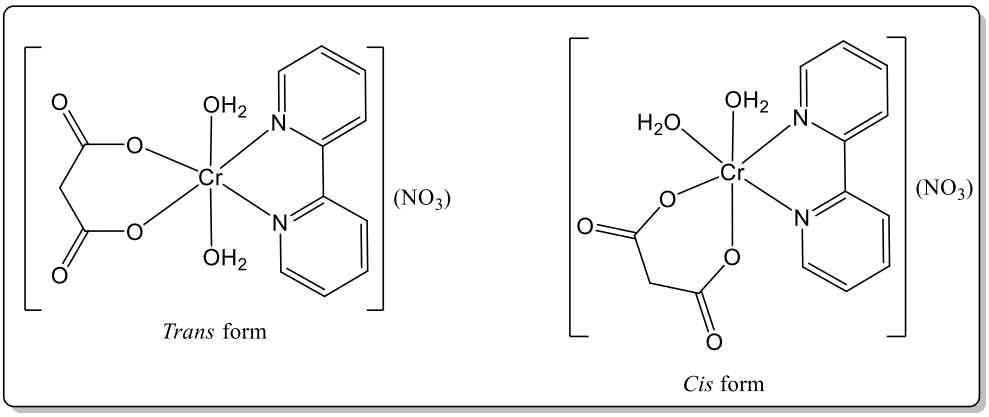


**Figure 5.6:** Chemical structures of *trans*- and *cis*-[Cr(mal)(bpy)$(H_2O)_2$][$NO_3$].

Baro *et al.* published the six coordinate complex [Cr(dipic)(phen)Cl]·1/2$H_2O$, **Figure 5.7**, **(**dipic = dipicolinate, phen = 1,10-phenantroline) where the Cr(III) ion is in an octahedral environment. The Cr(III) ion is coordinated to one phen molecule through the two nitrogen atoms and one nearly perpendicular dipic anion acting as tridentate ligand through one oxygen of each carboxylate group and the pyridinic nitrogen atom. The sixth site is occupied by a chloride atom.[25]

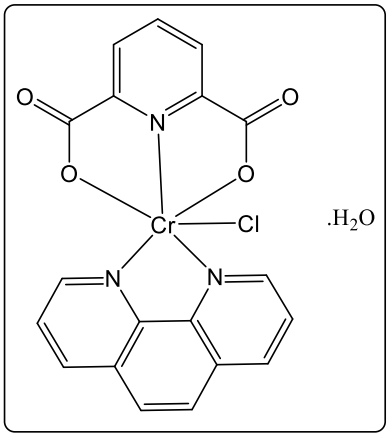


**Figure 5.7:** Chemical structure of [Cr(dipic)(phen)Cl]·1/2$H_2O$

The Cr(III) complex $LCrCl_3$, **Figure 5.8**, contains tridentate ligand of 2-imino-1,10-phenanthroline, (L = 2-(((2,6-di-isopropylphenyl)imino)methyl)1,10-phenanthroline) was synthesized by Zhang *et al*. X-ray crystallographic analysis reveals that the geometry around the chromium atom is octahedral. The complex exhibited high activity for ethylene oligomerization and moderate activity for ethylene polymerization.[26]

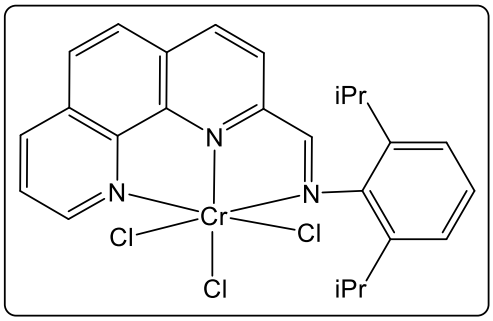


**Figure 5.8:** Chemical structure of $LCrCl_3$

However, to the best of our knowledge, and according to the CCDC, no reports focused on the synthesis of Cr(III) complexes of mixed ligands of HQ derivatives and bpy or phen. In this present study, the new Cr(III) complexes with HQ derivatives were synthesized by refluxing the quinoline derivatives with $CrCl_3.6H_2O$ in 2:1 and 3:1 equivalent ratio respectively and then fully characterised. The Cr(III) complexes of mixed ligands of HQ derivatives and bpy or phen were synthesized by two steps. First, synthesis at room temperature of $[Cr(phen)_2(CF_3SO_3)_2](CF_3SO_3)$ or $[Cr(bpy)_2(CF_3SO_3)_2](CF_3SO_3)$ as reported before[27] secondly, stirring at room temperature the mixture solution of the prepared Cr complexes with HQ derivative in the presence of $KPF_6$. In this chapter, the Cr(III) complexes of HQ derivatives and the mixed ligands of it and bpy or phen have been synthesised and fully characterised. The redox-behaviour of all the new Cr(III) species has also been probed by electrochemical studies. The photoluminescence and optical properties of all the new Cr(III) complexes have been investigated to explore if these complexes are emissive and whether they show phosphorescence or fluorescence properties.

# 5.2 Experimental

## 5.2.1 Instrumentation

The details regarding the collection of experimental data are the same as reported in previous chapters.

## 5.2.2 Synthesis of complexes (5.1-5.12)

### 5.2.2.1 Synthesis of $[Cr^{III}(Q)_2(H_2O)_2]Cl$ (5.1)

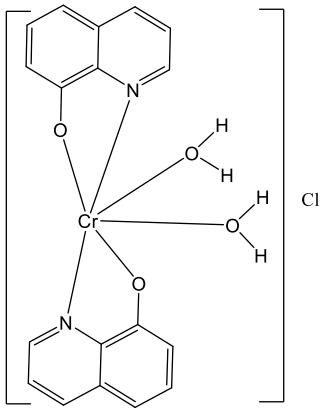

The solution of $CrCl_3.6H_2O$ (0.5 g, 1.9 mmol) in 5 $cm^3$ water was poured into the solution of HQ (0.545 g, 3.8 mmol) in 15 $cm^3$ ethanol. The mixture was heated to reflux for 3 hours. The colourless solution changed to dark green and then brown. After this time, the mixture solution was concentrated to 5 $cm^3$. The formed brown precipitate was filtered, washed with acetone 20 $cm^3$ and ether 10 $cm^3$ and then dried under vacuum. Yield (0.38 g, 71 %); brown powder; ESI-MS *(m/z)*(%): 376.06 [M+] (70%); Mass: 376.0753, Calc. Mass: 376.0761; FT-IR ($cm^{-1}$): ν(O-H) strech 3420, ν(O-H) deformation 1377, ν(C=N) 1554, ν(C-O) 1109; UV-vis. spectrum, $\lambda_{max}$ nm (εM, $M^{-1}$ $cm^{-1}$): 315(2390), 403(1780) and 565(77). Anal. Calcd. for $\mathbf{C_{18}H_{16}ClCrN_2O_4.2H_2O}$ (%): C,48.28; H, 4.50; N, 6.26. Found (%): C, 48.95; H, 4.86; N, 6.39.

### 5.2.2.2 Synthesis of $[Cr^{III}(Q)_3]$ (5.2)

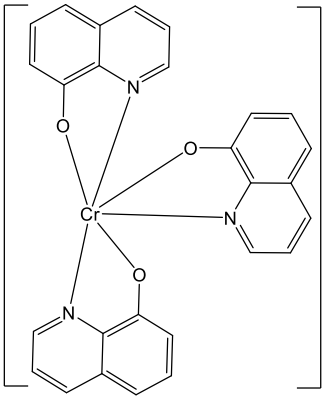

Using the same procedure as described for **5.1**: HQ (0.83 g, 5.7 mmol) and $CrCl_3.6H_2O$ (0.5 g, 1.9 mmol). Yield: (0.87 g, 80%); green powder; ESI-MS (*m/z*)(%): 484.08 [M] (100%); Mass: 484.0754, calc. Mass: 484.0753; FT-IR ($cm^{-1}$): ν(C=N) 1570, ν(C-O) 1110; UV-vis. spectrum, $\lambda_{max}$ nm (εM, $M^{-1}cm^{-1}$): 319(5360), 413(3505) and 546(108). Anal. Calcd. for $\mathbf{C_{27}H_{18}CrN_3O_3.CH_3CH_2OH}$ (%): C, 65.66; H, 4.56; N, 7.92. Found (%): C, 65.25; H, 4.88; N, 7.96.

### 5.2.2.3 Synthesis of $[Cr^{III}(QM)_2(H_2O)_2]Cl$ (5.3)

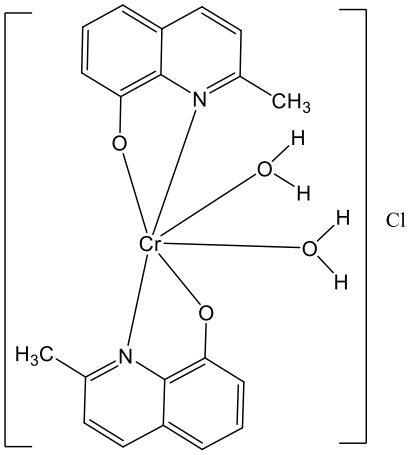

Using the same procedure as described for **5.1**: 8-hydroxy-2-methylquinoline (HQM) (0.6 g, 3.8 mmol) and $CrCl_3.6H_2O$ (0.5 g, 1.9 mmol). Dark green crystals of **5.3** were grown by slow evaporation at room temperature for 3 days. Yield: (0.41 g, 69%); green crystal; ESI-MS (*m/z*)(%): 404.08 [M+] (81%); Mass: 404.0903, calc. Mass: 404.0884; FT-IR ($cm^{-1}$): ν(O-H) strech 3428, ν(O-H) deformation 1369, ν(C=N) 1541, ν(C-O) 1105; UV-vis. spectrum, $\lambda_{max}$ nm (εM, $M^{-1}cm^{-1}$): 291(1305), 402(470) and 563(39). **$C_{20}H_{20}ClCrN_2O_4.H_2O.CH_3CH_2OH$** (%): C, 52.44; H, 5.60; N, 5.56. Found (%): C, 53.04; H, 6.03; N, 5.68.

### 5.2.2.4 Synthesis of $[Cr^{III}(QM)_3]$ (5.4)

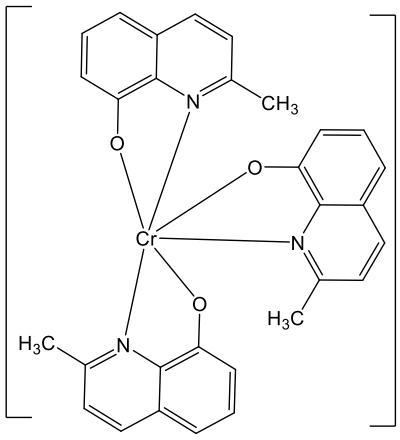

Using the same procedure as described for **5.1**: 8-hydroxy-2-methylquinoline (HQM) (0.91 g, 5.7 mmol) and $CrCl_3.6H_2O$ (0.5 g, 1.9 mmol). Yield: (0.95 g, 80%); green powder; ESI-MS (*m/z*)(%): 526.12 [M] (90%); Mass: 526.1223, calc. Mass: 526.1223; FT-IR ($cm^{-1}$): ν(C=N) 1550, ν(C-O) 1107; UV-vis. spectrum, $\lambda_{max}$ nm (εM, $M^{-1}cm^{-1}$): 308(3865), 404(2515) and 579(43); Anal. Calcd. for **$C_{30}H_{24}CrN_3O_3.3H_2O$** (%): C, 62.06; H, 5.21; N, 7.24. Found (%): C, 62.41; H, 5.05; N, 7.50.

### 5.2.2.5 Synthesis of $[Cr^{III}(QN)_2(H_2O)_2]Cl$ (5.5)

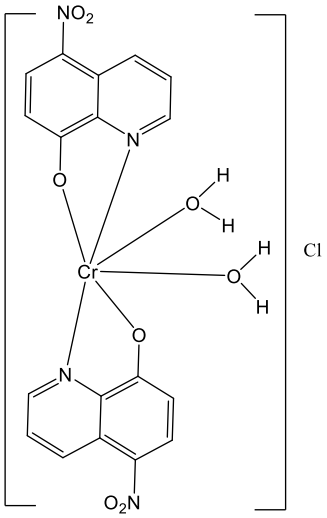

Using the same procedure as described for **5.1**: 8-hydroxy-5-nitroquinoline (HQN) (0.71 g, 3.8 mmol) and $CrCl_3.6H_2O$ (0.5 g, 1.9 mmol). Yield: (0.56 g, 79%); brown powder; ESI-MS (*m/z*)(%): 504.00 [$M+K^+$] (67%); FT-IR ($cm^{-1}$): ν(O-H) strech 3437, ν(O-H) deformation 1380, ν(C=N) 1566, ν(C-O) 1101; UV-vis. spectrum, $\lambda_{max}$ nm (εM, $M^{-1}cm^{-1}$): 332(3225), 427(1660) and 594(121). Anal. Calcd. for: **$C_{18}H_{14}ClCrN_4O_8$** (%): C,43.09; H, 2.81; N,11.17. Found (%): C, 43.29; H, 3.15; N, 11.25.

### 5.2.2.6 Synthesis of $[Cr^{III}(QN)_3]$ (5.6)

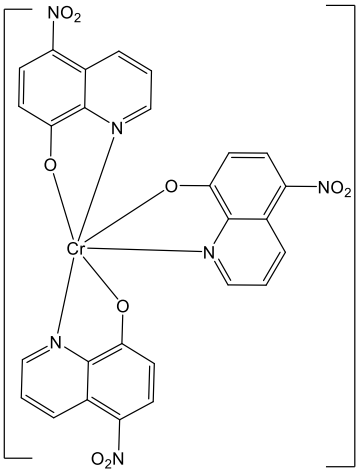

Using the same procedure as described for **5.1**: 8-hydroxy-5-nitroquinoline (HQN) (1.08 g, 5.7 mmol) and $CrCl_3.6H_2O$ (0.5 g, 1.9 mmol). Yield: (1.05 g, 74%); brown powder; ESI-MS (*m/z*)(%): 618.95 [M] (75%); Mass: 619.0296, calc. Mass: 619.0306; FT-IR ($cm^{-1}$): ν(C=N) 1570, ν(C-O) 1099; UV-vis. spectrum, $\lambda_{max}$ nm (εM, $M^{-1}cm^{-1}$): 333(7300), 408(2325) and 529(389); Anal. Calcd. for **$C_{27}H_{15}CrN_6O_9$** (%): C,52.35; H, 2.44; N,13.57. Found (%): C, 52.28; H, 2.57; N, 13.49.

### 5.2.2.7 Synthesis of $[Cr^{III}(phen)_2(Q)](PF_6)_2$ (5.7)

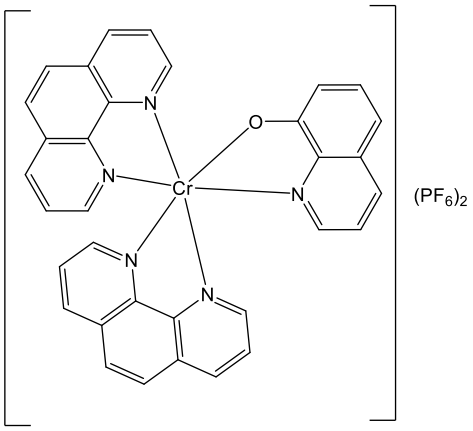


The starting material $[Cr(phen)_2Cl_2]Cl$ and $[Cr(phen)_2(CF_3SO_3)_2](CF_3SO_3)$ was prepared as described before.[27] The Cr(III) complex **5.7** was prepared by stirring at room temperature, the mixture solution of $[Cr(phen)_2(CF_3SO_3)_2](CF_3SO_3)$ (0.5 g, 0.58 mmol) in 10 $cm^3$ MeCN and HQ (0.085 g, 0.58 mmol) in 5 $cm^3$ MeCN for 3 hours. Concentration of the dark red solution to 5 $cm^3$, and then addition of $KPF_6$ (0.42 g, 2.3 mmol) in 2 $cm^3$ $H_2O$ resulted in a brown precipitate which was stirrer for 30 minutes. The brown precipitate was filtered, washed with 3 $cm^3$ $H_2O$ and 2 $cm^3$ MeCN and then dried under vacuum. Red crystals of **5.7** were obtained by vapor diffusion of diethyl ether into MeCN solution of the complex. Yield: (0.32 g, 64%); ESI-MS (*m/z*)(%): 578.03 [M+Na] (68%); FT-IR ($cm^{-1}$): ν(C=N) 1564, ν(C-O) 1107, ν($PF_6$-) 829; UV-vis. spectrum, $\lambda_{max}$ nm (εM, $M^{-1}cm^{-1}$): 273(2680), 366(1320) and 507(41); Anal. Calcd. for **$C_{33}H_{22}CrF_{12}N_5OP_2.4H_2O$ (%):** C, 43.15; H, 3.29; N, 7.62. Found (%): C, 43.05; H, 2.86; N, 7.49.

### 5.2.2.8 Synthesis of $[Cr^{III}(phen)_2(QM)](PF_6)_2$ (5.8)

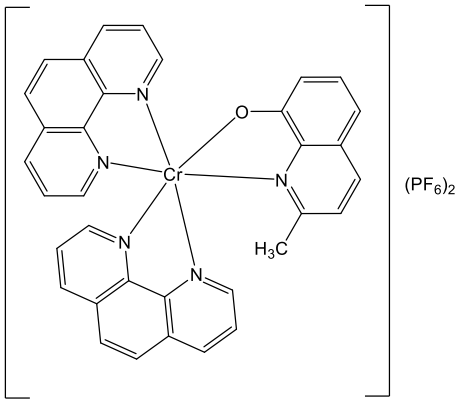


Using the same procedure as described for **5.7**: $[Cr(phen)_2(CF_3SO_3)_2]$ $(CF_3SO_3)$ (0.5 g, 0.58 mmol), HQM (0.093 g, 0.58 mmol) and $KPF_6$ (0.42 g, 2.3 mmol). Yield: (0.34 g, 68%); brown powder; ESI-MS (*m/z*)(%): 570.87 [M+] (65%); FT-IR ($cm^{-1}$): ν(C=N) 1558, ν(C-O) 1104, ν($PF_6$-) 830; UV-vis. spectrum, $\lambda_{max}$ nm (εM, $M^{-1}cm^{-1}$): 276(3370), 374(1805) and 515(45); Anal. Calcd. for **$C_{34}H_{24}CrF_{12}N_5OP_2$** (%): C, 47.46; H, 2.81; N, 8.14. Found (%): C, 47.59; H, 2.98; N, 8.05.

### 5.2.2.9 Synthesis of $Cr^{III}(phen)_2(QN)](PF_6)_2$ (5.9)

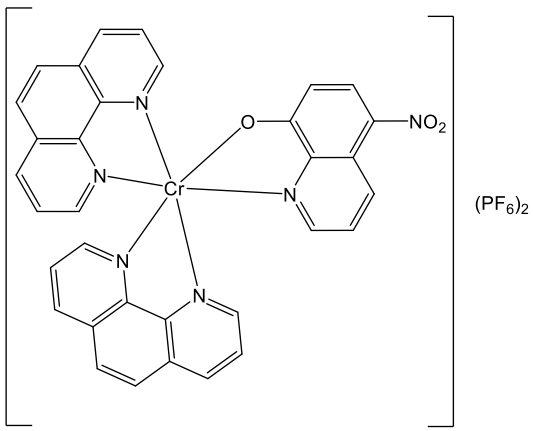


Using the same procedure as described for **5.7**: $[Cr(phen)_2(CF_3SO_3)_2]$ $(CF_3SO_3)$ (0.5 g, 0.58 mmol), HQN (0.11 g, 0.58 mmol) and $KPF_6$ (0.42 g, 2.3 mmol). Yield: (0.3 g, 61%); brown powder; ESI-MS (*m/z*)(%): 601.03 [M+] (75%); Mass: 601.0277, calc. Mass: 601.0302; FT-IR ($cm^{-1}$): ν(C=N) 1581, ν(C-O) 1116, ν($PF_6$-) 832; UV-vis. spectrum, $\lambda_{max}$ nm (εM, $M^{-1}cm^{-1}$): 271(2360), 385(1670) and 531(81); Anal. Calcd. for $\mathbf{C_{33}H_{21}CrF_{12}N_6O_3P_2}$ (%): C, 44.46; H, 2.37; N, 9.43. Found (%): C, 44.58; H, 2.47; N, 9.61.

### 5.2.2.10 Synthesis of $[Cr^{III}(bpy)_2(Q)](PF_6)_2$ (5.10)

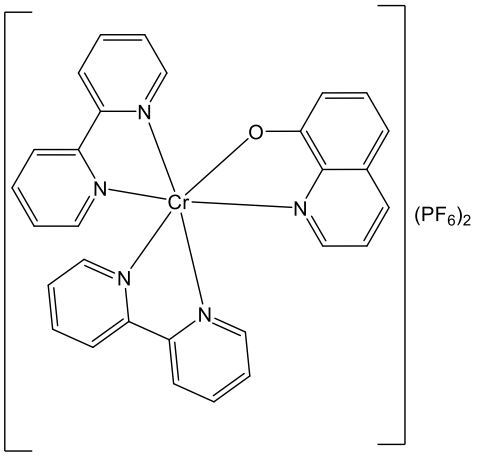


The starting material $[Cr(bpy)_2Cl_2]Cl$ and $[Cr(bpy)_2(CF_3SO_3)_2](CF_3SO_3)$ was prepared as described before.[27] The Cr(III) complex **5.10** was prepared by stirring at room temperature, the solution of $[Cr(bpy)_2$ $(CF_3SO_3)_2](CF_3SO_3)$ (0.5 g, 0.62 mmol) in 10 $cm^3$ MeCN and HQ (0.089 g, 0.62 mmol) in 5 $cm^3$ MeCN for 3 hours. Concentration of the dark red solution to 5 $cm^3$, and then addition of $KPF_6$ (0.45 g, 2.46 mmol) in 2 $cm^3$ $H_2O$ gave a brown precipitate that was filtered, washed with 3 $cm^3$ $H_2O$ and 2 $cm^3$ MeCN and then dried under vacuum. Yield: (0.4 g, 80%); brown powder; ESI-MS (*m/z*)(%): 508.15 [M+] (80%); FT-IR ($cm^{-1}$): ν(C=N) 1565, ν(C-O) 1115, ν($PF_6$-) 833; UV-vis. spectrum, $\lambda_{max}$ nm (εM, $M^{-1}cm^{-1}$): 304(8415), 386(810) and 545(131). Anal. Calcd. for $\mathbf{C_{29}H_{22}CrF_{12}N_5OP_2.4H_2O}$ (%): C,40.01; H, 3.47; N, 8.05. Found (%): C, 40.59; H, 3.67; N, 8.17.

### 5.2.2.11 Synthesis of $[Cr^{III}(bpy)_2(QM)] (PF_6)_2$ (5.11)

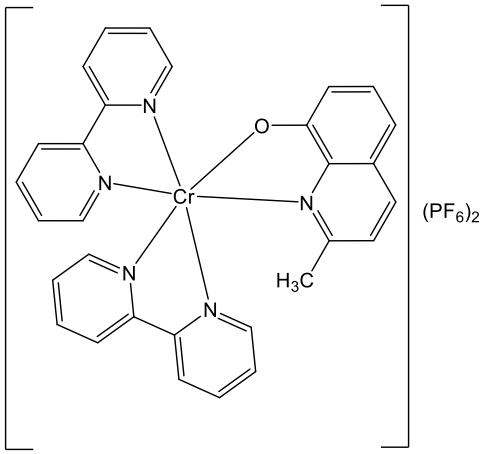


Using the same procedure as described for **5.10**:$[Cr(bpy)_2(CF_3SO_3)_2]$ $(CF_3SO_3)$ (0.5 g, 0.62 mmol), HQM (0.1 g, 0.62 mmol) and $KPF_6$ (0.45 g, 2.46 mmol). Red crystals of **5.11** were obtained by vapour diffusion of diethyl ether into a concentrated MeCN solution of the complex. Yield: (0.33 g, 67%); ESI-MS (*m/z*)(%): 545.13 [M+Na] (80%); FT-IR ($cm^{-1}$): ν(C=N) 1560, ν(C-O) 1109, ν($PF_6$-) 835; UV-vis. spectrum, $\lambda_{max}$ nm (εM, $M^{-1}cm^{-1}$): 305(4000), 441(115) and 533(50); Anal. Calcd. for $\mathbf{C_{30}H_{24}CrF_{12}N_5OP_2}$ (%): C, 44.35; H, 2.98; N, 8.62. Found (%): C, 44.49; H, 3.10; N, 8.84.

### 5.2.2.12 Synthesis of $[Cr^{III}(bpy)_2(QN)](PF_6)_2$ (5.12)

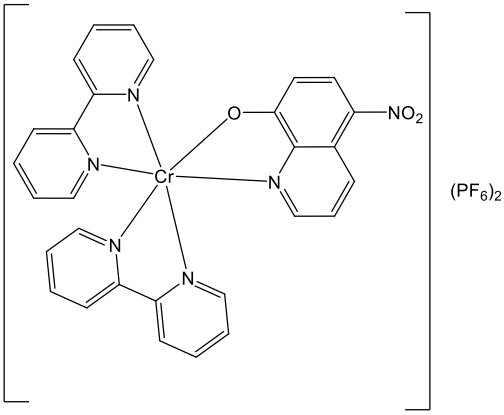


Using the same procedure as described for **5.10**: $[Cr(bpy)_2(CF_3SO_3)_2]$ $(CF_3SO_3)$ (0.5 g, 0.62 mmol), HQN (0.12 g, 0.62 mmol) and $KPF_6$ (0.46 g, 2.48 mmol). Red crystals of **5.12** were obtained by vapour diffusion of diethyl ether into a concentrated MeCN solution of the complex. Yield: (0.29 g, 57%); ESI-MS (*m/z*)(%): 553.03 [M+] (65%); Mass: 554.1350, calc. Mass: 554.1367; FT-IR ($cm^{-1}$): ν(C=N) 1575, ν(C-O) 1120, ν($PF_6$-) 837; UV-vis. spectrum, $\lambda_{max}$ nm (εM, $M^{-1}cm^{-1}$): 306(1950), 399(975) and 533(106). Anal. Calcd. for $\mathbf{C_{29}H_{21}CrF_{12}N_6O_3P_2.2H_2O}$ **(%)**: C, 39.61; H, 2.87; N, 9.56. Found (%): C, 40.22; H, 3.23; N, 9.73.

# 5.3 Results and discussion

## 5.3.1 Synthesis of complexes (5.1- 5.12)

The Cr(III) complexes **5.1-5.6** were synthesised by heating to reflux for 3 hours the mixture of HQ ligand derivatives, HQ (**5.1**, **5.2**), HQM (**5.3**, **5.4**) or HQN (**5.5**, **5.6**)) with $CrCl_3.6H_2O$ in ethanol/$H_2O$. The 2:1 and 3:1 equivalent ratio (HQ derivative:$CrCl_3.6H_2O$) was carried out to form **5.1**, **5.3**, **5.5** and **5.2**, **5.4**, **5.6** respectively. A brown precipitate formed for the preparations of **5.1**, **5.5**, **5.6** and a green precipitate formed with **5.2**, **5.3**, **5.4**. The precipitates were washed with acetone and then by ether and then recrystallization of **5.3** in ethanol solution to obtain green crystals. The complexes **5**.**7**-**5.12** were synthesised by stirring at room temperature for 12 hours the mixture of $[Cr(phen)_2(CF_3SO_3)_2](CF_3SO_3)$ or $[Cr(bpy)_2(CF_3SO_3)_2](CF_3SO_3)$ with the HQ derivative in acetonitrile. $KPF_6$ was added to help precipitate the product. The brown precipitate was washed with water and then acetonitrile and recrystallization of **5.7**, **5.11** and **5.12** from acetonitrile solution yielded red crystals. The yields for complexes **5.1-5.12** were 57-80%.

## 5.3.2 Spectroscopic studies of the Cr(III) complexes (5.1 – 5.12)

### 5.3.2.1 Infrared spectra

The FT-IR spectra of the Cr(III) complexes (**5.1**–**5.12**) were recorded over the range 4000–400 $cm^{-1}$. The important IR spectral bands for the complexes are presented in the experimental section and listed in **Table 5.1**. For the free HQ ligands the bands at 3435-3445 and 1365-1390 $cm^{-1}$ are assigned to the O-H stretching vibration and deformation modes of the hydroxyl group. However, an important feature of the IR spectra of the Cr(III) complexes **5.1**, **5.3** and **5.5** is the presence of O-H peaks which are likely due to the presence of the two coordinated $H_2O$ molecules with Cr(III) ion. The other Cr(III) complexes, **5.2**, **5.4**, **5.6**, **5.7**, **5.8**, **5.9**, **5.10**, **5.11**, **5.12** did not show peaks related to an O-H group. The (C-O) band was observed in all complexes in the range 1099-1120 $cm^{-1}$ and at lower frequency when compared with their free ligands 1135-1145 $cm^{-1}$. The absence of O-H bands and shifting of the C-O band suggest complex formation.

The band observed at 1580, 1570 and 1589 $cm^{-1}$ in the free ligands, HQ, 8-HQM and HQN respectively are assigned to a C=N stretch and there is a clear shift to lower frequency at 1554-1570 $cm^{-1}$ of unsubstituted HQ complexes (**5.1**, **5.2**, **5.7**, **5.10**), 1541-1560 $cm^{-1}$ of methyl-substituted HQM complexes (**5.3**, **5.4**, **5.8**, **5.11**), and 1575-1583 $cm^{-1}$ of $NO_2$-substituted HQN complexes (**5.5**, **5.6**, **5.9**, **5.12**) respectively when compared to their corresponding free ligands.

The IR spectra were also obtained on Cr(III) complexes **5.7-5.12** highlighting the hexafluorophosphate counter anion (ca. 833 $cm^{-1}$).

**Table 5.1:** Infrared spectral assignments ($cm^{-1}$) for Cr(III) complexes (**5.1**- **5.12**).

| Compound | ν (O-H) Stretching vibration | δ (O-H) deformation mode | ν (C=N) | ν (C-O) | ν $PF_6^-$ |
|---|---|---|---|---|---|
| **HQ** | 3440 | 1379 | 1580 | 1137 | - |
| **5.1** | 3420 | 1377 | 1554 | 1109 | - |
| **5.2** | - | - | 1570 | 1110 | - |
| **HQM** | 3435 | 1365 | 1570 | 1132 | - |
| **5.3** | 3428 | 1369 | 1541 | 1105 | - |
| **5.4** | - | - | 1550 | 1107 | - |
| **HQN** | 3445 | 1390 | 1589 | 1145 | - |
| **5.5** | 3437 | 1380 | 1566 | 1101 | - |
| **5.6** | - | - | 1570 | 1099 | - |
| **5.7** | - | - | 1564 | 1107 | 829 |
| **5.8** | - | - | 1558 | 1104 | 830 |
| **5.9** | - | - | 1583 | 1116 | 832 |
| **5.10** | - | - | 1565 | 1115 | 833 |
| **5.11** | - | - | 1560 | 1109 | 835 |
| **5.12** | - | - | 1575 | 1120 | 837 |

## 5.3.2.2 UV-vis. absorption and emission properties

In recent decades, the photochemical and optical properties of octahedral Cr(III) complexes have been investigated by many researchers.[28,29] The Cr(III) ion has the electronic configuration [Ar]$3d^3$ with a ground state $^4A_{2g}$ under octahedral symmetry. There are three quartet excited states ($^4T_{2g}$, $^4T_{1g}$, and $^4T_{1g}$). In UV-visible studies, three spin-allowed transitions are observed for octahedral Cr(III) complexes, which are attributed to $^4A_{2g}\rightarrow{}^4T_{2g,}$ $^4A_{2g}\rightarrow{}^4T_{1g}$ (F) and $^4A_{2g}\rightarrow{}^4T_{1g}$ (P) transitions.[29] Generally a rapid and non radiative internal conversion (IC) may occur from the excited state $^4T_{1g}$ to $^4T_{2g}$ ($^4T_{1g}\rightarrow{}^4T_{2g}$). Fluorescence emission is uncommonly observed for $^4T_{2g}\rightarrow{}^4A_{2g}$ at room temperature in solution, but intersystem crossing (ISC) from the $^4T_{2g}$ state to the doublet state $^2E_{2g}$ (spin forbidden $^4T_{2g}\rightarrow{}^2E_{2g}$) can also occur efficiently. The doublet states $^2T_{1g}$ and $^2E_{2g}$ therefore represents the lowest-lying excited state and can decay to give metal centred emissions ($^2E_{2g}\rightarrow{}^4A_{2g}$) and ($^2T_{1g}\rightarrow{}^4A_{2g}$) that are attributed to the phosphorescence process (see **Figure 5.9**). The photoluminescence data of previously reported diimine Cr(III) complexes are collected in **Table 5.2**. These Cr(III) complexes have two emission wavelengths around 700 and 730 nm which are consistent with the phosphorescence transitions ($^2E_{2g}\rightarrow{}^4A_{2g}$) and ($^2T_{1g}\rightarrow{}^4A_{2g}$) respectively.

**Table 5.2**: Overview of photoluminescence data for different Cr(III) complexes. (bpy= 2,2′-bipyridine, 5,5′-$Me_2$bpy= 5,5′-dimethyl bipyridine, phen= 1,10-phenanthroline).

| Compound | $\lambda_{emission}$ nm $^2T_{1g} \rightarrow {}^4A_{2g}$ | $\lambda_{emission}$ nm $^2E_{2g} \rightarrow {}^4A_{2g}$ | Solvent |
|---|---|---|---|
| $[Cr(bpy)_3][PF_6]_3$ [30, 31] | 699 | 728 | $CH_2Cl_2$/water |
| $[Cr(bpy)_3][PF_6]_3$ [27] | 703 | 730 | water |
| $[Cr(bpy)_3][PF_6]_3$ | 701 | 728 | MeCN |
| $[Cr(bpy)_2(5,5'\text{-}Me_2bpy)][PF_6]_3$ | 701 | 730 | water |
| $[Cr(5,5'\text{-}Me_2bpy)_3][PF_6]_3$ | 703 | 731 | water |
| $[Cr(5,5'\text{-}Me_2bpy)_3][PF_6]_3$ | 701 | 730 | MeCN |
| $[Cr(phen)_3][PF_6]_3$ [32] | 700 | 730 | water |
| $[Cr(phen)_2(5,5'\text{-}Me_2bpy)][PF_6]_3$ | 702 | 730 | MeCN |

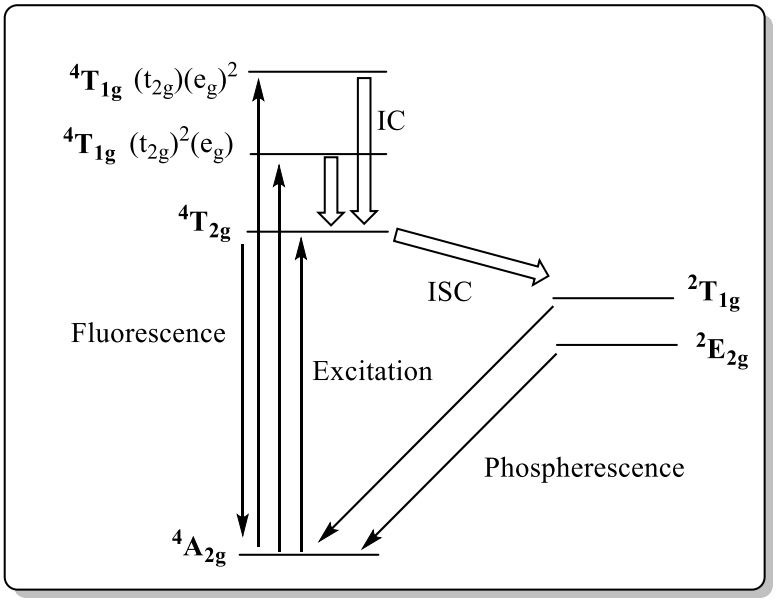


**Figure 5.9:** General diagram showing the energy levels for Cr(III) complexes and their three allowed transitions (IC refers to internal conversion and ISC to intersystem crossing).

### 5.3.2.2.1 The UV-vis. properties and the electronic spectra

The electronic spectra of the Cr(III) complexes with HQ derivatives were measured in DMF solutions and their spectral data are tabulated in **Table 5.3**. In the spectra of the Cr(III) complexes (**5.1-5.12**), two spin allowed transition bands, (271-333 nm) and (366-441) are observed and assigned to $\pi \rightarrow \pi^*$ and LMCT transitions respectively. All Cr(III) complexes (**5.1-5.12**) showed one *d-d* transition. The second and third transitions $^4A_{2g} \rightarrow {}^4T_{1g}(F)$ ($v_2$) and $^4A_{2g} \rightarrow {}^4T_{1g}(P)$ ($v_3$) respectively have been obscured by ligand-metal charge transfer LMCT band centered around 400 nm (see **Figures 5.10** and **5.11**, **Table 5.3**). The absorption band observed in the range (507-594 nm) corresponds to a *d-d* transition.[33]

While the first transition $\pi \rightarrow \pi^*$ is observed as sharp and higher intensity in the Cr(III) complexes (**5.1-5.12**), the LMCT is observed as a shoulder and at a lower intensity. The *d-d* transition is observable as a broad band but tends to be much weaker than the other two transitions due to it being a Laporte forbidden transition. The Cr(III) complex, **5.2** was previously reported by Freitas *et al.* and the UV data is in good agreement with the Cr(III) complex $[Cr(Q)_3]$, HQ= 8-hydroxyquinoline which also reveals transitions at 324, 420 and 558 nm close to the transitions in **5.1-5.12**.[34] **Figures 5.10** and **5.11** show the electronic spectra of Cr(III) complexes **5.3** and **5.11** respectively.

The Cr(III) ion is a $d^3$ ion for which the electronic spectra and magnetic properties of its complexes have been extensively investigated. The energy level diagram for $d^3$ ion in an octahedral field is shown in **Figure 5.12**. The ground term for the free ion is $^4F$ and the next higher energy term is $^4P$. In an octahedral field the $^4F$ term splits into $^4A_{2g}$, $^4T_{2g}$ and $^4T_{1g}$ and the three transitions have been assigned to $^4A_{2g} \rightarrow {}^4T_{2g}$ ($v_1$), $^4A_{2g} \rightarrow {}^4T_{1g}(F)$ ($v_2$) and $^4A_{2g} \rightarrow {}^4T_{1g}(P)$ ($v_3$) respectively.[35]

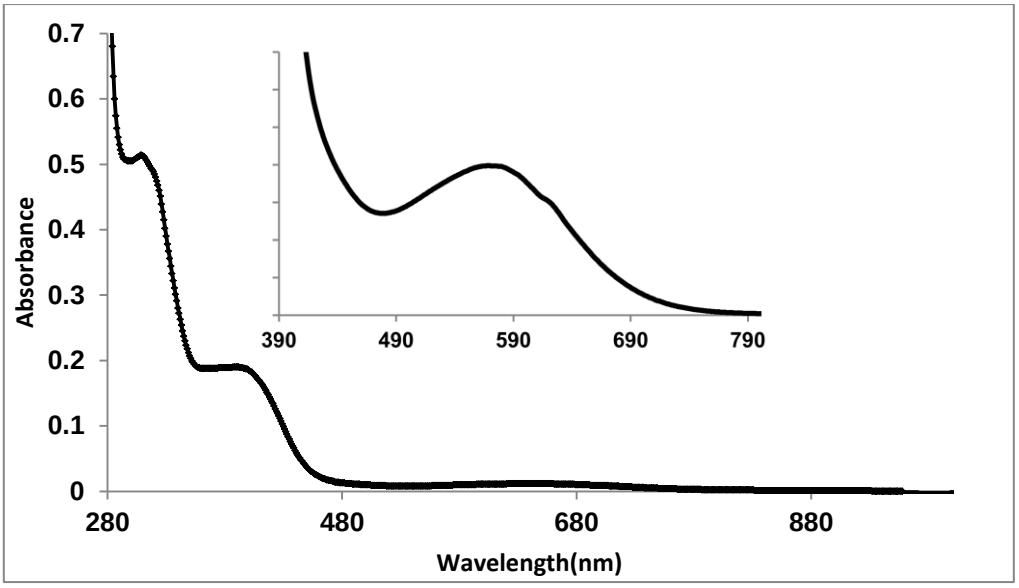


**Figure 5.10:** The electronic spectrum of octahedral Cr(III) complex **5.3.**

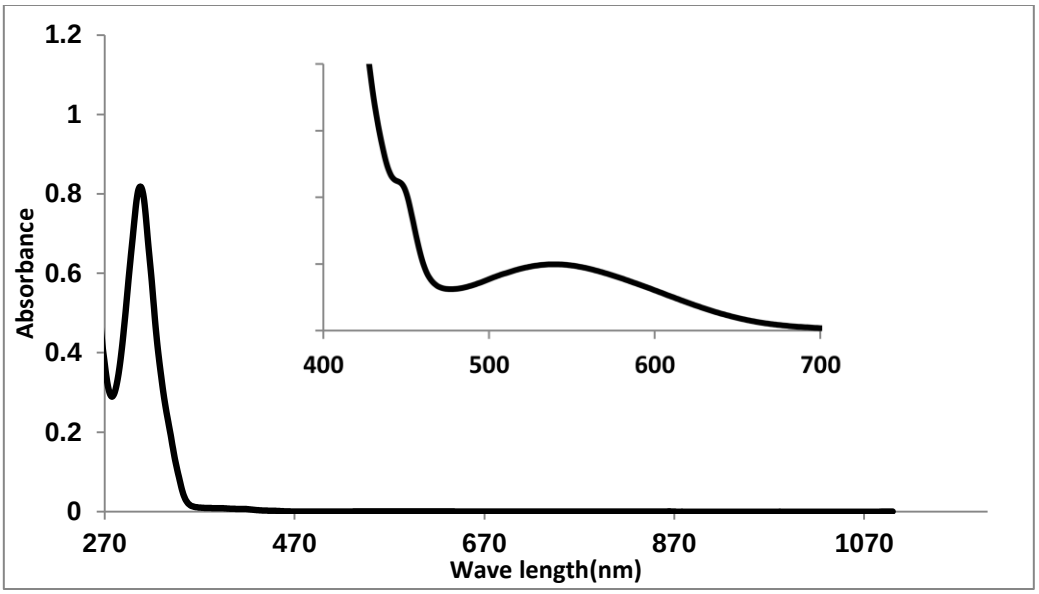


**Figure 5.11:** The electronic spectrum of octahedral Cr(III) complex **5.11.**

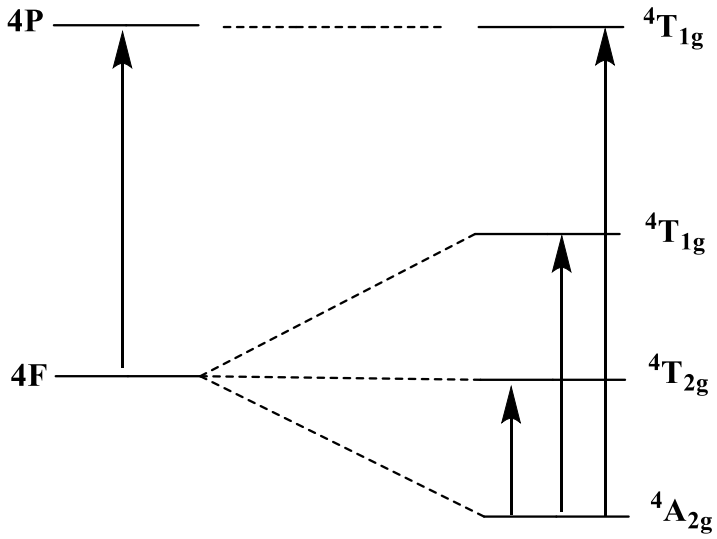


**Figure 5.12**: Term diagram for a Cr(III) in an octahedral field.

**Table 5.3:** Electronic spectral assignment for Cr(III) complexes **5.1-5.12**.

| compound | d-d transition $\lambda_{max}$ nm, ($\varepsilon$, $M^{-1}$ $cm^{-1}$) | | |
|---|---|---|---|
| | $\pi \rightarrow \pi^*$ | LMCT | *d-d* $^4A_{2g} \rightarrow {}^4T_{2g}$ |
| **5.1** | 315(2390) | 403(1780) | 565(77) |
| **5.2** | 319(5360) | 413(3505) | 546(108) |
| **5.3** | 291(1305) | 402(470) | 563(39) |
| **5.4** | 308(3865) | 404(2515) | 579(43) |
| **5.5** | 332(3225) | 427(1660) | 594(121) |
| **5.6** | 333(7300) | 408(2325) | 529(389) |
| **5.7** | 273(2680) | 366(1320) | 507(41) |
| **5.8** | 276(3370) | 374(1805) | 515(45) |
| **5.9** | 271(2360) | 385(1670) | 531(81) |
| **5.10** | 304(8415) | 386(810) | 545(131) |
| **5.11** | 305(4000) | 441(115) | 533(50) |
| **5.12** | 306(1950) | 399(975) | 533(106) |

### 5.3.2.2.2 Luminescence studies of the Cr(III) complexes (5.1-5.12)

Although a considerable amount of literature has been published and much research concerning the coordination chemistry of Cr(III) complexes, the photoluminescence properties of the Cr(III) complexes with HQ derivatives have not been reported. On the other hand, photoluminescence studies were published for different metal complexes with HQ derivatives, the review of these studies perhaps providing an explanation of the origins of the photoluminescence results. For example, in 2009 Shi *et al.*[36] designed and prepared the Al(III) complexes $Al(Q)_3$, $Al(6FQ)_3$ and $Al(4M6FQ)_3$, [HQ=8-hydroxyquinoline, 6FHQ=6-fluoro-8-hydroxyquinoline and 4M6FQ= 4-methyl-6-fluoro-8-hydroxyquinoline]. They studied the photoluminescence properties for these complexes and the effect of fluoro and methyl groups as withdrawing and donating groups respectively on these properties was investigated. $Al(Q)_3$ emitted green light (515 nm) while $Al(6Fq)_3$ emitted bluish green light (495 nm). $Al(4M6FQ)_3$ showed bigger blue shift of fluorescence (467 nm) than these complexes. The reason for the blue shift in $Al(6FQ)_3$ when compared with $Al(Q)_3$ is due to the strong electronegativity of the F-atom reducing and lowering the HOMO levels significantly. While the large blue shift in $Al(4M6FQ)_3$ is due to the effect of F-atom as above, in addition to the role of methyl group keeps of the lowest LUMO state and then broadened the band gap. It is worth mentioning that the fluorescence emission of these complexes originate from the electronic transition $\pi \rightarrow \pi^*$ in the ligands from a HOMO lying on the phenoxide ring to a LUMO located on the pyridyl ring, for example Al (III) complexes of HQ derivatives.[37,38]

The photoluminescence peaks of $Al(QS)_3$ and $Zn(QS)_2$, [QS= 8-Hydroxy-5-piperidinylquinolinesulfonamide] were compared with un-substituted HQ complexes, $Al(Q)_3$ and $Zn(Q)_2$ by Hopkins *et al.*. $Al(QS)_3$ and $Zn(QS)_2$exhibit emission peak in 480 and 502 nm respectively which are blue shift when compared with $Al(Q)_3$ and $Zn(Q)_2$ in 515 and 535 nm respectively due to the presence of strong withdrawing sulfonamide group.[39]

In 2014, Duvenhage *et al.* described the luminescence properties of the Al(III) complexes, $Al(Q)_3$, HQ=8-hydroxyquinoline and $Al(QM_2)_3$ (5,7-dimethyl-8-hydroxy quinoline) aluminum. The dimethyl substituted complex exhibits red shifted of the singlet emission peak to 556 nm when compared to 515 nm of $Al(Q)_3$. This red shift is due to the presence of the electron two donating methyl groups. They attributed the origin emission of $Al(Q)_3$ the ligand's electronic π–π* transitions.[40] Five years prior, the photoluminescence of the Zn(II) complex with the same ligand as above (5,7-dimethyl-8-hydroxyquinoline) was investigated by Singh *et al.* and exhibited similar wavelengths of the fluorescence emission spectra compared with (5,7-dimethyl-8-hydroxyquinoline) aluminum. In addition, they prepared the Zn(II) complex, 5,7-dimethyl-8-hydroxyquinolinato(2-(2-pyridyl) benzimidazole) Zn(II) which showed fluorescence emission spectra in 571 nm.[41] However the photoluminescence spectrum of a beryllium complex with HQ, $[Be(Q)_2]$ had been reported at 520 nm.[42,43] In 2016, Singh *et al.* reported that the photoluminescence spectrum of bis(5,7-dimethyl-8-hydroxyquinolinato) Be(II) complex as a light emissive material with a strong emission peak at 558 nm.[44] According to the previous review,[40-44] metal complexes of HQ derivatives, showed one fluorescence emission peak (467-571 nm) attributed to the electronic transition $\pi \rightarrow \pi^*$ in the ligands. These literature findings are consistent with our results for the fluorescence emission peak range 463-511 nm which we will discuss.

The optical properties of the complexes were investigated by measuring the luminescence for the Cr(III) complexes (**5.1**-**5.12**). **Figures 5.13**–**5.23** show the emission and the excitation spectra for the Cr(III) complexes with HQ derivatives of the different complexes (**5.1**-**5.11**) dissolved in acetonitrile. All the photoluminescence emission spectra of the Cr(III) complexes (**5.1**-**5.12**) exhibit an emission peak in the range 463-511 nm. The peaks are broad and structureless in appearance. Further, multiple strong excitation peaks are observed in the range 256-366 nm and a weaker broad peak around 440 nm. **Table 5.4** presents the wavelength of the emission and the excitation spectra for the Cr(III) complexes (**5.1**-**5.12**). In summary, all complexes gave one emission peak around 500 nm

with a corresponding short lifetime (<10 ns). These observations suggest a ligand-centred fluorescence process for the complexes.

The results of this investigation show that the electron donating group (such as methyl group) causes a red shift of the emission and the excitation peaks as compared with the un-substituted complexes (**Table 5.4**). The effect of the electron donating groups is also reported by Qin *et al.*[45] These electron donating groups and their ability of extending π conjugation at the 2-position of the phenoxide ring cause the higher energy level of the HOMO and thus smaller HOMO–LUMO gap. Other Cr(III) complexes of HQM, (**5.3**, **5.4**, **5.8** and **5.11**) showed the same behaviour when compared with their unsubstituted Cr(III) complexes (**5.1**, **5.2**, **5.7** and **5.10**) respectively.

The electron withdrawing group (such as $NO_2$ group) shifts emission and excitation wavelengths of (**5.5**, **5.6**, **5.9** and **5.12**) to the blue region compared to the un-substituted HQ derivatives of Cr(III) complexes (**5.1**, **5.2**, **5.7** and **5.10**) respectively. The emission peaks are also significantly weaker which is consistent with the well-known excited state quenching ability of nitro groups.[46] **Figure 5.24** shows the emission spectra for **5.1**, **5.3** and **5.5**.

One of the more significant findings to emerge from this study is the role of the coordinated $H_2O$ molecule in complexes (**5.1**, **5.3** and **5.5**) where a decrease in the wavelength of the emission and the excitation peak as compared with the tri HQ derivatives of Cr(III) complexes (**5.2**, **5.4** and **5.6**) was noted. For example, **5.5** showed shift from 476 to 463 nm (compared to **5.6**) due to the displacement of two $H_2O$ molecules by HQ. The Cr(III) complex, **5.3** exhibits the same effect compared with **5.4**. **Figure 5.25** shows the emission spectra for **5.3** and **5.4**.

The presence of a phen molecule instead of the bpy causes an increase in the emission wavelength. **Figure 5.26** shows the emission spectra for **5.7** and **5.10** and the potential effect of rigidity of the phen ligand.

**Figures 5.13-5.23** illustrate a significant change of the intensity of the emission peaks of the Cr(III) complexes. It is clear from the Cr(III) complexes which

containing the electron donating substituent groups (methyl group) on the aromatic ring of HQ (**5.3**, **5.4**, **5.8** and **5.11**) that the electron donating groups significantly affect the luminescence properties and they can effectively strengthen the fluorescence emission intensities, showing a higher integrated intensity than the corresponding Cr(III) complexes with un-substituted HQ (**5.1**, **5.2**, **5.7** and **5.10**) respectively. The contrary effect was exhibited by the Cr(III) complexes with the electron withdrawing groups ($NO_2$ group) (**5.5**, **5.6**, **5.9** and **5.12**) which gave a lower intensity of the emission peak. To understand the reason of these effects, Sapochak *et al.* suggested the effect depends on the stronger coupling of the metal–ligand stretching coordinating to the electronic transition in $Al(Q)_3$ complex (HQ = 8-hydroxyquinoline) and may give additional paths for non-radiative decay.[47]

For these Cr(III) complexes there was no evidence of any emission peaks in 700-750 nm that could be attributed to metal-centred luminescence.

**Table 5.4:** presents the wavelength of the emission and the excitation spectra for the Cr(III) complexes (**5.1**-**5.12**).

| No. | compound | $\lambda_{emission}$ nm | $\lambda_{excitation}$ nm |
|---|---|---|---|
| **1** | **5.1** | 495 | 285, 313, 350, 436 |
| **2** | **5.2** | 500 | 287, 449 |
| **3** | **5.3** | 504 | 307, 318, 356, 438 |
| **4** | **5.4** | 511 | 309, 319, 358, 449 |
| **5** | **5.5** | 463 | 256, 311, 344, 429 |
| **6** | **5.6** | 476 | 277, 348, 414, 445 |
| **7** | **5.7** | 500 | 316, 341, 363, 424 |
| **8** | **5.8** | 507 | 344, 365, 429 |
| **9** | **5.9** | 492 | 361, 422 |
| **10** | **5.10** | 484 | 318, 359, 423 |
| **11** | **5.11** | 493 | 364, 427 |
| **12** | **5.12** | 472 (Weak) | - |

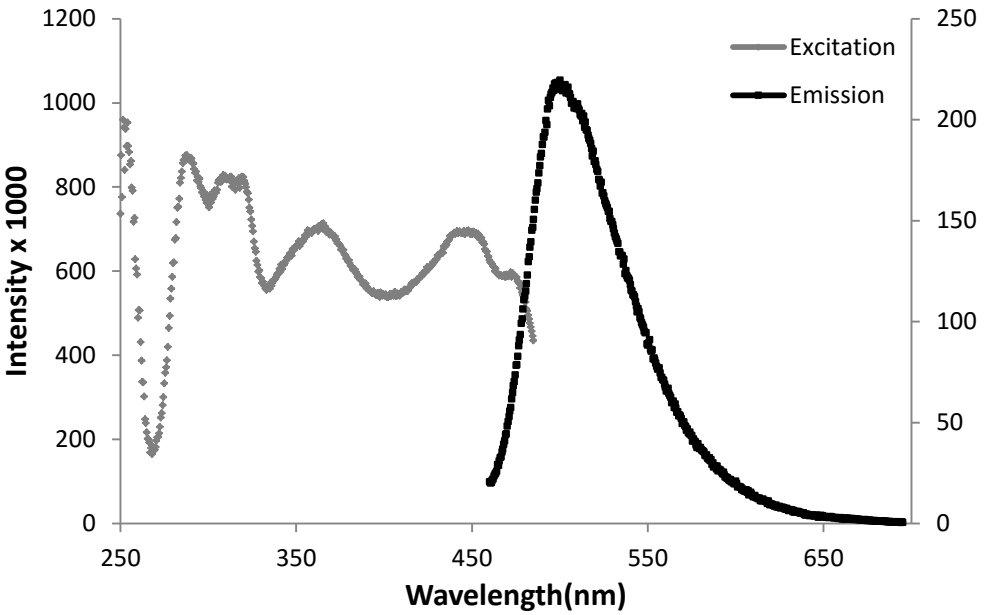


**Figure 5.13:** Steady state excitation (grey) and emission (black) spectra for **5.1**.

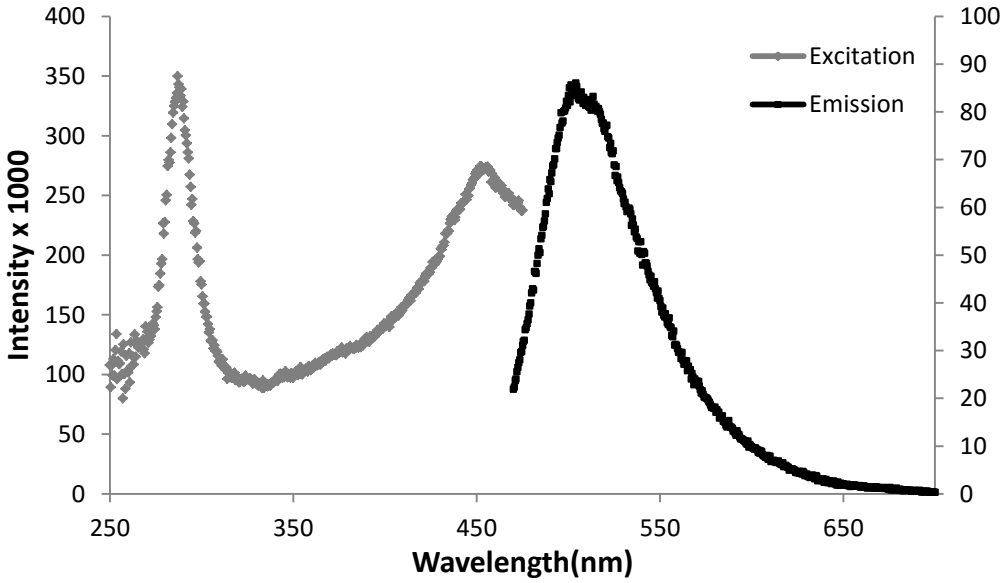


**Figure 5.14:** Steady state excitation (grey) and emission (black) spectra for **5.2**.

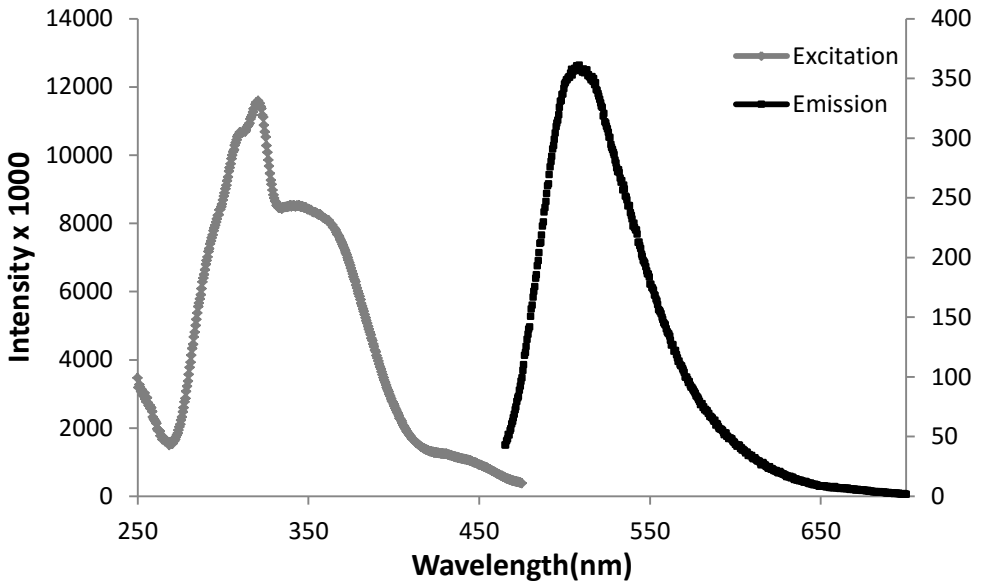


**Figure 5.15:** Steady state excitation (grey) and emission (black) spectra for **5.3**.

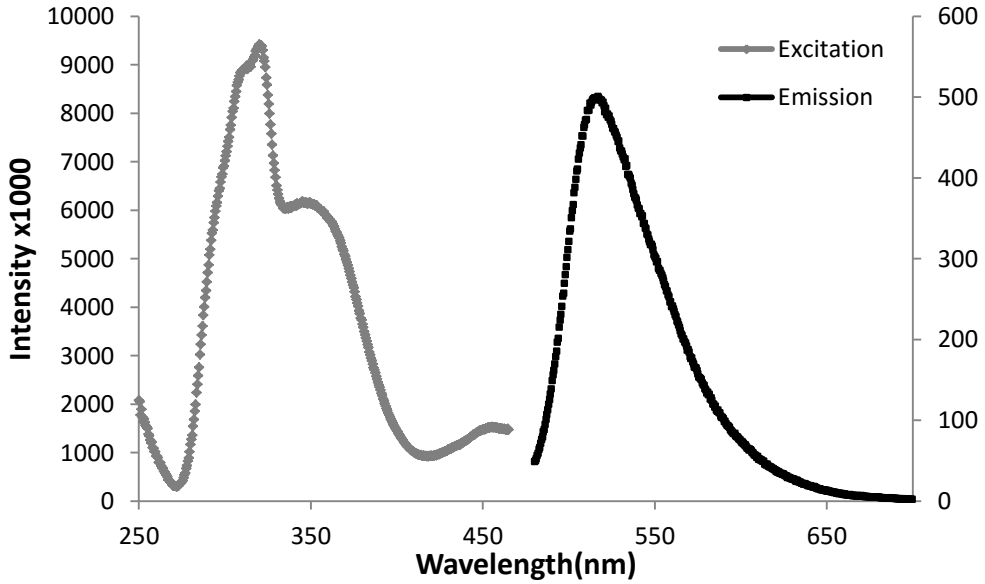


**Figure 5.16:** Steady state excitation (grey) and emission (black) spectra for **5.4**.

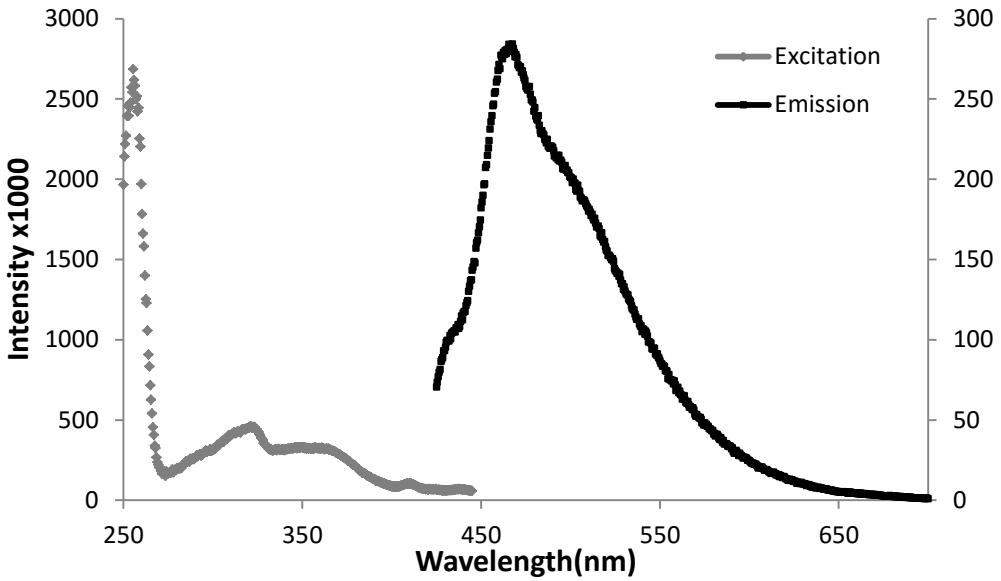


**Figure 5.17:** Steady state excitation (grey) and emission (black) spectra for **5.5**.

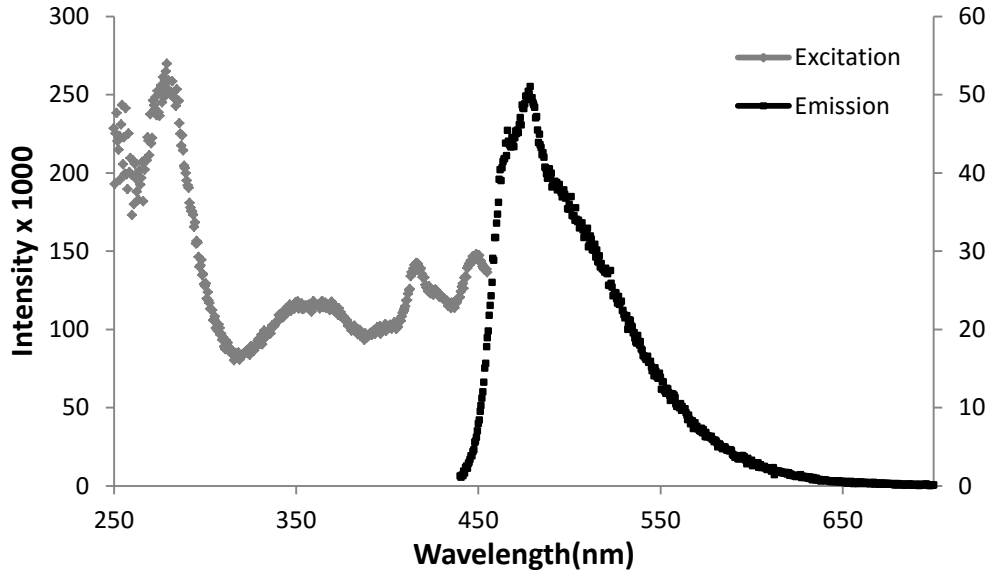


**Figure 5.18:** Steady state excitation (grey) and emission (black) spectra for **5.6**.

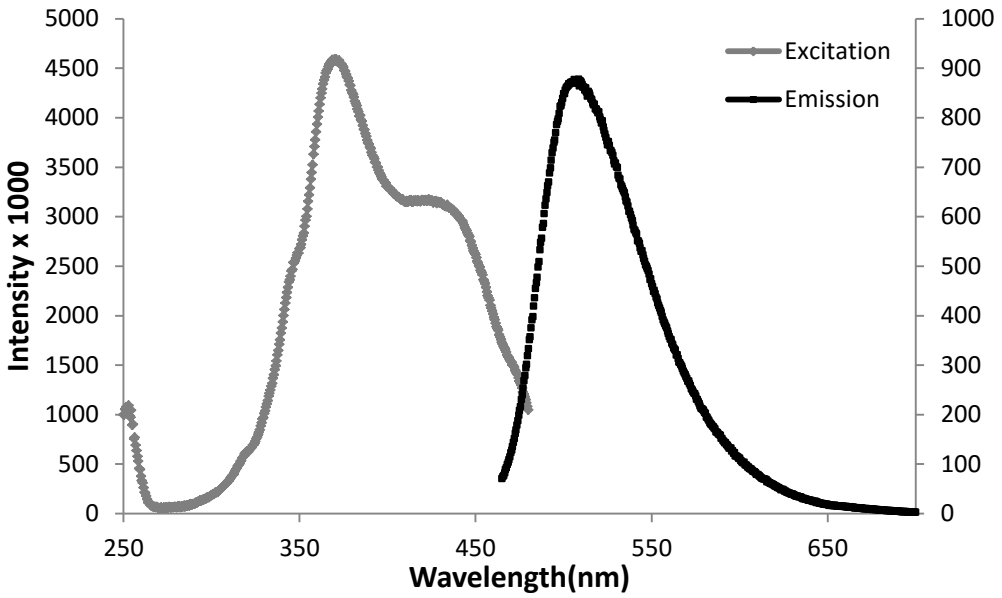


**Figure 5.19:** Steady state excitation (grey) and emission (black) spectra for **5.7**.

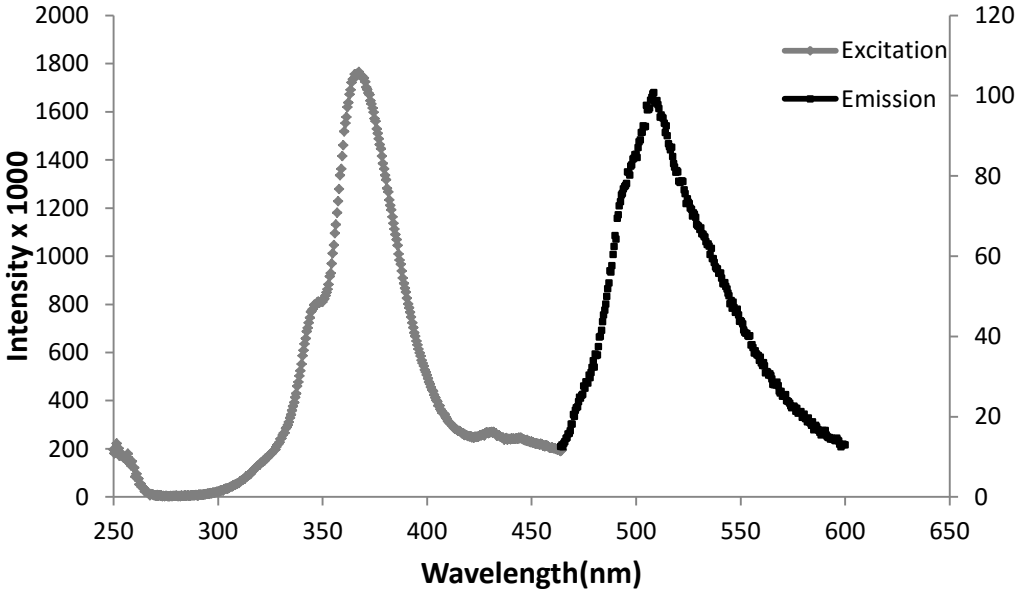


**Figure 5.20:** Steady state excitation (grey) and emission (black) spectra for **5.8**.

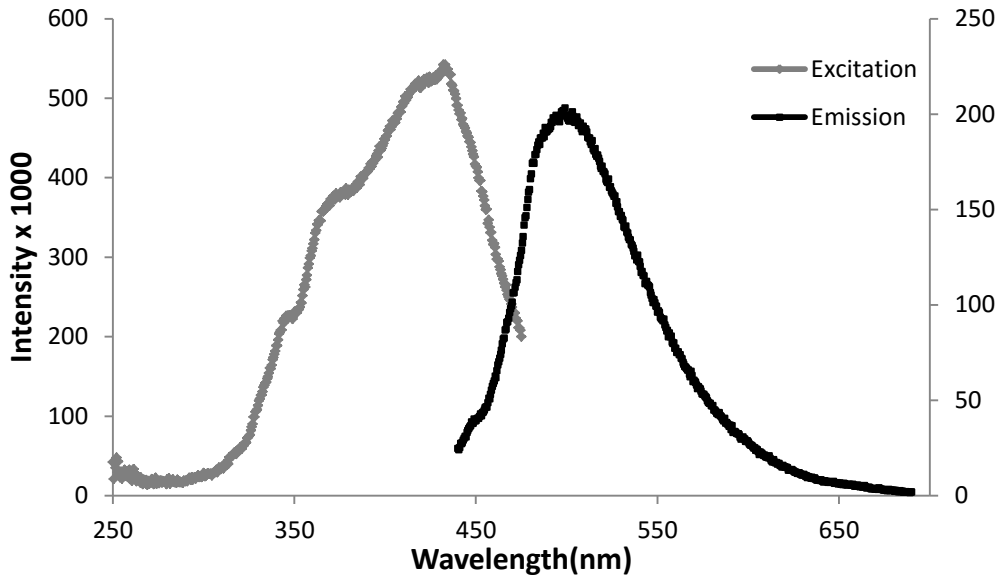


**Figure 5.21:** Steady state excitation (grey) and emission (black) spectra for **5.9**.

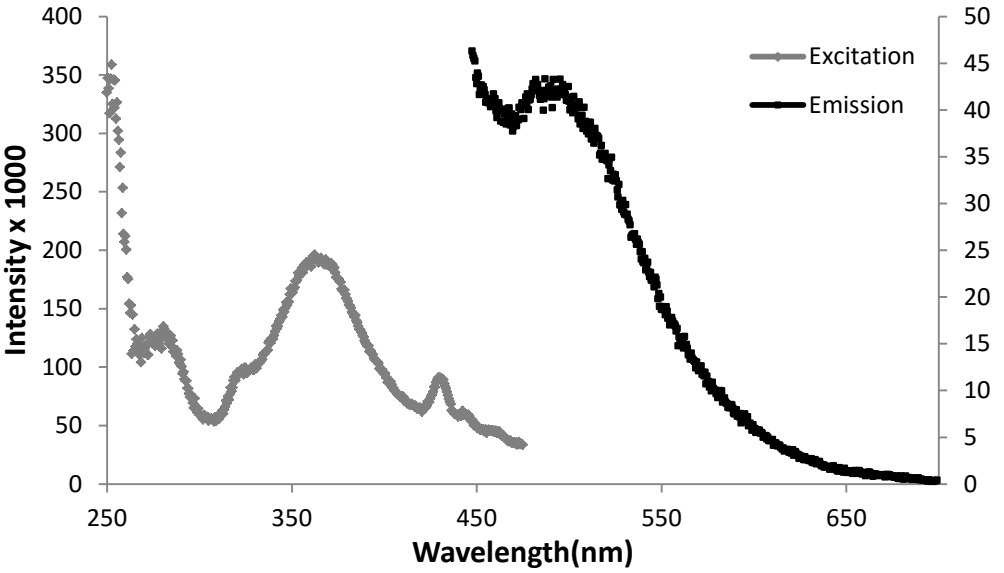


**Figure 5.22:** Steady state excitation (grey) and emission (black) spectra for **5.10**.

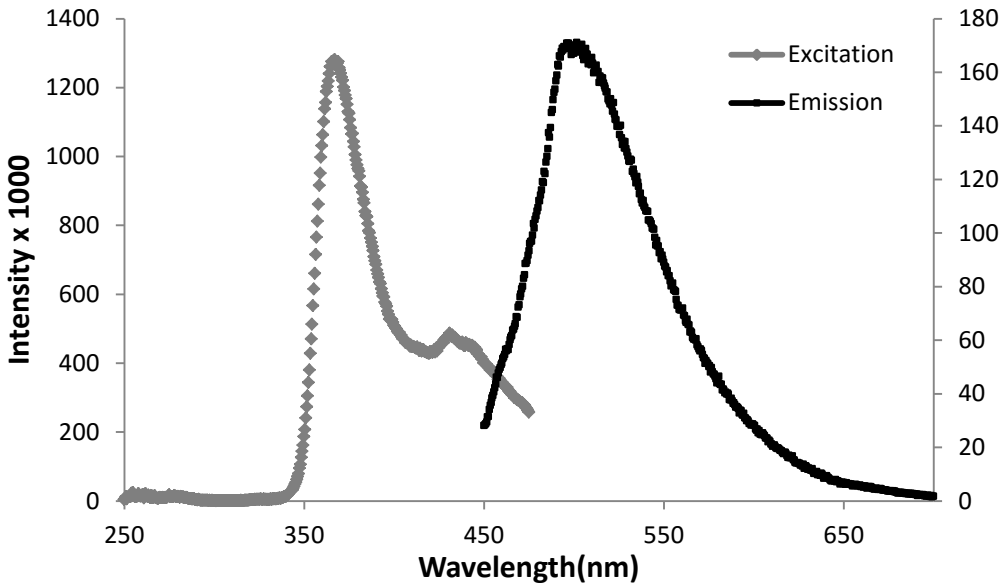


**Figure 5.23:** Steady state excitation (grey) and emission (black) spectra for **5.11**.

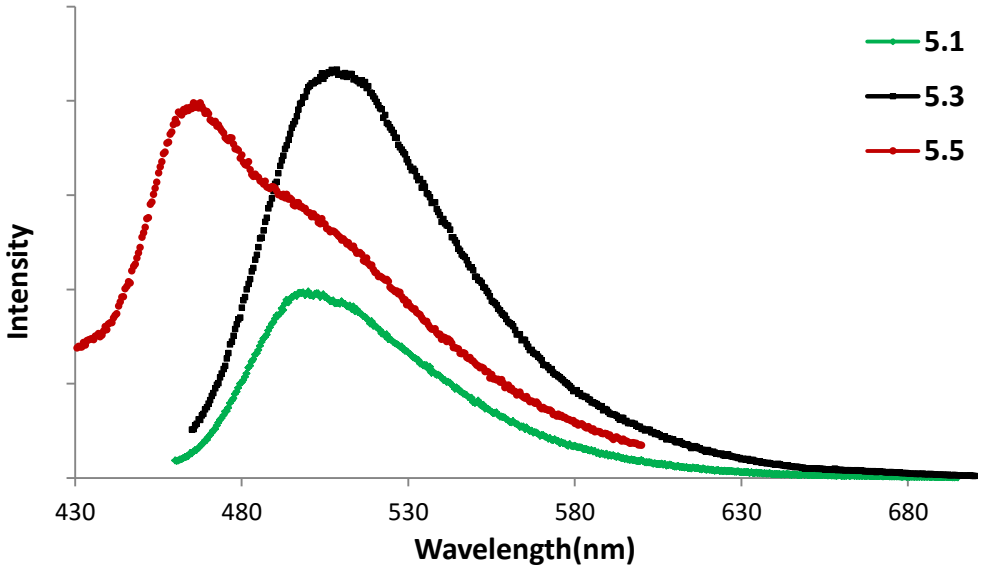


**Figure 5.24:** Emission spectra for **5.1**, **5.3** and **5.5** show their effecting by electron donating and electron withdrawing groups. .

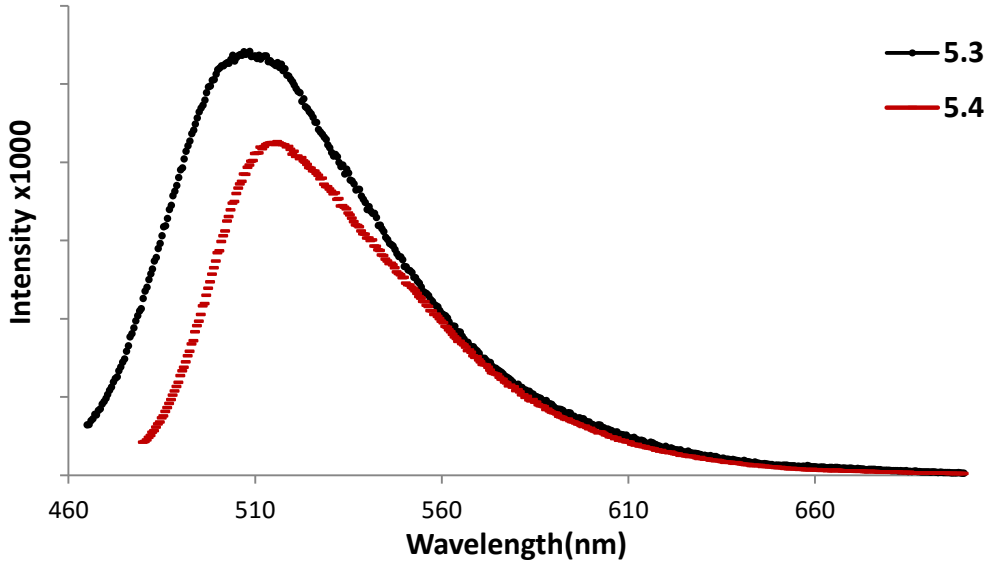


**Figure 5.25:** Emission spectra for **5.3** and **5.4** show their effecting in the presence of two $H_2O$ molecules.

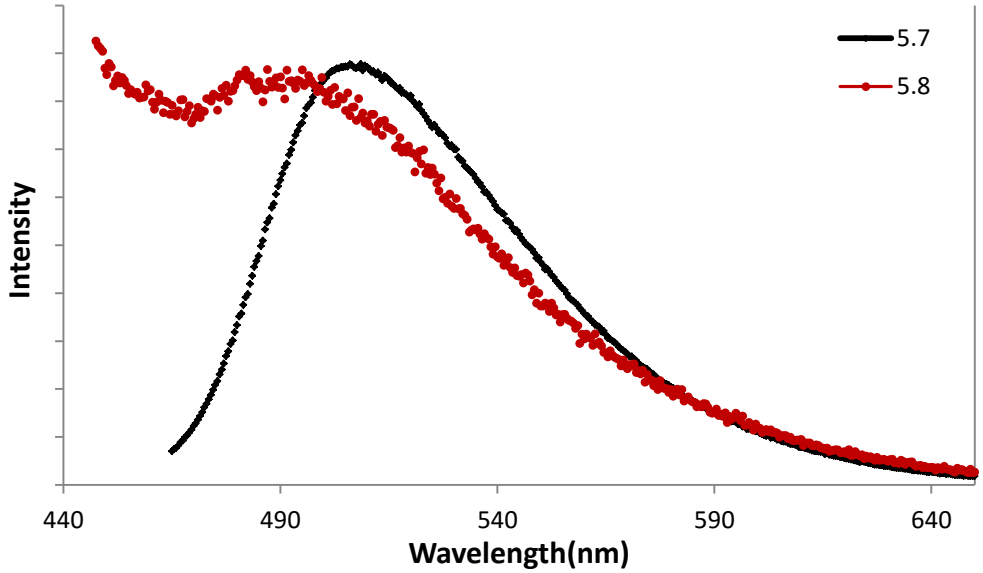


**Figure 5.26:** shows the emission spectra for **5.7** and **5.10** and their effecting by rigidity of phen molecule and the flexibility of bpy molecule.

## 5.3.3 Magnetic susceptibility measurements

The magnetic moment ($\mu_{eff}$) of the Cr(III) complexes were measured by using the Evans' method[48] in DMSO solvent at room temperature and listed in **Table 5.5**. The observed magnetic moment of all Cr(III) complexes (**5.1-5.12**) are 3.73-4.08 B.M. which is consistent with a $d^3$ configuration and corresponds to three unpaired electrons. These magnetic moment values confirmed the paramagnetic and high spin octahedral geometry.[49-53] The magnetic moment of all complexes (**5.1-5.12**) confirmed the presence of a $d^3$, Cr(III) ion and that it is not a $d^4$, Cr(II) ion which is expected to have magnetic moment range (3.2-3.3 B.M) for a $d^4$ low spin ($t_{2g}^4$) or (4.7-4.9 B.M) for a $d^4$ high spin ($t_{2g}^3$ $e_g^1$). **Table 5.5** shows the magnetic data which includes mass magnetic susceptibility, $\chi_{mass}$, molar magnetic susceptibility, $\chi_M$, and magnetic moments $\mu_{eff.}$.

**Table 5.5:** Magnetic data of octahedral Cr(III) complexes (**5.1**-**5.12**).

| **Complex.** | $\chi_{mass}$ **x10$^{-6}$** | $\chi_M$ **x10$^{-6}$** | $\mu_{obs}$ **B.M. experimental** |
|---|---|---|---|
| **5.1** | 14.646 | 6030.93 | 3.785 |
| **5.2** | 13.266 | 6407.26 | 3.863 |
| **5.3** | 14.133 | 6205.094 | 3.839 |
| **5.4** | 11.131 | 5861.03 | 3.731 |
| **5.5** | 12.198 | 6120.58 | 3.813 |
| **5.6** | 9.941 | 6157.95 | 3.825 |
| **5.7** | 8.11 | 6864.46 | 4.038 |
| **5.8** | 7.703 | 6628.81 | 3.968 |
| **5.9** | 7.843 | 6992.02 | 4.075 |
| **5.10** | 8.44 | 6738.92 | 4.000 |
| **5.11** | 7.994 | 6495.00 | 3.928 |
| **5.12** | 7.58 | 6393.35 | 3.890 |

## 5.3.4 Electrochemical studies of the Cr(III) complexes (5.1-5.12)

The electrochemical data for the Cr(III) complexes were performed in acetonitrile using $[Bu_4N][PF_6]$ (0.1 M) as supporting electrolyte. The data is tabulated for all Cr(III) complexes in **Table 5.6**. The cyclic voltammograms of these complexes **(5.1-5.12**) are similar, showing two reversible processes in the reductive regions -1.34 to -1.66 V and -1.91 to -2.17 V (vs $Fc/Fc^+$). These processes are typical to reversible processes with peak to peak separation 59-72 mV (see **Table 5.6**). Furthermore, the ratio of $i_{pc}$ to $i_{pa}$ is ~1, which also supports the reversible nature of these processes. The first potential at (-1.34 to -1.66 V) is attributed to formation of lower metal oxidation state Cr(III)/Cr(II) couple,[54-57] while the second potential at (-1.91 to -2.17 V) is close to the reduction potential of the HQ ligand. This is in good agreement with work reported by Monzon *et al.* for the Cr(III) complex $[Cr(L^1)_3]$ ($L^1$=(8-hydroxyquinoline) which shows two reversible peaks at -1.54 and -2.03 V (VS $Fc/Fc^+$) which is attributed to Cr(III)/Cr(II) couple and electron-transfer reaction involving the quinoline system respectively.[58] As specific observations, the nitro derivatives of Cr(III) complexes are observed at more anodic potentials than the Cr(III) complexes of HQ and its methyl group derivatives. For example, the complex **5.12** showed two reversible peaks at -1.37 and -1.93 V while **5.11** presented them at -1.57 and -2.10 V (VS $Fc/Fc^+$). This may be due to the presence of the strong withdrawing nitro group in **5.12** which leads to a more electropositive Cr(III) ion meaning that it is easier to reduce. The electron donating methyl group behaves oppositely; **Figures 5.27** and **5.28** show the cyclic voltammograms of the complexes **5.3** and **5.4**.

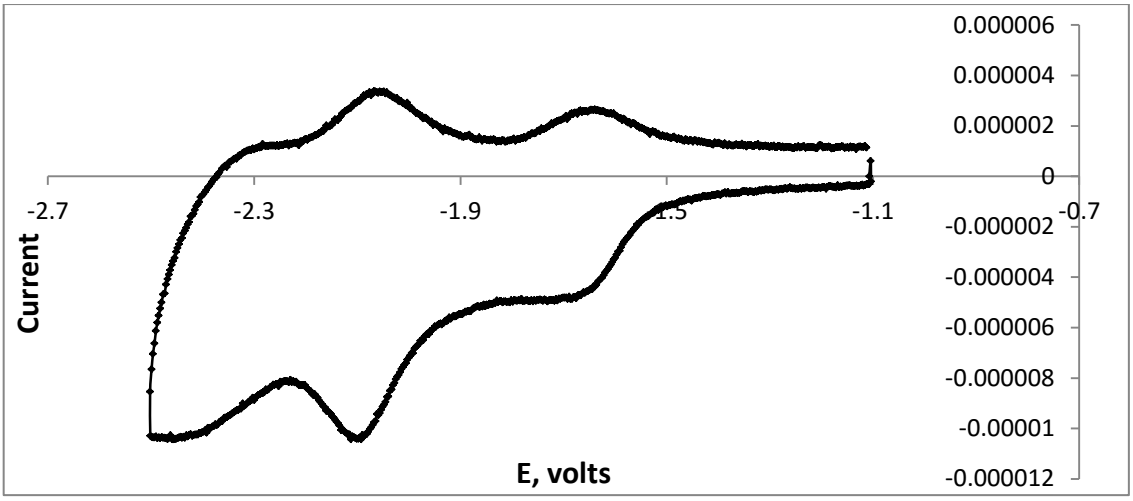


**Figure 5.27**: Cyclic voltammogram of complex **5.3** shows reversible processes.

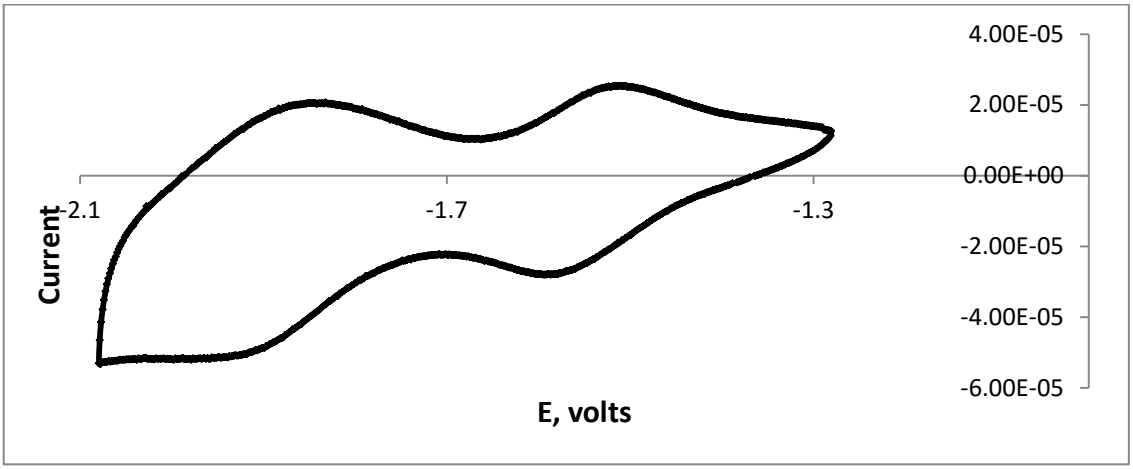


**Figure 5.28**: Cyclic voltammogram of complex **5.6** shows reversible processes.

**Table 5.6:** Electrochemical parameters for the two **reversible** processes exhibited by Cr(III) complexes **(5.1-5.12)** in acetonitrile solution, supporting electrolyte $[Bu_4N][PF_6]$ (0.1 M),T =25º C measured at 100 mv/sec. (Potentials Vs. $Fc/Fc^+$).

| Complex | reversible process (1) | | reversible process (2) | |
|---|---|---|---|---|
| | $E_{1/2}$ V | ΔE mv | $E_{1/2}$ V | ΔE mv |
| **5.1** | -1.48 | 59 | -2.02 | 60 |
| **5.2** | -1.56 | 60 | -2.07 | 61 |
| **5.3** | -1.64 | 62 | -2.14 | 59 |
| **5.4** | -1.66 | 59 | -2.17 | 70 |
| **5.5** | -1.39 | 61 | -1.92 | 63 |
| **5.6** | -1.42 | 70 | -1.95 | 59 |
| **5.7** | -1.46 | 63 | -2.06 | 72 |
| **5.8** | -1.57 | 59 | -2.12 | 74 |
| **5.9** | -1.34 | 71 | -1.91 | 59 |
| **5.10** | -1.43 | 59 | -2.02 | 64 |
| **5.11** | -1.57 | 64 | -2.10 | 60 |
| **5.12** | -1.37 | 60 | -1.93 | 61 |

## 5.3.5 Crystallographic studies

### 5.3.5.1 Crystal structure of $[Cr^{III}(QM)_2(H_2O)_2]Cl.\ 3/2H_2O$ (5.3)

The complex crystallises in the triclinic space group *P-1.* The Cr(III) cation lies at the centre of a slightly distorted octahedral configuration formed from two HQM ligands and two aqua molecules arranged as a cis isomer, see **Figure 5.29**. The CCDC shows that there are 297 Cr(III) complexes coordinated by six donor atoms comprising 2N and 4O. However, only 13 crystal structures of Cr(III) complexes contain the HQ ligand and all of them exhibit six coordinate octahedral geometry.[59-61] It is apparent from **Table 5.7** that the Cr-O41 and Cr-O42 bond lengths are

longer than Cr-O1 and Cr-O11 due to the freedom of movement of the coordinated $H_2O$ molecules which containing the O41 and O42 atoms. Hydrogen bonding with the coordinated $H_2O$ molecule may also elongate it. The Cr-O coordinative bond lengths range from 1.924(3) to 1.995(3) Å, and the Cr-N bond lengths are signeficantly longer and range from 2.094(4) to 2.098(3) Å due to the higher electronegativity of the oxygen atom than the nitrogen atom which reduces the Cr-O bond length. It is typical in Cr(III) complexes coordinated by six donor atoms (2N, 2O and (2O from two $H_2O$ molecules) that the bond length of Cr-O is shorter than Cr-N, and Cr-O shorter than Cr-$OH_2$:Cr-O distances range from 1.917-1.958, and Cr-$OH_2$ range from 1.982-2.006 and Cr-N range from 2.030-2.067 Å.[62-64] Similar bond lengths for Cr-O and Cr-N in **5.3** were observed in octahedral complex $[Cr(QM)(\mu\text{-}HQM)(\mu_3\text{-}OH)(\mu\text{-}OH)(\mu\text{-}CH_3COO)_2\ \{Ln(hfac)_2\}_2]$, HQM = 2-methyl-8-hydroxyquinoline, Ln = Eu, **6**; Tb, **7**; Er, **8** and hfa= hexafluoro acetyl acetonate reported by Xu *et al.*[65] (1.952-2.006 Å) for the four Cr-O bonds and 2.095 Å for two Cr-N bonds. The bond angles O11–Cr1–O1 and O42–Cr1–N11 are 172.41(13)º and 167.57(14)º respectively, (see **Table 5.7**). The pyridyl ring in each HQM is nearly perpendicular to the other HQM molecule (N11-Cr1-N1 91.92(14)º). Two intermolecular hydrogen bonds are observed. First, between the hydrogen atom in the coordinated $H_2O$ and the $Cl^-$ ion (O42–H42B···Cl1 at 2.20 Å), and the other hydrogen bond between the hydrogen atom of the same coordinated $H_2O$ molecule and the oxygen atom in the uncoordinated $H_2O$ (O42–H42A···$O45^i$ and the bond length is 1.72 Å). Furthermore, the uncoordinated $H_2O$ molecule H-bonds with the oxygen atom of HQM (O45–H45A···O11, the bond length is 1.97 Å, see **Figure 5.29**.

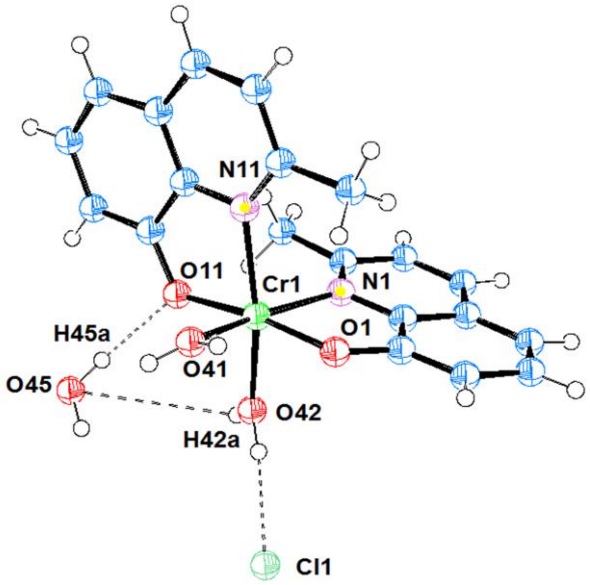


**Figure 5.29:** ORTEP diagram of complex **5.3** showing some atomic numbering scheme.

**Table 5.7:** Selected bond lengths (Å) and bond angles (º) for **5.3**

| | | | |
|---|---|---|---|
| **Bond length (Å)** | | | |
| Cr1–O11 | 1.924(3) | Cr1–O41 | 1.995(3) |
| Cr1–O1 | 1.948(3) | Cr1–N11 | 2.094(4) |
| Cr1–O42 | 1.983(3) | Cr1–N1 | 2.098(3) |
| **Bond Angles (º)** | | | |
| O11–Cr1–O1 | 172.41(13) | O42–Cr1–N11 | 167.57(14) |
| O11–Cr1–O42 | 85.56(13) | O41–Cr1–N11 | 87.02(13) |
| O1–Cr1–O42 | 88.86(13) | O11–Cr1–N1 | 103.14(13) |
| O11–Cr1–O41 | 91.26(12) | O1–Cr1–N1 | 81.88(13) |
| O1–Cr1–O41 | 84.10(12) | O42–Cr1–N1 | 89.09(14) |
| O42–Cr1–O41 | 95.09(13) | O41–Cr1–N1 | 165.29(14) |
| O11–Cr1–N11 | 82.15(15) | N11–Cr1–N1 | 91.92(14) |
| O1–Cr1–N11 | 103.55(15) | | |

### 5.3.5.2 Crystal structure of $[Cr^{III}(phen)_2(Q)] (PF_6)_2.MeCN$ (5.7)

The complex crystallises in the triclinic space group *P-1* and contains a single complex within the asu (**Figure 5.30**). Red crystals of **5.7** were obtained by vapour diffusion of diethyl ether into an acetonitrile solution of the complex. Based on the bond angles about the metal centre which range from 79.86(7)-99.49(7)º and 168.44(7)-175.81(7)º, the geometry of the complex is best considered as a slightly distorted octahedral, see **Table 5.8**. There are five nitrogen and one oxygen donors within the coordination sphere. One of the $PF_6^-$ counter ions is disordered in two positions with the fluorine atoms in the $PF_6^-$ fragment. This disorder is due to the non-directional ionic forces between the organometallic moiety and the $PF_6^-$ anion. As is clear in **Figure 5.30**, two possible orientations for the $PF_6^-$ fragment are observed.

Four of the nitrogen donor atoms (N11, N12, N31 and N32) originate from the two phen molecules while the fifth and sixth coordinating atoms are the nitrogen and oxygen donor atoms, N1 and O1 from HQ molecule. Crystal structure of **5.7** shows each phen molecule perpendicular to the other molecule and the HQ, with bond angles N1-Cr1-N32 93.42(7)º and N11-Cr1-N32 95.41(7)º. From a CCDC search, is relatively unusual for Cr(III) to be surrounded by 5N and 1O in an octahedral geometry. Only 30 compounds with related crystal structures with this donor set have been published,[66-70] but this is the first example of HQ derivatives to be crystallographically characterized with a $N_5O$ coordination sphere around a Cr(III) centre. The Cr-N and Cr-O bond lengths in **5.7** are similar to **5.3** and range from 2.098(3)-2.094(4) Å for Cr-N and is 1.924(3) Å for Cr-O bond. In addition, there is no hydrogen bonding observed in the crystal structure of **5.7** (**Figure 5.30**, **Table 5.8**).

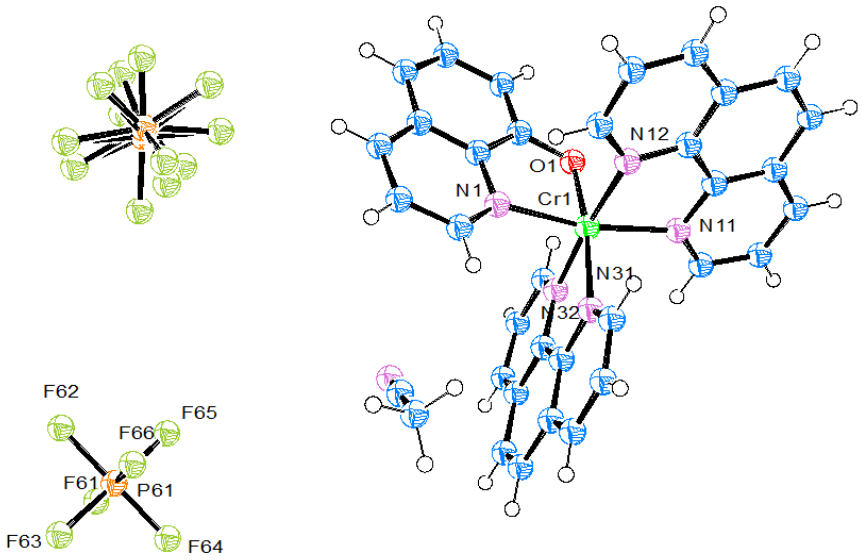


**Figure 5.30:** ORTEP diagram of complex **5.7** showing some atomic numbering scheme.

**Table 5.8:** Selected bond lengths (Å) and bond angles (º) for **5.7**

| | | | |
|---|---|---|---|
| **Bond length (Å)** | | | |
| Cr1–O1 | 1.9090(15) | Cr1–N32 | 2.0528(18) |
| Cr1–N1 | 2.0505(18) | Cr1–N12 | 2.0741(18) |
| Cr1–N11 | 2.0515(18) | Cr1–N31 | 2.0770(18) |
| **Bond Angles (º)** | | | |
| O1–Cr1–N1 | 83.16(7) | N11–Cr1–N12 | 80.53(7) |
| O1–Cr1–N11 | 89.19(7) | N32–Cr1–N12 | 175.81(7) |
| N1–Cr1–N11 | 168.44(7) | O1–Cr1–N31 | 169.84(7) |
| O1–Cr1–N32 | 91.25(7) | N1–Cr1–N31 | 92.40(7) |
| N1–Cr1–N32 | 93.42(7) | N11–Cr1–N31 | 96.48(7) |
| N11–Cr1–N32 | 95.41(7) | N32–Cr1–N31 | 79.86(7) |
| O1–Cr1–N12 | 89.74(7) | N12–Cr1–N31 | 99.49(7) |
| N1–Cr1–N12 | 90.74(7) | | |

### 5.3.5.3 Crystal structures of $[Cr^{III}(bpy)_2(QM)](PF_6)_2.H_2O$ (5.11) and $[Cr^{III}(bpy)_2(QN)](PF_6)_2.2$ MeCN (5.12)

Red crystals of **5.11** were obtained by vapour diffusion of diethyl ether into an acetonitrile solution of the complex. The complex crystallises in the monoclinic space group $P2_1/n$ and contains a single complex within the asu (**Figure 5.31**). Similar to the coordination style in **5.7**, the Cr(III) ion is surrounded by five nitrogen and one oxygen atoms within the coordination sphere, with two $PF_6^-$ counter ions within the lattice framework. One of the $PF_6^-$ counter ions is again disordered as reported in **5.7**, and for the same reason. Two molecules of bpy coordinate through (N11, N12, N21 and N22) while the fifth and sixth coordinating atoms are the N1 and O1 from HQM molecule. **5.11** shows a slightly distorted octahedral geometry which is similar to **5.7** and in the same range of the bond angles about the Cr(III) ion 78.16(8)-103.00(7)º and 166.78(7)-173.33(7)º (see **Table 5.9**). Complex **5.12** is similar to the octahedral geometry of **5.11**, except HQN is used instead of HQM (see **Table 5.10** and **Figure 5.32**). Crystallographic data are reported in **Table 5.11**.

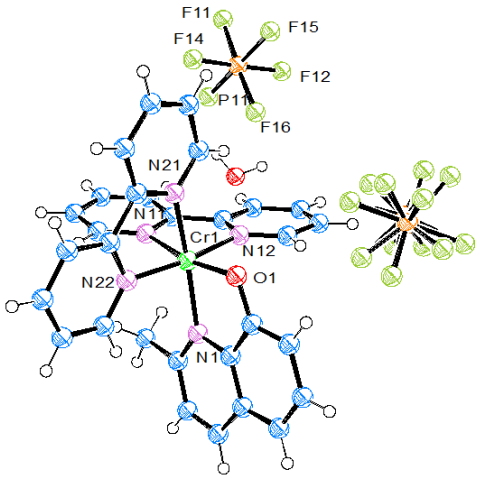


**Figure 5.31:** ORTEP diagram of complex **5.11** showing some atomic numbering scheme.

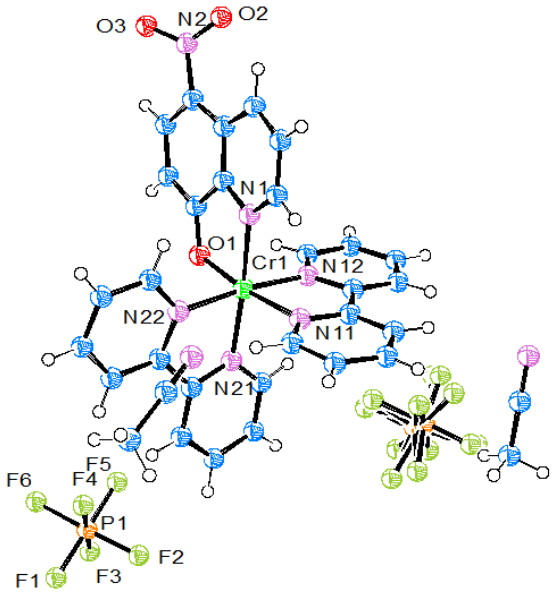


**Figure 5.32:** ORTEP diagram of complex **5.12** showing some atomic numbering scheme.

**Table 5.9:** Selected bond lengths (Å) and bond angles (º) for **5.11**

| | | | |
|---|---|---|---|
| **Bond length (Å)** | | | |
| Cr1–O1 | 1.9034(15) | Cr1–N22 | 2.0746(19) |
| Cr1–N21 | 2.0491(18) | Cr1–N11 | 2.0755(18) |
| Cr1–N12 | 2.0582(19) | Cr1–N1 | 2.0870(18) |
| **Bond Angles (º)** | | | |
| O1–Cr1–N21 | 88.41(7) | N12–Cr1–N11 | 78.16(8) |
| O1–Cr1–N12 | 92.26(7) | N22–Cr1–N11 | 96.23(7) |
| N21–Cr1–N12 | 96.76(8) | O1–Cr1–N1 | 83.20(7) |
| O1–Cr1–N22 | 92.94(7) | N21–Cr1–N1 | 166.78(7) |
| N21–Cr1–N22 | 79.22(7) | N12–Cr1–N1 | 93.78(7) |
| N12–Cr1–N22 | 173.33(7) | N22–Cr1–N1 | 90.99(7) |
| O1–Cr1–N11 | 168.80(7) | N11–Cr1–N1 | 103.00(7) |
| N21–Cr1–N11 | 87.02(7) | | |

**Table 5.10:** Selected bond lengths (Å) and bond angles (º) for **5.12**

| | | | |
|---|---|---|---|
| **Bond length (Å)** | | | |
| Cr1–O1 | 1.917(2) | Cr1–N12 | 2.047(3) |
| Cr1–N1 | 2.041(3) | Cr1–N21 | 2.049(3) |
| Cr1–N22 | 2.047(2) | Cr1–N11 | 2.061(3) |
| **Bond Angles (º)** | | | |
| O1–Cr1–N1 | 82.19(10) | N22–Cr1–N12 | 173.42(10) |
| O1–Cr1–N22 | 89.74(10) | N22–Cr1–N21 | 79.47(10) |
| N1–Cr1–N22 | 97.16(10) | O1–Cr1–N21 | 95.41(10) |
| O1–Cr1–N12 | 94.18(10) | N1–Cr1–N21 | 175.90(10) |
| N1–Cr1–N12 | 88.62(10) | N12–Cr1–N21 | 94.88(10) |
| N12–Cr1–N11 | 79.07(11) | N22–Cr1–N11 | 97.35(10) |
| O1–Cr1–N11 | 172.22(10) | N11–Cr1–N1 | 93.69(10) |
| N21–Cr1–N11 | 89.07(10) | | |

**Table 5.11:** Crystallographic data for of $[Cr^{III}(QM)_2(H_2O)_2]Cl.3/2H_2O$ **(5.3)**, $[Cr^{III}(phen)_2(Q)](PF_6)_2.MeCN$ **(5.7**), $[Cr^{III}(bpy)_2(QM)](PF_6)_2.H_2O$ **(5.11)** and $[Cr^{III}(bpy)_2(QN)](PF_6)_2.2MeCN$ **(5.12)**

| **Compound** | **5.3** | **5.7** | **5.11** | **5.12** |
|---|---|---|---|---|
| **Chemical Formula** | $C_{20}H_{23}ClCrN_2O_{5.50}$ | $C_{35}H_{25}CrF_{12}N_6OP_2$ | $C_{30}H_{26}CrF_{12}N_5O_2P_2$ | $C_{33}H_{27}CrF_{12}N_8O_3P_2$ |
| **Mr. g.mol$^{-1}$** | 466.85 | 887.55 | 830.50 | 925.56 |
| **Crystal system** | Triclinic | Triclinic | Monoclinic | Triclinic |
| **Space group** | *P*–1 | *P*–1 | $P2_1/n$ | *P*–1 |
| **T(K)** | 100(2) | 100(2) | 100(2) | 100(2) |
| **a, Å** | 12.0542(8) | 10.3697(7) | 10.0548(3) | 9.7304(3) |
| **b, Å** | 12.1609(9) | 12.7892(9) | 14.2079(3) | 12.3940(5) |
| **c, Å** | 14.9483(10) | 14.8184(10) | 23.8326(5) | 17.3435(5) |
| **α, degree** | 88.512(5) | 101.290(4) | 90° | 107.542(3)° |
| **β, degree** | 84.401(5) | 96.941(4) | 101.681(2)° | 95.630(2)° |
| **γ, degree** | 82.019(5) | 111.476(4) | 90° | 109.673(3)° |
| **Z** | 4 | 2 | 4 | 2 |
| **Dc. Mg/m$^3$** | 1.436 | 1.681 | 1.654 | 1.679 |
| **μ($M_O$ K α), mm$^{-1}$** | 0.689 | 0.523 | 0.545 | 0.510 |
| **Reflections collected** | 31525 | 27800 | 47627 | 29457 |
| **Unique reflections** | 9809 | 8022 | 7631 | 8439 |
| **$R_{int}$** | 0.0782 | 0.0513 | 0.0355 | 0.0295 |
| **R1[I>2σ<(I)]** | 0.0786 | 0.0485 | 0.0462 | 0.0644 |
| **wR2(all data)** | 0.2035 | 0.1385 | 0.1309 | 0.1920 |

## 5.4 Conclusion

The synthesis and characterization of 12 Cr(III) complexes with HQ derivatives (**5.1**-**5.12**) are presented. The synthesized complexes have been fully characterized using methods such as low and high resolution mass spectrometry, IR, UV-vis and luminescence spectroscopies, and analytical techniques such as room temperature magnetic susceptibility measurements, cyclic voltammetry as well as elemental analysis. The molecular structures of **5.3**, **5.7**, **5.11** and **5.12** have been confirmed by X-ray crystallography which show the anticipated coordination geometry around Cr(III). The optical properties were investigated of the Cr(III) complexes (**5.1**-**5.12**) by photoluminescence studies. The results of the lifetimes (<10 nanosecond) and the observation of one emission peak at 463-511 nm for all these complexes suggest that emission is due to ligand centred fluorescence, which is consistent with the more common Al(III) species of HQ derivatives. One of the more significant findings to emerge from this study is the tuneability of the luminescence wavelength. These findings show that **5.3**, **5.4**, **5.8** and **5.11** have a red shifted emission as compared with **5.1**, **5.2**, **5.7** and **5.10** due to the methyl group. **5.5**, **5.6**, **5.9** and **5.12** exhibit a blue shift due to the presence of a $NO_2$ group. The photoluminescence studies also show that Cr(III) complexes with two coordinated $H_2O$ molecules (**3.1**, **3.3** and **3.5**) retain good emission properties. Cyclic voltammetry (CV) in acetonitrile solutions showed two reversible processes in the reductive region at -1.34 to -1.66 V and -1.91 to -2.17 V (vs $Fc/Fc^+$). The first potential at -1.34 to -1.66 V is attributed to the Cr(III)/Cr(II) couple while the second potential at -1.91 to -2.17 V is a HQ reduction. It is noticed from the CV that the nitro derivatives were observed at less reductive potentials than the Cr(III) complexes of HQ and its methyl derivative. In summary a new series of paramagnetic Cr(III) complex has been reported which shows tuneable visible luminescence properties and ease of further functionalization at the coordination sphere through the use of labile ligands.

**5.5 Future work:** We are so interesting in the possibal act of the acyl thiourea and thiosemicarbazone derivatives and their complexes in the biological fields. So we are going to test them as antibacterial, antimalarial and antifungal.

## 5.6 References


**(1)** P. A. Adlard, R. A. Cherny, D. I. Finkelstein, E. Gautier, E. Robb, M. Cortes, I. Volitakis, X. Liu and J. P. Smith, Rapid restoration of cognition in Alzheimer's transgenic mice with 8-hydroxyquinoline analogs is associated with decreased interstitial Abeta., *Neuron*, **2008**, 59, 43-55.

**(2)** M. A. Saleh, M. F. Abdel Megeed, M. A. Aldo and A. M. Shokr, *Molecules*, **2003**, 8, 363-373.

**(3)** M. I. Mohamed, G. Krishnamoorthy and B. R. Venkatraman, *Res. J. Chem. Environ.*, **2006**, 10(*4*), 93-96.

**(4)** R. Musiol, J. Jampilek, K. Kralova, B. Podeszwa, J. Finster and J. Palanski, "New quinoline derivatives possessing herbicidal activity", *IX International Electronic Conference on Synthetic Organic Chemistry*, Poland, **2005**.

**(5)** S. N. Pandeya, V. S. Lakshmi and A. Pandey, *Indian J. Phama. Sci.,* **2003**, 65(*3*), 213.

**(6)** M. M. Mashaly, Z. H. Abd-Elwahabb and A. A. Faheimb, *J. Chin. Chem. Soc.*, **2004**, 51(*5*), 901-915.

**(7)** M. Thirumalaikumar, S. Sivakolunthu, A. Ponnuswamy and S. Sivasubramanian, *Ind. J. Chem.*, **1999**, 38(*7*), 720-722.

**(8)** H. E. Howard-Lock and C. J. L. Lock, "Uses in therapy," *in Comprehensive Coordination Chemistry*, G. Wilkinson, R. D. Gillard and J. A. McCleverty, Eds., Pergamon Press, Oxford, UK, **1987**, 6, 755.

**(9)** S. S. Patil, G. A. Thakur and M. M. Shaikh, *ISRN Pharm.*, **2011**, 2011, 1–6.

**(10)** S. Elmas, M. A. Subhani, M. Harrer, W. Leitner, J. Sundermeyer and T. E. Muller, *Catal.Sci.Technol.*, **2014**, 4, 1652-1657.

**(11)** F. Chen, X. Lu, X. Chen, H. Li and Y.Hu, *Inorg. Chim. Acta,* **2012**, 387, 407-411.

**(12)** X. Lu, H. Yang and X. Chen, *Chin. J. Struct. Chem.*, **2009**, 28(*6*), 673-676.

**(13)** W. A. Wickaramasinghe, P. H. Bird, M. A. Jamieson, N. Serpone and M. Maestri, *Inorganica Chimica Acta*, **1982**, 64(*2*), 85-86.

**(14)** M. Ardon and A. Bino, *J. Am. Chem. Soc.*, **1983**, 105(*26*), 7747-7748.

**(15)** L. Andros, M. Juric, K. Molcanov and P. Planinic, *Dalton Trans.,* **2012**, 41(*48*), 14611-14624.

**(16)** E. Coronado, M. C. Gimenez, C. J. Garcia and F. M. Romero, *Polyhedron*, **2003**, 22(*23*), 3115-3122.

**(17)** L. J. Batchelor, M. Sander, F. Tuna, M. Helliwell, F. Moro and E. J. Mclnnes, *Dalton Trans*, **2011**, 40(*19*), 5278-5284.

**(18)** Y. Tong and Y. Lin, *Inorg. Chim. Acta*, **2009**, 362(*7*), 2167-2171.

**(19)** S. Vasudevan, J. A. Smith, M. Wojdyla, T. McCabe, N. C. Fletcher, S. J. Quinn and J. M. Kelly, *Dalton Trans,* **2010**, 39(*16*), 3990-3998.

**(20)** W. Chen and J. Mi, *Polyhedron*, **2015**, 85, 117-123.

**(21)** L. Andros, M. Juric, J. Popovic, D. Pajic, K. Zadro, K. Molcanov, D. Zilic and P. Planinic, *Eur. J. Inorg. Chem.*, **2014**, 5703-5713.

**(22)** S. Nastase, C. Maxim, F. Tuna, C. Duhayon, J. P. Sutter and M. Andruh, *Polyhedron*, **2009**, 28(*9*), 1688-1693.

**(23)** C. M. Grant, B. J. Stamper, M. J. Knapp, K. Folting, J. C. Huffman, D. N. Hendrickson and G. Christou., *J. Chem. Soc. Dalton.Trans.*, **1999**, 19, 3399-3405.

**(24)** M. Molina, P. A. Luis, C. Perez, F. Lloret and M. Julve, *Inorganica Chemica Acta*, **2001**, 313(*1*), 87-94.

**(25)** A. C. Baro, R. Diez, O. E. Piro and B. S. Costa, *Polyhedron*, **2008**, 27(*2*), 502-512.

**(26)** S. Zhang, S. Jie, Q. Shi and W. Sun, *J. Mol. Catal. :A. Chem.*, **2007**, 276(*1*), 174-183.

**(27)** J. M. Schönle, Synthesis and Characterisation of Chromium(III) Complexes with Polypyridyl Ligands, PhD thesis , Basel, **2014**.

**(28)** L. S. Forster, *Chem. Rev*., **1990**, 90, 331-353.

**(29)** V. Balzani, G. Bergamini, S. Campagna and F. Puntoriero, *Top Curr Chem*, **2007**, 37-67.

**(30)** M. Maestri, F. Bolletta, L. Moggi, V. Balzani, M. S. Henry and M. Z. Hoffman, *J. Am. Chem. Soc,* **1978**, 100, 2694-2701.

**(31)** E. König and S. Herzog, *J. Inorg. Nucl. Chem.,* **1970**, 32, 585-599.

**(32)** R. A. Marusak, K. Doan and S. D. Cummings, *Integrated approach to coordination chemistry an inorganic laboratory guide*, WILEY-INTERSCIENCE, Hoboken, 1st edn., **2007**, pp. 202-206.

**(33)** A.B.P. Lever, *INORGANIC ELECTRONIC SPECTROSCOPY*, second eddition, (Amsterdam: Elsevier), **1986**, 534.

**(34)** A. R. Freitas, M. Silva, M. L. Ramos, L. L. G. Justino, S. M. Fonseca, M. M. Barsan, C. M. A. Brett, M. R. Silva and H. D. Burrows, *Dalt. Trans.*, **2015**, 44, 11491–11503.

**(35)** A. Beran and E. Libowitzky, Spectroscopic Methods in Mineralogy, Eötvös University Press, Budapest, **2004**.

**(36)** M. M. Shi, J. J. Lin, Y. W. Shi, M. Ouyang, M. Wang and H. Z. Chen, *Materials chemistry and physics*, **2009**, 115, 841-845.

**(37)** P. E. Burrows, Z. Shen, V. Bulovic, M. McCarty, S. R. Forrest, J. A. Cronin and M. E. Thompson, *J. Appl. Phys.*, **1996**, 79, 7991-8006.

**(38)** A. Curioni, M. Boero and W. Andreoni, *Chem. Phys. Lett*., **1998**, 294, 263-271.

**(39)** T. A. Hopkins, K. Meerholz, S. Shaheen, M. L. Anderson, A. Schmidt, B. Kippelen, A. B. Padias, H. K. Hall, N. Peyghambarian and N. R. Armstrong, *Chem. Mater.*, **1996**, 8(*2*), 344-351.

**(40)** M. M. Duvenhage, H. G. Visser, O. M. Ntwaeaborwa and H. C. Swart, *Phys. B Condens. Matter*, **2014**, 439, 46–49.

**(41)** K. Singh, A. Kumar, R. Srivastava, P. S. Kadyan, M. N. Kamalasanan and I. Singh, *Opt. Mater*., **2011**, 34, 221-227.

**(42)** L. S. Hung and C. H. Chen, *Mater. Sci. Eng.*, **2002**, 39, 143-222.

**(43)** T. Sano, Y. Nishio, Y. Hamada, H. Takahashi, T. Usuki and K. Shibata, *J. Mater. Chem.*, **2000**, 10, 157-161.

**(44)** D. Singh, K. Singh, S. Bhagwan, R. K. Saini, P. S. Kadyan and I. Singh, *J. Luminescence*, **2016**,169, 9–15.

**(45)** Y. Qin, I. Kiburu, S. Shah and F. Jakle, *Org. Lett.*, **2006**, 8, 5227-5230.

**(46)** J. Kwak, O. Choi, E. Sim and S. Lee, *Analyst*, **2015**, 140, 5354-5360.

**(47)** L. S. Sapochak, A. Padmaperuma, N. Washton, F. Endrino, G. T. Schmett, J. Marshall, D. Fogerty, P. E. Burrows and S. R. Forrest, *J. Am. Chem. Soc.*, **2001**, 123, 6300-6307.

**(48)** D. F. Evans, *J. Chem. Soc.*, **1959**, 2003–2005.

**(49)** F. A. Cotton and G. Wilkinson. "Advanced Inorganic Chemistry'' 3rd edn, Jon Wiley and Sons, *Inorganic Chem*. **1972**, 11, 838-844.

**(50)** A. M. A. Alaghaz, H. A. Bayoumi, Y. A. Ammar and S. A. Aldhlmani, *J Molec Struct.*, **2013**, 1035, 383– 399.

**(51)** A. M. A. Alaghaz and R. A. Ammar, *Eur. J. Med. Chem.*, **2010**, 45, 1314–1322.

**(52)** C. M. Sharaby, *Spectrochim. Acta*, **2007**, 66, 1271–1278.

**(53)** S. Chandra and S. Verma, *J. Inorg. Nucl. Chem*., **1975**, 37, 2429–2434.

**(54)** C. Combellas, F. Kanoufi, M. Stoytcheva and A. Thiebault, *J. Phys. Chem. B,* **2004**, 108, 2756.

**(55)** A. J. Fry, *Tetrahedron*, **2006**, 62, 6558-6565.

**(56)** S. Santi, L. Orian, C. Durante, A. Bisello, F. Benetollo, L. Crociani, P. Ganis and A. Ceccon, *Chem. Eur. J.* **2007**, 13, 1955-1968.

**(57)** S. V. Rosokha, D. Sun, J. Fisher and J. K. Kochi, *Chem. Phys.,* **2008**, 9, 2406-2413.

**(58)** L. M. A. Monzon, F. Burke and J. M. D. Coey, *J. Phys. Chem. C.,* **2011**, 115, 9182–9192

**(59)** N. Takenaka, G. Xia and H. Yamamoto, *J.AM.Chem.Soc.,* **2004**,126, 13198-13199.

**(60)** X. Lu, H. Yang and X. Chen, *Chin.J.Struct. Chem.,* **2009**, 28(*6*), 673-676.

**(61)** F. Chen, X. Lu, X. Chen, H. Li and Y. Hu, *Inorg.Chim.Acta,* **2012**, 387, 407-411.

**(62)** Kanthimathi, D. Jebanesan and B. U. Nair, *Transition Metal Chemistry*, **2002**, 27, 895–901.

**(63)** E. G. Petkova, R. D. Lampeka, M. V. Gorichko, G. V. Palamarchuk and *Z.Naturforsch, B. Chem.Sci.,* **2008**, 63, 841.

**(64)** J. Song, Y. Chen, Z. Li, R. Zhou, X. Xu, J. Xu and T. Wang, *Polyhedron*, **2007**, 26, 4397–4410.

**(65)** H. Xu, J. Li, L. Zhang, X. Huang, B. Li and Z. Chen, *Cry. Growth Des.,* **2010**, 10, 4101.

**(66)** A. L. Barra, A. Dossing, T. Morsing and J. Vibenholt, *Inorg. Chim.Acta*, **2011**, 373(*1*), 266-269.

**(67)** N. J. Nichols, G. D. Fallon, B. Moubaraki, K. S. Murray and B. O .West, *Polyhedron*, **1993**, 12(*18*), 2205-2213.

**(68)** R. Harada, Y. Mustada, H. Ökawa, R. Miyamoto, S. Yamauchi and T. Kojima, *Inorg. Chim. Acta*, **2005**, 358(*8*), 2489-2500.

**(69)** Z. Ni, H. Kou, L. Zhang, C. Ge, R. Wang and A. Cui, *J.Chem.Cryst.,* **2006**, 36(*8*), 465-472.

**(70)** P. Albores, L. D. Slep, T. Weyhermuller, E. Rentschler and L. M. Baraldo, *Dalton Trans.*, **2006**, 7, 948-954.

# Appendix: x-ray crystal structure data

## Tables of Bond Distances and Angles

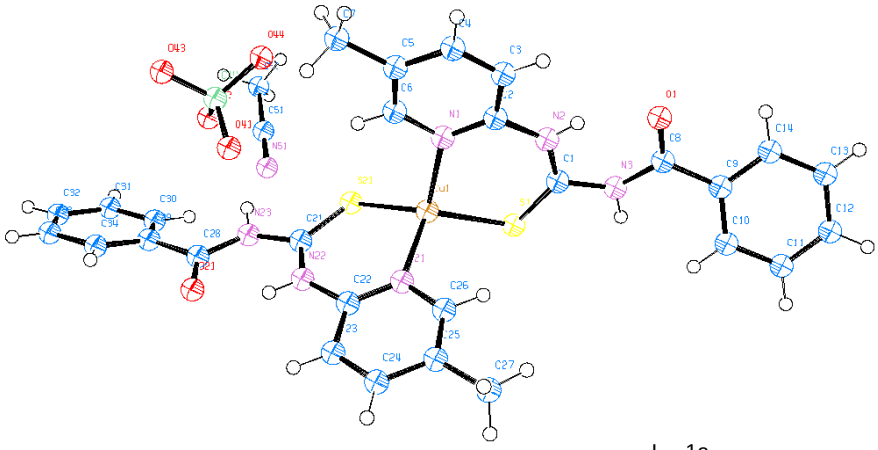

**Table A.1:** Crystal data and structure refinement for [ $Cu^{I}(L^{1a})_2$ ]($ClO_4$).$CH_3CN$ **2.1**

| | |
|---|---|
| Identification code | **2014ncs0359 / ALI-$L_1$Cu-P113** |
| Empirical formula | $C_{30}H_{29}ClCuN_7O_6S_2$ |
| Formula weight | 746.71 |
| Temperature | 100(2) K |
| Wavelength | 0.71075 Å |
| Crystal system | Monoclinic |
| Space group | $P2_1/n$ |
| Unit cell dimensions | $a$ = 15.4602(11) Å $\alpha$ = 90° |
| | $b$ = 9.7669(7) Å $\beta$ = 109.196(2)° |
| | $c$ = 21.9107(15) Å $\gamma$ = 90° |
| Volume | 3124.5(4) $Å^3$ |
| $Z$ | 4 |
| Density (calculated) | 1.587 Mg / $m^3$ |
| Absorption coefficient | 0.975 $mm^{-1}$ |
| $F(000)$ | 1536 |
| Crystal | Needle; Red |
| Crystal size | 0.270 × 0.030 × 0.020 $mm^3$ |
| $\theta$ range for data collection | 3.362 – 27.485° |
| Index ranges | $-14 \le h \le 20$, $-11 \le k \le 12$, $-28 \le l \le 24$ |
| Reflections collected | 20493 |
| Independent reflections | 7132 [$R_{int}$ = 0.0530] |
| Completeness to $\theta$ = 25.242° | 99.6 % |
| Absorption correction | Semi–empirical from equivalents |
| Max. and min. transmission | 1.000 and 0.545 |
| Refinement method | Full-matrix least-squares on $F^2$ |
| Data / restraints / parameters | 7132 / 0 / 443 |
| Goodness-of-fit on $F^2$ | 1.024 |
| Final $R$ indices [$F^2 > 2\sigma(F^2)$] | $R1$ = 0.0440, $wR2$ = 0.1029 |
| $R$ indices (all data) | $R1$ = 0.0701, $wR2$ = 0.1136 |
| Extinction coefficient | n/a |
| Largest diff. peak and hole | 0.398 and –0.571 e $Å^{-3}$ |

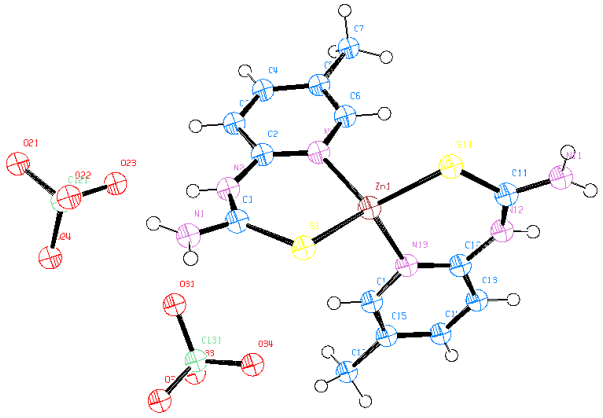

**Table B.1:** Crystal data and structure refinement for $[Zn^{II}(L^{1C})_2](ClO_4)_2$ **2.4.**

| | | |
|---|---|---|
| Identification code | **2014ncs0935 / $L_1$Zn-16/11** | |
| Empirical formula | $C_{14}H_{18}Cl_2N_6O_8S_2Zn$ | |
| Formula weight | 598.73 | |
| Temperature | 100(2) K | |
| Wavelength | 0.71075 Å | |
| Crystal system | Monoclinic | |
| Space group | $P2_1$ | |
| Unit cell dimensions | $a$ = 5.1243(2) Å | $\alpha$ = 90° |
| | $b$ = 11.4452(3) Å | $\beta$ = 91.109(3)° |
| | $c$ = 18.1830(5) Å | $\gamma$ = 90° |
| Volume | 1066.21(6) Å$^3$ | |
| $Z$ | 2 | |
| Density (calculated) | 1.865 Mg / m$^3$ | |
| Absorption coefficient | 1.656 mm$^{-1}$ | |
| *F(000)* | 608 | |
| Crystal | Prism; Colourless | |
| Crystal size | 0.110 × 0.060 × 0.050 mm$^3$ | |
| $\theta$ range for data collection | 2.103 – 27.548° | |
| Index ranges | $-6 \le h \le 6$, $-14 \le k \le 14$, $-23 \le l \le 23$ | |
| Reflections collected | 7361 | |
| Independent reflections | 7361 [$R_{int}$ = ?] | |
| Completeness to $\theta$ = 25.242° | 99.9 % | |
| Absorption correction | Semi–empirical from equivalents | |
| Max. and min. transmission | 1.00000 and 0.80208 | |
| Refinement method | Full-matrix least-squares on $F^2$ | |
| Data / restraints / parameters | 7361 / 1 / 301 | |
| Goodness-of-fit on $F^2$ | 1.131 | |
| Final $R$ indices [$F^2 > 2\sigma(F^2)$] | $R1$ = 0.0323, $wR2$ = 0.1060 | |
| $R$ indices (all data) | $R1$ = 0.0330, $wR2$ = 0.1102 | |
| Absolute structure parameter | 0.021(9) | |
| Extinction coefficient | n/a | |
| Largest diff. peak and hole | 0.553 and –0.420 e Å$^{-3}$ | |

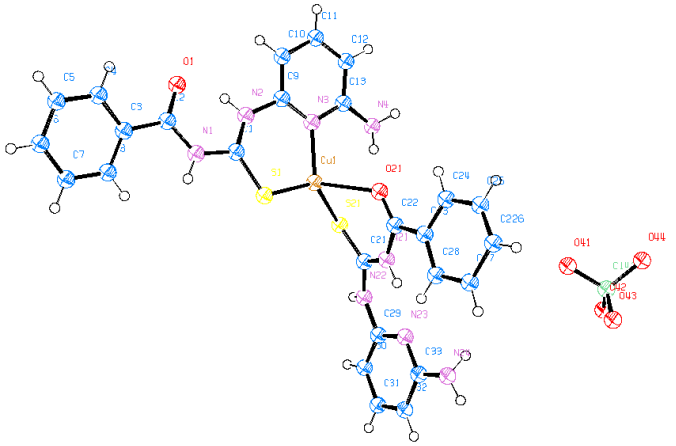

**Table C.1:** Crystal data and structure refinement for $[Cu^{I}(L^{2a})_2](ClO_4)$ **2.6**

| | |
|---|---|
| Identification code | **2014ncs0429 / ALI-$L_2$Cu-P70** |
| Empirical formula | $C_{26}H_{24}ClCuN_8O_6S_2$ |
| Formula weight | 707.64 |
| Temperature | 100(2) K |
| Wavelength | 0.71075 Å |
| Crystal system | Monoclinic |
| Space group | $P2_1/c$ |
| Unit cell dimensions | $a$ = 10.4870(7) Å $\alpha$ = 90° |
| | $b$ = 17.9141(13) Å $\beta$ = 106.4260(10)° |
| | $c$ = 15.3930(11) Å $\gamma$ = 90° |
| Volume | 2773.8(3) Å$^3$ |
| $Z$ | 4 |
| Density (calculated) | 1.695 Mg / m$^3$ |
| Absorption coefficient | 1.094 mm$^{-1}$ |
| $F(000)$ | 1448 |
| Crystal | Blade; Dark Orange |
| Crystal size | 0.130 × 0.070 × 0.010 mm$^3$ |
| $\theta$ range for data collection | 2.925 – 27.484° |
| Index ranges | $-13 \le h \le 10$, $-23 \le k \le 22$, $-19 \le l \le 19$ |
| Reflections collected | 36950 |
| Independent reflections | 6352 [$R_{int}$ = 0.0449] |
| Completeness to $\theta$ = 25.242° | 99.8 % |
| Absorption correction | Semi–empirical from equivalents |
| Max. and min. transmission | 1.000 and 0.757 |
| Refinement method | Full-matrix least-squares on $F^2$ |
| Data / restraints / parameters | 6352 / 1 / 430 |
| Goodness-of-fit on $F^2$ | 1.021 |
| Final $R$ indices [$F^2 > 2\sigma(F^2)$] | $R1$ = 0.0362, $wR2$ = 0.0930 |
| $R$ indices (all data) | $R1$ = 0.0467, $wR2$ = 0.0987 |
| Extinction coefficient | n/a |
| Largest diff. peak and hole | 0.656 and –0.334 e Å$^{-3}$ |

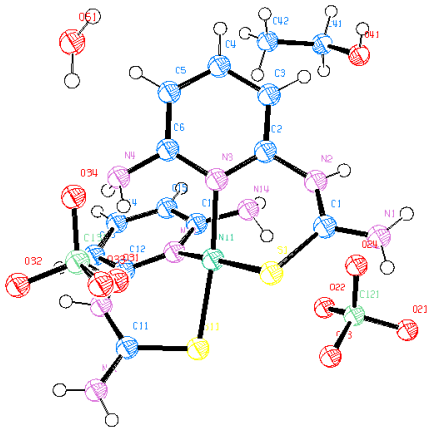

**Table D.1:** Crystal data and structure refinement for $[Ni^{II}(L^{2C})_2](ClO_4)_2.H_2O.CH_3CH_2OH$ **2.7.**

| | | |
|---|---|---|
| Identification code | **2014ncs0714 / $L_2$Ni-19Aug** | |
| Empirical formula | $C_{14}H_{24}Cl_2N_8NiO_{10}S_2$ | |
| Formula weight | 658.14 | |
| Temperature | 100(2) K | |
| Wavelength | 0.71075 Å | |
| Crystal system | Monoclinic | |
| Space group | $P2_1/c$ | |
| Unit cell dimensions | $a$ = 14.5292(10) Å | $\alpha$ = 90° |
| | $b$ = 17.4502(11) Å | $\beta$ = 106.2890(10)° |
| | $c$ = 10.2498(7) Å | $\gamma$ = 90° |
| Volume | 2494.4(3) Å$^3$ | |
| $Z$ | 4 | |
| Density (calculated) | 1.753 Mg / m$^3$ | |
| Absorption coefficient | 1.226 mm$^{-1}$ | |
| *F(000)* | 1352 | |
| Crystal | Plate; Red | |
| Crystal size | 0.090 × 0.030 × 0.010 mm$^3$ | |
| $\theta$ range for data collection | 2.334 – 27.485° | |
| Index ranges | $-18 \le h \le 18$, $-20 \le k \le 22$, $-13 \le l \le 13$ | |
| Reflections collected | 37562 | |
| Independent reflections | 5704 [$R_{int}$ = 0.0612] | |
| Completeness to $\theta$ = 25.242° | 99.8 % | |
| Absorption correction | Semi–empirical from equivalents | |
| Max. and min. transmission | 1.000 and 0.792 | |
| Refinement method | Full-matrix least-squares on $F^2$ | |
| Data / restraints / parameters | 5704 / 0 / 341 | |
| Goodness-of-fit on $F^2$ | 1.036 | |
| Final $R$ indices [$F^2 > 2\sigma(F^2)$] | $R1$ = 0.0426, $wR2$ = 0.1140 | |
| $R$ indices (all data) | $R1$ = 0.0506, $wR2$ = 0.1212 | |
| Extinction coefficient | n/a | |
| Largest diff. peak and hole | 0.902 and –0.594 e Å$^{-3}$ | |

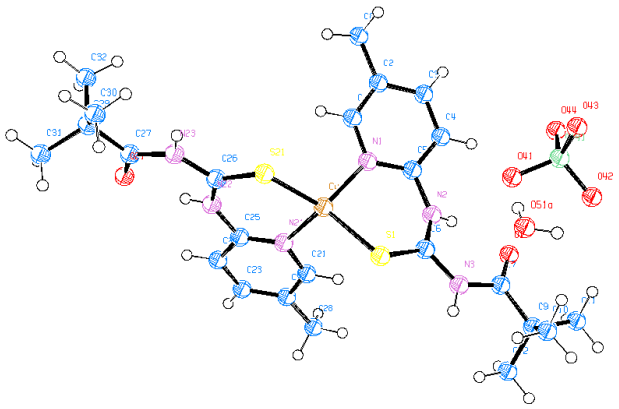

**Table E.1:** Crystal data and structure refinement for $[Cu^{I}(L^{1b})_2](ClO_4)(H_2O)$ **2.15**.

| | | |
|---|---|---|
| Identification code | **2014ncs0938 / L1bCu-2/12** | |
| Empirical formula | $C_{24}H_{36}ClCuN_6O_7S_2$ | |
| Formula weight | 683.70 | |
| Temperature | 100(2) K | |
| Wavelength | 0.71075 Å | |
| Crystal system | Orthorhombic | |
| Space group | $P2_12_12_1$ | |
| Unit cell dimensions | $a$ = 9.0770(3) Å | $\alpha$ = 90° |
| | $b$ = 17.2213(8) Å | $\beta$ = 90° |
| | $c$ = 19.5201(6) Å | $\gamma$ = 90° |
| Volume | 3051.3(2) $Å^3$ | |
| $Z$ | 4 | |
| Density (calculated) | 1.488 Mg / $m^3$ | |
| Absorption coefficient | 0.992 $mm^{-1}$ | |
| *F(000)* | 1424 | |
| Crystal | Plate; Orange | |
| Crystal size | 0.110 × 0.090 × 0.010 $mm^3$ | |
| $\theta$ range for data collection | 1.577 – 27.480° | |
| Index ranges | $-11 \le h \le 11$, $-22 \le k \le 22$, $-25 \le l \le 23$ | |
| Reflections collected | 35113 | |
| Independent reflections | 6990 [$R_{int}$ = 0.1008] | |
| Completeness to $\theta$ = 25.242° | 100.0 % | |
| Absorption correction | Semi–empirical from equivalents | |
| Max. and min. transmission | 1.00000 and 0.77214 | |
| Refinement method | Full-matrix least-squares on $F^2$ | |
| Data / restraints / parameters | 6990 / 30 / 383 | |
| Goodness-of-fit on $F^2$ | 1.041 | |
| Final $R$ indices [$F^2 > 2\sigma(F^2)$] | $R1$ = 0.0659, $wR2$ = 0.1259 | |
| $R$ indices (all data) | $R1$ = 0.1069, $wR2$ = 0.1418 | |
| Absolute structure parameter | –0.016(12) | |
| Extinction coefficient | n/a | |
| Largest diff. peak and hole | 1.110 and –0.701 e $Å^{-3}$ | |

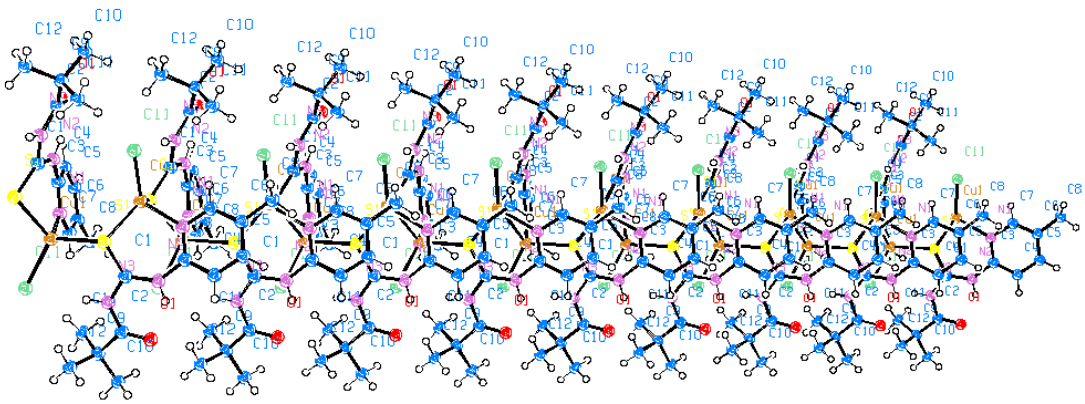

**Table F.1:** Crystal data and structure refinement for [$Cu^{I}(L^{1b})Cl$] **2.16.**

| | |
|---|---|
| Identification code | **2014ncs0760 / L1bCuCl-14Oct** |
| Empirical formula | $C_{12}H_{17}ClCuN_3OS$ |
| Formula weight | 350.33 |
| Temperature | 100(2) K |
| Wavelength | 0.71075 Å |
| Crystal system | Monoclinic |
| Space group | $P2_1/c$ |
| Unit cell dimensions | $a$ = 12.5881(9) Å $\alpha$ = 90° |
| | $b$ = 6.0555(4) Å $\beta$ = 101.012(2)° |
| | $c$ = 19.3671(14) Å $\gamma$ = 90° |
| Volume | 1449.12(18) $Å^3$ |
| $Z$ | 4 |
| Density (calculated) | 1.606 Mg / $m^3$ |
| Absorption coefficient | 1.830 $mm^{-1}$ |
| *F(000)* | 720 |
| Crystal | Needle; Red |
| Crystal size | 0.290 × 0.010 × 0.010 $mm^3$ |
| $\theta$ range for data collection | 2.143 – 27.554° |
| Index ranges | $-14 \le h \le 16$, $-7 \le k \le 7$, $-25 \le l \le 25$ |
| Reflections collected | 14551 |
| Independent reflections | 3349 [$R_{int}$ = 0.0518] |
| Completeness to $\theta$ = 25.242° | 100.0 % |
| Absorption correction | Semi–empirical from equivalents |
| Max. and min. transmission | 1.000 and 0.637 |
| Refinement method | Full-matrix least-squares on $F^2$ |
| Data / restraints / parameters | 3349 / 0 / 176 |
| Goodness-of-fit on $F^2$ | 1.088 |
| Final $R$ indices [$F^2 > 2\sigma(F^2)$] | $R1$ = 0.0310, $wR2$ = 0.0814 |
| $R$ indices (all data) | $R1$ = 0.0393, $wR2$ = 0.0943 |
| Extinction coefficient | n/a |
| Largest diff. peak and hole | 0.562 and –0.385 e $Å^{-3}$ |

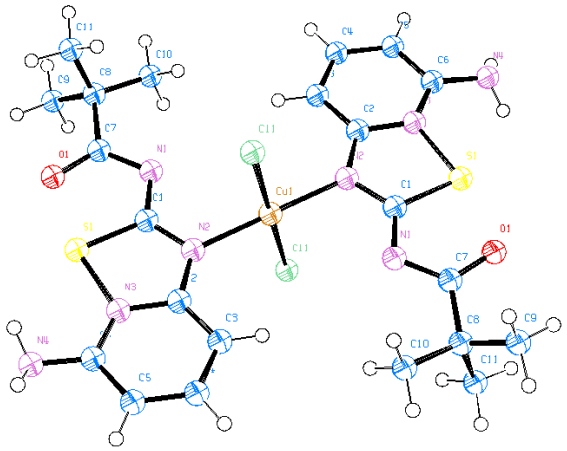

**Table G.1:** Crystal data and structure refinement for $[Cu^{II}(L^{2b*})_2Cl_2]$ **2.20.**

| | |
|---|---|
| Identification code | **2014ncs0802 / $L_2$bCuCl-15Oct** |
| Empirical formula | $C_{22}H_{28}Cl_2CuN_8O_2S_2$ |
| Formula weight | 635.08 |
| Temperature | 100(2) K |
| Wavelength | 0.71075 Å |
| Crystal system | Monoclinic |
| Space group | $P2_1/c$ |
| Unit cell dimensions | $a$ = 10.7026(8) Å $\alpha$ = 90° |
| | $b$ = 16.3850(11) Å $\beta$ = 97.287(2)° |
| | $c$ = 7.9196(5) Å $\gamma$ = 90° |
| Volume | 1377.58(16) Å$^3$ |
| $Z$ | 2 |
| Density (calculated) | 1.531 Mg / m$^3$ |
| Absorption coefficient | 1.175 mm$^{-1}$ |
| $F(000)$ | 654 |
| Crystal | Plate; Dark Green |
| Crystal size | 0.080 × 0.060 × 0.010 mm$^3$ |
| $\theta$ range for data collection | 2.286 – 27.537° |
| Index ranges | $-13 \le h \le 13$, $-21 \le k \le 18$, $-10 \le l \le 10$ |
| Reflections collected | 20899 |
| Independent reflections | 3166 [$R_{int}$ = 0.0958] |
| Completeness to $\theta$ = 25.242° | 99.6 % |
| Absorption correction | Semi–empirical from equivalents |
| Max. and min. transmission | 1.000 and 0.709 |
| Refinement method | Full-matrix least-squares on $F^2$ |
| Data / restraints / parameters | 3166 / 0 / 173 |
| Goodness-of-fit on $F^2$ | 1.067 |
| Final $R$ indices [$F^2 > 2\sigma(F^2)$] | $R1$ = 0.0631, $wR2$ = 0.1683 |
| $R$ indices (all data) | $R1$ = 0.0663, $wR2$ = 0.1740 |
| Extinction coefficient | n/a |
| Largest diff. peak and hole | 1.519 and –0.664 e Å$^{-3}$ |

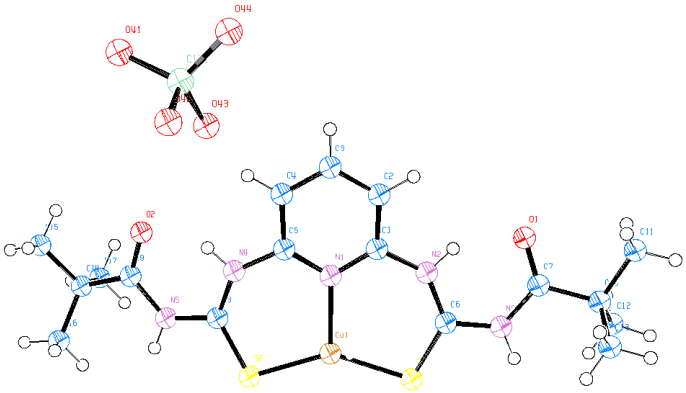

**Table H.1:** Crystal data and structure refinement for $[Cu^{I}(L^{3b})](ClO_4).0.5H_2O$ **2.24.**

| | |
|---|---|
| Identification code | **2015ncs0006 / ALI-L3bCu2-19/11** |
| Empirical formula | $C_{17}H_{26}ClCuN_5O_{6.50}S_2$ |
| Formula weight | 567.54 |
| Temperature | 100(2) K |
| Wavelength | 0.71075 Å |
| Crystal system | Monoclinic |
| Space group | $P2_1$ |
| Unit cell dimensions | $a$ = 12.3999(3) Å $\alpha$ = 90° |
| | $b$ = 14.2258(4) Å $\beta$ = 90.462(2)° |
| | $c$ = 13.3826(3) Å $\gamma$ = 90° |
| Volume | 2360.59(10) $Å^3$ |
| $Z$ | 4 |
| Density (calculated) | 1.597 Mg / $m^3$ |
| Absorption coefficient | 1.261 $mm^{-1}$ |
| $F(000)$ | 1172 |
| Crystal | Rod; Yellow |
| Crystal size | 0.130 × 0.040 × 0.010 $mm^3$ |
| $\theta$ range for data collection | 2.230 – 27.483° |
| Index ranges | $-15 \le h \le 16$, $-18 \le k \le 18$, $-17 \le l \le 17$ |
| Reflections collected | 30299 |
| Independent reflections | 10291 [$R_{int}$ = 0.0477] |
| Completeness to $\theta$ = 25.242° | 99.9 % |
| Absorption correction | Semi–empirical from equivalents |
| Max. and min. transmission | 1.00000 and 0.59658 |
| Refinement method | Full-matrix least-squares on $F^2$ |
| Data / restraints / parameters | 10291 / 143 / 681 |
| Goodness-of-fit on $F^2$ | 1.049 |
| Final $R$ indices [$F^2 > 2\sigma(F^2)$] | $R1$ = 0.0571, $wR2$ = 0.1507 |
| $R$ indices (all data) | $R1$ = 0.0686, $wR2$ = 0.1577 |
| Absolute structure parameter | –0.002(8) |
| Extinction coefficient | n/a |
| Largest diff. peak and hole | 1.255 and –0.794 e $Å^{-3}$ |

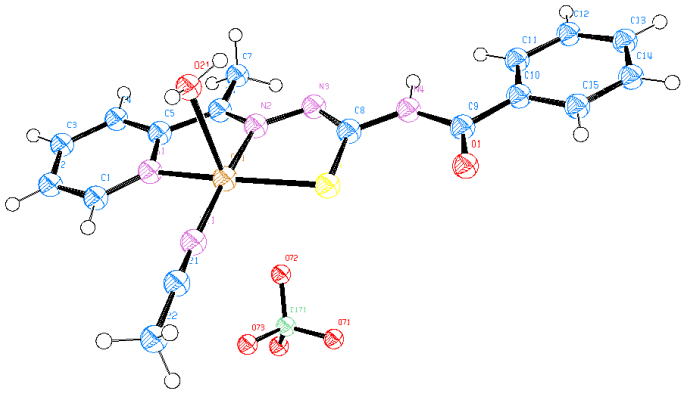

**Table I.1:** Crystal data and structure refinement for $[Cu^{II}(ACbe)(CH_3CN)(H_2O)]ClO_4$ **3.1**

| | | |
|---|---|---|
| Identification code | **2014ncs0457/ ALI-ACCU-16June** | |
| Empirical formula | $C_{17}H_{18}ClCuN_5O_6S$ | |
| Formula weight | 519.41 | |
| Temperature | 100(2) K | |
| Wavelength | 0.71075 Å | |
| Crystal system | Monoclinic | |
| Space group | $P2_1/n$ | |
| Unit cell dimensions | $a$ = 15.1334(11) Å | $\alpha$ = 90° |
| | $b$ = 15.1835(11) Å | $\beta$ = 107.0550(10)° |
| | $c$ = 18.4555(13) Å | $\gamma$ = 90° |
| Volume | 4054.2(5) Å$^3$ | |
| $Z$ | 8 | |
| Density (calculated) | 1.702 Mg / m$^3$ | |
| Absorption coefficient | 1.360 mm$^{-1}$ | |
| $F(000)$ | 2120 | |
| Crystal | Lath; Pale Green | |
| Crystal size | 0.240 × 0.040 × 0.020 mm$^3$ | |
| $\theta$ range for data collection | 2.921 – 27.485° | |
| Index ranges | $-18 \le h \le 19$, $-19 \le k \le 19$, $-23 \le l \le 23$ | |
| Reflections collected | 53507 | |
| Independent reflections | 9272 [$R_{int}$ = 0.0453] | |
| Completeness to $\theta$ = 25.242° | 99.8 % | |
| Absorption correction | Semi–empirical from equivalents | |
| Max. and min. transmission | 1.000 and 0.748 | |
| Refinement method | Full-matrix least-squares on $F^2$ | |
| Data / restraints / parameters | 9272 / 0 / 565 | |
| Goodness-of-fit on $F^2$ | 1.024 | |
| Final $R$ indices [$F^2 > 2\sigma(F^2)$] | $R1$ = 0.0342, $wR2$ = 0.0887 | |
| $R$ indices (all data) | $R1$ = 0.0432, $wR2$ = 0.0947 | |
| Extinction coefficient | n/a | |
| Largest diff. peak and hole | 0.823 and –0.606 e Å$^{-3}$ | |

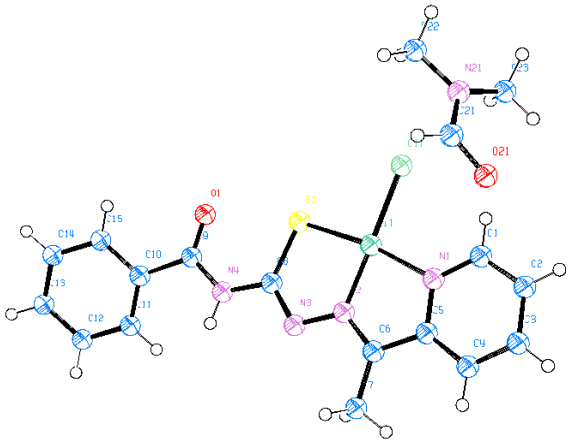

**Table J.1:** Crystal data and structure refinement details for [Ni(ACbe)Cl].DMF **3.5**

| | | |
|---|---|---|
| Identification code | **2015ncs0144 / ACbNiCl-24/2** | |
| Empirical formula | $C_{18}H_{20}ClN_5NiO_2S$ | |
| Formula weight | 464.61 | |
| Temperature | 100(2) K | |
| Wavelength | 0.71075 Å | |
| Crystal system | Triclinic | |
| Space group | *P*–1 | |
| Unit cell dimensions | *a* = 9.5241(7) Å | $\alpha$ = 111.950(5)° |
| | *b* = 10.0471(7) Å | $\beta$ = 91.708(4)° |
| | *c* = 11.4096(8) Å | $\gamma$ = 105.199(5)° |
| Volume | 967.20(13) Å$^3$ | |
| *Z* | 2 | |
| Density (calculated) | 1.595 Mg / m$^3$ | |
| Absorption coefficient | 1.274 mm$^{-1}$ | |
| *F(000)* | 480 | |
| Crystal | Plate; Red | |
| Crystal size | 0.130 × 0.120 × 0.020 mm$^3$ | |
| $\theta$ range for data collection | 2.688 – 27.513° | |
| Index ranges | $-12 \le h \le 10$, $-13 \le k \le 12$, $-14 \le l \le 14$ | |
| Reflections collected | 17855 | |
| Independent reflections | 4444 [$R_{int}$ = 0.0629] | |
| Completeness to $\theta$ = 25.242° | 99.8 % | |
| Absorption correction | Semi–empirical from equivalents | |
| Max. and min. transmission | 1.000 and 0.827 | |
| Refinement method | Full-matrix least-squares on $F^2$ | |
| Data / restraints / parameters | 4444 / 0 / 256 | |
| Goodness-of-fit on $F^2$ | 1.085 | |
| Final *R* indices [$F^2 > 2\sigma(F^2)$] | *R1* = 0.0350, *wR2* = 0.0896 | |
| *R* indices (all data) | *R1* = 0.0379, *wR2* = 0.0911 | |
| Extinction coefficient | n/a | |
| Largest diff. peak and hole | 0.656 and –0.497 e Å$^{-3}$ | |

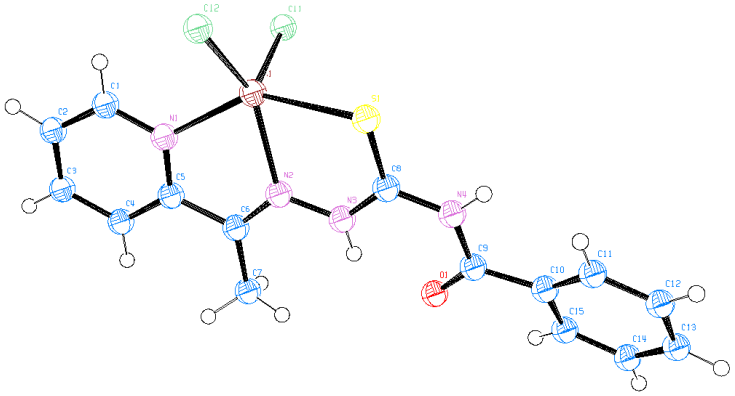

**Table K.1:** Crystal data and structure refinement details for [Zn(ACbe-H)$Cl_2$] **3.6**

| | |
|---|---|
| Identification code | **2015ncs0143 / ACbZnCl-24/2** |
| Empirical formula | $C_{15}H_{14}Cl_2N_4OSZn$ |
| Formula weight | 434.63 |
| Temperature | 100(2) K |
| Wavelength | 0.71075 Å |
| Crystal system | Monoclinic |
| Space group | $P2_1/c$ |
| Unit cell dimensions | $a$ = 11.6644(8) Å $\alpha$ = 90° |
| | $b$ = 18.0850(13) Å $\beta$ = 110.381(2)° |
| | $c$ = 8.5461(5) Å $\gamma$ = 90° |
| Volume | 1689.9(2) $Å^3$ |
| $Z$ | 4 |
| Density (calculated) | 1.708 Mg / $m^3$ |
| Absorption coefficient | 1.903 $mm^{-1}$ |
| *F(000)* | 880 |
| Crystal | Plate; Light Yellow |
| Crystal size | 0.090 × 0.060 × 0.010 $mm^3$ |
| $\theta$ range for data collection | 2.812 – 27.480° |
| Index ranges | $-15 \le h \le 14$, $-23 \le k \le 23$, $-11 \le l \le 10$ |
| Reflections collected | 20193 |
| Independent reflections | 3842 [$R_{int}$ = 0.0462] |
| Completeness to $\theta$ = 25.242° | 99.9 % |
| Absorption correction | Semi–empirical from equivalents |
| Max. and min. transmission | 1.000 and 0.748 |
| Refinement method | Full-matrix least-squares on $F^2$ |
| Data / restraints / parameters | 3842 / 0 / 218 |
| Goodness-of-fit on $F^2$ | 1.017 |
| Final $R$ indices [$F^2 > 2\sigma(F^2)$] | $R1$ = 0.0255, $wR2$ = 0.0657 |
| $R$ indices (all data) | $R1$ = 0.0287, $wR2$ = 0.0681 |
| Extinction coefficient | n/a |
| Largest diff. peak and hole | 0.458 and –0.394 e $Å^{-3}$ |

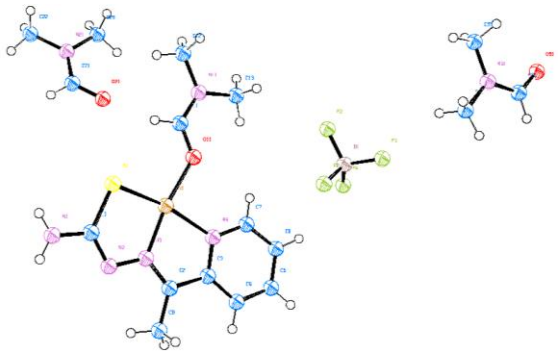

**Table L.1:** Crystal data and structure refinement details for [$Cu^{II}$(ACTM$^{\hat{}}$).DMF]($BF_4$).2DMF **3.7**

| | |
|---|---|
| Identification code | **2015ncs0141 / ACTMCu-24/2** |
| Empirical formula | $C_{17}H_{30}BCuF_4N_7O_3S$ |
| Formula weight | 562.89 |
| Temperature | 100(2) K |
| Wavelength | 0.71075 Å |
| Crystal system | Monoclinic |
| Space group | $P2_1/c$ |
| Unit cell dimensions | $a$ = 14.2666(8) Å $\alpha$ = 90° |
| | $b$ = 23.4497(14) Å $\beta$ = 101.593(6)° |
| | $c$ = 7.5245(4) Å $\gamma$ = 90° |
| Volume | 2465.9(2) Å$^3$ |
| $Z$ | 4 |
| Density (calculated) | 1.516 Mg / m$^3$ |
| Absorption coefficient | 1.034 mm$^{-1}$ |
| *F(000)* | 1164 |
| Crystal | Lath; Dark Green |
| Crystal size | 0.360 × 0.050 × 0.010 mm$^3$ |
| $\theta$ range for data collection | 2.267 – 27.562° |
| Index ranges | $-18 \le h \le 18$, $-30 \le k \le 30$, $-9 \le l \le 8$ |
| Reflections collected | 27241 |
| Independent reflections | 5630 [$R_{int}$ = 0.0792] |
| Completeness to $\theta$ = 25.242° | 99.9 % |
| Absorption correction | Semi–empirical from equivalents |
| Max. and min. transmission | 1.000 and 0.436 |
| Refinement method | Full-matrix least-squares on $F^2$ |
| Data / restraints / parameters | 5630 / 92 / 360 |
| Goodness-of-fit on $F^2$ | 1.071 |
| Final $R$ indices [$F^2 > 2\sigma(F^2)$] | $R1$ = 0.0769, $wR2$ = 0.1669 |
| $R$ indices (all data) | $R1$ = 0.1063, $wR2$ = 0.1814 |
| Extinction coefficient | n/a |
| Largest diff. peak and hole | 1.326 and –0.714 e Å$^{-3}$ |

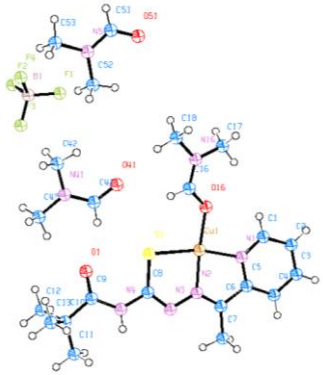

**Table M.1:** Crystal data and structure refinement details for [$Cu^{II}$(ACTM).DMF]($BF_4$).1.5 DMF **3.8**

| | | |
|---|---|---|
| Identification code | **2015ncs0420 / ACTMCu-15/6** | |
| Empirical formula | $C_{20.50}H_{34.50}BCuF_4N_{6.50}O_{3.50}S$ | |
| Formula weight | 610.45 | |
| Temperature | 100(2) K | |
| Wavelength | 0.71073 Å | |
| Crystal system | Monoclinic | |
| Space group | $P2_1/n$ | |
| Unit cell dimensions | $a$ = 6.59390(10) Å | $\alpha$ = 90° |
| | $b$ = 25.9958(5) Å | $\beta$ = 91.328(2)° |
| | $c$ = 31.1516(5) Å | $\gamma$ = 90° |
| Volume | 5338.38(16) $Å^3$ | |
| $Z$ | 8 | |
| Density (calculated) | 1.519 Mg / $m^3$ | |
| Absorption coefficient | 0.963 $mm^{-1}$ | |
| *F(000)* | 2536 | |
| Crystal | Blade; Dark Green | |
| Crystal size | 0.410 × 0.050 × 0.020 $mm^3$ | |
| $\theta$ range for data collection | 1.524 – 27.621° | |
| Index ranges | $-8 \le h \le 8$, $-33 \le k \le 33$, $-39 \le l \le 40$ | |
| Reflections collected | 13725 | |
| Independent reflections | 13725 [$R_{int}$ = ?] | |
| Completeness to $\theta$ = 25.242° | 100.0 % | |
| Absorption correction | Semi–empirical from equivalents | |
| Max. and min. transmission | 1.00000 and 0.83669 | |
| Refinement method | Full-matrix least-squares on $F^2$ | |
| Data / restraints / parameters | 13725 / 168 / 759 | |
| Goodness-of-fit on $F^2$ | 1.145 | |
| Final $R$ indices [$F^2 > 2\sigma(F^2)$] | *R1* = 0.0553, *wR2* = 0.1143 | |
| $R$ indices (all data) | *R1* = 0.0686, *wR2* = 0.1183 | |
| Extinction coefficient | n/a | |
| Largest diff. peak and hole | 0.610 and –0.342 e $Å^{-3}$ | |

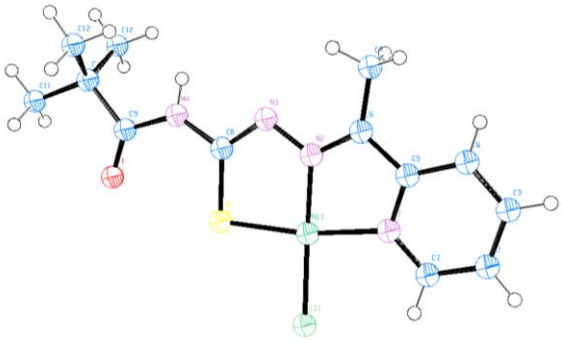

**Table N.1:** Crystal data and structure refinement details for [Ni$^{II}$(ACTM)Cl] **3.10**

| | |
|---|---|
| Identification code | **2015ncs0142 / ACTMNiCl-26/2** |
| Empirical formula | $C_{13}H_{17}ClN_4NiOS$ |
| Formula weight | 371.52 |
| Temperature | 100(2) K |
| Wavelength | 0.71075 Å |
| Crystal system | Monoclinic |
| Space group | $P2_1/m$ |
| Unit cell dimensions | $a$ = 8.5126(5) Å $\alpha$ = 90°<br>$b$ = 6.7302(5) Å $\beta$ = 102.009(3)°<br>$c$ = 13.6860(10) Å $\gamma$ = 90° |
| Volume | 766.93(9) Å$^3$ |
| $Z$ | 2 |
| Density (calculated) | 1.609 Mg / m$^3$ |
| Absorption coefficient | 1.578 mm$^{-1}$ |
| $F(000)$ | 384 |
| Crystal | Lath; Orange |
| Crystal size | 0.130 × 0.030 × 0.010 mm$^3$ |
| $\theta$ range for data collection | 2.598 – 27.490° |
| Index ranges | $-10 \le h \le 10$, $-8 \le k \le 7$, $-17 \le l \le 17$ |
| Reflections collected | 8271 |
| Independent reflections | 1893 [$R_{int}$ = 0.0705] |
| Completeness to $\theta$ = 25.242° | 99.7 % |
| Absorption correction | Semi–empirical from equivalents |
| Max. and min. transmission | 1.000 and 0.519 |
| Refinement method | Full-matrix least-squares on $F^2$ |
| Data / restraints / parameters | 1893 / 0 / 126 |
| Goodness-of-fit on $F^2$ | 1.051 |
| Final $R$ indices [$F^2 > 2\sigma(F^2)$] | $R1$ = 0.0536, $wR2$ = 0.1389 |
| $R$ indices (all data) | $R1$ = 0.0638, $wR2$ = 0.1464 |
| Extinction coefficient | n/a |
| Largest diff. peak and hole | 1.530 and –0.863 e Å$^{-3}$ |

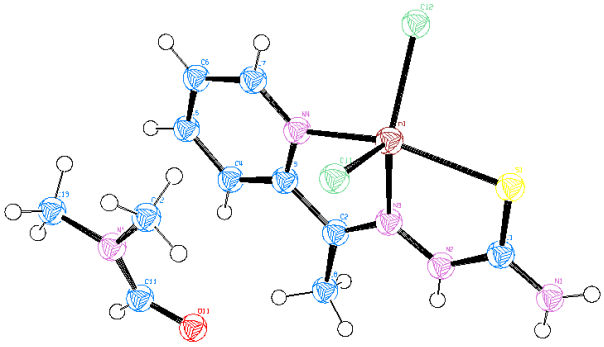

**Table O.1:** Crystal data and structure refinement details for $[Zn^{II}(ACTM^{\hat{}}\text{-}H)Cl_2]$ DMF **3.11**

| | |
|---|---|
| Identification code | **2015ncs0167 / ACTMZnCl-3/3** |
| Empirical formula | $C_{11}H_{17}Cl_2N_5OSZn$ |
| Formula weight | 403.62 |
| Temperature | 100(2) K |
| Wavelength | 0.71075 Å |
| Crystal system | Triclinic |
| Space group | *P*–1 |
| Unit cell dimensions | *a* = 7.4133(6) Å $\alpha$ = 101.623(7)° |
| | *b* = 9.2268(8) Å $\beta$ = 95.663(7)° |
| | *c* = 11.9719(11) Å $\gamma$ = 91.170(7)° |
| Volume | 797.50(12) Å$^3$ |
| *Z* | 2 |
| Density (calculated) | 1.681 Mg / m$^3$ |
| Absorption coefficient | 2.010 mm$^{-1}$ |
| *F(000)* | 412 |
| Crystal | Plate; Yellow |
| Crystal size | 0.120 × 0.080 × 0.010 mm$^3$ |
| $\theta$ range for data collection | 2.255 – 27.764° |
| Index ranges | $-8 \le h \le 9$, $-12 \le k \le 12$, $-15 \le l \le 15$ |
| Reflections collected | 9733 |
| Independent reflections | 9733 [$R_{int}$ = ?] |
| Completeness to $\theta$ = 25.242° | 100.0 % |
| Absorption correction | Semi–empirical from equivalents |
| Max. and min. transmission | 1.00000 and 0.58524 |
| Refinement method | Full-matrix least-squares on $F^2$ |
| Data / restraints / parameters | 9733 / 0 / 194 |
| Goodness-of-fit on $F^2$ | 1.045 |
| Final *R* indices [$F^2 > 2\sigma(F^2)$] | *R1* = 0.0861, *wR2* = 0.2416 |
| *R* indices (all data) | *R1* = 0.0917, *wR2* = 0.2476 |
| Extinction coefficient | n/a |
| Largest diff. peak and hole | 1.123 and –1.237 e Å$^{-3}$ |

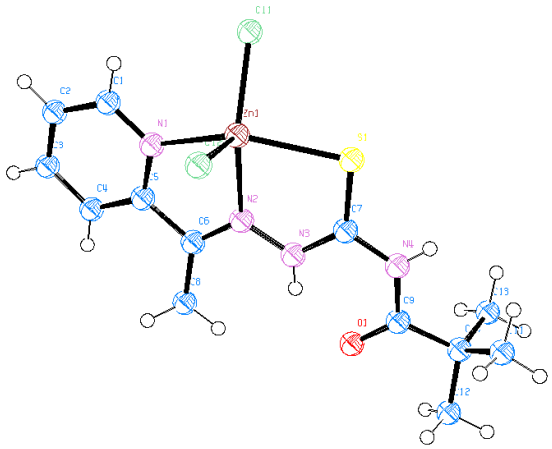

**Table P.1:** Crystal data and structure refinement details for [Zn(ACTM-H)$Cl_2$] **3.12**

| | | |
|---|---|---|
| Identification code | **2015ncs0433 / ACTMZnCl-23/6** | |
| Empirical formula | $C_{13}H_{18}Cl_2N_4OSZn$ | |
| Formula weight | 414.64 | |
| Temperature | 100(2) K | |
| Wavelength | 0.71075 Å | |
| Crystal system | Monoclinic | |
| Space group | $P2_1/c$ | |
| Unit cell dimensions | $a$ = 10.9082(8) Å | $\alpha$ = 90° |
| | $b$ = 8.5805(5) Å | $\beta$ = 101.553(2)° |
| | $c$ = 18.5869(13) Å | $\gamma$ = 90° |
| Volume | 1704.4(2) $Å^3$ | |
| $Z$ | 4 | |
| Density (calculated) | 1.616 Mg / $m^3$ | |
| Absorption coefficient | 1.882 $mm^{-1}$ | |
| *F(000)* | 848 | |
| Crystal | Block; Yellow | |
| Crystal size | 0.080 × 0.070 × 0.030 $mm^3$ | |
| $\theta$ range for data collection | 2.624 – 27.490° | |
| Index ranges | $-14 \le h \le 14$, $-10 \le k \le 11$, $-24 \le l \le 19$ | |
| Reflections collected | 23535 | |
| Independent reflections | 3882 [$R_{int}$ = 0.0376] | |
| Completeness to $\theta$ = 25.242° | 99.9 % | |
| Absorption correction | Semi–empirical from equivalents | |
| Max. and min. transmission | 1.000 and 0.889 | |
| Refinement method | Full-matrix least-squares on $F^2$ | |
| Data / restraints / parameters | 3882 / 0 / 211 | |
| Goodness-of-fit on $F^2$ | 1.029 | |
| Final $R$ indices [$F^2 > 2\sigma(F^2)$] | *R1* = 0.0221, *wR2* = 0.0530 | |
| $R$ indices (all data) | *R1* = 0.0265, *wR2* = 0.0549 | |
| Extinction coefficient | n/a | |
| Largest diff. peak and hole | 0.353 and –0.342 e $Å^{-3}$ | |

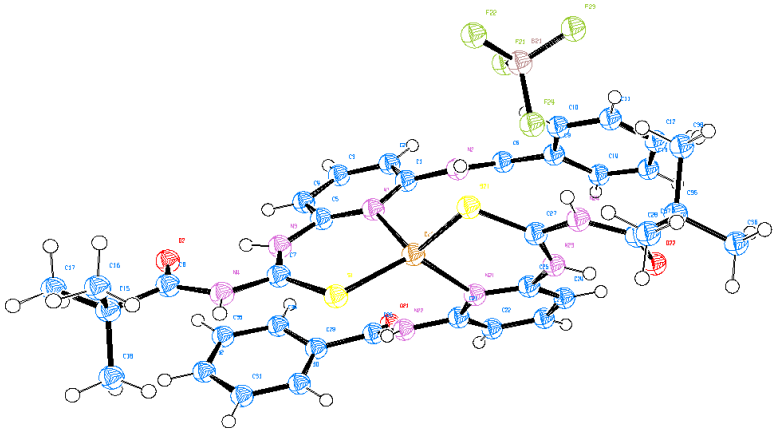

**Table Q.1;** Crystal data and structure refinement details for $[Cu^{I}(L^{5A})_2]BF_4 .0.17CH_2Cl_2$ **4.4**

| | | |
|---|---|---|
| Identification code | **2015ncs0599 / L5ACu-8-9** | |
| Empirical formula | $C_{36.17}H_{40.33}BCl_{0.33}CuF_4N_8O_4S_2$ | |
| Formula weight | 877.38 | |
| Temperature | 100(2) K | |
| Wavelength | 0.71073 Å | |
| Crystal system | Triclinic | |
| Space group | *P*–1 | |
| Unit cell dimensions | *a* = 18.1001(2) Å | $\alpha$ = 91.9450(10)° |
| | *b* = 18.1085(2) Å | $\beta$ = 93.0850(10)° |
| | *c* = 18.2115(2) Å | $\gamma$ = 90.1550(10)° |
| Volume | 5956.96(11) Å$^3$ | |
| *Z* | 6 | |
| Density (calculated) | 1.467 Mg / m$^3$ | |
| Absorption coefficient | 0.746 mm$^{-1}$ | |
| *F(000)* | 2718 | |
| Crystal | Block; Orabge | |
| Crystal size | 0.140 × 0.080 × 0.040 mm$^3$ | |
| $\theta$ range for data collection | 2.241 – 27.559° | |
| Index ranges | $-23 \le h \le 23$, $-23 \le k \le 23$, $-23 \le l \le 23$ | |
| Reflections collected | 106128 | |
| Independent reflections | 27419 [$R_{int}$ = 0.0261] | |
| Completeness to $\theta$ = 25.242° | 99.9 % | |
| Absorption correction | Semi–empirical from equivalents | |
| Max. and min. transmission | 1.00000 and 0.83466 | |
| Refinement method | Full-matrix least-squares on $F^2$ | |
| Data / restraints / parameters | 27419 / 23 / 1620 | |
| Goodness-of-fit on $F^2$ | 1.065 | |
| Final *R* indices [$F^2 > 2\sigma(F^2)$] | *R1* = 0.0387, *wR2* = 0.0958 | |
| *R* indices (all data) | *R1* = 0.0467, *wR2* = 0.0992 | |
| Extinction coefficient | n/a | |
| Largest diff. peak and hole | 0.792 and –0.543 e Å$^{-3}$ | |

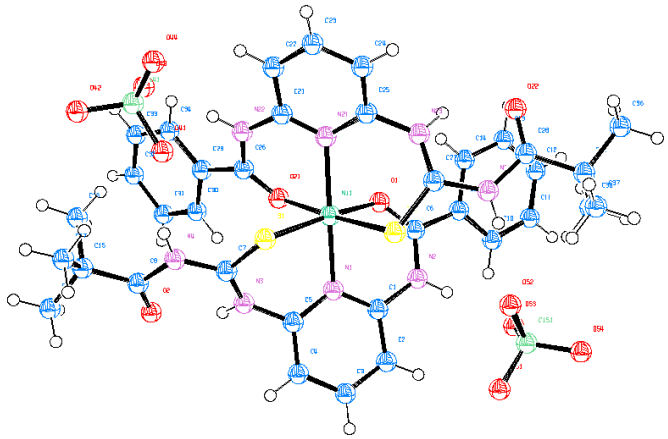

**Table R.1:** Crystal data and structure refinement details for $[Ni(L^{5A})_2](ClO_4)_2$ **4.6**

| | | |
|---|---|---|
| Identification code | **2015ncs0647 / $(L5A)_2$Ni-12-10** | |
| Empirical formula | $C_{36}H_{40}Cl_2N_8NiO_{12}S_2$ | |
| Formula weight | 970.49 | |
| Temperature | 100(2) K | |
| Wavelength | 0.71073 Å | |
| Crystal system | Triclinic | |
| Space group | *P*–1 | |
| Unit cell dimensions | *a* = 12.902(3) Å | $\alpha$ = 70.747(18)° |
| | *b* = 15.043(3) Å | $\beta$ = 74.247(18)° |
| | *c* = 15.061(3) Å | $\gamma$ = 84.912(16)° |
| Volume | 2656.1(10) Å$^3$ | |
| *Z* | 2 | |
| Density (calculated) | 1.213 Mg / m$^3$ | |
| Absorption coefficient | 0.601 mm$^{-1}$ | |
| *F(000)* | 1004 | |
| Crystal | Blade; Pale Green | |
| Crystal size | 0.150 × 0.060 × 0.010 mm$^3$ | |
| $\theta$ range for data collection | 1.906 – 25.026° | |
| Index ranges | $-13 \le h \le 15$, $-17 \le k \le 17$, $-17 \le l \le 16$ | |
| Reflections collected | 25357 | |
| Independent reflections | 8915 [$R_{int}$ = 0.1940] | |
| Completeness to $\theta$ = 25.000° | 95.1 % | |
| Absorption correction | Semi–empirical from equivalents | |
| Max. and min. transmission | 1.00000 and 0.53718 | |
| Refinement method | Full-matrix least-squares on $F^2$ | |
| Data / restraints / parameters | 8915 / 525 / 556 | |
| Goodness-of-fit on $F^2$ | 1.037 | |
| Final *R* indices [$F^2 > 2\sigma(F^2)$] | *R1* = 0.1678, *wR2* = 0.3741 | |
| *R* indices (all data) | *R1* = 0.2837, *wR2* = 0.4479 | |
| Extinction coefficient | n/a | |
| Largest diff. peak and hole | 2.420 and –0.955 e Å$^{-3}$ | |

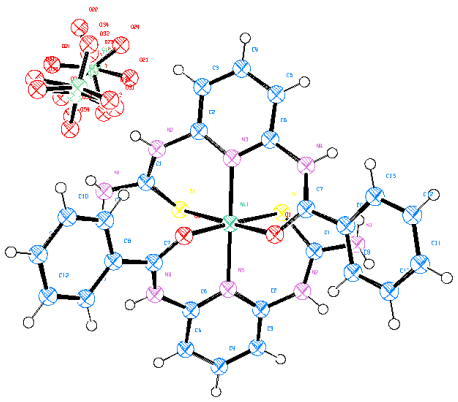

**Table S.1:** Crystal data and structure refinement for $[Ni(L^{5A*})_2](ClO_4)_2.(CH_3CH_2)_2O$ **4.7**

| | |
|---|---|
| Identification code | **2014ncs0677 / L5ANi-5Aug** |
| Empirical formula | $C_{30}H_{34}Cl_2N_8NiO_{11}S_2$ |
| Formula weight | 876.38 |
| Temperature | 100(2) K |
| Wavelength | 0.71075 Å |
| Crystal system | Monoclinic |
| Space group | *C*2/*c* |
| Unit cell dimensions | *a* = 12.6740(9) Å $\alpha$ = 90° |
| | *b* = 23.9734(15) Å $\beta$ = 103.616(7)° |
| | *c* = 12.1220(9) Å $\gamma$ = 90° |
| Volume | 3579.6(4) Å$^3$ |
| *Z* | 4 |
| Density (calculated) | 1.626 Mg / m$^3$ |
| Absorption coefficient | 0.879 mm$^{-1}$ |
| *F(000)* | 1808 |
| Crystal | Blade; Light Green |
| Crystal size | 0.100 × 0.080 × 0.010 mm$^3$ |
| $\theta$ range for data collection | 3.039 – 27.483° |
| Index ranges | $-14 \le h \le 16$, $-31 \le k \le 31$, $-15 \le l \le 15$ |
| Reflections collected | 22195 |
| Independent reflections | 4108 [$R_{int}$ = 0.0733] |
| Completeness to $\theta$ = 25.242° | 99.8 % |
| Absorption correction | Semi–empirical from equivalents |
| Max. and min. transmission | 1.00000 and 0.60958 |
| Refinement method | Full-matrix least-squares on $F^2$ |
| Data / restraints / parameters | 4108 / 94 / 313 |
| Goodness-of-fit on $F^2$ | 1.043 |
| Final *R* indices [$F^2 > 2\sigma(F^2)$] | *R1* = 0.0800, *wR2* = 0.1959 |
| *R* indices (all data) | *R1* = 0.1323, *wR2* = 0.2266 |
| Extinction coefficient | n/a |
| Largest diff. peak and hole | 0.841 and –0.557 e Å$^{-3}$ |

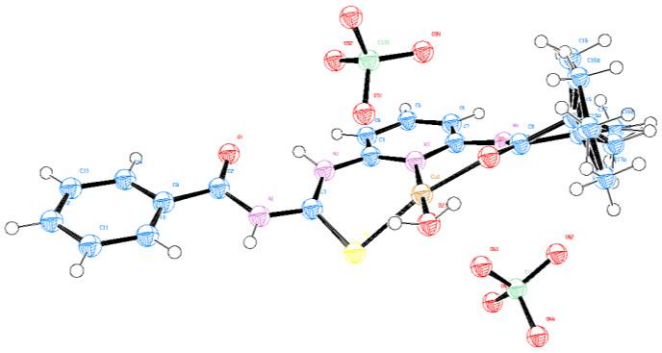

**Table T.1:** Crystal data and structure refinement for $[Cu^{II}(L^{7})(H_2O)](ClO_4)_2.CH_3COCH_3.H_2O$ **4.9**

| | |
|---|---|
| Identification code | **2014ncs0653 / L7Cu-21Aug** |
| Empirical formula | $C_{22}H_{32}Cl_2CuN_4O_{12}S$ |
| Formula weight | 711.01 |
| Temperature | 100(2) K |
| Wavelength | 0.71075 Å |
| Crystal system | Triclinic |
| Space group | *P*–1 |
| Unit cell dimensions | *a* = 7.7655(5) Å $\alpha$ = 78.858(7)° |
| | *b* = 13.5019(10) Å $\beta$ = 87.457(8)° |
| | *c* = 14.3687(11) Å $\gamma$ = 87.924(8)° |
| Volume | 1476.10(19) $Å^3$ |
| *Z* | 2 |
| Density (calculated) | 1.600 Mg / $m^3$ |
| Absorption coefficient | 1.058 $mm^{-1}$ |
| *F(000)* | 734 |
| Crystal | Blade; Pale Green |
| Crystal size | 0.290 × 0.090 × 0.020 $mm^3$ |
| $\theta$ range for data collection | 2.627 – 27.529° |
| Index ranges | $-10 \le h \le 10$, $-17 \le k \le 17$, $-18 \le l \le 18$ |
| Reflections collected | 21866 |
| Independent reflections | 6724 [$R_{int}$ = 0.0962] |
| Completeness to $\theta$ = 25.242° | 99.8 % |
| Absorption correction | Semi–empirical from equivalents |
| Max. and min. transmission | 1.000 and 0.481 |
| Refinement method | Full-matrix least-squares on $F^2$ |
| Data / restraints / parameters | 6724 / 213 / 466 |
| Goodness-of-fit on $F^2$ | 1.058 |
| Final *R* indices [$F^2 > 2\sigma(F^2)$] | *R1* = 0.0715, *wR2* = 0.1846 |
| *R* indices (all data) | *R1* = 0.0923, *wR2* = 0.1980 |
| Extinction coefficient | n/a |
| Largest diff. peak and hole | 1.679 and –0.650 e $Å^{-3}$ |

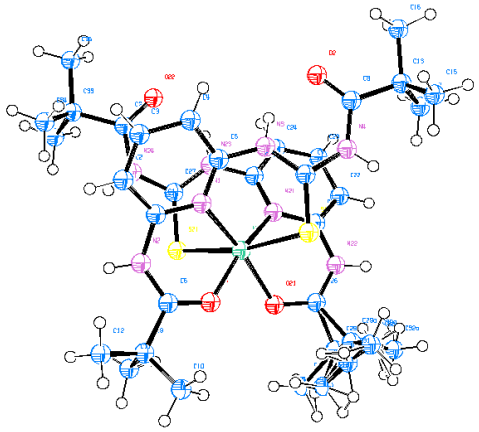

**Table U.1:** Crystal data and structure refinement details for $[Ni(L^{7A})_2](ClO_4)_2$ **4.13**

| | | |
|---|---|---|
| Identification code | **2015ncs0646 / $(L7A)_2$Ni-10-8** | |
| Empirical formula | $C_{32}H_{48}Cl_2N_8NiO_{12}S_2$ | |
| Formula weight | 930.51 | |
| Temperature | 100(2) K | |
| Wavelength | 0.71073 Å | |
| Crystal system | Monoclinic | |
| Space group | $P2_1/n$ | |
| Unit cell dimensions | $a$ = 12.4984(5) Å | $\alpha$ = 90° |
| | $b$ = 16.4192(7) Å | $\beta$ = 103.963(5)° |
| | $c$ = 25.5823(17) Å | $\gamma$ = 90° |
| Volume | 5094.7(5) Å$^3$ | |
| $Z$ | 4 | |
| Density (calculated) | 1.213 Mg / m$^3$ | |
| Absorption coefficient | 0.623 mm$^{-1}$ | |
| *F(000)* | 1944 | |
| Crystal | Blade; Green | |
| Crystal size | 0.160 × 0.070 × 0.020 mm$^3$ | |
| $\theta$ range for data collection | 1.640 – 27.484° | |
| Index ranges | $-14 \le h \le 16$, $-21 \le k \le 21$, $-33 \le l \le 33$ | |
| Reflections collected | 63663 | |
| Independent reflections | 11858 [$R_{int}$ = 0.1133] | |
| Completeness to $\theta$ = 25.000° | 100.0 % | |
| Absorption correction | Semi–empirical from equivalents | |
| Max. and min. transmission | 1.00000 and 0.89833 | |
| Refinement method | Full-matrix least-squares on $F^2$ | |
| Data / restraints / parameters | 11858 / 881 / 647 | |
| Goodness-of-fit on $F^2$ | 1.359 | |
| Final $R$ indices [$F^2 > 2\sigma(F^2)$] | *R1* = 0.1508, *wR2* = 0.4061 | |
| $R$ indices (all data) | *R1* = 0.2289, *wR2* = 0.4425 | |
| Extinction coefficient | n/a | |
| Largest diff. peak and hole | 0.944 and –0.727 e Å$^{-3}$ | |

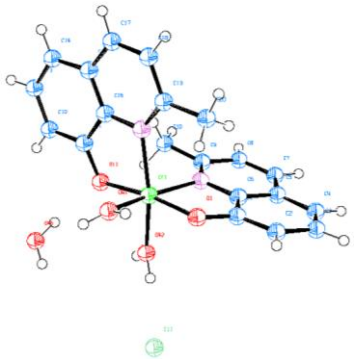

**Table V.1:** Crystal data and structure refinement for $[Cr^{III}(QM)_2(H_2O)_2]Cl.3/2H_2O$ **5.3**

| | |
|---|---|
| Identification code | **2014ncs0840 / HYM$_2$Cr-5-11** |
| Empirical formula | $C_{20}H_{23}ClCrN_2O_{5.50}$ |
| Formula weight | 466.85 |
| Temperature | 100(2) K |
| Wavelength | 0.71075 Å |
| Crystal system | Triclinic |
| Space group | *P*–1 |
| Unit cell dimensions | *a* = 12.0542(8) Å $\alpha$ = 88.512(5)°<br>*b* = 12.1609(9) Å $\beta$ = 84.401(5)°<br>*c* = 14.9483(10) Å $\gamma$ = 82.019(5)° |
| Volume | 2159.5(3) Å$^3$ |
| *Z* | 4 |
| Density (calculated) | 1.436 Mg / m$^3$ |
| Absorption coefficient | 0.689 mm$^{-1}$ |
| *F(000)* | 968 |
| Crystal | Plate; Pale Dark Green |
| Crystal size | 0.160 × 0.090 × 0.010 mm$^3$ |
| $\theta$ range for data collection | 2.090 – 27.484° |
| Index ranges | –15 ≤ *h* ≤ 14, –15 ≤ *k* ≤ 15, –19 ≤ *l* ≤ 18 |
| Reflections collected | 31525 |
| Independent reflections | 9809 [$R_{int}$ = 0.0782] |
| Completeness to $\theta$ = 25.242° | 99.2 % |
| Absorption correction | Semi–empirical from equivalents |
| Max. and min. transmission | 1.000 and 0.511 |
| Refinement method | Full-matrix least-squares on $F^2$ |
| Data / restraints / parameters | 9809 / 0 / 537 |
| Goodness-of-fit on $F^2$ | 1.111 |
| Final *R* indices [$F^2 > 2\sigma(F^2)$] | *R1* = 0.0786, *wR2* = 0.1914 |
| *R* indices (all data) | *R1* = 0.1024, *wR2* = 0.2035 |
| Extinction coefficient | n/a |
| Largest diff. peak and hole | 1.344 and –0.839 e Å$^{-3}$ |

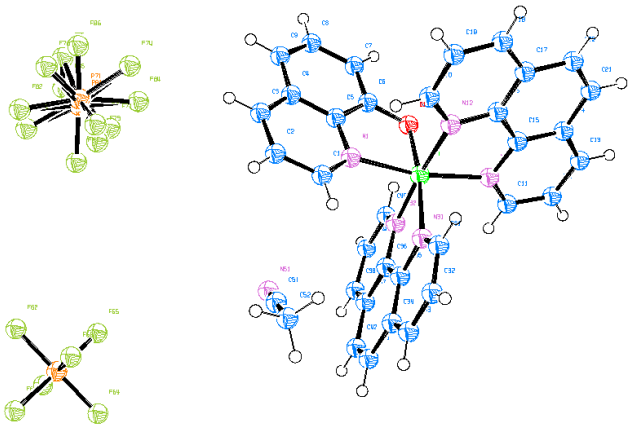

**Table W.1:** Crystal data and structure refinement for $[Cr(phen)_2(Q)](PF_6)_2.MeCN$ **5.7**

| | | |
|---|---|---|
| Identification code | **2014ncs0880 / $CrPCF_3h_2$=11Nov** | |
| Empirical formula | $C_{35}H_{25}CrF_{12}N_6OP_2$ | |
| Formula weight | 887.55 | |
| Temperature | 100(2) K | |
| Wavelength | 0.71075 Å | |
| Crystal system | Triclinic | |
| Space group | *P*–1 | |
| Unit cell dimensions | *a* = 10.3697(7) Å | $\alpha$ = 101.290(4)° |
| | *b* = 12.7892(9) Å | $\beta$ = 96.941(4)° |
| | *c* = 14.8184(10) Å | $\gamma$ = 111.476(4)° |
| Volume | 1753.0(2) $Å^3$ | |
| *Z* | 2 | |
| Density (calculated) | 1.681 Mg / $m^3$ | |
| Absorption coefficient | 0.523 $mm^{-1}$ | |
| *F(000)* | 894 | |
| Crystal | Plate; Red | |
| Crystal size | 0.100 × 0.070 × 0.020 $mm^3$ | |
| $\theta$ range for data collection | 2.159 – 27.524° | |
| Index ranges | $-13 \le h \le 13$, $-16 \le k \le 16$, $-19 \le l \le 18$ | |
| Reflections collected | 27800 | |
| Independent reflections | 8022 [$R_{int}$ = 0.0513] | |
| Completeness to $\theta$ = 25.242° | 99.8 % | |
| Absorption correction | Semi–empirical from equivalents | |
| Max. and min. transmission | 1.000 and 0.523 | |
| Refinement method | Full-matrix least-squares on $F^2$ | |
| Data / restraints / parameters | 8022 / 495 / 544 | |
| Goodness-of-fit on $F^2$ | 1.044 | |
| Final *R* indices [$F^2 > 2\sigma(F^2)$] | *R1* = 0.0485, *wR2* = 0.1329 | |
| *R* indices (all data) | *R1* = 0.0549, *wR2* = 0.1385 | |
| Extinction coefficient | n/a | |
| Largest diff. peak and hole | 0.961 and –0.492 e $Å^{-3}$ | |

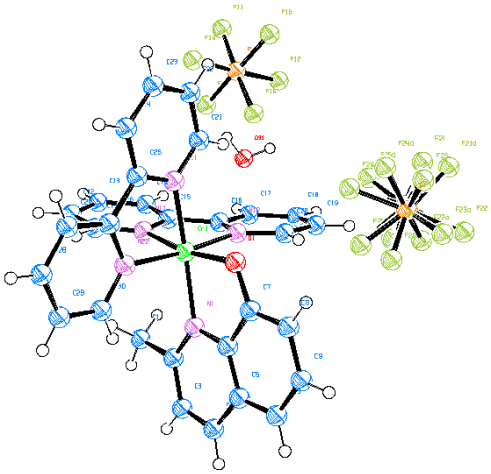

**Table X.1:** Crystal data and structure refinement details for $[Cr^{III}(bpy)_2(QM)]\ (PF_6)_2.H_2O$ **5.11**

| | | |
|---|---|---|
| Identification code | **2015ncs0415 / CrdhmPF3-10/6** | |
| Empirical formula | $C_{30}H_{26}CrF_{12}N_5O_2P_2$ | |
| Formula weight | 830.50 | |
| Temperature | 100(2) K | |
| Wavelength | 0.71073 Å | |
| Crystal system | Monoclinic | |
| Space group | $P2_1/n$ | |
| Unit cell dimensions | $a$ = 10.0548(3) Å | $\alpha$ = 90° |
| | $b$ = 14.2079(3) Å | $\beta$ = 101.681(2)° |
| | $c$ = 23.8326(5) Å | $\gamma$ = 90° |
| Volume | 3334.16(14) Å$^3$ | |
| $Z$ | 4 | |
| Density (calculated) | 1.654 Mg / m$^3$ | |
| Absorption coefficient | 0.545 mm$^{-1}$ | |
| $F(000)$ | 1676 | |
| Crystal | Blade; Red | |
| Crystal size | 0.130 × 0.040 × 0.010 mm$^3$ | |
| $\theta$ range for data collection | 1.678 – 27.485° | |
| Index ranges | $-10 \le h \le 13$, $-18 \le k \le 18$, $-30 \le l \le 30$ | |
| Reflections collected | 47627 | |
| Independent reflections | 7631 [$R_{int}$ = 0.0355] | |
| Completeness to $\theta$ = 25.242° | 100.0 % | |
| Absorption correction | Semi–empirical from equivalents | |
| Max. and min. transmission | 1.00000 and 0.63721 | |
| Refinement method | Full-matrix least-squares on $F^2$ | |
| Data / restraints / parameters | 7631 / 252 / 538 | |
| Goodness-of-fit on $F^2$ | 1.020 | |
| Final $R$ indices [$F^2 > 2\sigma(F^2)$] | $R1$ = 0.0462, $wR2$ = 0.1236 | |
| $R$ indices (all data) | $R1$ = 0.0566, $wR2$ = 0.1309 | |
| Extinction coefficient | n/a | |
| Largest diff. peak and hole | 0.973 and –0.563 e Å$^{-3}$ | |

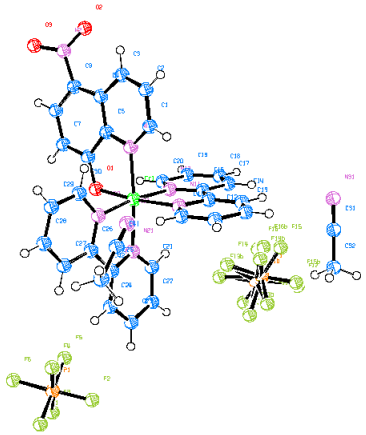

**Table Y.1:** Crystal data and structure refinement details $[Cr^{III}(bpy)_2(QN)](PF_6)_2.2$ MeCN

**5.12**

| | | |
|---|---|---|
| Identification code | **2015ncs0426 / CrdhNPF$_3$-18/6** | |
| Empirical formula | $C_{33}H_{27}CrF_{12}N_8O_3P_2$ | |
| Formula weight | 925.56 | |
| Temperature | 100(2) K | |
| Wavelength | 0.71073 Å | |
| Crystal system | Triclinic | |
| Space group | *P*–1 | |
| Unit cell dimensions | *a* = 9.7304(3) Å | $\alpha$ = 107.542(3)° |
| | *b* = 12.3940(5) Å | $\beta$ = 95.630(2)° |
| | *c* = 17.3435(5) Å | $\gamma$ = 109.673(3)° |
| Volume | 1830.94(12) Å$^3$ | |
| *Z* | 2 | |
| Density (calculated) | 1.679 Mg / m$^3$ | |
| Absorption coefficient | 0.510 mm$^{-1}$ | |
| *F(000)* | 934 | |
| Crystal | Block; Red | |
| Crystal size | 0.110 × 0.100 × 0.050 mm$^3$ | |
| $\theta$ range for data collection | 2.280 – 27.559° | |
| Index ranges | $-12 \le h \le 12$, $-16 \le k \le 16$, $-22 \le l \le 22$ | |
| Reflections collected | 29457 | |
| Independent reflections | 8439 [$R_{int}$ = 0.0295] | |
| Completeness to $\theta$ = 25.242° | 99.9 % | |
| Absorption correction | Semi–empirical from equivalents | |
| Max. and min. transmission | 1.00000 and 0.88263 | |
| Refinement method | Full-matrix least-squares on $F^2$ | |
| Data / restraints / parameters | 8439 / 252 / 598 | |
| Goodness-of-fit on $F^2$ | 1.065 | |
| Final *R* indices [$F^2 > 2\sigma(F^2)$] | *R1* = 0.0644, *wR2* = 0.1804 | |
| *R* indices (all data) | *R1* = 0.0791, *wR2* = 0.1920 | |
| Extinction coefficient | n/a | |
| Largest diff. peak and hole | 0.904 and –0.534 e Å$^{-3}$ | |